UNIVERSITÀ DI SIENA 1240

Department of Biotechnology, Chemistry and Pharmacy

PhD in Chemical and Pharmaceutical Sciences

Cycle XXXV

Coordinator: Prof. Maurizio Taddei

Antibody-drug conjugates charged with unconventional payloads

Tutor:
Prof. Elena Petricci

CHIM/06- Organic Chemistry

PhD candidate:
Giovanni Ievoli

Giovanni Ievoli
26.05.2023 06:45:43
GMT+01:00

Academic year:
2021/2022

Abstract

Antibody-drug conjugates (ADCs) represent one of the most advanced selective therapy that have attracted a lot of interest in recent years. ADCs consist of monoclonal antibodies (mAbs) that are bound to bioactive molecules (payloads) through specific linkers. The linker is one of the most important part of ADC due to its ability to stabilize the conjugates in the bloodstream, enhance the solubility of the ADC, prevent non-specific release of payload and finally release the bioactive compound in the target cell.

ADCs are effective systems for target therapy in particular in treatment of cancer but also for bacterial infections resistant to conventional antibiotics. Less explored are the use of these systems for the treatment of viral infections. In this thesis, various linkers suitable for the bioconjugation of several payloads were synthesized and conjugated with mAbs to make novel ADCs for the treatment of cancer, bacterial and viral infections.

The other part of the thesis was made in collaboration with a leading Italian pharmaceutical company. In this context, new synthetic strategies were explored for the preparation of intermediates useful for the synthesis of biological active compounds.

Abstract

Gli *Antibody-drug conjugates* (ADCs) rappresentano una delle terapie selettive più avanzate che hanno suscitato molto interesse negli ultimi anni. Gli ADCs sono formati da un anticorpo monoclonale (mAb) legato a molecole bioattive (*payloads*) tramite uno specifico *linker*. Il linker è una delle parti più importanti del sistema poichè stabilizza il bioconiugato nel circolo sistemico, aumenta la solubilità dell'ADC, previene un rilascio non specifico del *payload* e favorisce il rilascio della molecola attiva nelle cellule target.

Gli ADCs sono dei sistemi molto efficaci nel trattamento del cancro ma anche nelle infezioni batteriche resistenti agli antibiotici convenzionali. Tuttavia, il loro utilizzo come agenti antivirali è stato meno esplorato. In questo lavoro di tesi, vari *linkers* adatti per la bioconiugazione di *payloads* con mAbs sono stati sintetizzati per dare vita a nuovi ADCs per il trattamento del cancro e di infezioni batteriche e virali.

L'altra parte di questa tesi è stata svolta in collaborazione con un'industria farmaceutica italiana. In questo caso, sono state esplorate nuove strategie sintetiche per la preparazione di intermedi utili per la sintesi di molecole biologicamente attive.

Index

List of abbreviations

5-FU	5-Fluorouracil
AAC	Antibody-Antibiotic Conjugate
ABF	4-azidobenzoyl fluoride
ACN	acetonitrile
Ac_2O	acetic anhydride
AcONa	sodium acetate
ADC	Antibody-Drug Conjugate
ADCC	Antibody-Dependent Cell-mediated Cytotoxicity
ADCP	antibody dependent cell-mediated phagocytosis
Ala	alanine
Alk	alkyl
AML	acute myeloid leukemia
AMPs	antimicrobial peptides
AMR	antimicrobial resistance
API	Active Pharmaceutical Ingredient
Arg	arginine
Asn	asparagine
ATP	adenosine triphosphate
BCC	basal cell carcinoma
bs	broad singlet
β-GlcNAc-WTA	β-N-acetylglucosamine cell-wall teichoic acid
CA	cinnamaldehyde
CD	cluster of differentiation
Ce6	chlorin e6
Ces1C	carboxyesterase 1C
CEX	Cation exchange chromatography
Cit	citrulline
COVID-19	Coronavirus Disease 2019
COX-2	cyclooxygenase-2
Ctx	Cetuximab
CuAAC	Copper(I)-Catalyzed Azide-Alkyne Cycloaddition
Cys	cysteine
d	doublet
DAR	drug-to-antibody ratio
DBCO	dibenzocyclooctyne
DBCO-NH_2	dibenzocyclooctyne-amine
DBU	diazabicyclo[5,4,0]undec-7-ene
DCM	dichloromethane
dd	doublet of doublets
ddd	doublet of doublets of doublets
dddd	doublet of doublets of doublets of doublets

DFT	density functional theory
Dhh	Desert Hedgehog
DHP	dihydropyridine
DHPMs	dihydropyrimidinones
DPPH	2,2-diphenyl-1-picrylhydrazyl
DHPS	dihydropteroate synthase
DIPEA	N,N-diisopropylethylamine
DLBCL	diffuse large B-cell lymphoma
DM1	Mertansine or Emtansine
DM4	Ravtansine or Soravtansine
DMA	dimethylacetamide
DMAP	4-dimethylaminopyridine
DME	dimethoxyethane
DMF	dimethylformamide
DMSO	dimethyl sulfoxide
DMSO-d_6	deuterated dimethyl sulfoxide
DNA	deoxyribonucleic acid
DOXO	Doxorubicin
DPD	dihydropyrimidine dehydrogenase
DTT	Dithiothreitol
EVD	Ebola virus infection
EDC	1-ethyl-3-(3-dimethylaminopropyl)carbodiimide
EDGs	electron-donating groups
EGFR	epidermal growth factor receptor
EMA	European Medicines Agency
EPPS	(N-(2-Hydroxyethyl)piperazine-N′-(3-propanesulfonic acid))
ESI	electrospray ionization
EtOAc	ethyl acetate
EtOH	ethanol
EWGs	electron-withdrawing groups
Fab	fragment antigen-binding
Fc	fragment constant
FcRns	neonatal Fc receptors
FcγRs	Fc-gamma receptors
FDA	Food and Drug Administration
FGE	formylglicine-generating enzymes
fGly	formylglycine
FID	free induction decay
GC-MS	gas chromatography-mass spectrometry
Gly	glycine
GPCR	G-protein-coupled receptor
GSH	reduced glutathione
HAT	histone acetyltransferase
HCL	refractory hairy cell leukemia

HDAC	histone deacetylase
HDX-MS	hydrogen deuterium exchange mass spectrometry
HER2	human epidermal growth factor receptor 2
HETCOR	heteronuclear correlation
HH	Hedgehog pathway
HHPMs	hexahydropyrimidinones
HIC	Hydrophobic Interaction Chromatography
HIV	human immunodeficiency virus
HL	Hodking lymphoma
HLM	human liver microsomes
HMPO	5-(hydroxymethyl) pyrogallol orthoester
HPG	hyperbranched polyglycerol
HPLC	high-performance liquid chromatography
HRMS	high-resolution mass analyser
HSA	human serum albumin
HSV	herpex simplex virus
IC_{50}	half maximal inhibitory concentration
IgA	immunoglobulin A
IgE	immunoglobulin E
IgD	immunoglobulin D
IgG	immunoglobulin G
IgM	immunoglobulin M
IGN	indolinobenzodiazepins
Ihh	Indian hedgehog
IM-MS	ion-mobility mass spectrometry
iNOS	inducible nitric oxide synthase
KHMDS	potassium bis(trimethylsilyl)amide
Leu	leucine
Lys	lysine
m	multiplet
mAbs	monoclonal antibodies
MALDI	matrix-assisted laser desorption/ionization
MC	maleidocaproic acid
MCC	maleimidomethyl cyclohexane-1-carboxylate
MCRs	multicomponent reactions
MDR1	multidrug resistance protein 1
MeCN	acetonitrile
MEM	methoxyethoxymethyl ether
MIC	minimal inhibition concentration
MMAE	Monomethyl Auristatin-E
MMAF	Monomethyl Auristatin-F
MOM	methoxymethyl ether
MPLC	medium pressure liquid chromatography
MPXV	Monkeypox virus

MRSA	methicillin-resistant Staphylococcus aureus
MS	mass spectroscopy
MTD	maximum tolerated dose
MTDB	1,5,7-triazabicyclo[4.4.0]dec-5-ene
mTG	microbial transglutaminases
mTNBC	with metastatic triple-negative breast cancer
MTT	(3-[4,5-dimethylthiazol-2-yl]-2,5 diphenyl tetrazolium bromide)
MW	microwave
ncAAs	non-canonical amino acids
NCHB	network of cooperative hydrogen bonds
NCL	Niclosamide
NEBIs	*N*-ethoxybenzylimidazoles
NHS	N-hydroxysuccinimide
NMR	nuclear magnetic resonance
NOESY	Nuclear Overhauser Enhancement SpectroscopY
NMP	*N*-methyl pyrrolidone
NSCLC	non-small cell lung cancer
PABA	*p*-aminobenzyl alcohol
PABC	*p*-aminobenzyloxyacarbonyl
PABQ	*p*-aminobenzyl quaternary salt
pAcF	*p*-acetylphenylalanine
pAzF	*p*-azidophenylalanine
PBS	phosphate-buffered saline
PBD	pyrrolobenzodiazepine
PE	petroleum ether
PEG	polyethylene glycol
PG	protecting group
PHB	*p*-hydroxybenzyl
Phe	phenylalanine
PK	pharmacokinetic
PPE	polyphosphoric ester
Pro	proline
PRRT	peptide receptor radionuclide therapy
PTCH	12-pass transmembrane receptor Patched
PTSA	*p*-toluenesulfonic acid
Py	pyridine
q	quartet
Q-TOF	Quadrupole Time of Flight
RLM	rat liver microsomes
RNA	ribonucleic acid
RNS	reactive nitrogen species
ROS	reactive oxygen species
RPLC	reversed-Phase Liquid Chromatography
Rt	retention time

r.t.	room temperature
s	singlet
SAHA	Vorinostat, suberanilohydroxamic acid
sALCL	relapsed systemic anaplastic large-cell lymphoma
SEC	size-Exclusion Chromatography
Shh	Sonic hedgehog
SMCC	succinimidyl-4-(N-maleimidomethyl)cyclohexane-1-carboxylate
SMDCs	Small Molecule-Drug Conjugates
SMO	Smoothened receptor
S_NAr	nucleophilic aromatic substitution
S-NHS	*N*-hydroxysulfosuccinimide
SPAAC	strain-promoted azide–alkyne cycloaddition
SpiDO	Spiro-Di-Orthoester
t	triplet
TBAB	N-tetrabutylammonium bromide
TCEP	(tris(2-carboxyethyl)phosphine)
TCO	trans-cyclooctene
TFA	trifluoroacetic acid
THF	tetrahydrofuran
Thr	threonine
TLC	thin-layer chromatography
TMG	1,1,3,3-tetramethylguanidine
TMSCl	chlorotrimethylsilane
TPGS	DL-α-tocopherol methoxypolyethylene glycol succinate
TRPA1	transient receptor potential A1 inhibitors
TSs	transition states
Tyr	tyrosine
UV/Vis	ultraviolet-visible spectroscopy
Val	valine
vc	valine-citrulline
VEGF	vascular endothelial growth factor
VREF	vancomycin-resistant *Enterococcus faecium*
WHO	World Health Organization
WTA	wall teichoic acid
ZBG	zinc-binding group

SECTION A

Antibody-drug conjugates charged with unconventional payloads

CHAPTER 1- Introduction

1.1 Cancer disease, bacterial and viral infections: classical therapies versus target-base approaches

In the last century the expectancy of life has increased. This is correlated with the improvements in medical field, nutrition, sanitation, and the discovery of new drugs. [1] Although many advances have been made in treating cancer or bacterial and viral infections, these diseases remain a global problem requiring attention. In the following chapters there is an overview of the main strategies used in clinic with a particular focus on antibody-drug conjugates (ADCs) that represent the main topic of this thesis project.

1.1.1 Cancer: from old drugs to target therapy

Now more than ever, cancer is a leading cause of death worldwide; about 10 million deaths in 2020 as reported in the last data sheet of WHO. [2] The 20th century can be considered the starting point for the classic chemotherapy. Indeed, especially after the observation of the effects of nitrogen mustards in World War I and II, these compounds followed by folic acid antagonist were used in clinic to treat haematological malignancies. [3] During the time, other kind of drugs such as antimetabolites and alkylating agents were developed to increase the response in the patients. Nowadays, chemotherapy is still the first choice leading to a higher toxicity or drug resistance. The major issue is the lack of selectivity towards rapidly dividing cells causing hair loss, sickness, and tiredness. Other classic treatments include immunotherapy, surgery, radiation, stem cell therapy, laser treatment, photodynamic therapy, and hyperthermia. [3,4] Therefore, there is a need to develop new drugs to increase the selectivity and reduce the side effects. The first concept associated with target therapy was developed by Paul Erlich with his “magic bullet” referring to chemical drugs able to target microorganisms in a specific manner without harming the human body. [5] This dreaming vision postulated by Erlich, flows into four main types of target therapy:

- kinase inhibitors;
- monoclonal antibodies (mAb);
- antibody-drug conjugates (ADCs);

- small molecule-drug conjugates (SMDCs). [6]

Even if none of these categories are free from side-effects, great improvements have been observed over the years.

In 2001 the FDA approved Imatinib (Gleevec®, Figure 1), the first kinase inhibitor for the treatment of chronic myeloid leukemia.

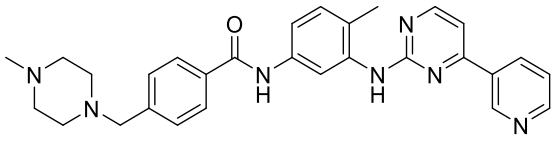

Figure 1- Structure of Imatinib.

After Imatinib, more than 60 inhibitors were approved by the FDA with some of these for the treatment of multiple cancer diseases. [7,8] As the overexpression of specific kinases (tyrosine and serine or threonine) are involved in different types of cancer, these drugs work by blocking the activity of the catalytic domain of transmembrane kinase receptors through a competition with ATP binding. [9] Despite a good result to reduce the off-target toxicity, kinase inhibitors still show low activity in many solid tumors along with a limited variety of targeted enzymes. [10]

The use of chemotherapeutics based on monoclonal antibodies (mAbs) started in the 1970s after the introduction of hybridoma technique to produce mAbs developed by Kohler and Milstein. [11] The idea behind this approach involved a specific binding between mAbs and antigen on tumor cells leading a more selective therapies with a reduction of side effects related to the off-target toxicity typical of classic chemotherapeutic agents. With >100 mAbs approved by FDA for cancer and non-cancer indications and more than 400 mAbs under investigation in clinical phases, this field is constantly growing. [12] A common structure shared by all antibodies is Y-shaped in which we can identify two heavy polypeptide chains and two light chains (Figure 2).

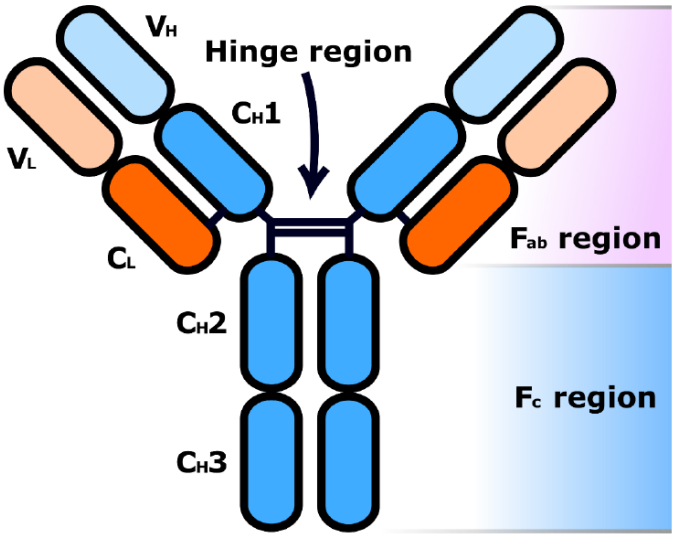

Figure 2- Y-shape structure. Heavy chains in blue and light chains in orange. [13]

These chains also contain constant (C) and variable (V) regions linked by disulphide and non-covalent bonds. The hinge region plays an important role in the rearrangement of antibodies for the binding with antigens which occurs on fragment antigen-binding (F_{ab}) region (Figure 2). [14] We can also classify the mAbs into five immunoglobulin classes: IgM, IgG, IgD, IgE and IgA on the basis of the different amino acid sequences located in constant regions. Amongst, IgG (in particular IgG1) isotype is the most frequently used either in immunotherapy and in antibody-drug conjugates (ADCs) systems because of its stability in plasma and higher binding for Fc-gamma receptors (FcγRs) giving more effective immune response. [15] An example of mAb used in clinic is Trastuzumab (Herceptin®), a humanised anti-HER2 IgG1 indicated for adjuvant treatment of HER2-positive breast cancer, in combination or monotherapy in metastatic breast cancer and metastatic gastric cancer. [16] Some problems in the use of mAbs are related to solid tumors, which express irregular vasculature affecting the biodistribution of drugs and resistance mechanisms. For example, although Trastuzumab has significantly improved outcome in breast cancer patients, less than 35% of HER2-positive breast cancer respond to the treatment because of the mechanisms of resistance to the drug. [17,18] Since 1977, when the first mAb Rituximab (anti CD20) was approved by FDA, other mAbs have come out to the market: ofatutumab (anti-CD20), alemtuzumab (anti-CD52), trastuzumab and pertuzumab (both anti-HER2), cetuximab and paninutumab (anti-EGFR), bevacizumab (anti-VEGF).

Another novel class of molecules that are gaining a lot of interest in recent years are small molecule-drug conjugates (SMDCs). As indicated by the name, these small molecules are

composed by a low molecular weight ligand linked to the cytotoxic drug by an appropriate linker. SMDCs are developed with the idea to overcome the problematic pharmacokinetic properties shown by naked antibodies or ADCs related to the large size of mAbs. [19] Usually, natural substances like vitamin or peptides are chosen as ligands. In contrast to ADCs, all small molecules are characterized by kidney uptake, meaning the renal clearance process. [20] Therefore, the development of SMDCs characterized by other elimination pathways remain a good challenge. [21,22] Regarding the mechanism of action, after the binding to its receptor, the conjugate goes into the cell by endocytosis to form an early endosome where there is the cleavage of conjugates from receptors (which is recycled on the cell surface). At the lysosome stage, the drug is released from its conjugate via deconjugation (or cleavage of linker) causing cell death (Figure 3).

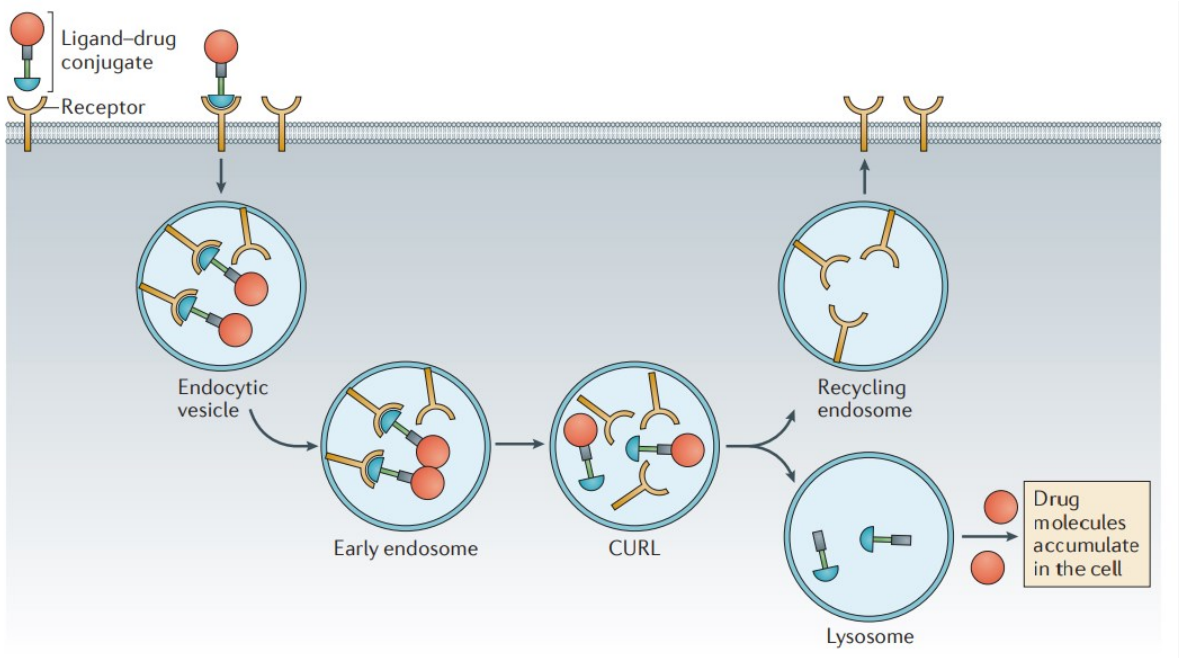

Figure 3- Mechanism of action of SMDCs. [19]

Recently, a peptide-based ^{177}Lu-DOTATE was approved in clinic by FDA and European Medicines Agency (EMA) for the treatment of neuroendocrine gastroenteropancreatic tumors (Figure 4).

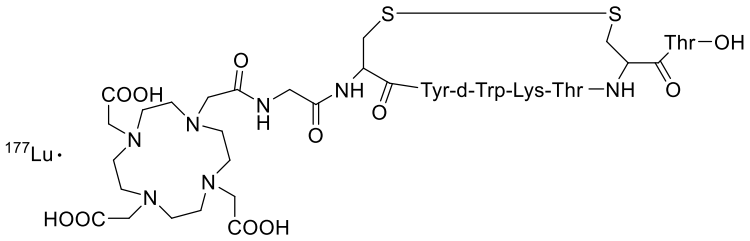

Figure 4- Structure of ^{177}Lu-DOTATE.

The use of ^{177}Lutetium (^{177}Lu) for radiotherapy belongs to a category of treatments know as peptide receptor radionuclide therapy (PRRT) in which the peptide targets the peptide receptors on the cell surface while the radionuclide allowing the use of radiation to treat the tumor. [23] The mechanism of the drug is related to its structure: a somatostatin analog (in this case octreotate) selectively binding to somatostatin receptor expressing cells and being internalized, along with isotope ^{177}Lu. [23] Although ^{177}Lu-DOTATE is the only drug approved for PRRT, other compounds are developed. This is the case of ^{90}Y-DOTATOC which seems to allow for greater efficacy for large metastatic tumor, but with some side effects (in particular nephrotoxicity) if compared to ^{177}Lu-DOTATE. [24] Peptides are not the only example of ligand. Some vitamins such as folic acid, cobalamine B_{12} and biotin are chosen as the tumor cells have an increased request of these compounds to satisfy their metabolic needs. Vintafolide (EC145) consists of a folic acid moiety linked to a novel vinca alkaloid agent desacetylvinblastinehydrazide via a cleavable disulfur linker that reached a phase III of clinical trials for ovarian cancer even if with a poor result to prove survival advantage. [25] In addition to kinase inhibithors, mAbs and SMDC, another important class of drugs for target therapy against cancer is antibody-drug conjugation (ADCs). ADCs are comprised of a monoclonal antibody that are covalently bound to cytotoxic molecules (known as payloads) via chemical linkers (Figure 5).

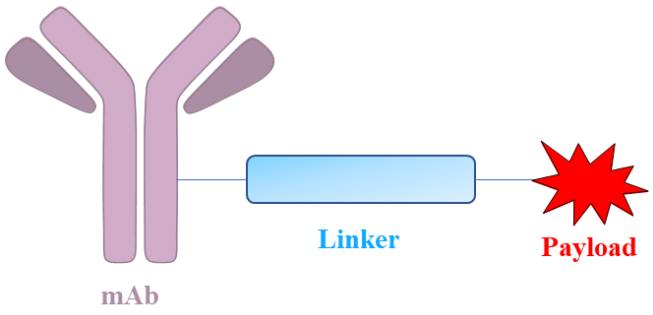

Figure 5- Structure of a generic ADC.

Combining the ability of mAbs to target cancer cells with the ability of payload to selectively kill cancer cells, ADCs represent the most sophisticated pharmaceuticals ever developed. [26] The linker is one of the challenging parts of ADCs as it has a greater impact on toxicity, specificity, stability and potency of the entire system. Thus, a wide range of chemical linkers have been investigated leading to two main classes: cleavable linkers and non-cleavable linkers. As the ADC is directed by mAb, the target antigen should be expressed in high concentration on tumor cells and not or poorly expressed in healthy cells. ADCs suffer from the same problems of mAb (as it is almost the 90% of the ADC), that is, a not optimal pharmacokinetic profile due to the large size of antibodies. [13] Usually, the payload is a high cytotoxic agent (IC_{50} 0.1 nM-1 pM) acts in the nucleus causing DNA or microtubules damage but there may be other mechanisms such as the modelling of genic transcription as in ADCs charged with HDAc inhibithors. [27] The amount of payload charged on ADC must be balanced because of its influence on pharmacokinetic properties. The drug-to-antibody ratio (DAR) is a useful parameter because it expresses the number of linker-payload *per* antibody. An optimal DAR remains to be established even if the majority of ADCs have a range from 0-8. [28] Regarding the mechanism of action, a typical example is reported in Figure 6. [29]

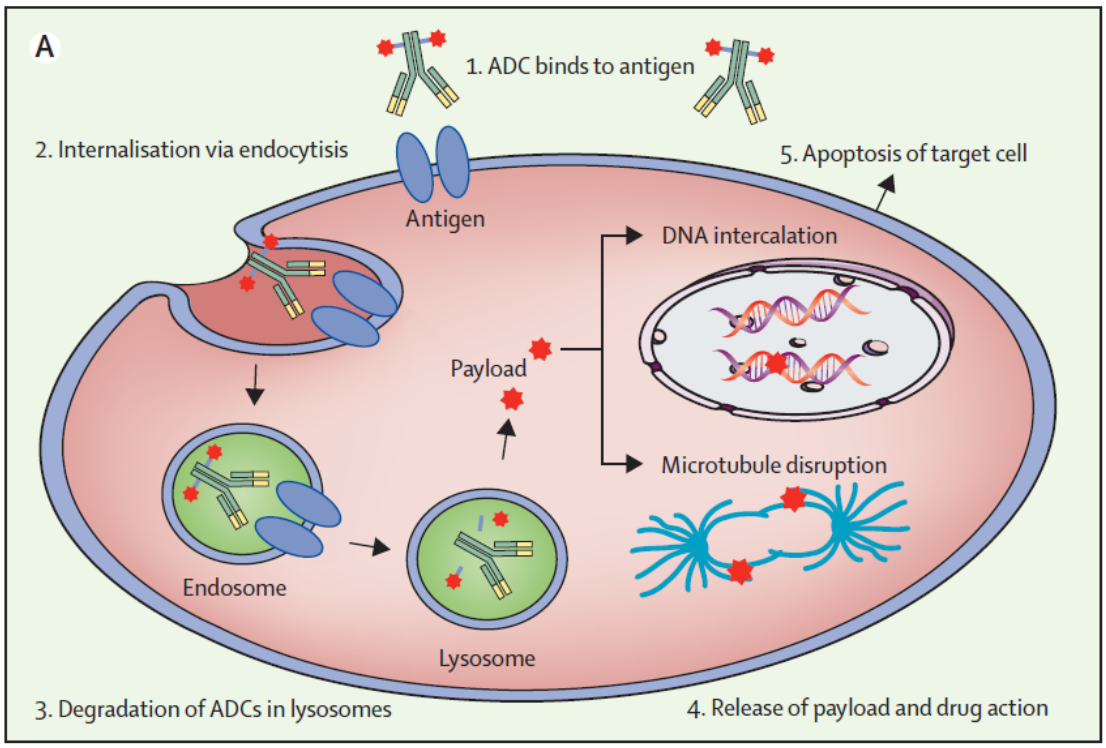

Figure 6- Mechanism of action of an ADC. [29]

First, circulating ADCs find and bind their antigen. Then the ADC-antigen complex becomes internalised mainly via clathrin-mediated endocytosis and forms an early endosome. [30,31] At this stage, depending on the nature of the linker, the payload can be released after an appropriate stimulus (such as pH variations, enzyme, difference in the redox potential) as the case of cleavable linkers, or the endosome can mature and fuse with lysosome. For non-cleavable linkers the ADC requires complete proteolytic digestion promoted by an acidic environment generated from a proton pump on lysosomes. The ADCs can also be recycled back to the cell surface because of the binding with the neonatal Fc receptors (FcRns) expressed in endosomes. [31] Once the payload has been released, it can act according to its mechanism leading to cell apoptosis. The payload can also kill nearby cells by the so-called bystander effect. This effect depends mainly on the hydrophobicity of payload. High hydrophobic and non-charged payload can diffuse through the plasmatic membrane and spread into neighbouring cells. Even though the bystander effect can improve the range of actions of ADCs to cells that do not express the target antigen (as in the case of some solid tumors), sometimes this can lead to the off-target toxicity when healthy cells are involved. Nowadays, the difficulty in finding new drugs for ADCs lies into non optimal pharmacokinetic/pharmacodynamic properties of many of these active molecules such as low hydrophobicity, high potency and chemical group that allows chemistry with the linker. All these features can be found in drugs that target DNA (*i.e.* duocarmycines, calicheamicines and pyrrolobenzodiazepines) or tubulin (*i.e.* auristatins and maytansinoid). The three components of ADCs (mAb, linker, payload) must be balanced in order to obtain conjugates with limited side effects and high activity and homogeneity in terms of DAR. In the following paragraphs there is a more in-depth discussion of the various aspects to be considered in the development of these conjugates with an outlook on ADCs in the market.

1.1.2 New approaches for bacterial infections

The use of ADCs is not limited to cancer, but over the years they have also been explored as antibacterials and antivirals. Considering bacterial infections, approximately two-thirds of antibiotics in clinic are natural or semisynthetic products. [32] Although their use has reduced mortality, many common infections are becoming resistant to classical antibiotics. In addition, poor pharmacokinetic properties and high toxicities related to some new potent antibacterial drugs, limited their use in clinic. Alternative therapies are represented by the use of antibodies or antibody-antibiotic conjugates (AACs). The discovery of antibodies (in

form of serum) against bacteria is due to Emil von Behring and Kitasoto in their studies on diphtheria and tetanus. [33] Unfortunately, the limited spectrum and heterogeneity between lots have complicated their use as antibiotics. [34] Thanks to the discovery of hybridoma technology and advances in mAbs there is a renewed interest in developing new antibacterial mAbs. So far, three mAbs have been approved to treat bacterial infections: Bezlotoxumba (Zinplava®, against *Clotridium difficile*), Obiltoxaximab (ANTHIM®, against *Bacillus antracis)* and Raxibacumab (ABthrax®, against *Bacillus antracis*). [35] The mechanisms of action of mAbs may be multiple. For example, the Fab region of antibody can bind an antigen (expressed on the bacterial cell surface) resulting in neutralization of toxins and preventing infection. [32] Another mechanism involves the Fc region of antibodies that can promote an immune response towards opsonized bacteria. However, the use of mAbs as monotherapy is limited due to several factors such as limited spectrum and hiding of essential epitopes on bacterial surfaces (*i.e.* teichoic acids by Gram positive). [36] A novel class of antibacterial are antibody-antibiotic conjugates (AACs) in which the idea is similar to classic ADCs but with some changes in mAbs and payloads. First, the mAb should target specific antigens (expressed on bacterial cells surface) selectively. Then the classic cytotoxic drugs, used as payloads in ADCs for cancer, may be replaced by antibacterial drugs. An example of AAC developed against *Staphylococcus aureus* is shown in Figure 7.

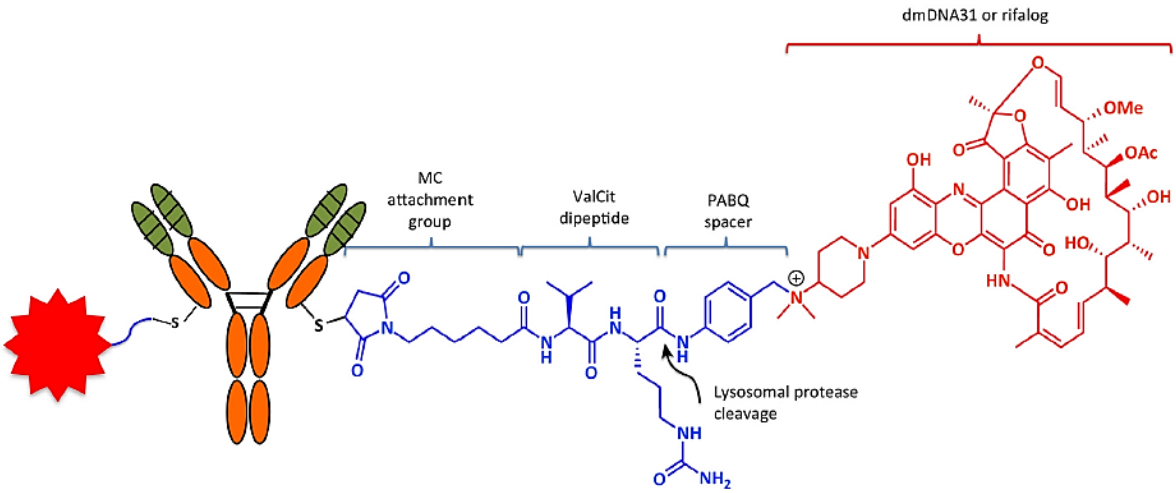

Figure 7- AAC based on THIOMAB™ technology for the treatment of *S. aureus.* [32]

In this example the mAb is an β-N-acetylglucosamine cell-wall teichoic acid (β-GlcNAc-WTA) engineering antibody. This mAb bind in a selective manner β-GlcNAc residues on the wall teichoic acid (WTA) through a specific antigen that is highly abundant and

expressed on *S. aureus* and absent in mammalian cells. [37,38] In addition, the THIOMAB™ technology (a form of engineered antibody with reactive cysteines at specific site) allows a more accurate bioconjugation leading a more homogeneous product in terms of DAR. [39] The cleavable MC-ValCit-PABQ linker consists of maleimide and caproic acid (MC) for antibody bioconjugation, valine citrulline (Val-Cit) sensible to lysosomal protease and p-aminobenzyl as quaternary salt (PABQ) which is the bridge between payload and linker and act as self-immolative spacer to promote the release of drug. The last difference is the payload. In this AAC the drug can be either rifampicin or DNA31 (a rifalazil analog) that inhibits RNA polymerase. [38] Even if both antibiotics have the right properties (chemical group for conjugation, high potency and good pharmacokinetics) to be included in AAC, only DNA31 is active when released due to its activity against persisted and stationary phase *S.aureus*. [38] The mechanism of action of this AAC shows the difference from the classic ADCs used for cancer. Actually, the antibody ensure that *S.aureus* are rapidly opsonized or tagged and then the complex AAC-bacteria are internalized by phagocytosis/non-phagocytosis mechanisms. [38] Once in the cells, the payload can be released (through cathepsins cleavage) and fulfill its function killing bacteria (Figure 7).

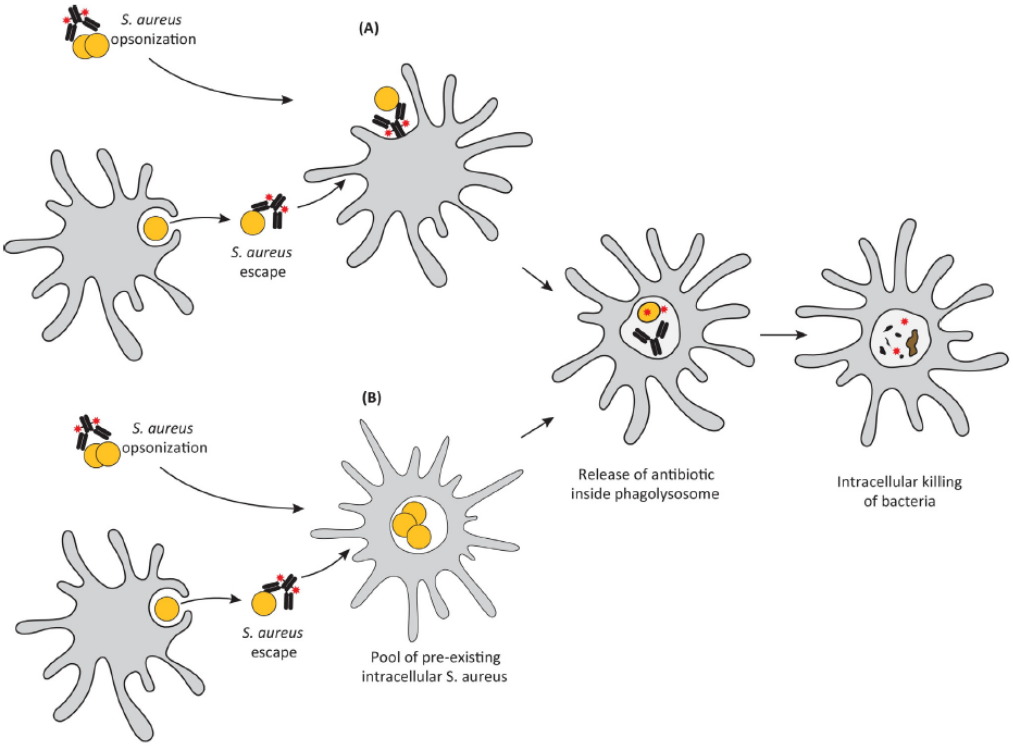

Figure 8- Mechanism of action of AAC against *S.aureus*. (A) Cells not infected with *S.aureus* and (B) cells already infected with *S.aureus*. [32]

As the opsonized *S.aureus* can enter into the cells already infected (in which the bacteria is "hidden" from AAC), the mechanism of action of this AAC relying in the elimination of tagged and untagged bacteria leading to better treatment of infection.
Recently, other promising alternatives emerged as the use of peptomimetics. [40] These molecules, also known as antimicrobial peptides (AMPs), have important properties such as low toxicity, potency and specificity along with a particular mechanism of action. [41] However, the main disadvantage is the poor physiological stability even if several AMPs can be found in preclinical and clinical development. [42–44]

1.1.3 Viral infections and therapeutical approaches

The recent Coronavirus Disease 2019 (COVID-19) pandemic and other kinds of infections like Ebola virus infection (EVD) or Monkeypox virus (MPXV) [45] stressed the importance in the development of new antiviral drugs. Different approaches are used for the treatment of viruses:

- Vaccines;
- specific antiviral drugs that block one or more steps during the virus cell cycle;
- plasma of healed patients containing antiviral antibodies or the corresponding mAbs.

Vaccines are very effective for some viruses but could become ineffective if the virus is constantly mutating. Sometimes, as well as antiviral drugs, it takes a long time for their development. Antiviral drugs are more effective against certain viruses but still suffer from mechanisms of resistance (like the case of HIV). [46] The use of plasma of healed patients is a very interesting approach as it is fast but the poor availability and the variability in terms of antibodies have limited its use in clinic. [47] Moreover, a randomized trial of convalescent plasma in Covid-19 (on 333 patients) shows no significance differences between patients treated with convalescent plasma and those treated with placebo. [48]
Thus, there is a need for new therapies that are effective and versatile against different types of viruses. In this context, ADCs may be an alternative to overcome the problems described above. Recently some examples of antibody-conjugates have been reported for a possible treatment of HIV even if none of these have been approved due to poor data in humans. [49] However, the use of ADCs in this field is a matter of intense research.

1.2 Antibody-drug conjugates

1.2.1 ADCs in the market: an in-depth look

Antibody-drug conjugates have made a lot of progress in the last 10 years. Since the first ADC gentuzumab ozogamicin, to-date 11 ADCs (plus 1 immunotoxine Lumoxiti® often included in ADCs) have been approved by FDA for cancer treatment and more than 80 are currently under clinical investigation (Table 1). [50]

Drug	Condition-Target	Trade name	Approval year
Gentuzumab ozogamicin	Relapsed acute myelogenous leukemia (AML)-CD33	Mylotarg®	2000 (withdrawn from the market); 2017
Brentuximab vedotin	Relapsed Hodking lymphoma (HL) and relapsed systemic anaplastic large-cell lymphoma (sALCL)-CD30	Adcetris®	2011
Trastuzumab ematansine	HER2-positive metastatic breast cancer-HER2	Kadcyla®	2013
Inotuzumab ozogamicin	relapsed or refractory CD22-positive B-cell precursor acute lymphoblastic leukemia- CD22	Besponsa®	2017
Moxetumomab pasudotox	adults with relapsed or refractory hairy cell leukemia (HCL)-CD22	Lumoxiti®	2018
Polatuzumab vedotin-piiq	relapsed or refractory (R/R) diffuse large B-cell lymphoma (DLBCL)-CD79	Polivy®	2019
Enfortumab vedotin	adult patients with locally advanced or metastatic urothelial cancer who have received a PD-1 or PD-L1 inhibitor, and a Pt-containing therapy- Nectin-4	Padcev®	2019
Trastuzumab deruxtecan	adult with unresectable or metastatic HER2-positive breast cancer who have received two or more prior anti-HER2 based regimens- HER2	Enhertu®	2019

Sacituzumab govitecan	adult with metastatic triple-negative breast cancer (mTNBC) who have received at least two prior therapies for patients with relapsed or refractory metastatic disease- Trop-2	Trodelvy®	2020
Belantamab mafodotin-blmf	adult patients with relapsed or refractory multiple myeloma-BCMA	Blenrep®	2020
Loncastuximab tesirine-lpyl	Large B-cell lymphoma-CD19	Zynlonta®	2021
Tisotumab vedotin-tftv	Recurrent or metastatic cervical cancer	Tivdak®	2021

Table 1- ADCs approved by FDA.

The first approved ADC was gentuzumab ozogamicin (Mylotarg®) in 2000 for the treatment of acute myeloid leukemia (Figure 9) but in 2010 was voluntarily withdrawn from the market when post approval study revealed a lack of clinical benefit and excess mortality. [51] Then, in 2017 was reapproved at lower dosages for the same indications after a further investigation in phase III. [52]

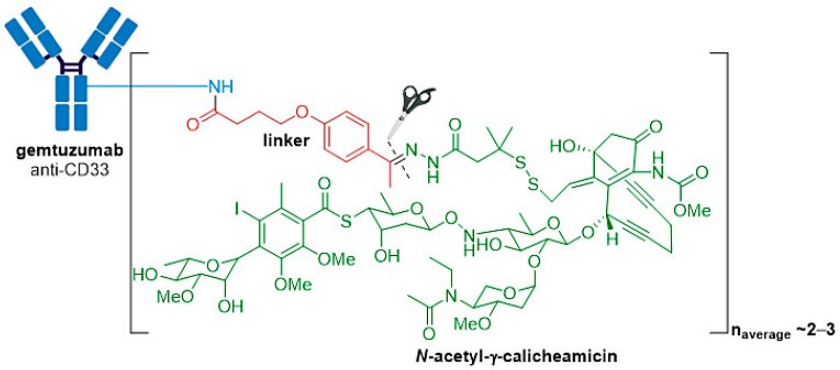

Figure 9- Mylotarg® [53]

Adcetris® (Figure 10) was approved in 2011 for the treatment of stage III or IV Hodgkin's lymphoma and for systemic anaplastic large lymphoma. [50] It contains an anti-CD-30 IgG1 linked with monomethyl auristatin E (MMAE) through a protease sensitive linker along with a *p*-aminobenzyl self-immolative spacer, a second generation of cleavable linkers (as described in next paragraphs). [54]

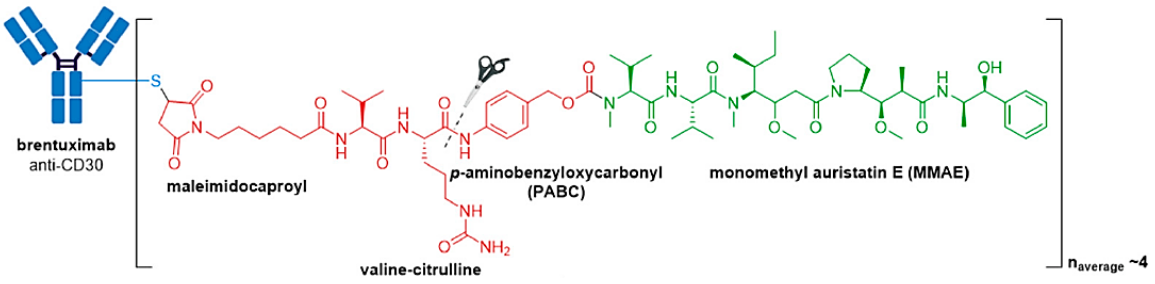

Figure 10- Adcetris® [53]

Kadcyla® (Figure 11), was the first ADC approved for solid tumors in 2013. [53] It is indicated for HER2-positive metastatic breast cancer-HER2 in patients who previously received trastuzumab (Herceptin®) and a taxane. [55] In this case the mAb is an IgG anti HER2 linked to Maytansinoid DM1 by a metabolic sensitive thioether linker. [56] This non-cleavable linker is more stable than their cleavable counterparts but require lysosomal degradation of the entire antibody linker (with the risk of some charged amino acids attached on the payload).

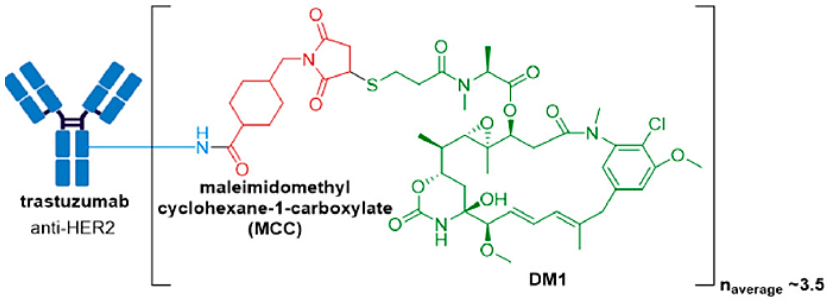

Figure 11- Kadcyla® [53]

Inotuzumab ozogamicin (Besponsa®, Figure 12), indicated for the treatment of acute and chronic lympocytic leukemia, was approved in 2017 by FDA. [50] It consists of an IgG4 antibody direct towards CD22 antigens. The linker is a cleavable hydrazone linker (pH sensitive) charged with Calicheamicin as payload. [57] Preclinical studies show that Besponsa® can tolerate high DAR (~6) without significant aggregation. [58]

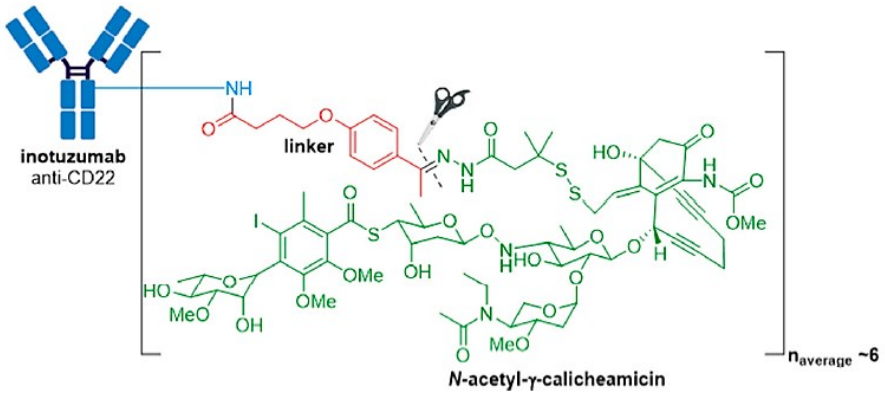

Figure 12- Besponsa® [53]

Lumoxity® be part of the drugs listed as ADCs, but it is quite different. It is an immunotoxin composed of a recombinant murine immunoglobulin that recognized CD22 antigens, fused to a 38kDa of Pseudomonas exotoxin, which inhibits protein synthesis. [59]

In 2019 three ADCs have been approved: Polivy®, Padcev® and Enhertu®. Polivy® and Padcev® (Figure 13), contain the same linker-payload (mc-vc-PABC-MMAE) but differ in mAbs. While the first is an anti-CD79 mAb, Padcev® is anti-Nectin-4 mAb. [53] These examples highlighted that only by changing the mAb we can obtain two different products with different indications in clinic.

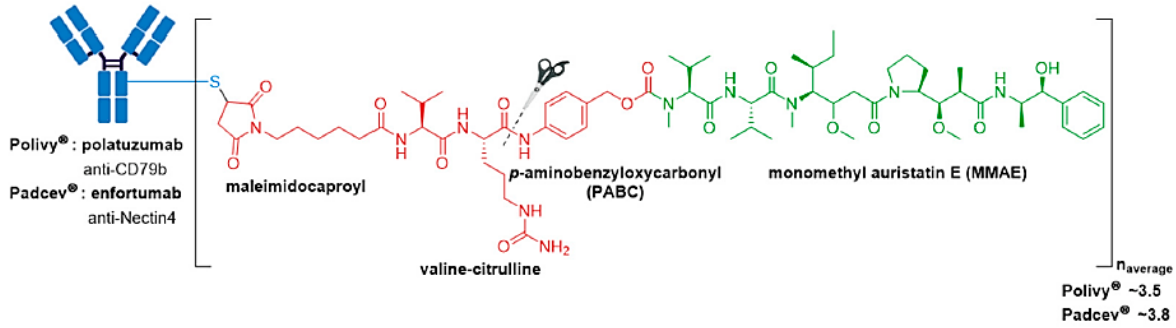

Figure 13- Polivy® and Padcev® [53]

Enhertu® (Figure 14) was first approved for treatment of patients with metastatic HER2 positive breast cancer and then in 2020-2021 for HER2-mutated non-small cell lung cancer (NSCLC) and for treatment of HER2 positive metastatic and advanced gastric or gastroesophageal cancer. [60,61]

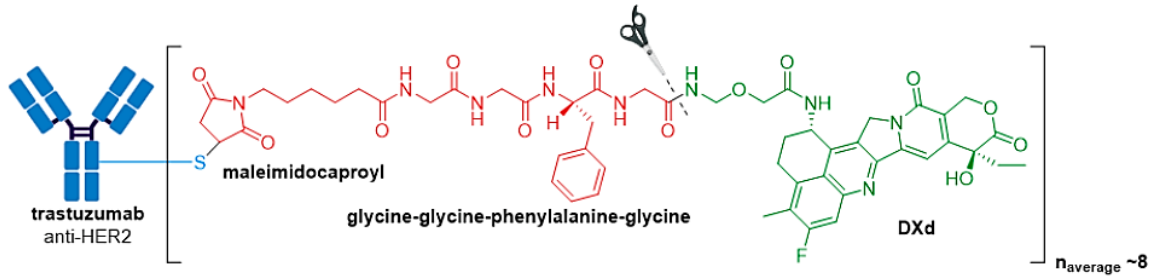

Figure 14- Enhertu® [53]

In 2020, Trodelvy® was approved for adults with metastatic triple-negative breast cancer (mTNBC) who have already received other two therapies. This ADC consists of a IgG1 (Sacituzumab Govitecan), an antineoplastic drug called SN-38 and a pH sensitive linker (Figure 15). [50] This ADC has generated a huge success, recording $137 million in 2020. [53]

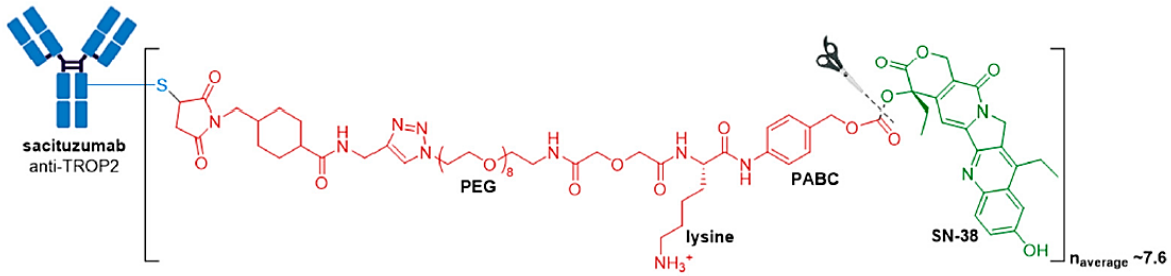

Figure 15- Trodelvy® [53]

Blenrep®, developed by GlaxoSmithKline and approved by FDA in 2020, is indicated for the treatment of relapsed or refractory multiple myeloma. It is composed of IgG1 Belantamab Mafodotin anti-BCMA connected to Auristatin MMAF through a non-cleavable maleimidocaproyl linker (Figure 16). This ADC along with Kadcyla®, is the only other FDA approved ADC with non-cleavable linker. [53]

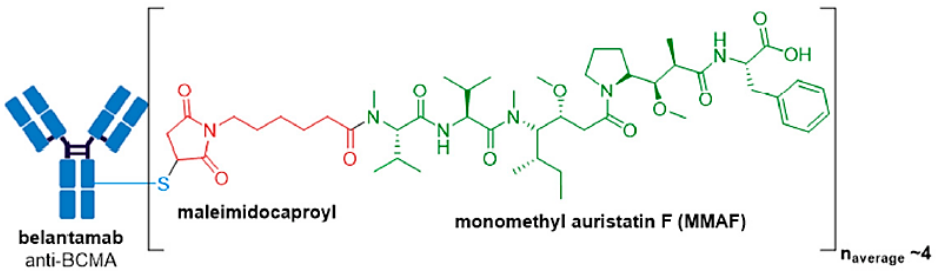

Figure 16- Blenrep® [53]

Zynlonta® (loncastuximab tesirine-lpyl) approved in 2021, is indicated for treatment of adult patients with relapsed or refractory large B-cell lymphoma after two or more systemic therapy, including diffuse large B-cell lymphoma (DLBCL). The IgG1 anti-CD19 (Loncastuximab Tesirine) charge a cleavable valine-alanine linked to a SG3249 PBD dimer (Figure 17). [50]

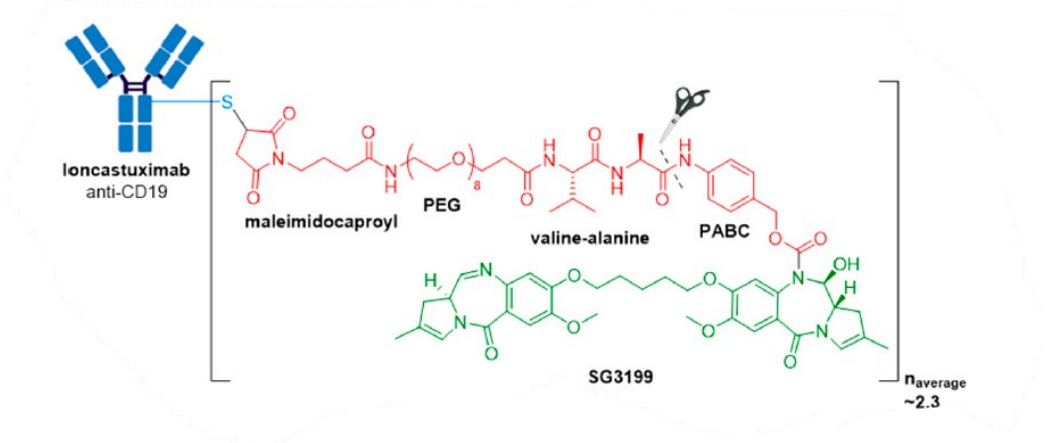

Figure 17- Zynlonta® [53]

The last ADC approved by FDA in 2021 is Tivdak® (Figure 18). It is a Tissue Factor (TF) directed ADC composed of a human anti-TF IgG1κ antibody conjugated to MMAE via protease-cleavable mc-vc-PABC linker (the same of Adcetris®, Polivy®, and Padcev®). [53] Tivdak® is used in clinic for recurrent or metastatic cervical cancer.

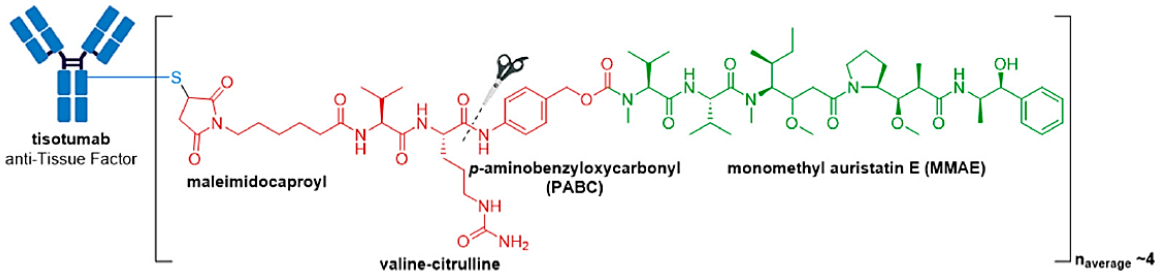

Figure 18- Tivdak® [53]

1.2.2 Antibodies and antigens

Target the right antigen with antibodies is one of the essential features for the development of ADCs. While antibodies found in humans are polyclonal, the antibodies used in clinic are usually monoclonal to allow a more targeted therapy. [13] The four main classes of mAbs used in clinic are:

- Murine;
- Chimeric;
- humanised;
- human.

Murine antibodies are 100% derived from mice. They were the first antibodies used in clinic but some issues such as high immunogenicity, poor efficacy in humans and short serum half-life led to a change from murine antibodies to chimeric antibodies. [62] Chimeric antibodies derived from 35% of mouse (variable regions) and 65% of human (constant regions) but suffer from the same immunogenicity problems of murine antibodies. [13] Nowadays, humanised (95% human with some synthetic or animal-derived domain on variable regions) and human antibodies are the first choice because, as we can see from ADC in the market, they show minimal immunogenicity and high affinity and specificity for antigens. [63] Among the main factors influencing the choice of mAb, probably the first is high target antigen specificity, because from this derive the success of the entire ADC or the appearance of side effects. [64] The IgG, in particular IgG1 subclass, are the most common in ADCs. In fact, if compared with IgG2 and IgG4, they have similar stability (21 days) but IgG1 antibodies are more effective in activation of immune response through its high affinity towards FcγRs. [15] The Fab regions of mAbs is responsible for the recognition and binding of antigens. Common types of antigens are glycoproteins, cell surface proteins and extracellular matrix proteins. [13] Besides the high expression on cells surface, the antigen should promote the internalisation of ADCs. In solid tumors, ADCs with high affinity for their antigens have a low penetration; [65] in this case a bystander effect can help the diffusion of drug. Other parameters to be noted are the distribution of cell surface antigens that have effect on the therapeutic window and, as the rate of internalisation varies for each tumor, high level of antigens do not always mean high effectiveness. [13,63,66] In addition, the mAb, through its Fc regions, promote an indirect cytotoxicity through the immune response as antibody dependent cell-mediated cytotoxicity (ADCC) and antibody dependent cell-mediated phagocytosis (ADCP), parameters to be considered in the development of ADCs. [29] Interesting, depending on the type of tumor, the activation of ADCC and ADCP can either

promote or reduce the activity of ADC. Another aspect to consider is the size of mAbs. Since they are the largest part of ADC, this means that the pharmacokinetic of the entire system mainly depends on antibodies.

1.2.3 Linkers

The design of the linkers is one of the most challenging parts in the development of ADCs. As we discussed before, the linker connects the payload with mAb. However, even if they seem only connectors, linkers have a great impact on ADC pharmacokinetic and pharmacodynamic properties and therapeutic window. [63]

The chemical structure of the linker must be balanced to avoid the premature release of the drug and therefore an off-target toxicity. We can divide it in three parts: one that binds the drugs, one is the spacer that can promotes the release of drugs and a chemical group that allows the bioconjugation with mAbs. The polarity of the linker is also an important factor because it's related to the aggregation of mAbs. Indeed, hydrophobic linkers promote the aggregation and affects the clearance of ADCs reducing their effectiveness. [67]

Furthermore, the linker also has an impact on the DAR of ADCs as it contains a chemical group for bioconjugations with mAbs. It is well known that high DAR can promote the aggregation of antibodies while a low DAR (usually <1) lead to a poor effect of ADCs. [68]

The release of the drug from the linker can be intracellular or extracellular depending on the design and the mechanism of action we want to achieve. Thus, the linker can also promote a by-stander effect by an extracellular cleavage allowing the diffusion of the drug in nearby cells (Figure 19). [69]

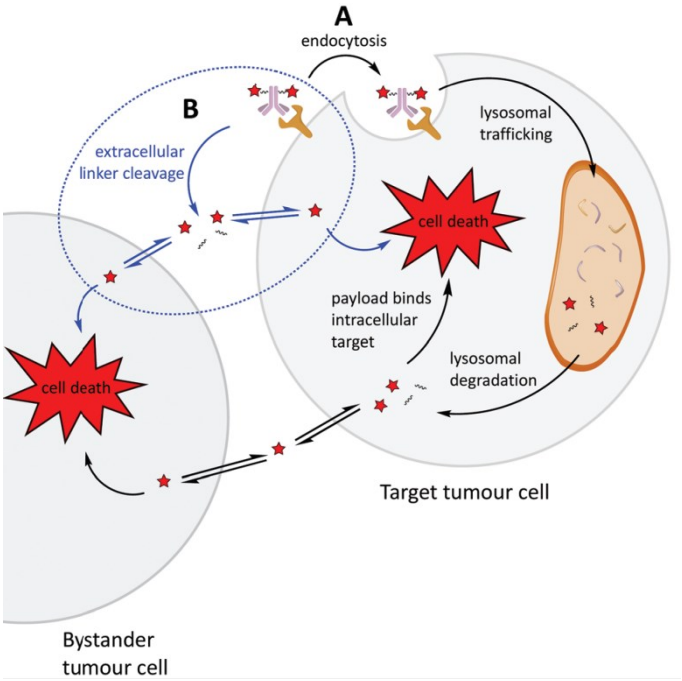

Figure 19- A) intracellular cleavage of the linker and B) extracellular cleavage of the linker. [69]

There are different categories of linkers but the classification is quite hard. A classical division is between "cleavable" linkers, that contain a specific group sensible at some *stimulus* in the tumor microenvironment, and "uncleavable" linkers, that require a complete degradation in lysosome to release the payload. We can also have a classification based on different external stimuli like chemically labile, enzymatic or metabolic sensitive linkers. To make clear the discussion on different type of linkers, in the following paragraphs there is a division between cleavable linker (that also contains chemically labile and enzymatic linkers) and non-cleavable linkers (also known as metabolic sensitive linkers).

1.2.3.1 Non-cleavable linkers

As we discussed above, non-cleavable linkers (or metabolic sensitive linkers) require a complete degradation in lysosome microenvironment for the release of the drug. [63] The main advantages of this kind of linkers are longer plasma half-lives and good stability at physiological pH leading a reduced off-target toxicity and wider therapeutic window. [70]
The most common non-cleavable linkers are based on a succinimide-thioether group, formed by a Michael reaction between maleimides and thiols such as succinimidyl-4-(N-

maleimidimethyl) cyclohexane-1-carboxylate (SMCC) and maleimido caproic acid (MC) (Figure 20).

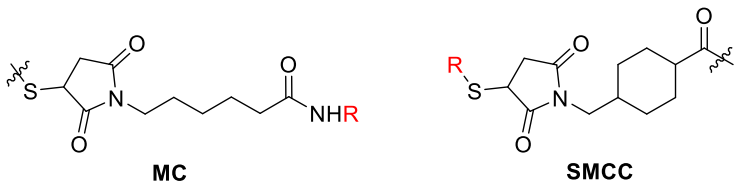

Figure 20- MC linker and SMCC linker; R = payload.

The exact mechanism of release is under investigation but the most accredited are based on the retro-Michael reaction of thiol ethers or the proteolytic degradation of mAb that release linker-payload system. [71]

These linkers can be found in ADCs in the market as trastuzumab emtansine (Kadcyla®, Figure 11) and Blenrep® (Figure 16). Interestingly, the cyclohexane ring in SMCC increases the steric hindrance and thus the stability of this linker. With non-cleavable linkers it is important to consider variances between parent drug and ADCs metabolites after lysosome digestion. For instance, after degradation the drug can be released attached with a charge amino acid derived from the antibodies affecting the pharmacokinetic properties of the original drug and limiting the bystander effect. [72]

In the development of maleimide linkers, we must consider that they are susceptible to hydrolysis even in physiological conditions. Therefore, these kinds of linkers can be hydrolysed leading to the more stable ring-opened derivates (Figure 21).

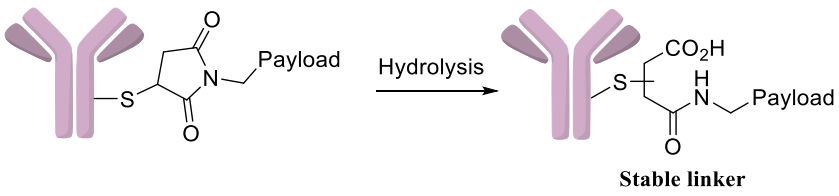

Figure 21- Ring opening of maleimide linkers.

As reported by Tumey et al., this hydrolyzed succinimide show equivalent cytotoxicity, improved in vitro stability, pharmacokinetic and efficacy as compared to their non hydrolyzed counterparts. [73] Following this trend, we can find several examples in literature of functionalized maleimides including *N*-aryl maleimides, beta amino maleimides and

acetal based maleimides that promote the hydrolysis of the ring and thus enhance the stability of the linker (Figure 22). [74]

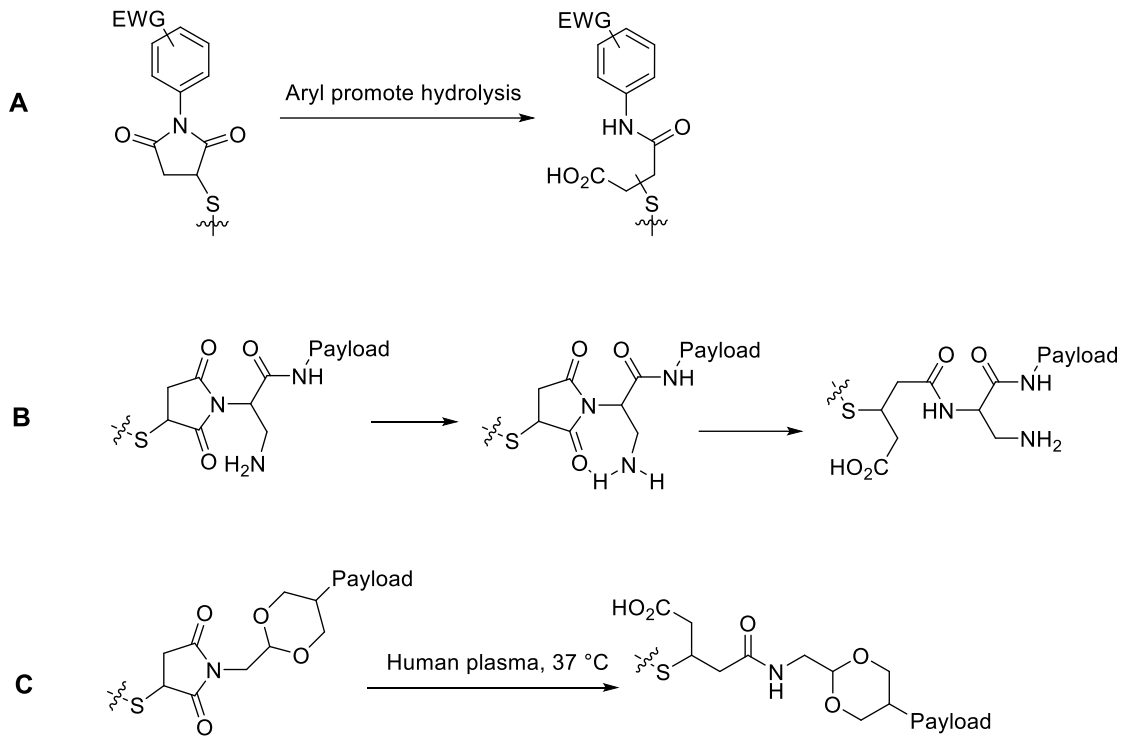

Figure 22- A: N-aryl maleimides; B: beta amino maleimides; C: acetal based maleimides.

1.2.3.2 Cleavable linkers

All linkers that are sensitive to external *stimuli* such as pH variations, enzymes or redox state belong to this category. In general, cleavable linkers are less stable than non-cleavable one but more versatile, increasing the range of applications. [69] However, some chemical modifications are possible with cleavable linkers in order to increase their stability and prevent the premature release of the drug. In the following paragraphs there are a description of the main categories of cleavable linkers:

- pH sensitive;
- enzymatic sensitive;
- reactive oxygen species (ROS) sensitive;
- reducible disulfide;
- biorthogonal and others.

1.2.3.2.1 pH sensitive linkers

This class is sensitive to the different pH between extracellular and intracellular environments, in particular in endosomes (pH 5.5-6.2) and lysosomes (pH 4.5-5). Subclasses of pH sensitive linkers are hydrazone, oximes, maleic acid derivative, acetal and orthoester.

HYDRAZONE AND OXIMES

Examples of hydrazone linkers can be found in Mylotarg® and Besponsa®. These are stable under physiological conditions (pH 7.4) but readily release the drug at pH 4.5. In addition, analysis *in vivo* on stability of Besponsa® showed that only 1.5-2% per day of hydrolysis occurred. [75]

The explanation for the stability of hydrazones or oximes involved the resonance structures of these compounds (Figure 23). [76]

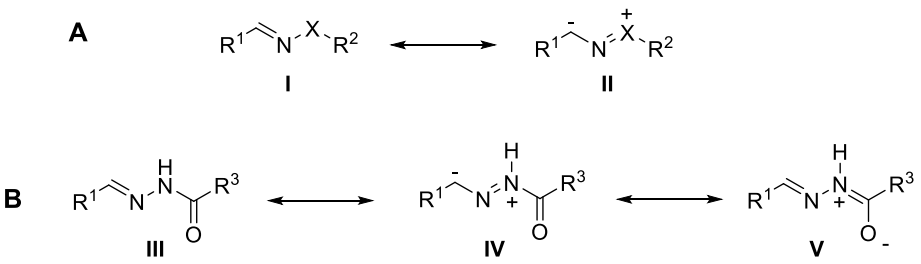

Figure 23- Possible explanation of stability of hydrazone (A) and acylhydrazones (B) through electron delocalization. X= N hydrazone; X= O oxime.

Structure II and IV (Figure 23) contain a negative charge on carbon, reducing its electrophilicity and thus a possible attack of water. In acidic conditions, the situation is quite different because, as it is also demonstrated by NMR studies, a protonation on N occurs. [76] Therefore, the carbon centre becomes more electrophilic and susceptible to water attack (Figure 24).

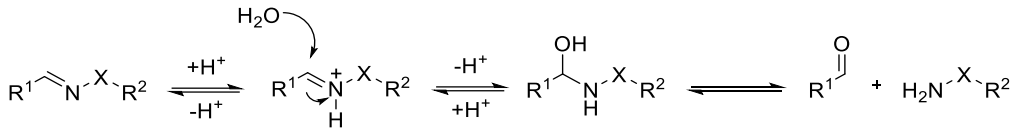

Figure 24- hydrolysis of hydrazone or oxime. X= N hydrazone; X= O oxime.

From the mechanism discussed above, we notice that an important parameter in hydrazone/oxime linker is a good balance between the resistance to hydrolysis at physiological pH and lability in acidic conditions. Acyl hydrazone are amongst the best group leading a more versatile choice for ADCs as in the case of Mylotarg® and Besponsa®. The major issue of this kind of linker concerns acidic conditions that are also present in other body compartments besides lysosomes, increasing the likelihood of side effects.

MALEIC ACID DERIVATIVE, CARBONATES, SILYL ETHER AND PHOSPHORAMIDE

Maleic acid linkers promote the release of payload through cyclization of di-substituted maleamic acid (Figure 25).

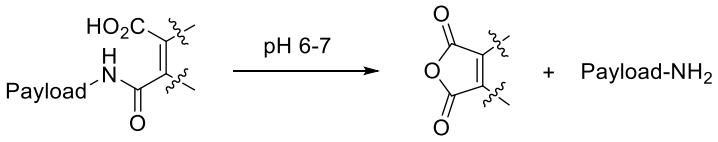

Figure 25- Release of the drug promoted by cyclization.

The cyclization requires a pH 6-7 that is the extracellular pH in some types of tumors. [77] In 2017, Zhang et al. tried to explain the mechanism of cyclization even if different pathways are possible. [78] The interesting thing is that these maleic acid derivatives act as prodrug; at pH 7.4 they are unreactive (maleimide form) but at pH 6-7 they can release the drug (Figure 26).

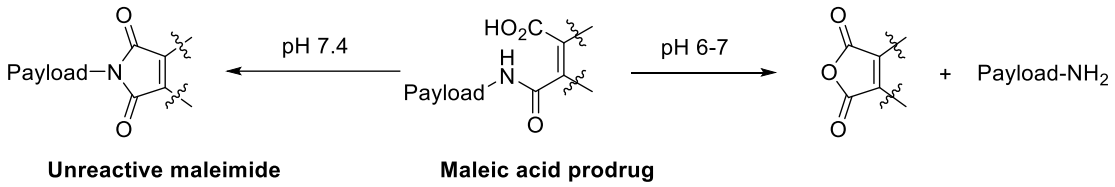

Figure 26- Behaviour of maleic acid at different pH.

As the release is in an extracellular environment, the drug must have the ability to pass the plasmatic membrane. Also in this case, a bystander effect can take place with possible application of this linker in solid tumors.

Other kind of pH sensitive linkers are carbonates, silyl ethers and phosphoramide (Figure 27):

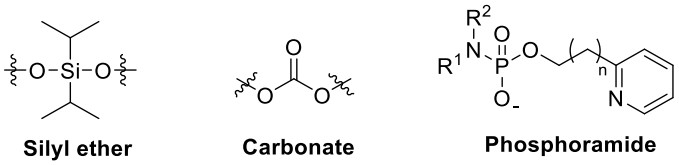

Figure 27- Silyl ether, carbonate and phosphoramide linkers.

Carbonate is used in ADC Trodelvy®, while silyl ether is recently developed proving a long half-life in plasma (> 7 days). [79] Silyl ethers can be used in combination with self-immolative spacer *p*-hydroxybenzyl (PHB) as reported by Wang et al. in their work (Figure 28).[79]

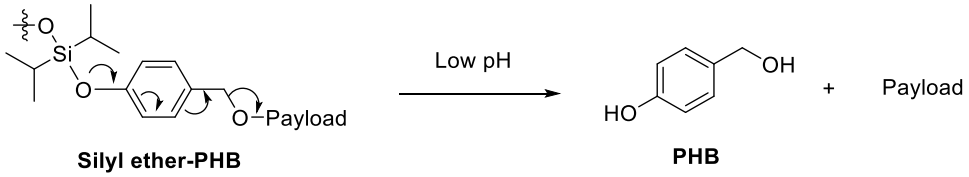

Figure 28- Release mechanism of silyl ethers.

Phosphoramides rely on pKa of pyridine which is lower than physiological pH resulting in unprotonated form at pH 7.4. In acidic conditions a protonation of nitrogen of pyridine occurs with the formation of eight or nine ring with the oxygen of phosphoramide in the

transition state. This intermediate is readily hydrolysed by water with the release of the drug (Figure 29). [80]

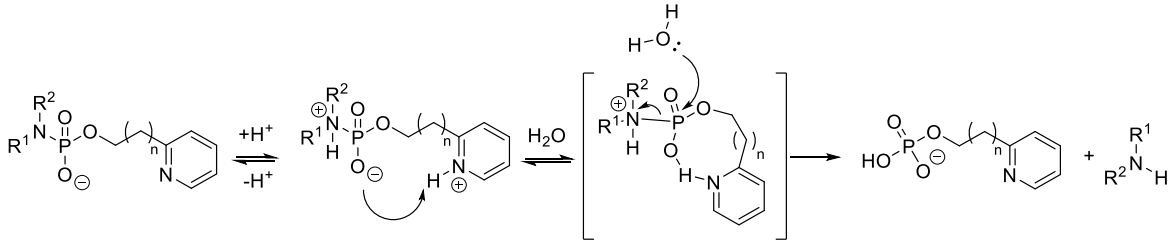

Figure 29- Release mechanism of phosphoramide.

ACETAL AND ORTHOESTER LINKERS

Acetal is an acid-labile group often used in organic chemistry as a protecting group. Thus, this instability at lower pH can be used to design pH sensitive linkers. In 2007, Kong et al. described for the first time *N*-ethoxybenzylimidazoles (NEBIs) as possible linkers for drug delivery. [81] NEBI linkers are able to release the payload almost 10 time faster in mildly acidic conditions (pH 6.4-6.9) compared to physiological pH 7.4, extending the effect even at lower pH (4.5-5.5). [81] The possible mechanism of release is shown in Figure 30.

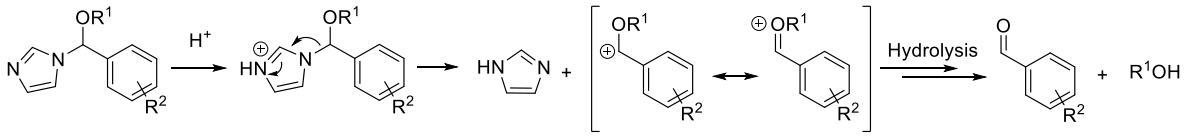

Figure 30- Hydrolysis of NEBIs in acidic conditions.

Later, Wagner et al. tried some modifications on benzaldehyde obtaining different derivatives with different $t_{1/2}$ in terms of time of hydrolysis. [82] The same research group designed a Spiro-Di-Orthoester linker (SpiDO) linker and compared its release profile with acylalkylhydrazone linker and non-hydrolysable linker. [83] As reported from the work, SpiDO platform (Figure 31) proved to be more sensitive in mild acidic conditions than the other linkers.

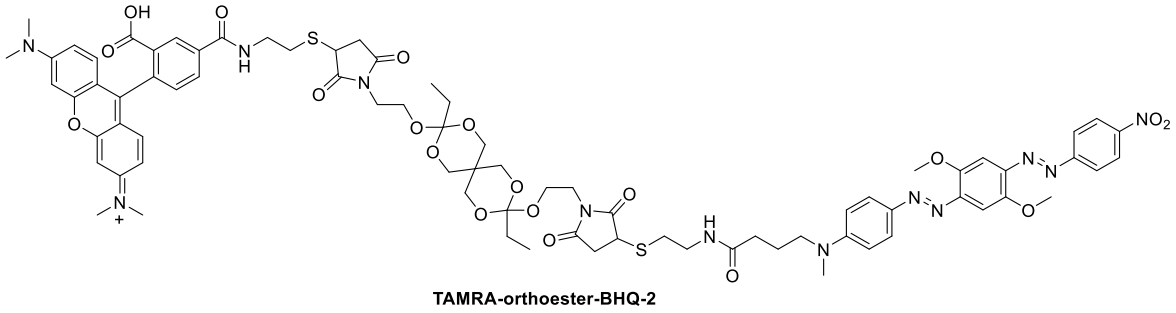

Figure 31- SpiDO platform

In general, for cyclic and acyclic acetals, the more is the degree of substitution on central carbon the faster is the hydrolysis. [84] This can be explain if we consider the carbocation formed during the hydrolysis of acetals which is more stable with more alkyl or alkoxy group.

1.2.3.2.2 Reducible disulfide

Disulfide along with hydrazones are the most prominent class found in ADCs. This kind of linker can be found in Mylotarg® and Besponsa®. Disulfides are stable at physiological pH but are more susceptible to nucleophilic attack from thiols. In humans, glutathione (GSH) can reduce the disulfide and, as tumor cells contain high concentrations of GSH, this strategy can be used for the selective release of the drug. [85] In addition, the oxidative stress generated by tumors often lead to elevated GSH levels. Besides GSH, other enzymes like disulfide isomerase may also promote disulfide reduction. [69] Even if there is a difference in GSH concentration between the blood plasma and cytoplasm (~5 mmol/L in blood plasma versus 1-10 mmol/L in cytoplasm), the present disulfide linkers still have some problems about stability and premature release of drug. Thomas et al. reported an example of disulfide linker attached to engineering cysteines through THIOMAB mAbs. [86] In this way, there is a protection of disulfide bond mediated by a steric hindrance from the mAb and thus an improvement in half-life of ADCs. In a similar way to hydrazones, the stability of disulfide can increase by adding a substituent near the sulfur atom. The combination of disulfide with carbamate as immolative spacer is also possible as described by researchers in Genentech in their work on pyrrolobenzodiazepine (PBD)-dimer (Figure 32). [87]

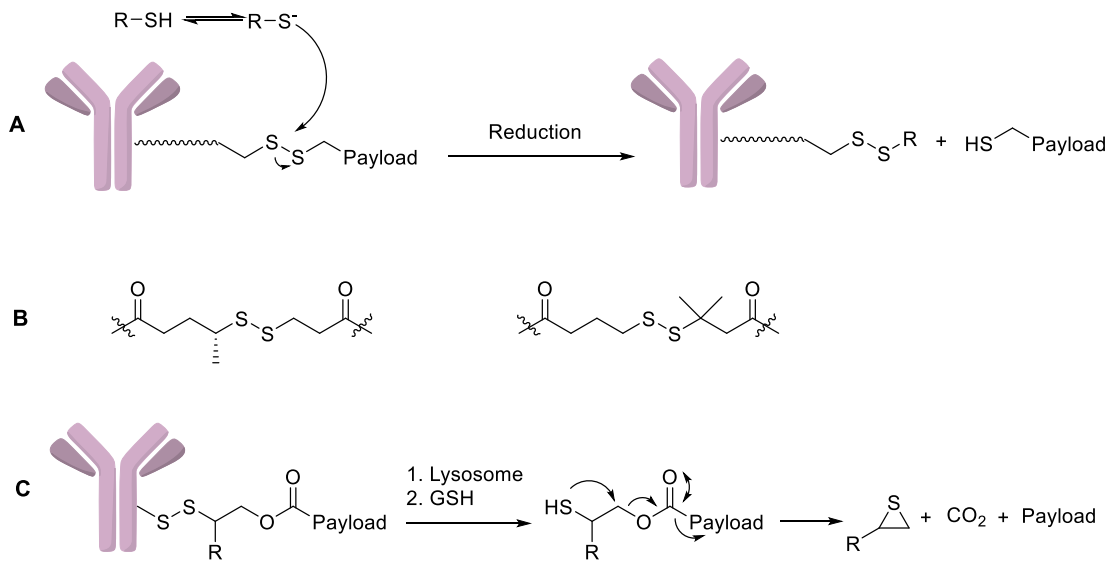

Figure 32- A) Reduction of disulfide bond; B) Examples of steric hindrance near the sulfur atoms C) Disulfide associated with carbamate immolative spacer.

ADCs with cleavable disulfide linkers can also follow the extracellular mechanism beside the traditional one. Neri et al. have demonstrated the extracellular reduction of this linker using a tumor vasculature-targeting antibody. [88] The release of the payload is due to the high concentrations of reductants released from the dying cells. Moreover, as the cells die, a growing concentration of reductant is released leading to a "chain reaction" in which the effect of ADC is broadened.

1.2.3.2.3 Enzymatic sensitive linkers

The enzymatic linkers are very attractive in the field of ADCs as they combine good stability with selective cleavability in intracellular environment. This class of linkers include protease, glycosidase (β-Glucuronidase and β-Galactosidase), phosphatase and sulfatase sensitive linkers.

PROTEASE SENSITIVE LINKERS

Nowadays, the most protease cleavable linkers are composed of dipeptides as we see from the approved brentuximab vedotin (Adcetris®). Indeed, tetrapeptides like Gly-Phe-Leu-Gly and Ala-Leu-Ala-Leu are not suitable for ADCs due to their slow release kinetics and

complexity. [69] Cathepsin B is an enzyme located mainly in lysosomes and overexpressed in a wide range of cancers. Thus, this protease is often targeted in the development of dipeptide linkers. Several combinations are possible even if Val-Cit and Val-Ala seems to be the best choice. [89] Dipeptides are usually associated with a *p*-aminobenzyl alcohols (PABA) self-immolative spacer which promotes the 1,6-elimination mechanism with the release of the payload (Figure 33).

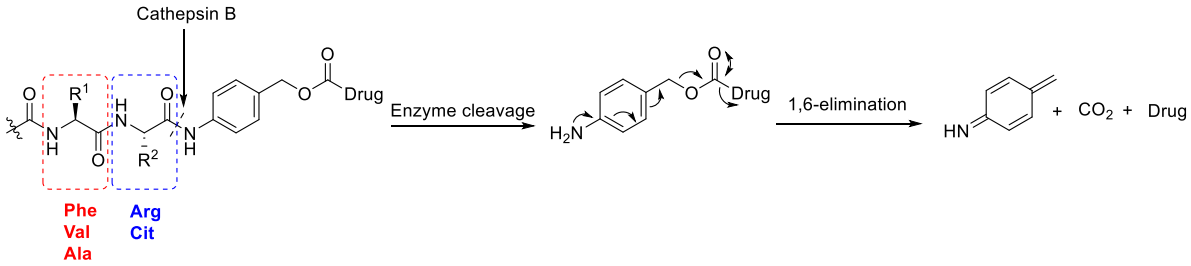

Figure 33- Various combinations of dipeptide linkers and 1,6-elimination promoted by PABA.

Cathepsin B, through its carboxypeptidase activity, recognized and cleaved peptide-spacer bonds. The role of the self-immolative spacer is not only related to the release mechanism but it also provides less steric hindrance near the peptides. For example, first studies on dipeptides charged with Doxorubicine showed that due to the steric bulk of the payload, a spacer was required for enzymatic activity. [89]

Val-Cit sequence (Figure 34) has been well studied in mice; the plasma instability of Val-Cit does not appear to be correlated directly with Cathepsin B but rather with other enzymes. [90] Furthermore the premature release of the drug is highly dependent from the conjugation site. Later, in 2016, Dorywalska et al. identify the responsible of Val-Cit hydrolysis in mouse plasma, turning out to be a carboxyesterase 1C (Ces1C). [91] In the same paper, they reported a series of modifications on Val-Cit to improve the stability without affecting the effect of Cathepsin B. Moreover, some tripeptides, particularly Glu-Val-Cit, are effective to reduce the effects of Ces1C and improve the stability of ADC. [92]

Although the Cathepsin B is the most known as protease enzymes for ADCs, incubation studies on isolated enzyme showed that also Cathepsin S seems to be more active towards Val-Cit motif. [93]

Val-Ala (Figure 34) has also emerged as protease sensitive linker. Compared to Val-Cit, it has a longer half-live and lower aggregation without negative influence on potency, toxicity and efficacy. [94]

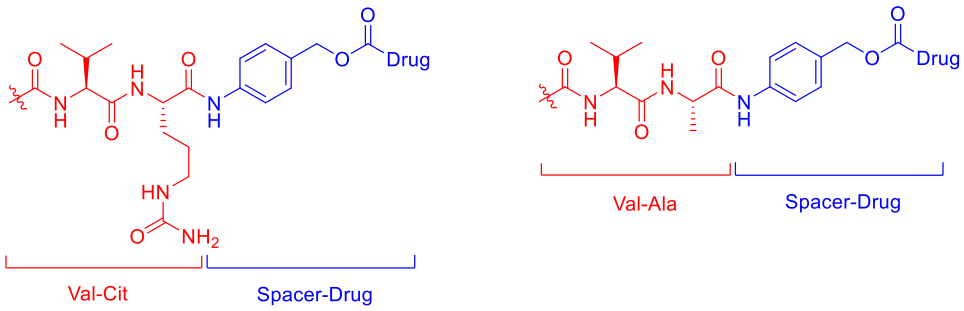

Figure 34- Val-Cit and Val-Ala dipeptides.

The lower aggregation is due to the less hydrophobicity of Val-Ala; thus, this dipeptide can be used with more hydrophobic payload such as MMAE and PBD-dimers. [94,95]

Although peptide-sensitive linkers are known as internalising dipeptides, some papers also show the use of Val-Cit-PABA for an extracellular release. In particular, Neri et al. developed a series of linkers to explore possible applications in some tumors targeting the extracellular space. [96,97]

GLYCOSIDASE CLEAVABLE LINKERS

β-Glucuronidase and β-Galactosidase sensitive linkers belong to this class, and both are cleaved by lysosomal enzymes. Usually, they are associated with self-immolative spacers PABA. β-Glucuronidase linkers (Figure 35) was first applied in 2006 when was seen that also charged a high amount of payload per antibody (DAR > 8) there was no aggregation of ADCs. [98] Interesting, comparative studies with Val-Cit using camptothecin analogues as payloads, show a very low aggregation in the case of β-Glucuronidase linkers even if the maximum tolerated dose (MTD) remains lower. [99]

β-Galactosidase sensitive linkers (Figure 35) are more recently developed. [100] They are very similar to β-Glucuronidase linkers but are substrate of β-Galactosidase overexpressed in certain tumors.

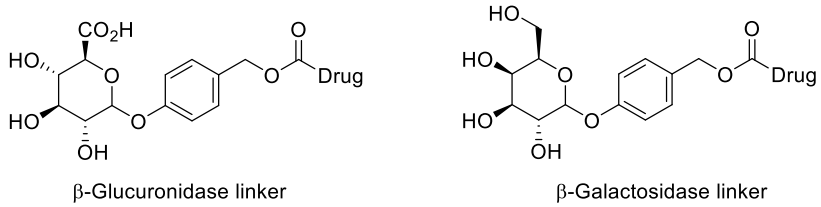

Figure 35- Glycosidase cleavable linkers

The strength of these linkers lies in their high hydrophilicity; therefore, this suggests possible applications when a very hydrophobic payload is used.

PHOSPHATASE CLEAVABLE LINKERS

Phosphate and pyrophosphate are cleavable linkers that, after proteolysis, release the drug with an alcohol moiety (Figure 36).

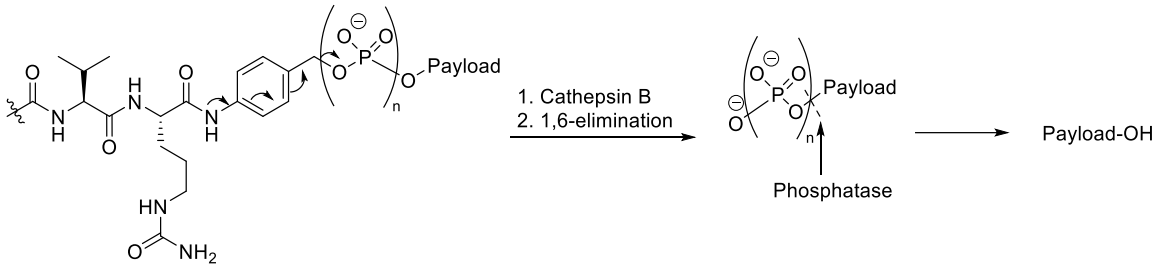

Figure 36- Release mechanism of phosphate linkers.

Usually, these linkers are used in combination with dipeptide-PABA spacer, where the payload is released after a sort of "cascade effect" started by Cathepsin B. Even if acid phosphatase and pyrophosphatase are thought to be the enzymes responsible for the cleavage of linkers, the mechanism remains to be proven. [69] Phosphatase sensitive linkers seems to be effective with hydrophobic payload with -OH moiety for conjugation as some glucocorticoids. [101]

SULFATASE CLEAVABLE LINKERS

Sulfatase sensitive linkers (Figure 37) was recently discovered by Bargh et al. in 2020. [102] Sulfatase is similar to β-Galactosidase, and it can be overexpressed in certain tumors. Sulfatase sensitive linkers prove to be highly stable in plasma (>7 days) and readily hydrolysed in presence of the enzyme ($t_{1/2}$ = 24 min.). [103]

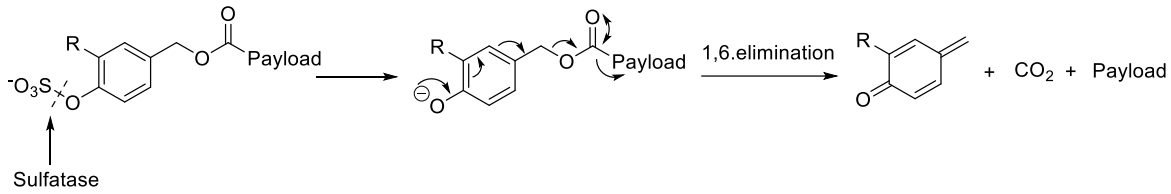

Figure 37- Release of payload from sulfatase sensitive linkers. R= H, NO_2.

The release mechanism is like other enzyme sensitive linkers; R can be a hydrogen or -NO_2 group which increase the activity of sulfatase towards electron-poor arylsulfates (Figure 37). Moreover, compared with the in vitro cytotoxicity of non-cleavable ADCs and Val-Ala containing ADCs, sulfatase-linkers result in higher cytotoxicity and a superior selectivity of the bioconjugate in HER2+ cells. [103]

1.2.3.2.4 Reactive oxygen species (ROS) sensitive

Reactive oxygen species (ROS) are generated during mitochondrial oxidative metabolism or in response to some alterations in cell metabolism such as cancer, inflammation or infections. ROS consist of superoxide anion (O^{2-}), hydrogen peroxide (H_2O_2), and hydroxyl radical (·OH); [104] when the level of ROS exceeds there is an oxidative stress which is typical of the pathologies described above providing a possible target in therapy. The oxidative environment leads to a modification of redox-reactive cysteine residues changing the structure and thus the function of some proteins. [104] Targeted ROS, these linkers are based on structures containing thioether, arylboronic acid, selenide/telluride, thioketal, aminoacrylate, oligoproline, peroxalate ester and mesoporous silicon. [105,106] The detailed description of all these linkers is beyond the scope of this thesis but a brief discussion of the most important, such as arylboronic acids and tioketals, is given below.

ARYLBORONIC ACID AND BORONATE ESTER

Boronic acids and boronate ester has been used as prodrugs in 5-FU, SAHA, SN-38, nitrogen mustard and NO donors. [107] The classic example is 5-FU which is used as anticancer drug but suffer from many side effects like myelosuppression and gastrointestinal e neurocentral toxicity. [108,109] Therefore, Xue et al. developed a prodrug of 5-FU based on boronic ester which avoids the metabolic degradation by dihydropyrimidine dehydrogenase (DPD) at N1

and thus enhances the stability. [110] Upon exposure to H_2O_2 the arylboronate group was hydrolysed releasing the active drug. Another example is a prodrug of SN-38, a chemotherapeutic drug derived from camptothecin (Figure 38) showed effective antitumor activity in a mouse model of metastatic lung disease. [111]

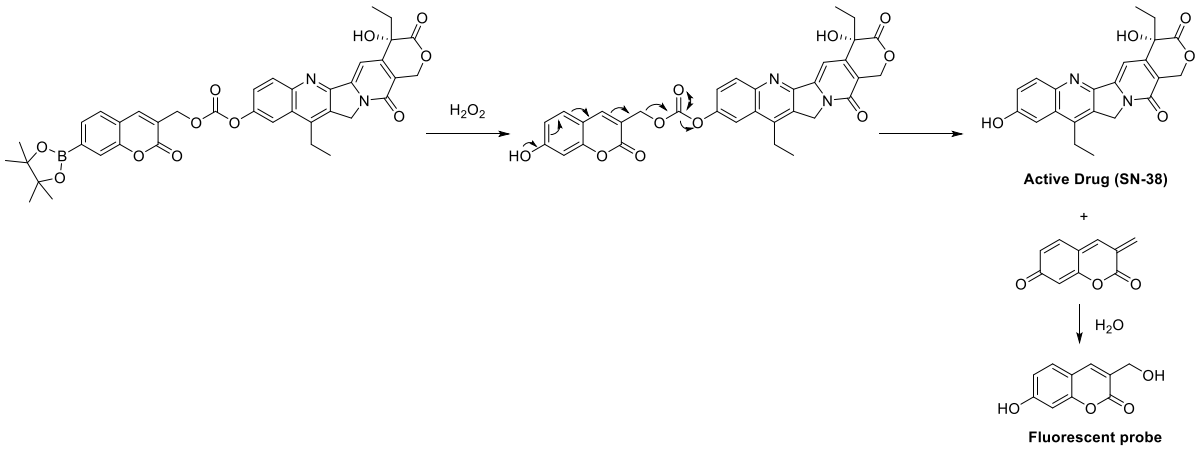

Figure 38- Prodrug of SN-38.

SN-38 release from prodrug was investigated by monitoring fluorescence after addition of H_2O_2 to the cancer cells. Anyway, the boric acid and ester side-products formed from the release mechanism are known to be well tolerated in humans. [108]

All these examples are prodrugs, but the release mechanism suggest a possible application also in drug delivery system.

THIOKETAL AND THIOETER LINKERS

Thioketals can be cleaved by ROS species releasing thiol and acetone (Figure 39). [112]

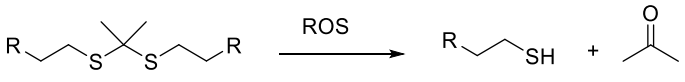

Figure 39- Hydrolysis of thioketal.

Using this linker, in 2012 Xia et al. developed a thioketal polymeric system with a possible application in prostate cancer. [113] Moreover, they studied the kinetic profile of the linker and

found a very slow degradation in presence of ROS. Thus, there must be other factors that induce an extra release of ROS. This was clear when Wang et al. synthesized nanoparticles in which polyphosphoric ester (PPE) was bind to Doxorubicine through thioketal linker. [114] The system was embedded with chlorin e6 (Ce6 is a photosensitizer sensible to red light) and they discovered that irradiation could generate an extra amount of ROS which promote an increased release of the drug if compared to the system without Ce6.

As we can see from the examples reported in literature, thioketals are stable under physiological conditions releasing the drug only after activation by ROS. However, the poor kinetics profile limits its use as linker in ADCs.

Regarding thioethers, they could be converted to a more hydrophilic sulfoxide or sulfones by ROS oxidation releasing the active drug. [115] The example based on thioethers can be found in the work of Zhu et al. in which they reported H_2O_2 sensitive polymeric micelles. [116] In that case, the thioether linker connect SN-38 (as cytotoxic drug) with an hyperbranched polyglycerol (HPG). Moreover, cinnamaldehyde (CA), that induces apoptotic cell death via ROS production, was encapsulated in the core; as CA was release from the micelles, the amount of ROS increased leading to the release of SN-38. [116]

As well as thioketals and arylboronic acids, thioethers found in literature are mainly prodrugs and for ADC applications they need further modification to allow the bioconjugation with antibodies.

1.2.3.2.5 Bioorthogonal and other linkers

Bioorthogonal chemistry refers to a chemical reaction that occurs in the body, without interfering with normal biological processes. [103] Indeed, the classical linker-drug conjugates technique still suffers from some properties of ADCs such as the number of receptors on cell surface, DAR and the stability of the system. Bioorthogonal chemistry can overcome these problems through the synthesis of "inactivate system" (or prodrugs) which, relying on biomolecular click reaction, is readily activated to release the active drug. Among the different strategies, click chemistry between the trans-cyclooctene (TCO) and azide or tetrazine have been developed (Figure 40). [117,118]

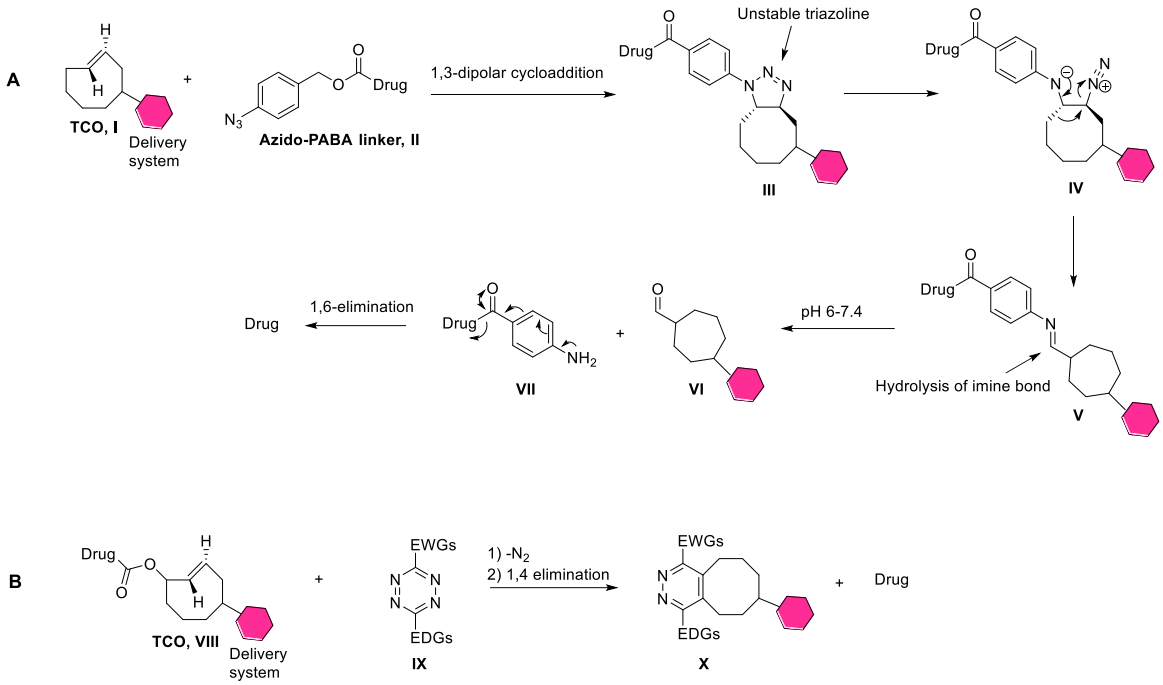

Figure 40- A) Click chemistry and release mechanism of TCO-azide linker; B) Click and release mechanism of TCO-tetrazine.

In the example A (Figure 40), 1,3-dipolar cycloaddition leads to an unstable triazoline (IV) that releases N_2 forming an imine (V); further hydrolysis gives the corresponding aldehyde (VI) and promote 1,6-elimination of self-immolative spacer (VII) for the release of the drug. [118] However, this release mechanism is not demonstrated *in vivo* until now. In the example B, cycloaddition of TCO (VIII) with tetrazine (IX) leads product X and the release of drug after 1,4-elimination mechanism. [117] As the presence of electron withdrawing groups (EWGs) accelerate cycloaddition step and electron donating groups (EDGs) are essential in the elimination step, the insertion of EWGs in position 3 and EDGs in position 6 of tetrazine can increase the rate of the cycloaddition-elimination step thus favouring the release of drug. [119] In this case, the click and release mechanism were demonstrated in vitro and in tumor-bearing mice by Rossin et al. in their experiment using Doxorubicine as a drug. [120] The design and development of biorthogonal linkers can be useful in non-internalized ADC, where a bystander effect is sought.

Other kinds of linkers are Fe (II) cleavable linkers and photosensitive cleavable linkers. In 2018, Spangler et al. reported a trioxolane scaffold as Fe (II) sensitive moiety for ADCs. [121] This linker relying on elevated levels of unbound ferrous iron in cancer cells and in the tumor microenvironment; after the activation mediated by Fe (II) a β-elimination occurs for the release of payload (Figure 41).

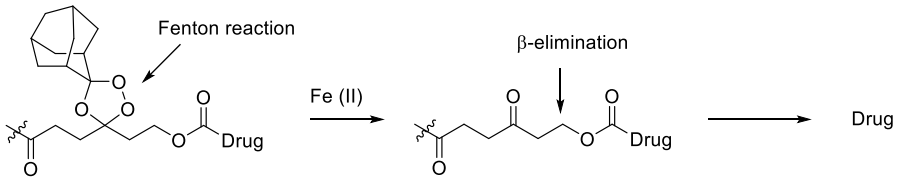

Figure 41- Release mechanism promoted by Fe (II).

Interestingly, this linker showed a comparable effect to Val-Cit linker in vitro studies even if a significant instability of ADC was found; they explain a possible interaction between the adamantane moiety and the nearby sites of antibody. [121]

Photosensitive linkers represent an emerging strategy for the controlled release of drugs. Recently, Zhou et al. discovered novel ADCs with UV-controlled cleavage mechanisms (Figure 42). [122]

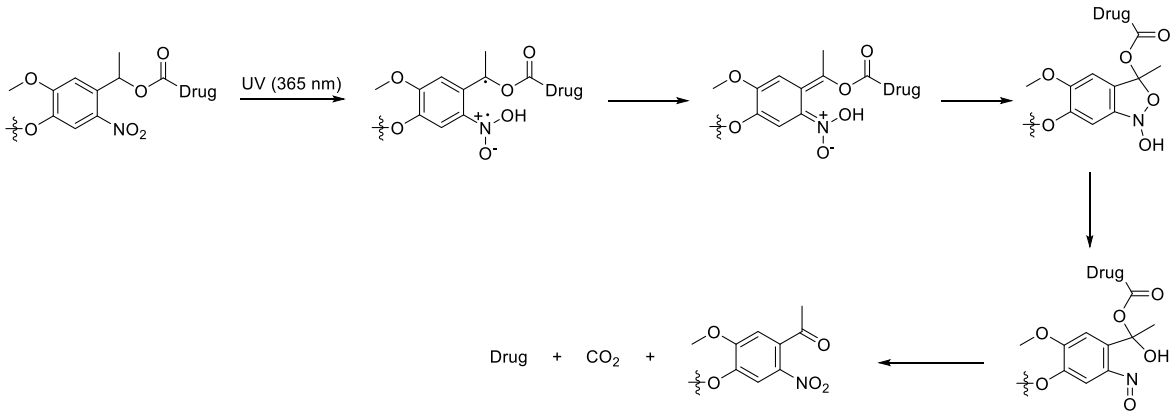

Figure 42- Photo-sensitive linker activated by UV irradiation.

This linker is stable under natural light (<1% of free payload detected after 6 days) but readily release the payload upon irradiation at 365 nm. [122] However, there are still some problems in development of these ADC due to the toxicity of high dosage of UV irradiations such as oxidative stress, photoaging and immunosuppression. [123,124]

1.2.3.3 Self-immolative spacer

Self-immolative spacers can be considered a part of linker that promote the release of the payload upon an appropriate stimulus. As we see from the previous chapters, a lot of ADCs

include a self-immolative spacer in their structure stressing the importance of the controlled release of drugs. These spacers rely on a protecting group (PG) which after modification (by specific stimulus) leads to a series of rearrangement with the release of the payload. In particular, two kinds of rearrangement are described:

- self-immolation by electronic cascade leads to 1,4-, 1,6-, 1,8- elimination;
- self-immolation by cyclization. [125]

In both cases, the protecting group masks the nucleophilicity of the heteroatom avoiding the self-immolative process that occurs only after a specific activation.

1,4-, 1,6-, 1,8- ELIMINATION

These spacers are composed of an aromatic ring bearing both the protecting group and the leaving group in specific positions. The electronic cascade starts when the protecting group is removed revealing the intrinsic nucleophilicity of the amino, hydroxy, or thiol group. The external *stimuli* can be varied and include chemical reagents, enzymes, or light. [126] The elimination process involves the formation of a quinone or azaquinone methide intermediate beyond the drug (Figure 43).

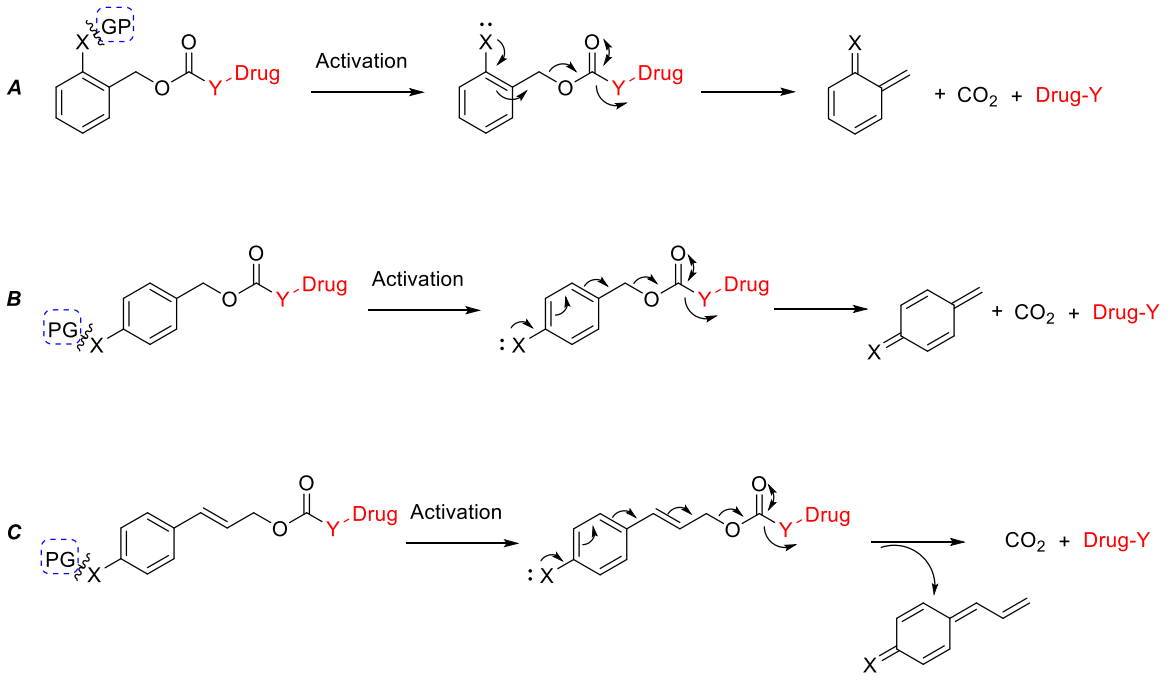

Figure 43- Self-immolative process by electronic cascade. A) 1,4-elimination; B) 1,6-elimination; C) 1,8-elimination. X= NH, O, S; Y= NH, NR, O; PG= protecting group.

Usually, these spacers include a carbamate or carbonate moiety, thus the liberation of CO_2 (increase in entropy) pushes the reaction towards the elimination. Moreover, the presence of EDGs on the aromatic ring seems to increase the rate of the self-immolative process due to stabilization of the transient state. [127,128] It is worth noting that spacers based on naphthalene or biphenyl rings don't give the elimination maybe due to the high energy barrier to break the aromaticity. [125]

One of the most important spacers is PABA-like based on 1,6-elimination mechanism. This is widely used in the development of ADCs especially with amine containing drugs that are bound to the spacer through a stable carbamate. Indeed, with alcohols the leaving group becomes a carbonate which is less stable in physiological conditions; an alternative strategy involves the use of phenols more stable at pH 7.4. [129,130] Different kinds of leaving group can be tertiary and heteroaryl amines. In this case they are included in the linker through the formation of quaternary ammonium salt; this approach generates a charged linker that increases the solubility of ADC and potentially reduces antibody aggregation. [131]

SELF-IMMOLATION BY CYCLIZATION

For the release of the payload, these spacers required the cyclization process leading to 5- or 6- member rings with the release of free drug (Figure 44).

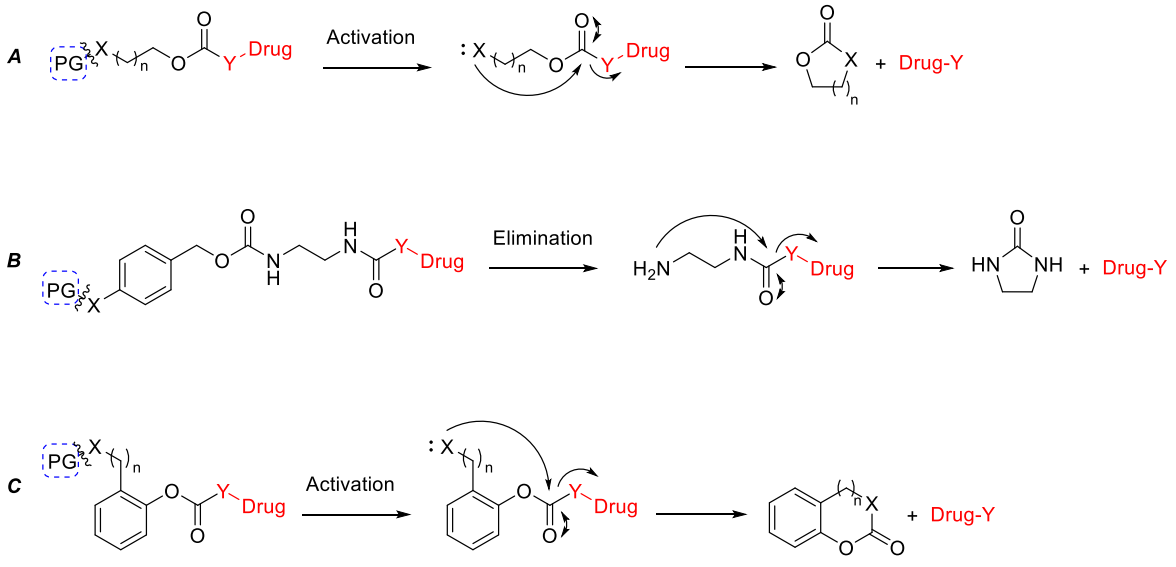

Figure 44- Self-immolative process by cyclization. X= O, -NH; -NMe, S; Y= -NH, -NR, O; PG= protecting group.

The cyclization is promoted by the nucleophilic attack of amines, alcohols or thiols on carbonyl group. The entire process relying on the formation of 5- or 6- member ring that are thermodynamically favoured. [132] If compared to the electronic rearrangement, the cyclization is slower and the kinetics depends on the conformational aspects (Thorpe-Ingold effect) and the electrophilicity/nucleophilicity of the group involved in the cyclization. [133,134] Sometimes, a spacer based on cyclization and the other based on 1,6 elimination (PABA-like) are combined; the resulting linker can be easily triggered leading to faster release of the payload.

One of the most important parameters for linkers/spacers is polarity. Although some cleavable linkers such as dipeptides or glycosides are polar enough, others need modifications to avoid the aggregation of antibodies and thus a fast clearance of ADCs. [67] Among the different strategies, we can find the insertion of PEG chain or charged groups as sulfonate or pyrophosphate ester. [68,101,135] In addition, the linkers and thus the mechanism of release must take into account the properties of the chosen payload.

1.2.4 Payloads

At first glance it may seem that all drugs that lead to cell death are suitable for ADCs. Unfortunately, only a few with specific properties can be charged on ADCs. Among the key factors there are high potency (IC_{50} in subnanomolar or picomolar range) [63] and chemical groups that allow the conjugation with the linker. But we also have some other aspects to consider:

- a limited amount of drug that can be charged on mAb (DAR);
- after administration, less than 0.01% of an injected dose of ADC actually binds to the tumor cells; [136]
- many cytotoxic drugs are hydrophobic and induce the antibody aggregation.

It is clear that all these features lead to some specific classes of molecules: auristatins, maytansinoids, tubulysins, calicheamicins, camptothecin analogues, pyrrolobenzodiazepines, duocarmycines and doxorubicin. Although auristatins and maytansinoids represent the majority of payloads used in ADCs, other kinds of warheads with different mechanisms of action have been explored in recent years.

AURISTATINS

Auristatins are widely used as payload in ADCs. [137] The most important drugs of this class are monomethyl auristatin E (MMAE) and monomethyl auristatin F (MMAF) both synthetic analogues of dolastatin 10 (Figure 45).

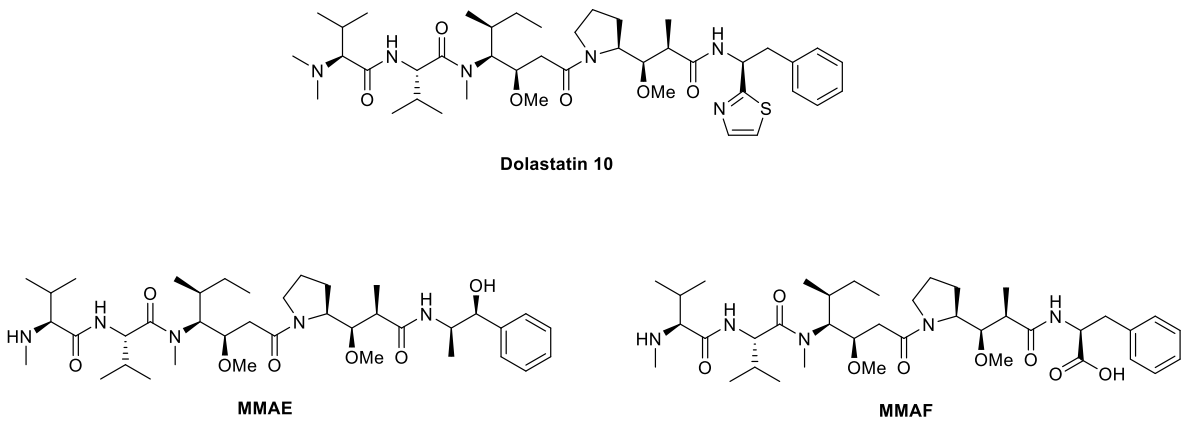

Figure 45- Dolastatin 10 and synthetic derivatives MMAE and MMAF.

Auristatins bind at the tubulin vinca alkaloid binding domain leading to metaphase cells cycle arrest.[138] The insertion of alcohol group in MMAE, the carboxylic group in MMAF and the presence of secondary amine in both compounds enhance the hydrophilicity of these molecules to give a better pharmacokinetic profile than dolastatin 10. Moreover, MMAF is less able to cross cell membranes (due to the carboxylic acid) but it has a lesser tendency to aggregate and shows lower systemic toxicity than MMAE. [139] Examples of ADCs charged with MMAE are Adcetris® (Figure 10) and Polivy® or Padcev® (Figure 13).

MAYTANSINOIDS

DM1 and DM4 (Figure 46) are derived from maytansine, a natural benzoansamacrolide isolated from the bark of the African shrub *Maytenus ovatus*. [56]

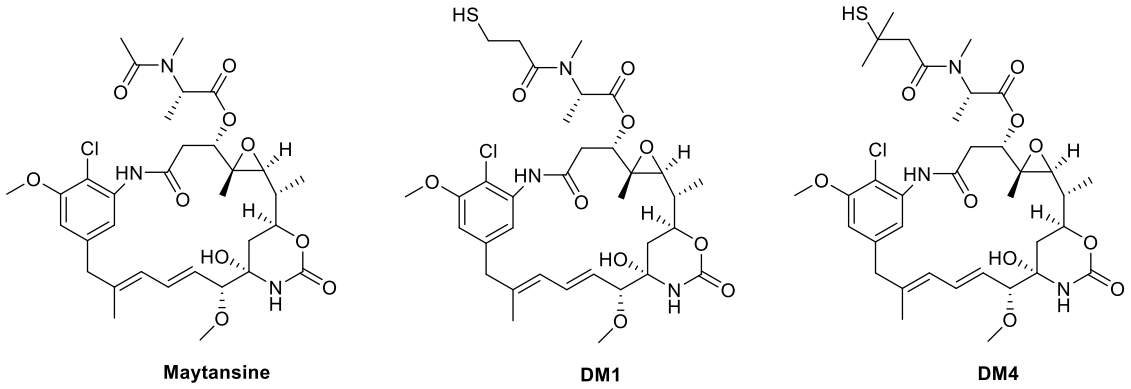

Figure 46- Structure of maytansine, DM1 and DM4.

These compounds bind the tubulin and inhibit microtubule assembly. [137] The main difference of DM1 and DM4 compared to maytansine is the -SH group (more hindered in DM4) which allows both the conjugation with the linker and control the clearance of the conjugates. [140] An example of ADC charged with DM1 is Kadcyla® (Figure 11), but many others maytansinoids with some structural modifications are under investigations for a possible application in the field of ADCs. [141]

TUBULYSINS AND AMATOXINS

Tubulysins and amatoxins are both based on peptides; while the first are linear tetrapeptides, the second are bicyclic octapeptides.

Tubulysins, isolated from myxobacterium *Archangium gephyra*, inhibit microtubule polymerization with the same mechanism of auristatins and have the advantage to bypass the efflux pumps for DM1. [142] An example of warhead is AZ13599185 (Figure 47) developed by Astrazeneca/MedImmune which has a lower picomolar potency than classic tubulysins. Moreover, AZ13599185 is an example of "biparatopic" ADC, where the payload is conjugates to four engineered cysteines and the ADC targets two different epitopes on HER2. [143]

Amatoxins, isolated from various species of mushrooms, are a promising class of payloads due to a great pharmacokinetics and high potency even if none in this class has reached clinical trials. Regarding the mechanism of action, amatoxins inhibit RNA-polymerase II. In this class, α-amanitin (Figure 47) and β-amanitin are well known for the toxic effects on humans but ADC based on this payload showed a significant effect in preclinical trials against colorectal tumor cells. [144]

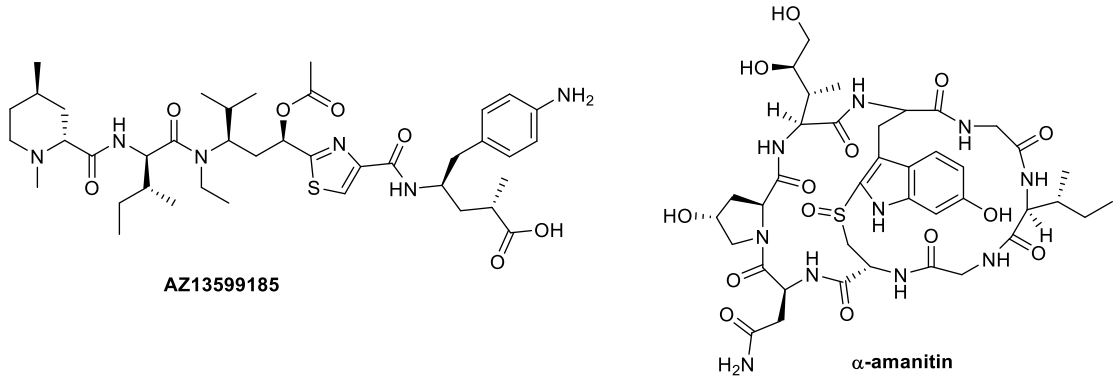

Figure 47- Structure of AZ13599185 an a-amanitin.

CALICHEAMICINS

Calicheamicins are highly potent antitumor agents isolated from the actinomycete *Micromonospora echinospora*; the mechanism of action involves the binding to the minor groove of DNA cleaving double-stranded DNA in a specific manner. [145] The main problem with calicheamicins is the high hydrophobicity that can induce the aggregation of mAbs. In this context, the DAR must be controlled to ensure a good balance between potency and stability of ADCs. Calicheamicin γ^{I}_{1} (Figure 48) is the most studied calicheamicins. It contains an aglycon moiety with bicyclo[7.3.1]tridec-9-ene-2,6-diyne system bearing a labile methyl trisulfide group.

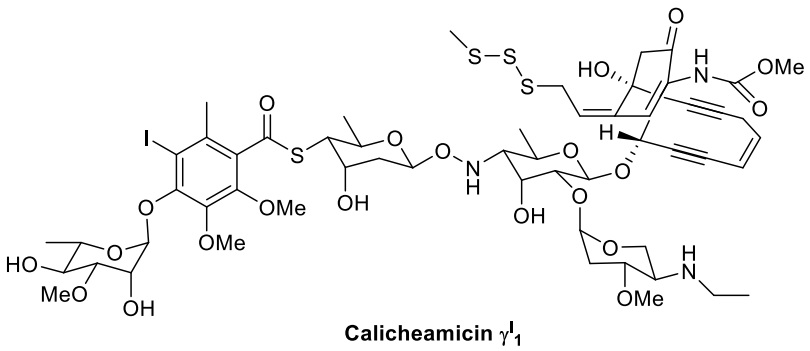

Figure 48- Structure of calicheamicin γ^{I}_{1}.

Unfortunately, due to the complexity of the structure is difficult to study new semisynthetic derivatives. [146] Among the ADCs on the market, Mylotarg® (Figure 9) and Besponsa® (Figure 12) contain calicheamicin payloads.

CAMPTOTHECIN ANALOGUES

Camptothecin is a topoisomerase inhibitor with a high cytotoxic activity. The main problems with camptothecin are low solubility, instability due to the lactone ring and high affinity for MDR1 (that means drug resistance mediated by efflux pumps). Different derivatives have been developed with better pharmacokinetics. [147] An example is SN-38 (active metabolite of irinotecan, Figure 49) used in recent ADC Trodelvy® (Figure 15).

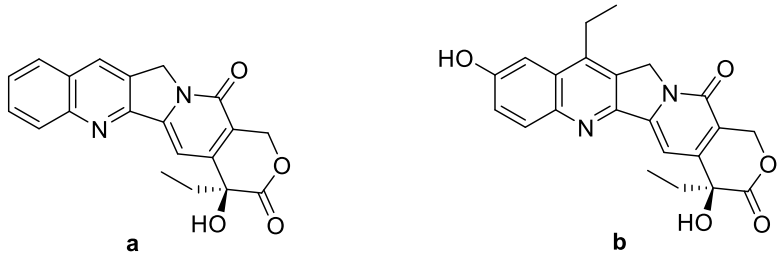

Figure 49- Structure of a) camptothecin and b) SN-38.

PYRROLOBENZODIAZEPINES

The pyrrolobenzodiazepines (PBDs) was first reported in 1965 after the isolation of anthramycin from *Streptomyces refuineus thermotolerans*. [148] The dimerization of two PBDs leads to symmetrical or non-symmetrical compounds that crosslink DNA through the binding to the N2 position of guanine. [149] PBDs dimers are very attractive because of their relatively easy synthesis and thus a lot of derivatives are possible. Indeed, they occupy the third position among the most used payload after auristatin and maytansinoids. [150] Several PBDs based ADCs are currently under investigation; [151] the most used are SG-1882 and SG-3199 (Figure 50) with the last found in Zynlonta®, an ADC recently approved for Large B-cell lymphoma.

A class related to PBDs are indolinobenzodiazepines (IGNs, Figure 50). Their structure is quite similar to PBDs but there are three main differences:

- the insertion of fourth ring near the pyrrole;
- an aromatic ring in the centre of PDB dimers, which increase the binding with the DNA and can be a possible attachment point for linkers;

- only one of the two indolinobenzodiazepins moieties contain an electrophilic imine group providing a monoalkylation of DNA and thus reducing the off-target toxicity. [150]

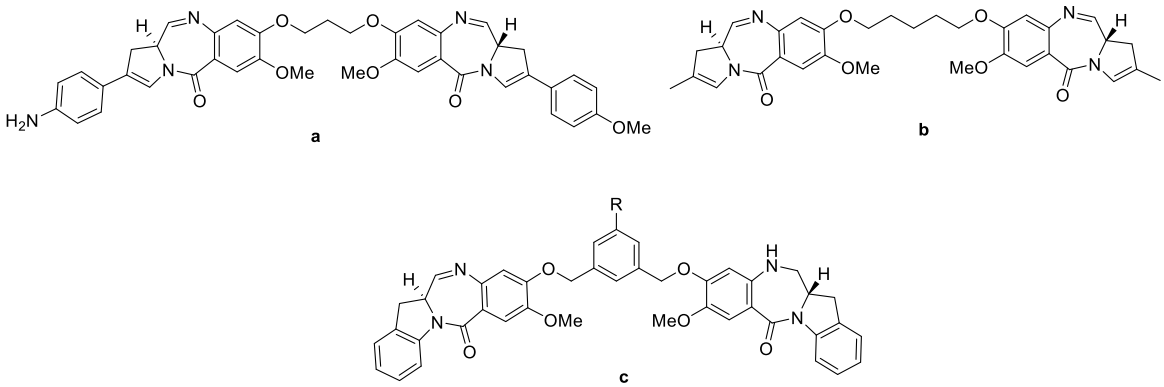

Figure 50- a) SG-1882; b) SG-3199; c) generic structure of IGNs.

DUOCARMYCINS

Isolated from *Streptomyces* bacteria in the 1970s, duocarmycins are a class of DNA alkylating products that covalently bind N3 position of adenine. [152] The first reported compound of this class is CC-1065 (Figure 51) formed by DNA-binding moiety and a DNA alkylating unit (spirocyclic cyclopropapyrroloindole moiety). [153] However, CC-1065 shows some side-effects including hepatotoxicity, thus several analogues have been developed. [154] DUBA and *seco*-DUBA (Figure 52) are examples; while DUBA contains the same cyclopropane moiety of CC-1065, *seco*-DUBA is a prodrug which needs an electronic cascade known as Winstein spyrocyclization for the conversion into the active drug (Figure 51). [153]

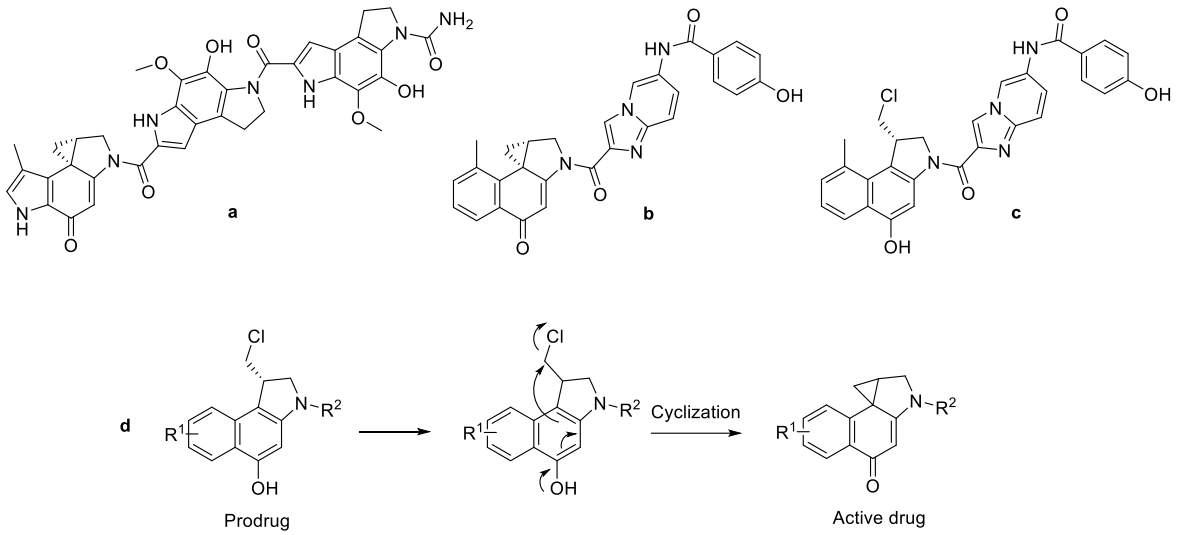

Figure 51- a) CC-1065; b) DUBA; c) *seco*-DUBA; d) cyclization of *seco*-compounds to give the active drug.

Beyond *seco*-DUBA, other *seco*-compounds have been developed also as dimers with PDBs. Unfortunately, to date none of ADCs based on duocarmycins have been approved for oncological applications.

DOXORUBICIN AND ANTHRACYCLINES

Doxorubicin (Figure 52) belongs to the class of anthracyclines extracted from *Streptomyces bacterium*. [155] Compared to the other drugs, Doxorubicin as well as the other anthracyclines, has a lower potency but this payload is still used in some developing ADCs. [156] The most attractive feature of Doxorubicin are the high hydrophilicity and different groups for the attachment of the linker.

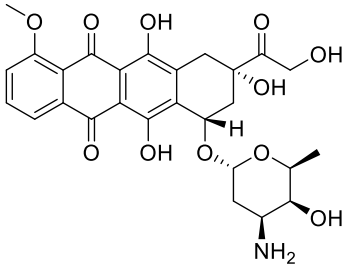

Figure 52- Doxorubicin.

Moreover, to reduce the side effects (the more common cardiotoxicity) of Doxorubicin, several strategies have been studied; [157] thus, its inclusion in ADC systems could be an additional promising strategy to overcome the well-known problems encountered in clinic.

COMBRETASTATINS

A brief introduction is needed for this class of drugs. The most famous is Combretastatin A4 (Figure 53) which is a tubulin inhibitor with structure associated to stilbenoids. [158]

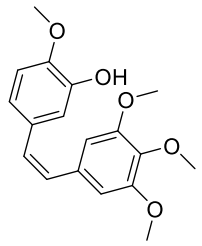

Figure 53- Combretastatin A4.

Although it is a potent cytotoxic agent, Combretastatin A4 has some problems regarding the solubility in water. Different analogues, also based on macrocyclic structure, have been developed as promising anticancer agents. [159] The structure of many compounds of this class is attractive as they have phenol group that can be useful for the attachment of the linker and thus the bioconjugation with mAbs.

1.2.4.1 Unconventional payloads

The choice of the payload, as we discussed in the previous chapters, is also an important parameter to be consider for the development of ADCs. Despite the potent cytotoxic agents available, only a few are suitable for ADCs. Together with new linkers and modified mAbs, the discovery of new payloads with different mechanisms of actions could be useful for the development of the next generation of ADCs. With the terms unconventional we refer to these payloads that are unexplored in drug delivery systems such as antibody-drug conjugates. In particular, epigenetic modulators (i.e. HDAc inhibitors), Hedgehog inhibitors,

antibacterial and antiviral drugs (i.e. Linezolid, Niclosamide, Doxorubicine) are reported as they are correlated to this thesis project.

EPIGENETIC MODULATORS

The degree of condensation of the DNA within histones are regulated by post-translational modifications such as methylations, ubiquitinations, phosphorylation and acetylation of histone proteins. Therefore, the epigenetic modulation is fundamental to maintain cell homeostasis. Acetylation and deacetylation of histones are perfectly balanced in healthy cells by the activities of histone acetyltransferases (HATs) and histone deacetylase (HDACs). However, the alteration of the functions of these enzymes are found in some type of cancers. [160] The main target for cancer therapy is HDAC enzymes that can be divided into four classes: class I, II and III are Zn-dependent while class IV are NAD^+-dependent. [161] The inhibition of HDAC led to the inhibition of the deacetylation of histones causing a dysregulation between pro- and antiapoptotic proteins leading to the cell death. [162] HDAC inhibitors are currently used in clinic for cancer and non-cancer indications, and in general their structure is based on hydroxamates, cyclic peptides, aliphatic acids and benzamides. [163] In 2014, a systematic study of medicinal chemistry aimed at identifying a new generation of HDAC inhibitors that showed different activities towards different HDAc isoforms. [164] These molecules are based on the introduction of a thiol zinc-binding group (ZBG) and on an amide-lactam at the ω-position of the polyethylene chain of the Vorinostat scaffold (Figure 54). [164] Based on this work, the research group where I did my project thesis have developed different ADCs charged with HDAC inhibitors tested in vitro and in vivo demonstrating that it's not necessary to have high cytotoxic payload for the efficiency of ADCs (Figure 54). [165,166]

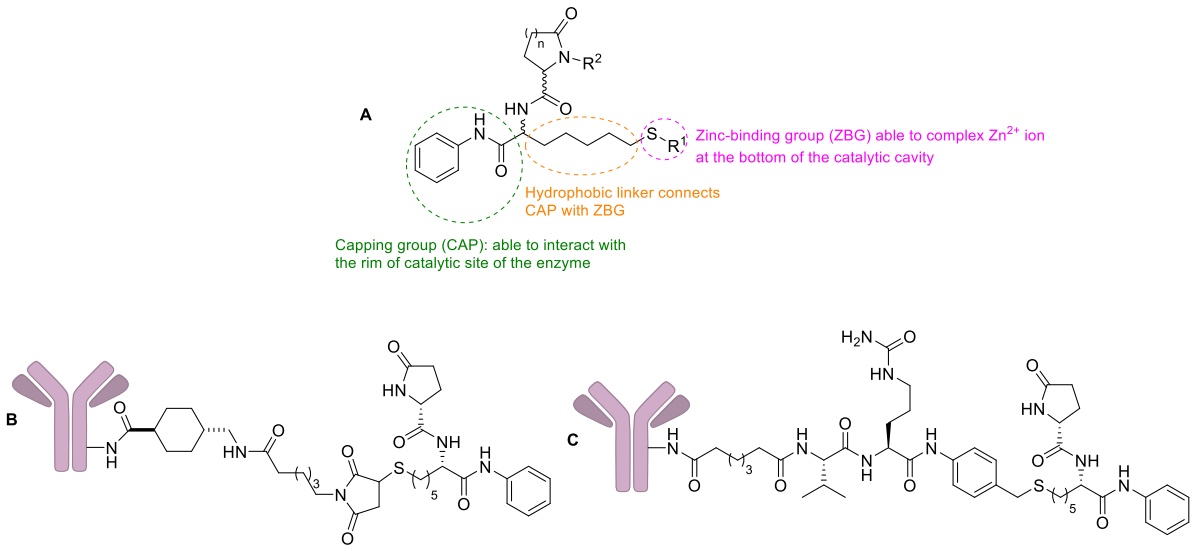

Figure 54- A) Some features of new generation of HDAC inhibitors; B) and C) examples of ADCs charged with epigenetic modulators.

These are the first examples reported in literature on ADC charged with unconventional payloads and could lead to new strategies for future explorations also in non-cancer therapies.

HEDGEHOG INHIBITORS AND CYCLOPAMINE

Hedgehog pathway (HH) was first described in the 1980s thanks to studies on *Drosophilae Melanogaster* when Nüsslein-Volhard and Wieschaus discovered the Hedgehog gene. [167] This signaling pathway is essential for the embryonic development and for tissue repairs in adults (i.e. breast, skin, neural, lung and pancreatic tissues) but an abnormal overactivation of HH seems to be correlated to basal cell carcinoma (BCC), medulloblastoma and melanoma. [168,169] Three isoforms of HH gene are identified: Desert Hedgehog (Dhh), Indian Hedgehog (Ihh) and Sonic Hedgehog (Shh) which encode for three proteins such as DHH, IHH and SHH. [170] These proteins have high affinity for a 12-pass transmembrane receptor Patched (PTCH) which normally inhibits another transmembrane G-protein-coupled receptor (GPCR) called smoothened receptor (SMO). SMO is a G inhibitory protein so in normal conditions there is an inhibition of proliferation or differentiation inputs. [171] When the ligand interacts with PTCH, there is a loss of inhibition of SMO which can translocate to the cilium and activate HH pathway. [172] This simplified description of HH is responsible for several types of tumors but other non-canonical pathways are possible. [169]

The first SMO inhibitor discovered was Cyclopamine. This alkaloid was found in the corn lily *Veratrum Californicum* responsible for the birth defects such as cyclopia and craniofacial deformations, observed in calves from livestock in 1966. [173] This effect is due to the inhibitions of SHH pathways which is important in the embryogenesis process and tissue differentiation as described above. The toxicity of Cyclopamine has not hampered the interest in the development of derivatives but some studies in vitro and in vivo showed that this compound could be a promising anticancer agent. [174–176] The main problems with this payload are related to the poor solubility in water (ca. 5 μg/mL) and acid lability. Indeed, in acidic environments Cyclopamine is readily convert to Veratramine which doesn't act as SHH inhibitor (Figure 55). [177]

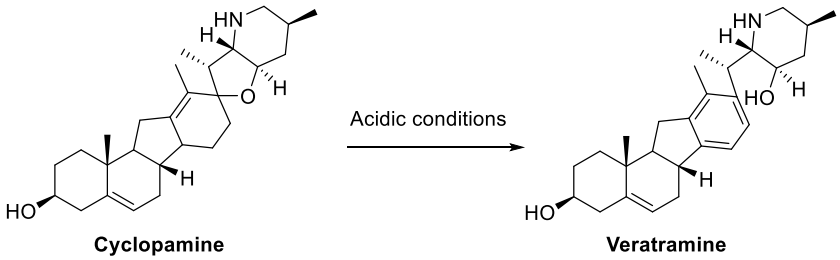

Figure 55- Acid lability of Cyclopamine.

To overcome these problems several semisynthetic derivatives have been developed like Saridegib, Vismodegib, Sonidegib, Glasdegib and Taladegib (Figure 56). Except the Taladegib, all drugs have been approved by FDA for different indications, but the problem related to drug resistance still remains. [178]

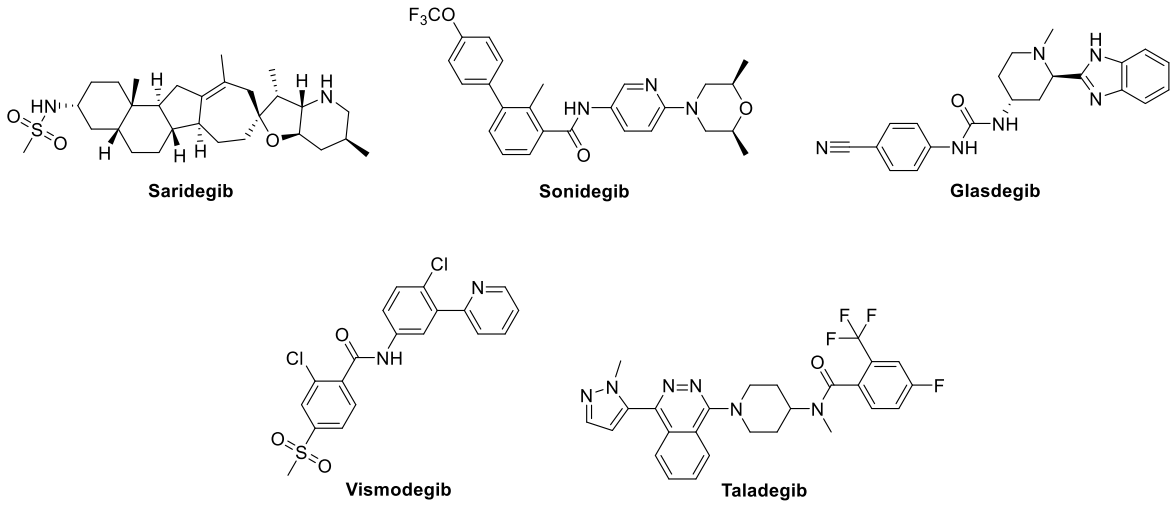

Figure 56- Other SMO inhibitors.

ANTIBACTERIAL AND ANTIVIRAL PAYLOADS

The use of ADCs for non-oncological indications is a growing field in which also non cytotoxic payloads are under investigation. [179] The most successful example in the antibacterial field is the AAC directed against intracellular *Staphylococcus aureus* (Figure 7) which is well described in the previous paragraph. In that case, Rifampicin analogues were conjugates. When we think about a suitable antibiotic payload for ADC, we have to considerer three points:

- the drug should have bactericidal potency in subnanomolar range;

- the antibiotic must contain a chemical group that allows the conjugation with the linker;

- the antibiotic should have good pharmacokinetics properties such as good water solubility and stability in physiological conditions. [180]

Even if Rifampicin-type payloads are the most promising class, different drugs (i.e. clindamycin, daptomycin, sitafloxacin, teicoplanin, triclosan, naphthyridine, radezolid, ampicillin, vancomycin, imipenem and many others) have been conjugated with antibodies and are under investigations. [181]

The rising of antimicrobial resistance (AMR) in recent years leads to reuse of well-known antibiotic drugs that can be conjugated in drug delivery systems. Indeed, the process of

discovery and development of new molecules is slow; [182] in this context ADC charged with drugs already used in clinic can be a useful and rapid strategy. Among the various payloads, Linezolid (Figure 57) is interesting for its pharmacokinetics and pharmacodynamic profile. [183] It can be considered the first member of oxazolidinone class which inhibits bacterial protein synthesis through the binding with rRNA.

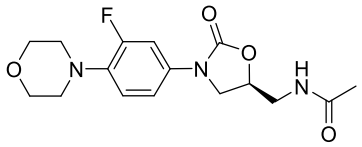

Figure 57- Structure of Linezolid.

Linezolid is used in clinic for several infections including MRSA, vancomycin-resistant *Enterococcus faecium* (VREF) and other critical infections. [183] One interesting structural feature of this drug is the amide moiety which can ideally be used for its inclusion in drug delivery systems.

To date, no ADCs based on antiviral drugs have been approved for clinical indications with a very few examples of antibody conjugates for the treatment of HIV-1 or influenza as emerging therapies. [49,184] This field is still unexplored, but the recent COVID-19 pandemic has highlighted the need for the development of alternative therapies. Interesting payloads are Doxorubicine (DOXO) and Niclosamide (NCL). Both have emerged as possible drugs for the treatment of COVID-19 disease and have chemical groups for linker conjugation (Figure 58, amino group for DOXO and phenol for NCL). [185,186]

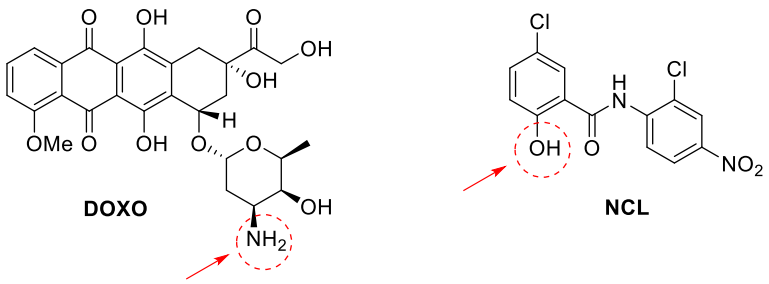

Figure 58- DOXO, NCL and possible attachment site for linker conjugation.

1.3 Bioconjugation: state of art and future perspectives

With the term bioconjugation we refer to the chemical process that allows the binding between the linker-payload system to mAb. Among the different strategies, the bioconjugation with lysine and cysteine are the most attractive. The reason is that they are nucleophilic enough (through amino and thiol moieties) and can easily react with the activated linkers. This process leads to a stable covalent bond without the modification of antibody and can be carried out in buffer conditions which are ideally for mAbs. In addition, amino and thiol groups of mAbs are available in solvent-accessible regions. [187] Although the classic bioconjugations with these amino acids are the most chosen, the main disadvantage of these methods is the high heterogeneity of the final product and thus a broad distribution of DAR. This is correlated with the aggregation of antibodies, increase of clearance rate and in general alteration of pharmacokinetic properties of ADCs. [188]

Alternative bioconjugation methods regarding the site-specific coupling with engineering amino acids. In this case more homogeneous ADCs can be obtained even if the process is more complicated and sometimes required an extensive genetic engineering of mAbs. [72]

1.3.1 Bioconjugation through native residues

As we discussed, this is the most common method for bioconjugation and involves amino and thiol groups of lysines and cysteines. The mAb is not modified, but the process requires the activation of the linker.

1.3.1.2 Lysine coupling

This coupling is used to produce the three marketed ADCs: Mylotarg® (Figure 9), Kadcyla® (Figure 11) and Besponsa® (Figure 12). As a typical IgG1 has more than 80 lysine residues, a lot of heterogeneity occurs; for industrial production the protocol is optimized to coupling the kinetically favoured lysines (about 8-10). [189] For example, Kadcyla® has an average DAR of 3.5 with 5% of unconjugated antibodies which can still impact the efficiency of the ADC. [63] Typically, for lysine conjugation the linker is activated as N-hydroxysuccinimide (NHS) ester which has a good solubility in water and thus can be used in buffer solution (Figure 59). [190]

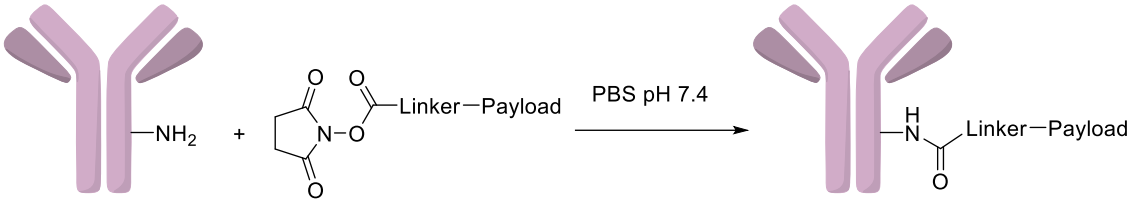

Figure 59- Coupling of activated NHS linker with lysine.

The main drawback of activated NHS esters is the low stability in water (the pH must be carefully controlled) and the lower selectivity, as it's reported that they can react also with serines, tyrosines and threonines. [189,191]

The activation of the linker using NHS is not the only method for lysine coupling. Other methods include isocyanate and isothiocyanate, 4-azidobenzoyl fluoride (ABF), β-lactams, phospha-Mannich reactions, α,β- unsatured sulfonamide and sulfonyl acrylate. [192] Schematic representation of all these methods is reported in Figure 60.

Isocyanates can react with amino groups to give a stable urea, but they are not selective towards lysines and are sensitive to the moisture. [193] The corresponding isothiocyanates can be used to avoid these problems as they seem more stable. [194]

The use of ABF is interesting because the bioconjugation can be performed through two steps: first there is the reaction of amino group with ABF and then copper-free strain-promoted azide–alkyne cycloaddition (SPAAC) with the linker (Figure 60). [195]

The β-lactam linker was developed by Barbas et al. [184] The resulting ADC was charged with Zanamivir, representing one of the few examples of ADC against viral infections in literature. In that case, bioconjugation with lysines occurs in 2 h in phosphate buffer solution (PBS) at room temperature and give an ADC with similar activity compared to the free drug Zanamivir. [184]

Phospha-Mannich reaction was applied to target lysines of several proteins but also Fabs of trastuzumab; like ABF, 2 steps are necessary to insert the linker-payload system. [192] The benzaldehyde can be functionalised with different groups on the aromatic ring to allow the insertion of the linker in the second step (Figure 60).

Until now, α,β- unsatured sulfonamide as linker for lysines coupling was applied only to human serum albumin (HSA). The interesting feature of this linker is that the coupling occurs in chemo- and regioselective manner unlike the other methods. [196]

Sulfonyl acrylate linker was applied for bioconjugation to prepare Trastuzumab-Crizotinib ADC. [192] This two-step protocol involves first the coupling between the sulfonyl moiety and unprotonated lysine (at pH=8) and then Michael addition of the payload on the double bond.

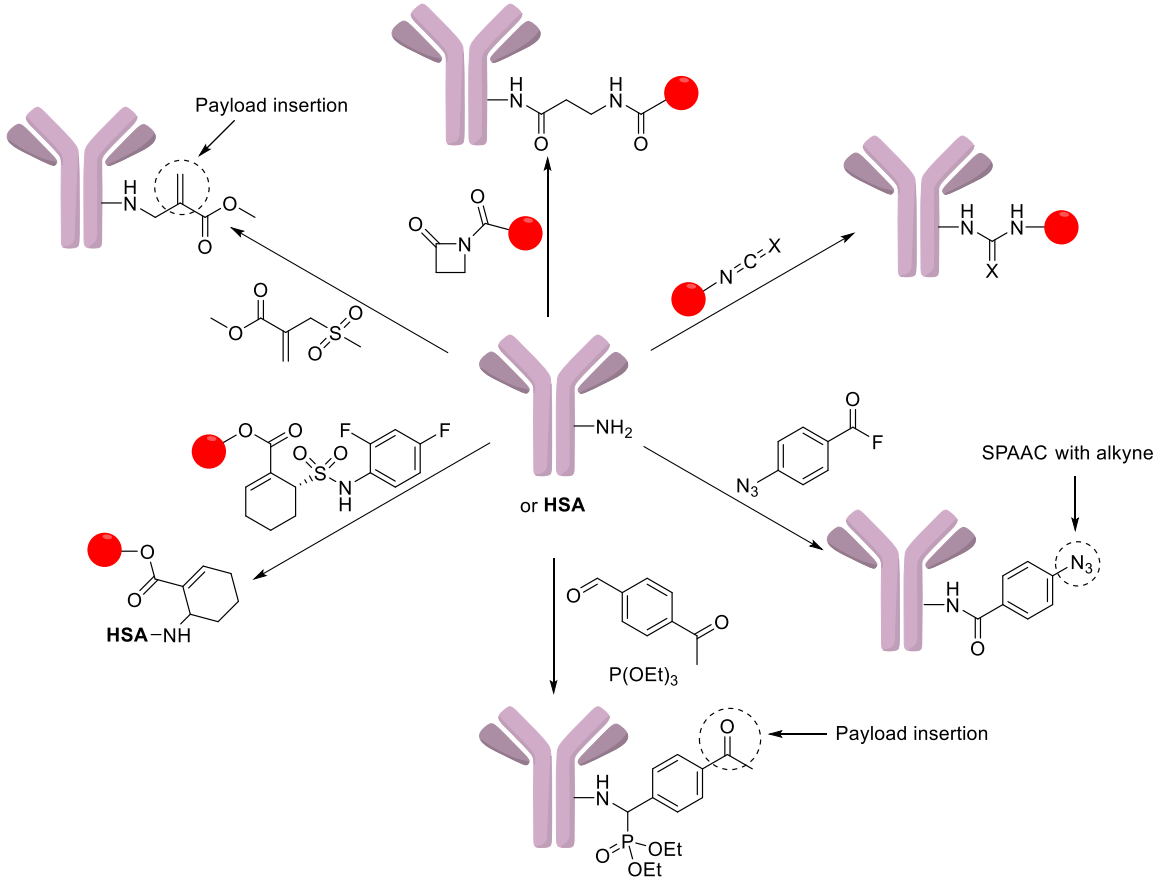

Figure 60- All possible conjugations with lysines. Payload in red. X= O,S.

1.3.1.3 Cysteine coupling

A typical IgG1 has 16 cysteine pairs (12 intra-chain and 4 inter-chain) but only 4 inter-chains are solvent accessible and thus can be used for bioconjugation. Conjugations with cysteines can be found in the remaining ADCs in the market thus demonstrating that this method is the most exploited. The main advantages of cysteines are more homogeneous ADC (less cysteines compared to lysines) and, as the thiol groups are soft nucleophiles, they interact mainly with soft electrophiles allowing selective reactions. To be used, cysteines need to be reduced with some chemical agents such as TCEP or DTT. [197] The reduction of disulfide is also a drawback in cysteine coupling because, if not balanced, can lead to denaturation of antibodies.

The most used method for cysteine coupling involves maleimide linker (Figure 61). It's important to notice that the resulting ADC is susceptible to retro-Michael reaction and two enantiomers (that readily undergo isomerization) are generated. [198,199] Moreover, thiosuccinimide is reported to be prone to ring hydrolysis even if this process avoids the retro-Michael reaction and increase the stability of ADC. [200]

Besides maleimide, many linkers have been developed and some of these are reported in Figure 61. A detailed description of all of them is beyond the scope of this thesis, so only a few are considered as examples.

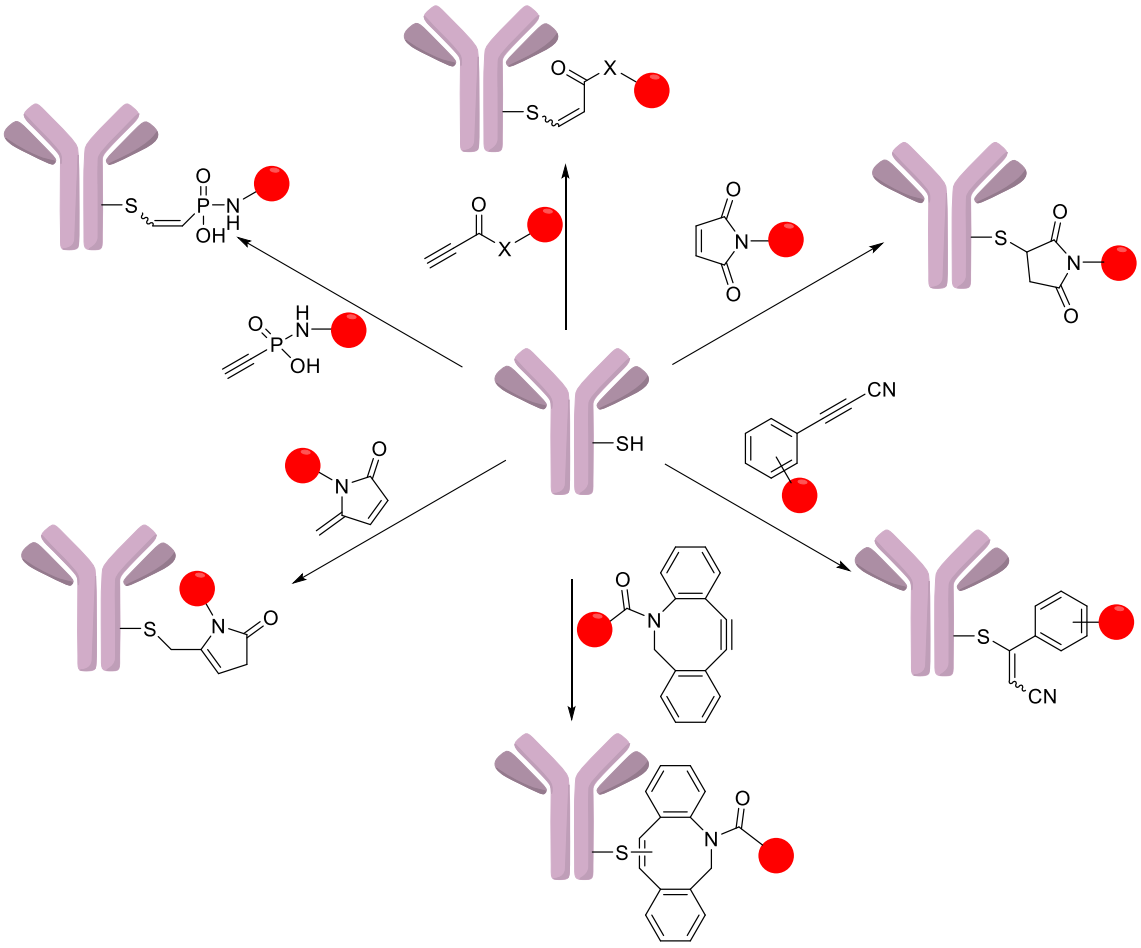

Figure 61- Some examples of cysteine coupling.

As shown in Figure 61, all these linkers can react with only one thiol group, but bis-reactive linkers are also described. [201] This method can be considered a site-specific bioconjugation because involves a specific modification of cysteines. When bis-reactive linkers are used, the process is called disulfide rebridging in which the first step is the reduction of disulfide

followed by reaction with a cysteine-selective cross-linking reagent (Figure 62). The main advantage is the production of ADC with more controlled DAR (4, 8 or 16).

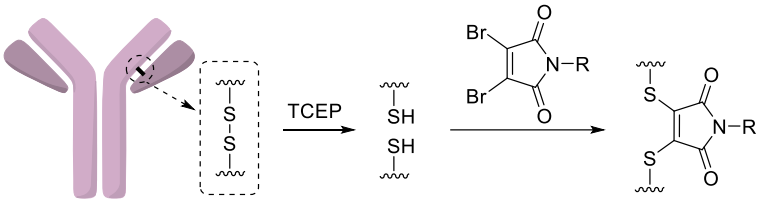

Figure 62- Example of disulfide rebridging.

One drawback of disulfide rebridging is the formation of "half-antibody", formed by intrachain bridging of the hinge region in heavy chain cysteines.

1.3.2 Other kinds of bioconjugation

Along with unmodified amino acids, there are other possibilities for bioconjugation, but in most cases they require a genetic engineering of mAb. Among these we find:

- Chemical modification of amino acids: engineering cysteines, disulfide rebridging (described above), bioconjugation with non-canonical amino acids (ncAAs) and other chemical methods like histidine, lysine and arginine modifications;

- enzymatic methods for bioconjugation;

- glycan modifications (glycoengineering mAbs). [201]

CHEMICAL MODIFICATION OF AMINO ACIDS.

Introduction of non-native cysteines not involved in disulfide bond can offers some advantages such as high homogeneous ADCs and increasing in stability of antibodies. Indeed, the modification site of antibody is carefully evaluated and some studies on aggregation, clearance, binding, and cytotoxicity of modified product are done. [202,203] One famous example of this modification is THIOMAB which is a cysteine-engineering antibody developed by Junutula and co-workers. [39] As they described in their work, the THIOMAB antibody was obtained after a series of modifications to insert free thiol moiety on Fab regions of antibody. Then, a selective bioconjugation occurred to give an antibody

conjugated with MMAE through mc-Val-Cit-PABC linker. They compared this highly homogeneous ADC (DAR 1.6) with an analogues heterogeneous ADC with DAR 3.1. Interestingly, the homogeneous ADC shows similar activity and less adverse effects in rats and monkeys than the heterogeneous one, despite the low drug loading. [39] Depending on the site of modification, the engineering cysteines can have various levels of solvent accessibility and thus the stability of ADC made with this technology can be adjusted. [204]

The expansion of genetic code in recent years, has allow the site-specific incorporation of non-canonical amino acids (ncAAs) on antibodies. This process is done using engineering tRNA *via* cell based or cell-free systems. [201] The site of incorporation is crucial for the development of ADC as it has an influence on the binding with antigens, pharmacokinetics, and stability of the system. [205,206] Usually the ncAAs are similar to the natural amino acids to reduce the immunogenicity but bearing some chemical groups for specific bioconjugation such as azide, ketones, cyclopropenes or dienes. [201] Some examples are *p*-acetylphenylalanine (pAcF) that contains a keto group suitable for an oxime ligation with alkoxy-amines linkers and *p*-azidophenylalanine (pAzF) which can undergo click reactions (Figure 63).

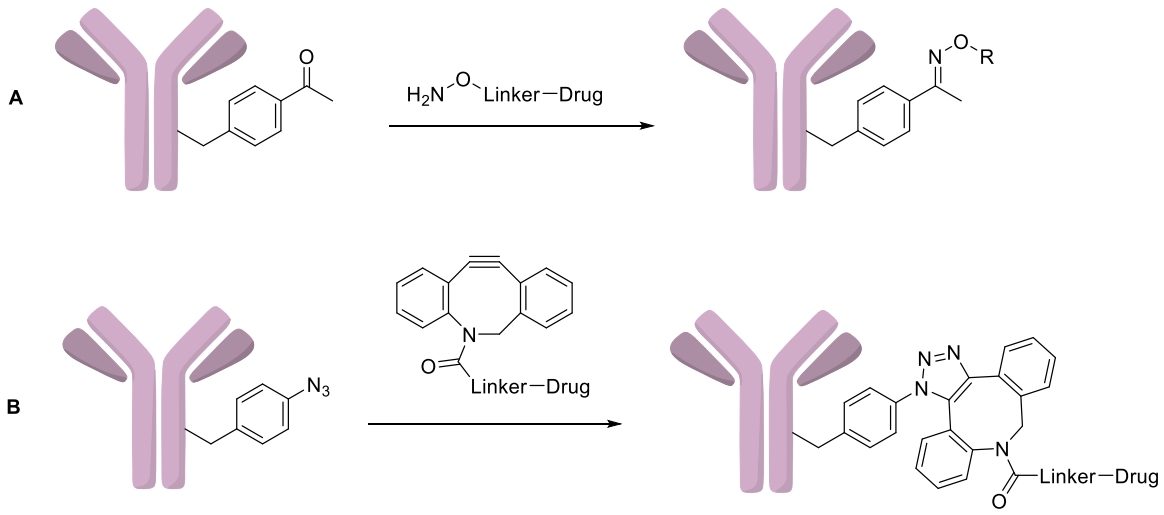

Figure 63- Bioconjugations of ncAAs containing: A) pAcF residue; B) pAzF residue.

A recent strategy involves the incorporation of selenocysteines in mAbs resulting in antibodies known as selenomabs. The key point is the acidity of selenol groups that are higher than thiols of natural cysteines giving a selective bioconjugation without catalyst or rebridging. [207]

Other chemical modifications on different amino acids like histidine and arginine are also reported in literature but described as more challenging respect lysines and cysteines. [201]

ENZYMATIC METHODS FOR BIOCONJUGATION

Enzymes can be used to achieve site-specific conjugations in two different manners: they can directly attach the payload to specific sequences on mAb or introduce reactive moiety on antibodies for a further conjugation with linker-payload system. The most used enzymes are transglutaminase, sortase and formylglicine-generating enzymes (FGE). Microbial transglutaminases (mTG) are a class of enzymes that catalysed the acyl transfer reaction between glutamines and lysines with the release of ammonia. [208] This specific activity can be applied in the field of ADC but, as human IgG contains a lot of lysines and glutamines, this approach can be challenging. As example, glutamine residues of deglycosylated antibodies can be conjugated with primary amine of the linker with a high controlled DAR of 2. [209]

Sortase-mediated antibody technology, also known as SMAC-technology™, uses a transpeptidase (sortase A) that recognise the sequence Lys-Pro-Glu- Thr-Gly and cleave Thr-Gly motif. After that, this enzyme catalysed the insertion of the new glycine-functionalised payload-linker. [210]

FGE oxidises cysteine residues to a formylglycine (fGly) unit in a Cys-X-Pro-X-Arg (X = any amino acids) sequence. The aldehyde can be further conjugated with hydrazine- or hydroxylamine-functionalised payloads. [211] This technology is known as SMARTag®.

The three methods described above are probably the most used, but other enzymatic methods for bioconjugation have been developed including: prenyltransferase (conjugation of functionalised isoprenoid group to cysteines and further oxime reaction), SpyLigase-mediated conjugation, tyrosinase-mediated strategy (for the oxidation of tyrosine and subsequent strain-promoted cycloaddition) and Horse-radish peroxidase tyrosine oxidation strategy. [201]

GLYCOENGINEERING mAbs

N-glycosylation at Asn^{297} of IgG can be exploited to make glycoengineering mAbs; glycosyltransferase transfers sugar to a residue of glycan to allow a functionalisation of

antibody which can further bioconjugate with a linker-payload system. [212] Conjugation to N-glycan give some advantages:

- the conjugation occurs in spatially distant from the site where the mAbs recognised the antigen, leading to a lower risk for the activity of ADCs;

- the glycosylation pattern is well conservated in antibodies, thus it's relatively simple to modify the site of interest;

- the carbohydrates are structurally different from peptides, allowing a site-specific conjugation. [201]

One method for glycan modification involves the oxidation of vicinal diols of sugars using $NaIO_4$. [213] The new aldehyde can react with a hydrazine linker to form a hydrazone. However, direct oxidation of sugars leads to a mixture of conjugates because galactose, fucose and sialic acid residues are all involved in oxidation. Neri and co-workers overcome this problem by developing antibodies which consist solely of G0F glycoforms (where G0 means 0 residues of galactose and F means 1 residue of fucose). [214] Thus, only one residue of fucose is sensitive to oxidation and then further functionalisation with the linker is possible.

Another strategy involves the transfer of galactose (using β-1,4-galactosyltransferase) and sialic acid (using α-2,6-sialyltransferase) on the native glycans. [215] Then, only a little amount of $NaIO_4$ (1 mM) is used for oxidation of sialic acids residues which can be functionalised to form an oxime bond with the linker. The main limitation of this technique is the lower drug loading because only two sialic acids can be introduced (one for heavy chain) allowing a maximum DAR of 2.

Along with the described methods, some papers report other glycan remodelling using enzymes as endoglycosidase and galactosyltransferase. [216,217] The idea is almost the same, first there is a modification of native glycans with these transglycosidases to insert modified sugars, and then the selective reaction with a specific linker.

1.3.3 Characterization of ADCs

The characterization of ADCs is crucial to evaluate the properties of the final product. There are three points of interest: the DAR, the site of conjugation and the aggregation. They are all correlated with the pharmacokinetics and stability of the final product, and this is the reason for the development of some technique to identify these parameters. The main methods involve UV/Vis spectroscopy, chromatography and mass spectrometry (MS).

UV/Vis SPECTROSCOPY

This is the simplest method to determine the DAR of the product without specific preparation of the sample. This technique relies on the different absorption (λmax) between each component of ADC. [218] The λmax of mAbs is usually 280 nm, so the payload should have a different λmax to perform a correct characterization. The main disadvantage of UV technique is represented by UV-sensitive payloads which therefore cannot be used.

CHROMATOGRAPHIC METHODS

Chromatographic methods have been widely used in pharmaceutical companies due to the characterization of several physiochemical parameters of ADCs. [219] In this context, there are three kinds of chromatography: Hydrophobic Interaction Chromatography (HIC), Reversed-Phase Liquid Chromatography (RPLC) and Size-Exclusion Chromatography (SEC).
HIC can be used to evaluate the average DAR and the distribution of the DAR. [220] Usually, payloads are hydrophobic and when conjugated with mAbs the resulting ADC is more hydrophobic than the native antibody. The hydrophobicity also increases with the number of drug loading (DAR) and through HIC we are able to see different peaks that are retain differently according to the DAR. The operation conditions such as temperature and the use of organic solvents must be carefully controlled to avoid the degradation of ADCs. [220] The main disadvantage of HIC is the use of buffer solution as mobile phase which is not compatible with MS detection. However, the coupling of HIC with RPLC, known as multidimensional chromatography, can overcome this issue. [221]
RPLC is used to determine the DAR, drug distribution in heavy and light chains and unconjugated payload. [222] The main advantage over HIC is the volatile mobile phase which allows the use of MS detection. However, antibodies have a strong tendency to remain in column due to their high affinity with reverse-phase column and a loss of material must be

considered. [223] Moreover, ADC is usually denaturated by the harsh conditions of RPLC, but DAR can be calculated based on the peaks (% area) of heavy and light chains. [220]

SEC is used to determine the presence of aggregate formed during the synthesis or storage of ADCs. [224] Interaction of ADC with the column can be electrostatic or hydrophobic resulting in different elution time and tailoring of the peaks. For example, by modulating the ionic strength of the mobile phase the electrostatic interaction can be reduced leading to a more reliable analysis. [220] This can be achieved using potassium salt that seems to stabilise the antibodies and avoid the interaction of aggregated antibodies with the column. [225] Beside the aggregation, SEC is widely used for desalting purposes and for the characterization of excipients in ADCs synthesis.

Cation exchange chromatography (CEX) is another technique for ADCs characterization even if less used than the others. CEX is useful when there is a variation of charge on antibodies; for example, a common application is found to see the reduction of charge of lysines after attachment of the payload. [226]

MASS SPECTROMETRY

Along with chromatography, MS is a key analysis for ADCs characterization. This powerful technique can detect small variations of mass (30-100 ppm) allowing the determination of DAR and giving information on heterogeneity and antigen binding. [227] Each component of ADC should be evaluated to choose the correct analysis such as MALDI, ESI or nano-ESI. For example, very high hydrophobic payload or ADC with high DAR tend to reduce ionization making the analysis more complex. [223] Quadrupole Time of Flight (Q-TOF) has also been used for determination of DAR due to the speed and resolution of analysis. [220] More often, MS is coupled with chromatography to have more detailed information. Recently, other MS powerful techniques like ion-mobility mass spectrometry (IM-MS), hydrogen deuterium exchange mass spectrometry (HDX-MS) or high-resolution mass analyser (HRMS) have been used to identify some specific characteristics of ADCs such as the site of conjugation or the binding with the antigen. [228,229]

1.3.4 Future outlook

Many methods have been developed for bioconjugation with native amino acids or through site-selective modifications. All the described techniques have their advantages and disadvantages and it is still unclear which is the best choice. [230] Engineering mAbs offer very homogeneous ADCs but require special technologies and qualified operators. On the other hand, conjugations with native amino acids involve simple reactions but lead to high heterogeneous products. Moreover, it's difficult to predict how the linker and the payload affect the properties of the final ADC. In addition, the therapeutic index of ADC seems not to be strictly correlated to the DAR; in this context other parameters that affect the activity of ADC are under investigation. [231]

Bioconjugation with other carriers such as nanobodies, DAR-Pins and peptide aptamers are also investigated and could be a real perspective for the future as they have lower cost, lower immunogenicity, and higher affinity binding than mAbs. [192]

1.4 Aim of this research work

Making a successful ADC can be very challenging as each component should be carefully evaluated. The linker is crucial for ADCs and, as we see from the various examples in literature (paragraph 1.2.3), it has a strong influence on ADCs properties such as PK and stability. Moreover, it is essential to have specific chemical groups that allow the conjugation with the drug and bioconjugation with antibodies.

On the other hand, the development of bioconjugation protocols is not very simple as they depend on the types of linker-payload system that we want bioconjugate.

The aims of this work are:

- Find new linkers, suitable both for payloads with different reactive moiety (such as alcohols, amines and amides) and for efficient bioconjugation with mAbs;

- Making ADCs charged with unconventional payloads (antibacterial, antivirals or Hedgehog inhibitors) by exploring new protocols for bioconjugation with mAbs.

1.4.1 A new pH sensitive linker for drug targeting delivery

Among cleavable linkers, the pH sensitive (paragraph 1.2.3.2.1) have been well studied and used for ADCs. The main issues of these linkers are premature release of the drug which increases off-target toxicity and sometimes the payload is released attached to a part of linker (as the case of NEBI linkers).

Our aim is to make a new acid labile linker started from Gallic acid, a safe and cheap molecule which can be converted into a pH sensitive platform called 5-(hydroxymethyl) pyrogallol orthoester (HMPO, Figure 64). HMPO contains an orthoester moiety which is stable at physiological pH 7.4 but readily releases the payload in acidic conditions (pH 5.5). In addition, we insert a chemical group to allow the bioconjugation with mAbs proving its applicability in the field of ADCs.

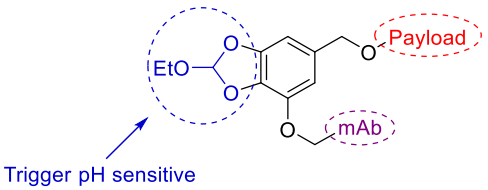

Figure 64- HMPO platform.

1.4.2 ADCs charged with unconventional payloads and exploration of new protocols for bioconjugation

As we discussed, cytotoxic drugs are not the only payloads that we can conjugate with ADCs. For cancer, we saw that other warheads with different mechanisms of action could be suitable for ADCs. Cyclopamine is a HH inhibitor that has never aroused interest due to the poor solubility and instability in acidic conditions. [177] In this context, our aim is to develop new ADCs charged with Cyclopamine through specific linkers to overcome the problematic PK of this payload.

Beyond cancers, ADCs can be used for various diseases such as bacterial and viral infections even if these fields are less explored. Our aim is to choose payloads with various indications in clinic that have chemical groups suitable for conjugation with several linkers (Figure 65). In particular, amide-based drugs (*i.e.* Linezolid, Enzalutamide, Tasimelteon and *p*-Toluensulfonamide) are reported since they represent one of the few examples of amide release in literature. [232–234]

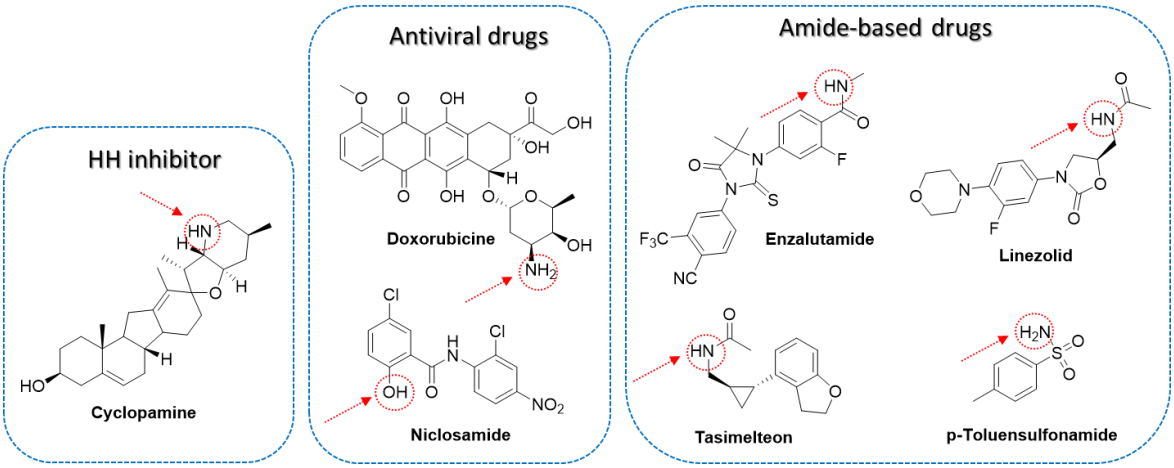

Figure 65- Payloads used in this work. In the red circle are the chemical groups available for conjugation with the linker.

Thanks to the past experience of the research group where I did this project thesis, we understand that the same bioconjugation protocol cannot be applied for all cases. The properties of the linker and the payload have a great influence on this process. Thus, our focus is to develop new bioconjugation protocols especially for high hydrophobic payload (*i.e.* Cyclopamine).

CHAPTER 2- Results and discussion

2.1 A new pH sensitive linker for drug targeting delivery

As we introduced in our discussion on pH sensitive linkers (paragraph 1.2.3.2.1), one of the most important features of these connectors is the selective release of the drug in acidic environments. This is a critical point as the premature release of the payload could lead to off-target toxicity. Moreover, most of these linkers require a complex synthetic chemistry and can be charged only with drugs bearing specific chemical groups. [107]

Regarding the mechanism of release, 1,6 self-immolative elimination process is well studied and proved to be effective in various ADCs. With all these in mind, for our purpose we thought of Gallic acid as a precursor for the synthesis of new pH sensitive linker which could be applied not only in the field of ADCs but also in other kinds of delivery systems. Gallic

acid represents a perfect starting material for our scope because it is a safe-handling and economic molecule which has three points of interest for further functionalizations:

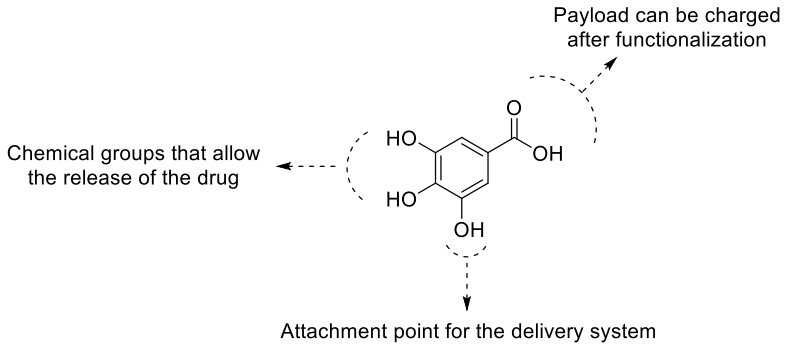

Figure 66

The carboxylic acid moiety can be transformed into benzylic alcohol, thus becoming more susceptible to drug loading. Two hydroxyl groups can undergo selective protection to insert the orthoester moiety, while the remaining -OH is suitable for a further functionalization and bioconjugation with mAbs.

2.1.1 Synthesis of HMPO platform

Starting from Gallic acid, the synthesis of HMPO platform can be achieved in 4 steps as described in the following Scheme:

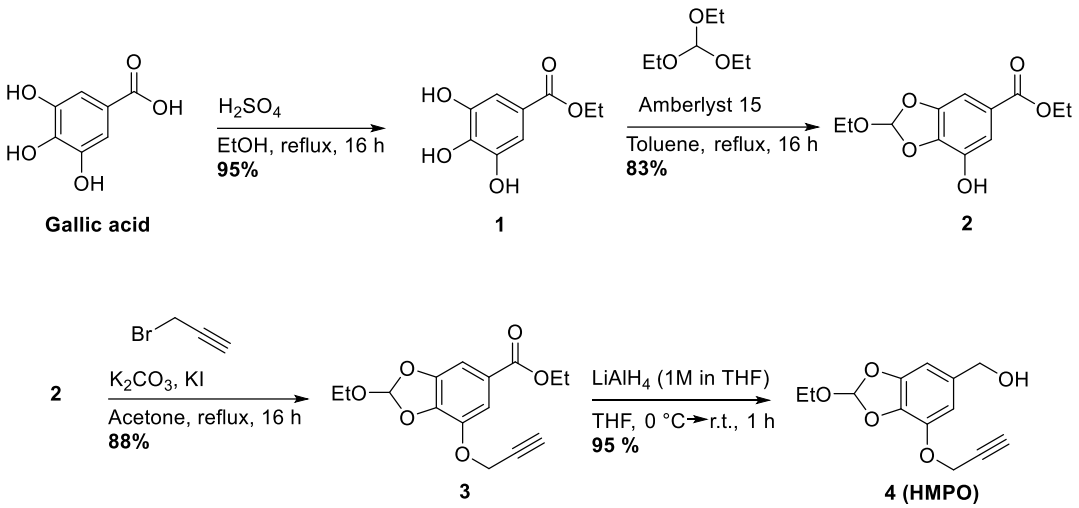

Scheme 1

The first step was the Fischer esterification which gave the product in excellent yield. The subsequent synthesis of orthoester moiety was originally catalyzed by *p*-toluenesulfonic acid (PTSA) but with low yield when applied on gram scale. Amberlyst® 15, an acid resin catalyst, was successfully employed in the synthesis of compound **2** (Scheme 1) even on larger scales (>5g). The insertion of propargyl group takes place by nucleophilic substitution; a catalytic amount of KI seems to be effective in promoting the reaction due to *in situ* I-Br exchange, which makes the propargyl moiety more reactive. The major issue of this step was the purification of the excess propargyl bromide, as some remained after flash chromatography or by evaporation under reduced pressure. Anyhow, an efficient method to remove propargyl bromide was trituration in Et_2O and further filtration of the pure product. In the last step, the ester was reduced with $LiAlH_4$ (1M in THF); it is worth noting that the addition at 0 °C reduced the amount of side products, leading to the final product **4** in excellent yield.

Once the synthesis of HMPO was achieved, we wanted to evaluate whether this linker could release the payload under acidic conditions and remained stable at physiological pH. For this scope, we decided to synthetize two model systems, one through the formation of a carbamate and the other through the formation of an ether.

2.1.2 Synthesis two model systems and evaluation of the HMPO hydrolysis profile

The first model system was made through the activation of HMPO **4** with *p*-nitrophenyl chloroformate and further alkylation with tryptamine (Scheme 2):

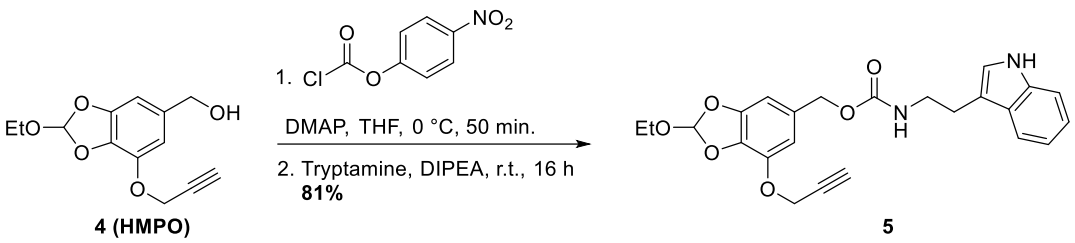

Scheme 2

The intermediate formed after activation with *p*-nitrophenyl chloroformate was rather unstable and difficult to purify without avoiding a partial degradation of the resulting product, which gave *p*-nitrophenol and the starting material **4**. Thus, the activated compound was treated with a solution of tryptamine and DIPEA in THF to give the product **5** in good yield.

The synthesis of the second model system was quite challenging; the chlorination of HMPO **4** required specific conditions to avoid the complete degradation of product **6**:

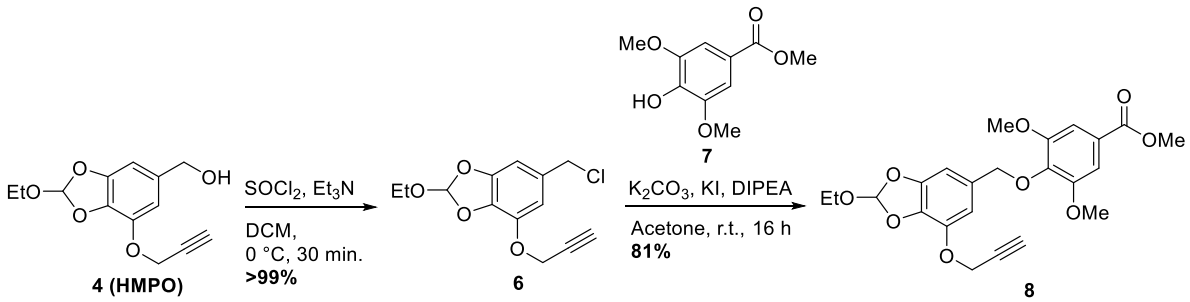

Scheme 3

A stochiometric amount of Et_3N was required to quench HCl which could hydrolyse the orthoester moiety. A further alkylation with compound **7** gave **8** in good yield.

Stabilities of compounds **5** and **8** were evaluated by HPLC at different pH values (5.5, 6.5, 7.4) and in water. Compound **5** released 93% of the payload after 6 h ($T_{1/2}$= 3 h, Figure 67) at pH 5.5 while remaining quite stable at pH of 6.5, 7.4 and in water.

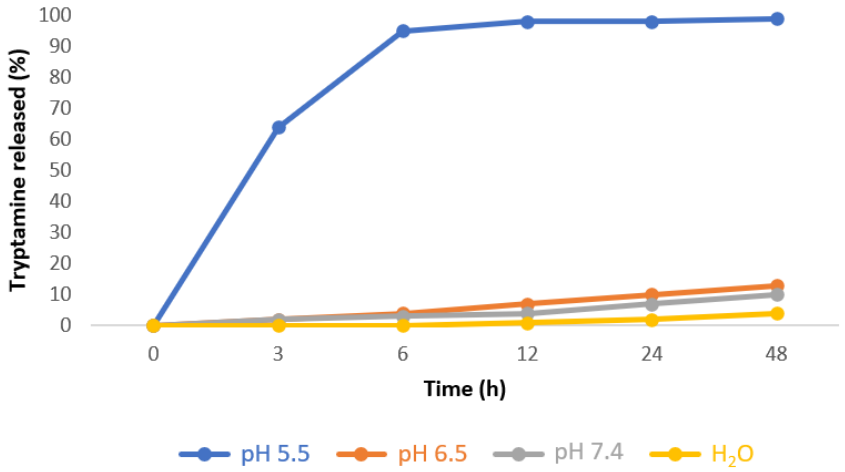

Figure 67- Hydrolysis kinetics of model system 5 at pH 5.5, 6.5, 7.4 and H_2O.

A similar outcome was observed with compound **8** which released about 95% of the payload after 7 h ($T_{1/2}$= 3 h, Figure 68) and remained stable at various pH and in water. In this case, only 25% of free payload was detected after 24 hours at pH 6.5.

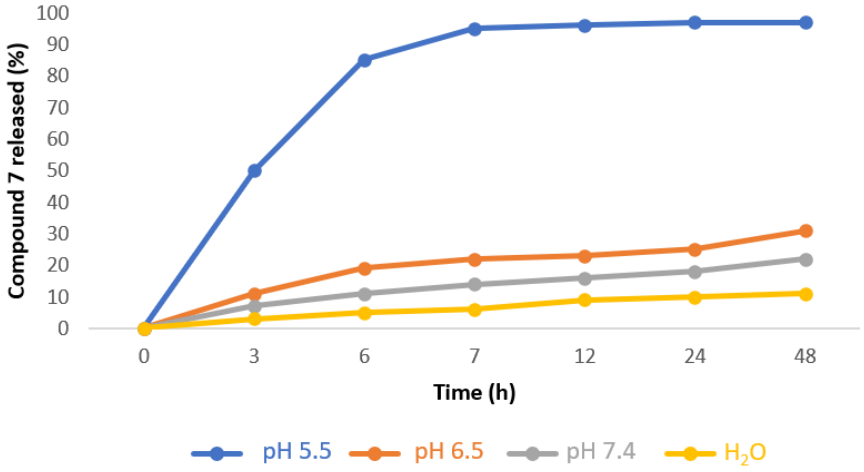

Figure 68- Hydrolysis kinetics of model system 8 at pH 5.5, 6.5, 7.4 and H_2O.

These data demonstrated that our linker based on orthoester was effective in releasing the respective payloads in an acidic environment. In addition, excellent stability in neutral conditions (pH 7.4 and H_2O) was achieved, proving a possible application in ADC systems. However, before continuing our discussion on ADCs containing HMPO as a linker, we performed some ^1H NMR studies to investigate a possible mechanism of release.

2.1.3 Hypothetical mechanism of release of HMPO

To investigate the hypothetical mechanism of release of HMPO, we decided to carry out some NMR studies of model system **8** at pH 5.5. Compound **8** was incubated in deuterated buffer at 37 °C and the FID recorded every 30 minutes. NMR spectra (see the experimental part) showed the shift of some important signals:

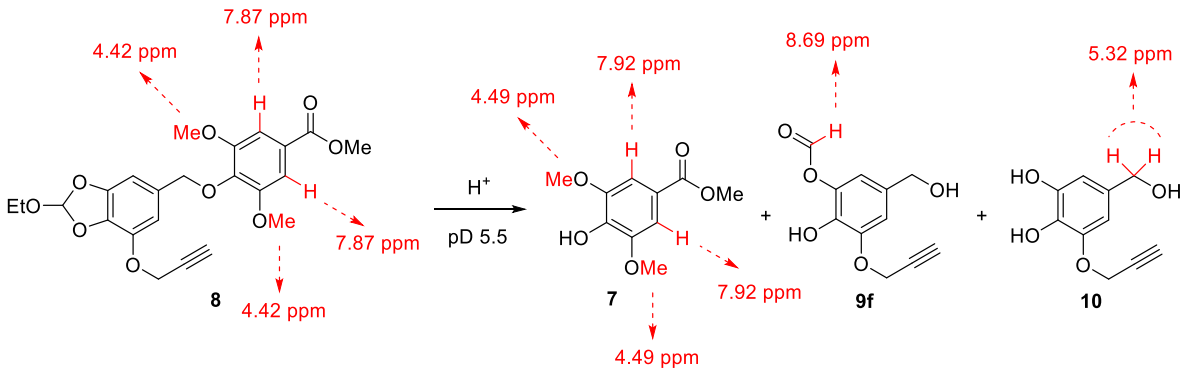

Scheme 4- Some characteristic signals detected by ^{1}H NMR.

In particular, the shifts of the aromatic signals from 7.87 to 7.92 ppm and of the singlet (-OMe groups) from 4.42 to 4.49 ppm suggest the release of phenol **7**. Furthermore, new peaks at 8.69 and 5.32 ppm confirmed the presence of transient compound **9f** and the phenol **10**. On the basis of these results, we supposed a hypothetical release mechanism (Scheme 5).

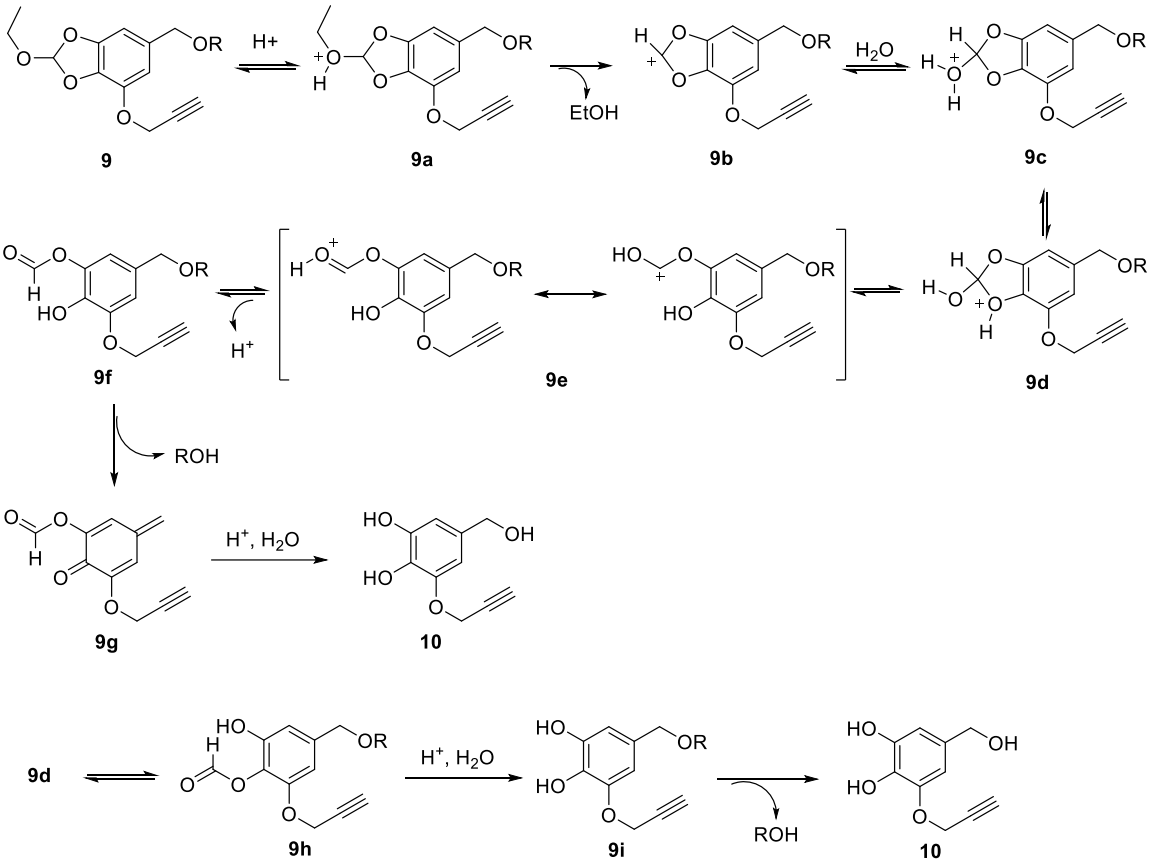

Scheme 5

Compound **9** is protonated in acidic conditions, thus releasing EtOH and forming the carbocation **9b.** The carbocation immediately reacts with water to form hydroxyacetal **9d**, which subsequently furnishes the formate **9f**. At this stage, 1,6-elimination occurs to give the free payload (ROH) and *p*-quinone methide **9g**. Further attack of water gives the pyrogallol **10**. Alternatively, **9d** can generate **9h** which, after hydrolysis, releases the payload (ROH) through 1,6-elimination process.

2.1.4 Synthesis of ADCs containing HMPO platform and evaluation of hydrolysis kinetics

At this point, we decided to charge the HMPO linker with two antitumor drugs, Doxorubicin and Combretastatin A-4, and bioconjugate the resulting systems with Cetuximab (Ctx). Cetuximab is a monoclonal antibody specific for the epidermal growth factor receptor (EGFR) which is overexpressed in certain tumors. The synthesis of these two products was very similar to that of the model systems. For Doxorubicin-containing ADC, HMPO linker

was activated using *p*-nitrophenyl chloroformate and treated with Doxorubicin to afford compound **11**. Then, a Copper-Catalyzed Azide-Alkyne Cycloaddition (CuAAC) with 6-azidohexanoic acid (**12**) gave the desired product **13** (Scheme 6).

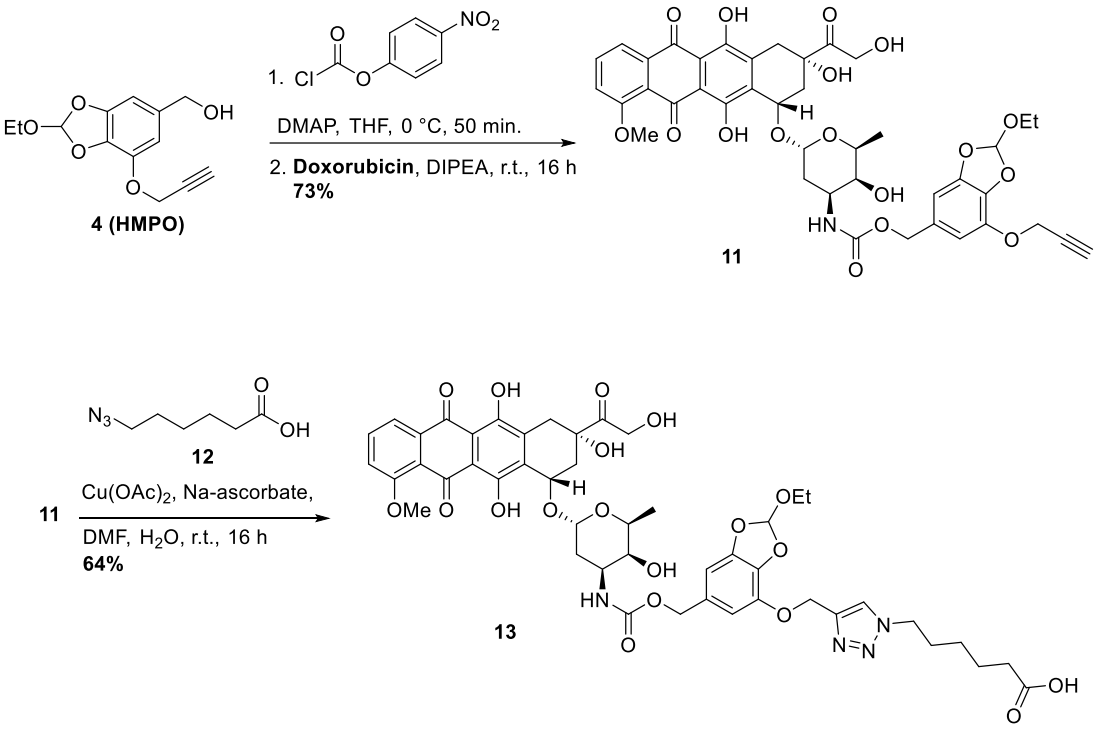

Scheme 6

For the synthesis of the system with Combretastatin A-4, HMPO was activated with $SOCl_2$ and treated with the payload to afford compound **14** (Scheme 7).

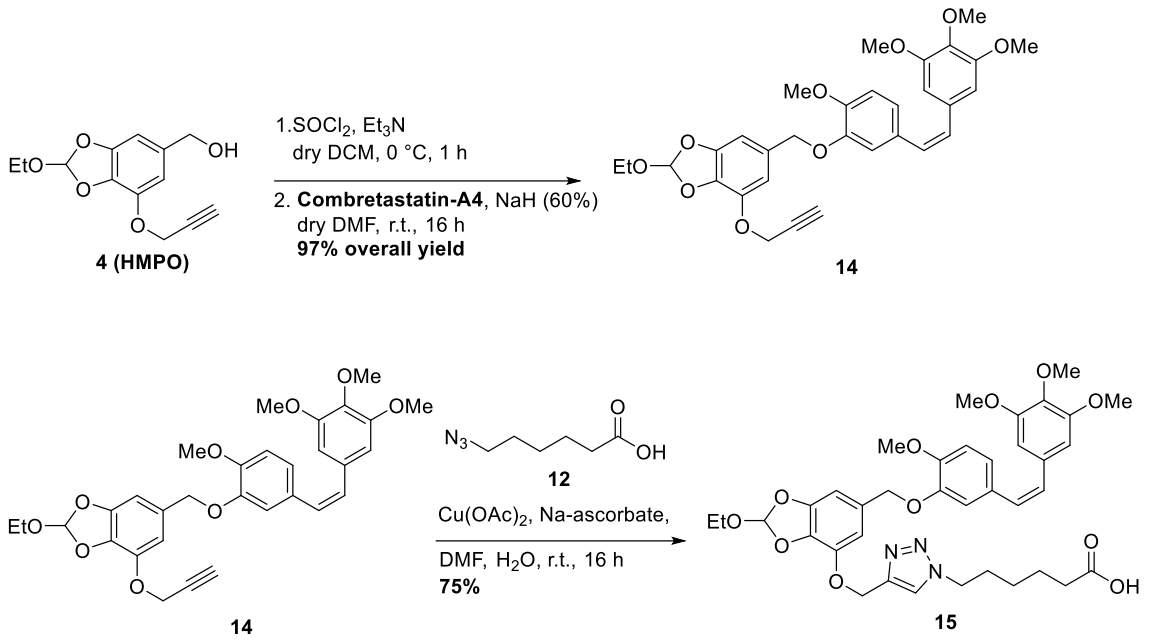

Scheme 7

The further CuAAC with 6-azidohexanoic acid gave compound **15** in good yield. In this case, the difficult step was the alkylation of the chloro derivative of compound **4**, as the classic conditions found for the model system **8** (K_2CO_3, KI) did not reach the product. NaH was the best choice and compound **14** was obtained in excellent yield.

When Doxorubicin or Combretastatin-A4 were inserted in the respective systems, the resulting compounds must be handled in dark conditions as both drugs are light sensitive (photodegradation for Doxorubicin and isomerization for Combretastatin-A4). [235,236]

Hydrolysis kinetics of compounds **11** and **14** were tested by HPLC at different pHs (5.5, 6.5, 7.4) in phosphate buffers and in water. For compound **11** the release of the payload at pH 5.5 was really fast and the *plateau* was reached after 6 hours (Figure 69):

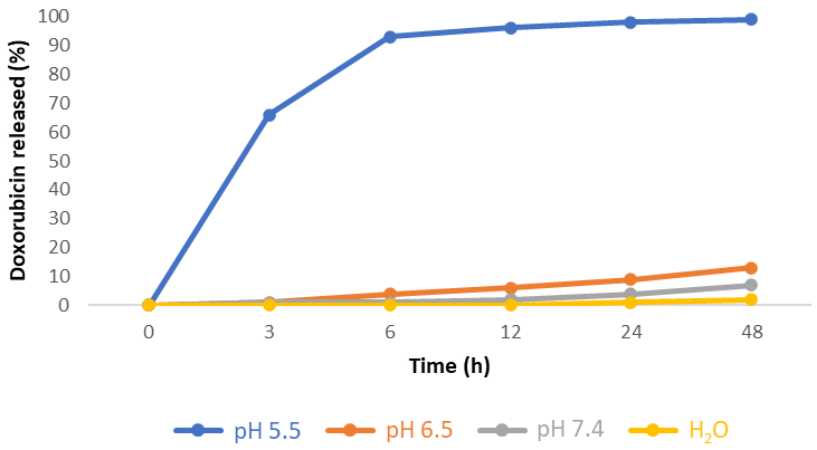

Figure 69- Hydrolysis kinetics of 11 at pHs 5.5, 6.5, 7.4 and H_2O.

On the other hand, the system remained stable at pHs 6.5, 7.4 and in H_2O at 37 °C for 48 hours. Similar results were obtained with compound **14**: only a little amount of Combretastatin-A4 was released after 48 hours at pH 6.5 and 7.4 but rapid hydrolysis occurred at pH 5.5 (Figure 70).

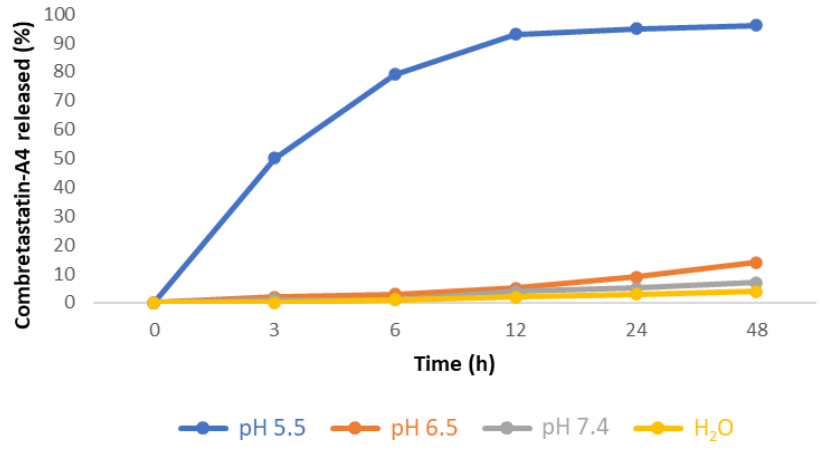

Figure 70- Hydrolysis kinetics of 14 at pHs 5.5, 6.5, 7.4 and H_2O.

In this case, the release of the payload was slightly slower than the system with Doxorubicin and the *plateau* was reached after 12 hours. The stability in plasma was also evaluated, showing that both compounds were quite stable (Table 2). With compound **11**, the T ½ value was in line with the general behaviour of Doxorubicin in plasma. [237]

Cmp.	H_2O [a]	pH 7.4, [a] $t_{1/2}$ [b]	pH 6.5, [a] $t_{1/2}$ [b]	Plasma, [a] $t_{1/2}$ [b]
11	99%	94%, >36 h	90%, >36 h	35%, 8.3 h
14	99%	95%, >36 h	93%, >36 h	89%, 27.6 h

Table 2- a) Value expressed as percentage of unmodified compound after 24 hours of incubation; b) Halflife (T ½) expressed as the amount of time it takes before half of the drug is hydrolyzed/degraded.

Once the stability/hydrolysis tests were achieved, the next step was the bioconjugation of compounds **13** and **15** with Cetuximab.

2.1.5 Bioconjugation of HMPO-payload systems with Cetuximab and biological tests

For bioconjugation with Cetuximab, we needed to activate carboxylic acid moieties of our systems. Indeed, the reaction involves the lysines of mAb which have -NH_2 groups available for the formation of amides.

Therefore, the carboxylic acids of compounds **13** and **15** were activated with *N*-hydroxysulfosuccinimide (S-NHS) and 1-ethyl-3-(3-dimethylaminopropyl)carbodiimide (EDC) to form the respective NHS-esters in PBS 7.4. Then, dialyzed Cetuximab (in PBS 7.4) was added to obtain the bioconjugate products **ADC-1** and **ADC-2** (Scheme 8).

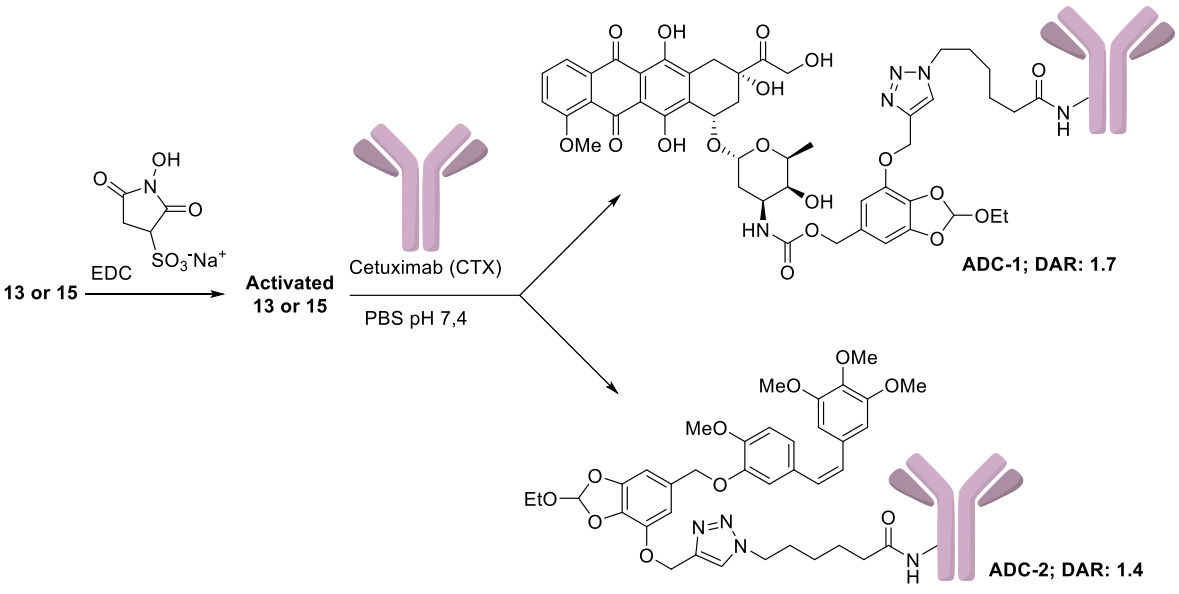

Scheme 8

The purification of **ADC-1** and **ADC-2** were carried out by dialysis using specific columns for cleanup of large biomolecules (such as proteins >5000 Mr) by removal of buffer salts and low molecular weight compounds. The DAR was determinated through MALDI analysis which showed good results (**ADC-1**: DAR= 1.7; **ADC-2**: DAR= 1.4).

The anti-proliferative activity (MTT assay) of **ADC-1** and **ADC-2** was evaluated in two cell lines: A549 (human lung carcinoma) and A431 (epidermoid carcinoma cell line). The results are reported in the following Figures:

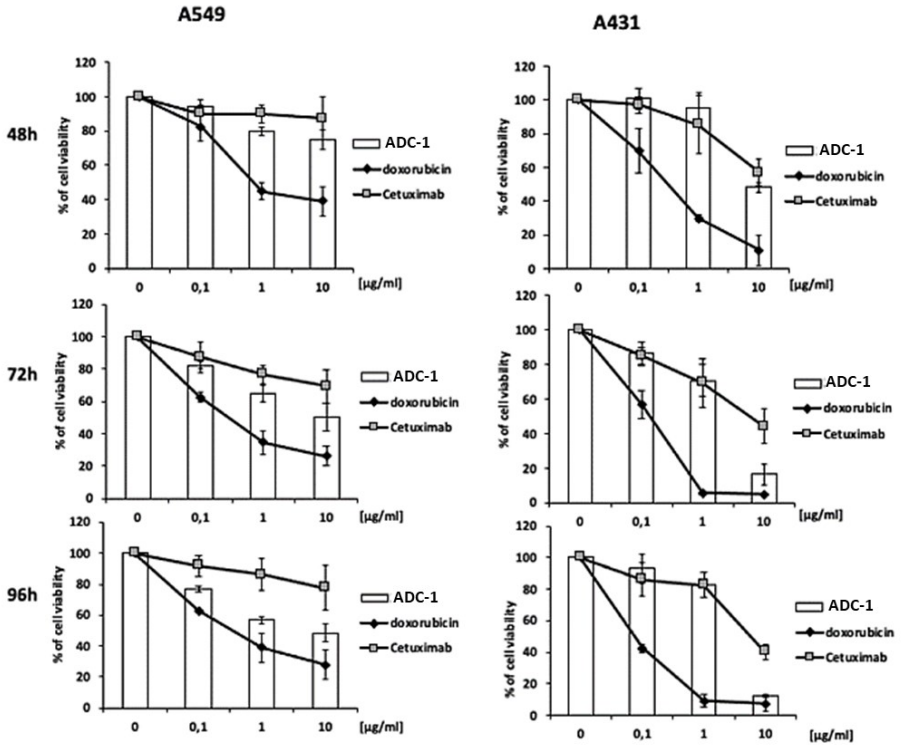

Figure 71- MTT assay of ADC-1.

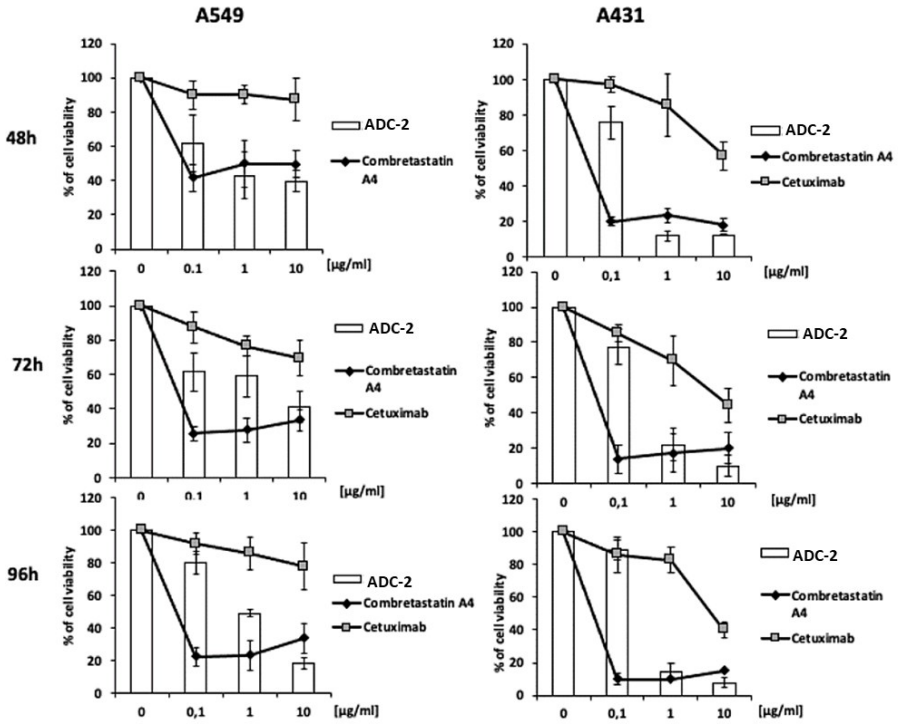

Figure 72- MTT assay of ADC-2.

In both cases, **ADC-1** and **ADC-2** showed an antiproliferative activity if compared to Cetuximab and the effect was comparable to the free drugs Doxorubicin and Combretastatin-A4. Moreover, HMPO linker alone was not toxic on cells employed in the tests.
These results demonstrated that HMPO was effective as linker for the release of various type of payloads; for this reason, we decided to use it also in our studies in ADCs charged with unconventional payloads.

2.2 ADCs charged with unconventional payloads and exploration of new protocols for bioconjugation

2.2.1 Amide-based drugs

As shown in the previous paragraph, HMPO can be employed to release the drugs containing amines, alcohols or phenols through formation of carbamates, carbonates or ethers. The 1,6-self-immolative process relies on molecules with high nucleofugacity, thus with amides the release of the drug can be very challenging. This is due to the low nucleophilicity of the amide nitrogen and the low acidity of amide hydrogen, which prevents nucleofugacity.

In this part of the work, we decided to investigate the use of *N*-acyl carbamates to develop a self-immolative linker for the release of amides (Scheme 9).

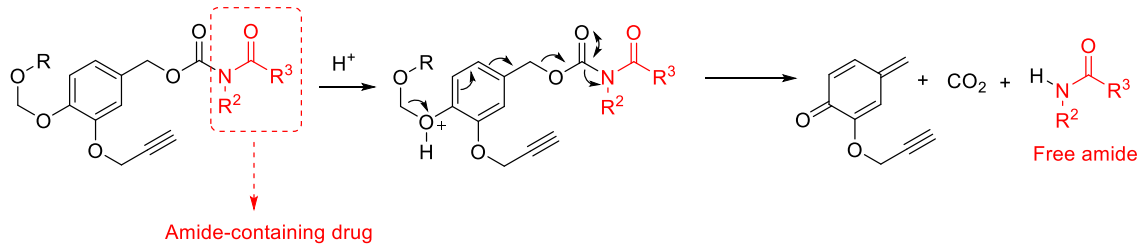

Scheme 9

As linkers we have chosen the HMPO, whose synthesis has been previously described, and the same scaffold in which the orthoester was replaced by methoxymethyl ether (MOM) or methoxyethoxymethyl ether (MEM). The synthesis of the last two linkers is reported in the following Scheme:

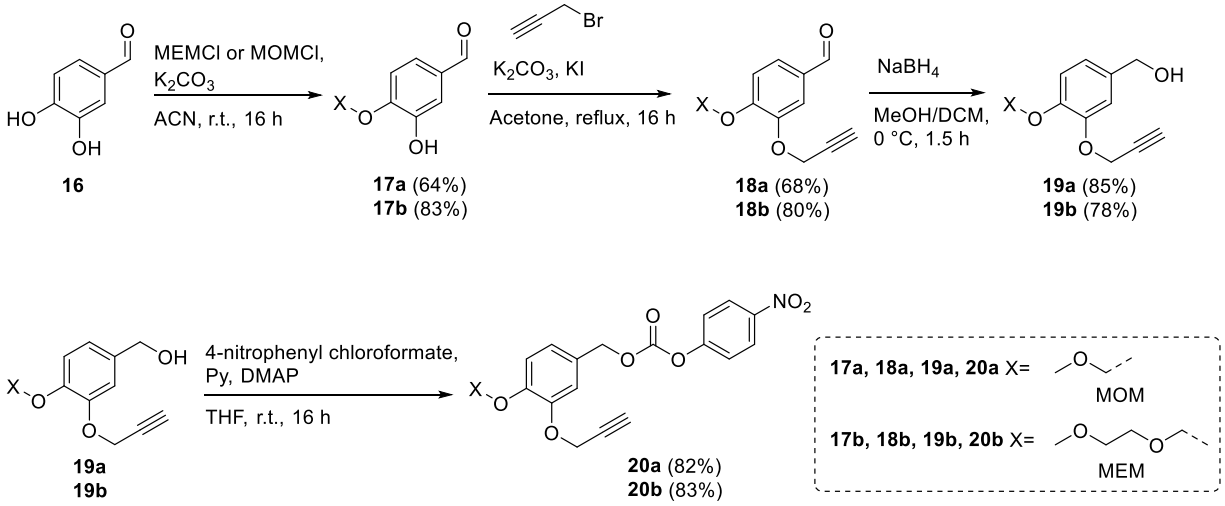

Scheme 10

In the first step, 3,4-dihydroxybenzaldehyde was protected in position 4 using MOMCl or MEMCl to obtain the corresponding products **17a** and **17b** in good yields. The other phenol group was alkylated with propargyl bromide using the same procedure applied for HMPO linker. Further reduction of **18a,b** with $NaBH_4$ gave alcohols **19a,b** which are the starting materials for the synthesis of *N*-acyl carbamates. Indeed, the activation of these linkers with

p-nitrophenyl chloroformate gave **20a,b**, which are relatively stable compounds and could be purified through flash chromatography. The yields of compounds with MOM protecting group were slightly worse than those with the MEM group due to purification issues. Compound **20a** was used to explore direct oxycarbonylation of Linezolid **21** or acylation of amine **22** (Table 3):

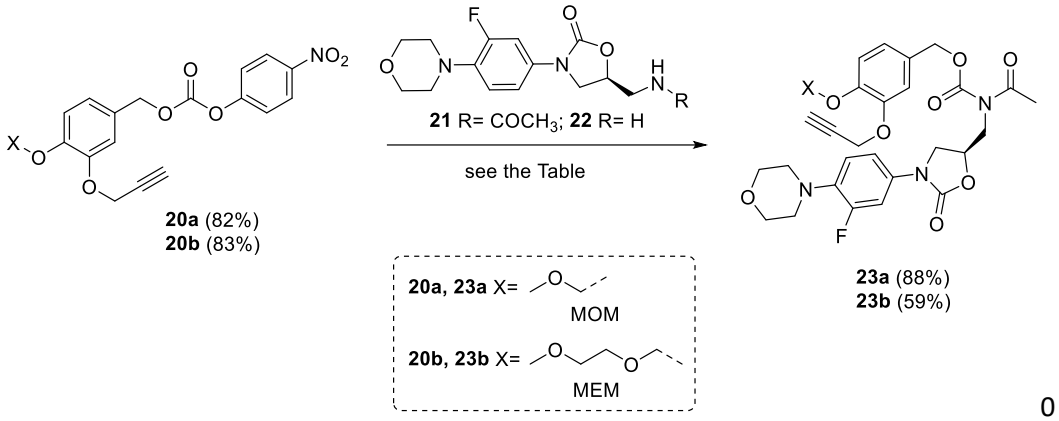

Entry	Reagents	Conditions	Product (Yield)
1	**20a**, **21**	DMAP (10%), Pyridine (2 eq.), DMF, r.t., 24 h	**23a** (-)
2	**20a**, **21**	DMAP (2 eq.), Pyridine (1 mL), DMF, r.t., 24 h	**23a** (10%)
3	**20a**, **21**	mTDB (2 eq.), DMF/THF, r.t., 24 h	**23a** (15%)
4	**20a**, **21**	NaH (2 eq.), THF, 0 °C → r.t., 24 h	**23a** (-)
5	**20a**, **22**	DIPEA, THF, r.t., 24 h then Ac_2O, DMAP (10%), Et_3N (4eq.), DCM, r.t., 24 h [a]	**23a** (21%)
6	**21, 20a**	KHMDS (1 eq.), THF, - 78 °C, 1 h then **20a**, THF, - 78 °C → -5 °C, 4 h	**23a** (88%)
7	**21, 20b**	KHMDS (1 eq.), THF, - 78 °C, 1 h then **20b**, THF, - 78 °C → -5 °C, 4 h	**23b** (59%)

Table 3- a) the intermediate carbamate was isolated as a crude product in 76% yield.

Treatment of **20a** with **21** in the presence of various bases and solvents gave only a little amount of the desired product, while a lot of unreacted starting materials were recovered (entries 1-4, Table 3). Better results were obtained by carbamoylation of amine **22**, which was carried out in good yields (entry 5, Table 3). However, acetylation of the resulting carbamate with Ac_2O, DMAP and Et_3N gave compound **23a** in low yield (entry 5, Table 3). Further attempts to increase the yield by changing the base were unsuccessful. The best result was obtained by deprotonation of amide **21** with KHMDS at -78 °C and subsequent reaction with **20a** at controlled temperature to obtain product **23a** in good yield (entry 6, Table 3). The same procedure was applied with compound **20b** to obtain **23b** in moderate yield (entry 7, Table 3).

Enzalutamide, a non-steroidal antiandrogen approved for the treatment of prostate cancer, [238] was chosen as a payload to obtain a similar system with a drug bearing different amide:

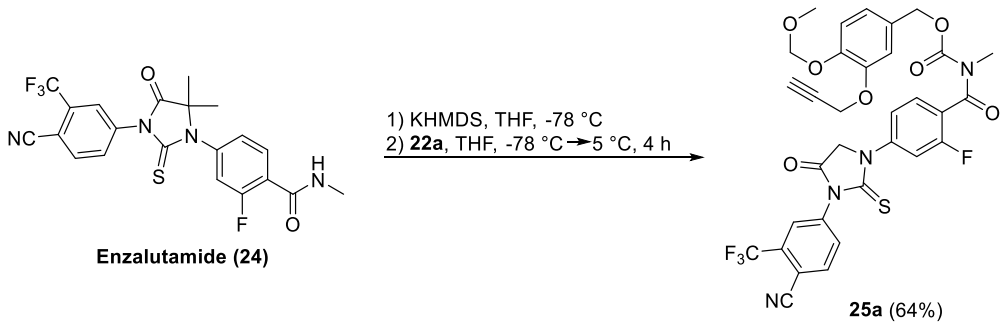

Scheme 11

The protocol was the same applied with Linezolid; the amide group of Enzalutamide was deprotonated with KHMDS and treated with the linker **22a** to obtain **25a** in moderate yields (Scheme 11). Once the synthesis linker-payload systems were achieved, we performed stability and release tests of **23a,b** and **25a** at pHs 4.5, 5.5 and 7.4 (Figures 73-75).

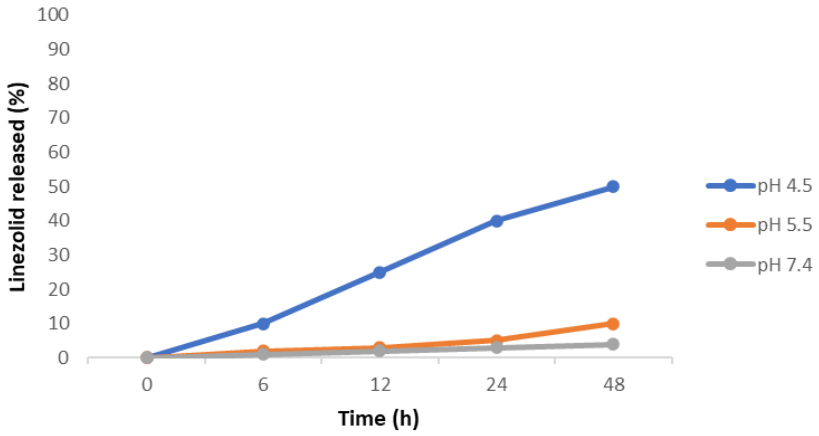

Figure 73- Stability and release tests of compound 23a.

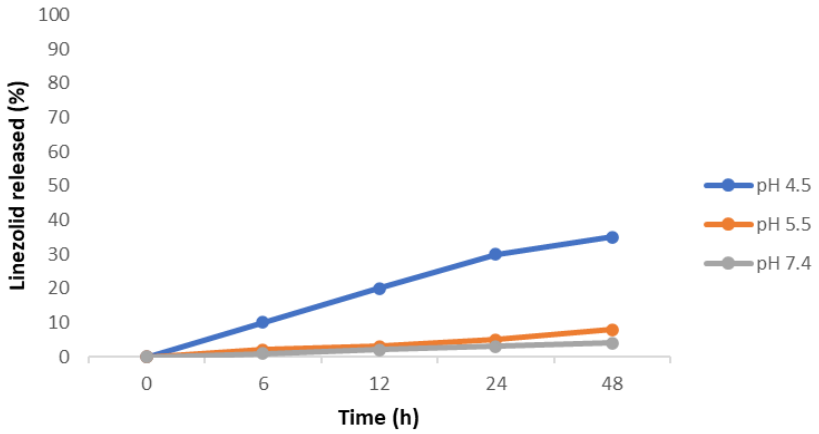

Figure 74- Stability and release tests of compound 23b.

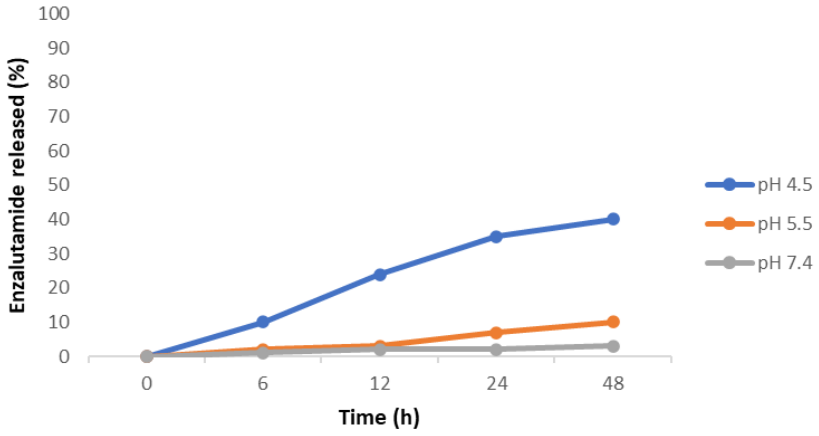

Figure 75- Stability and release tests of compound 25a.

These data show that the use of MOM and MEM protecting groups as triggers were ineffective in releasing the amide-based drugs. Compounds **23a,b** and **25a** were stable at pH 7.4 for 48 h but only about 40-50% of respective payloads were released after 48 hours at pH 4.5.

Therefore, we decided to explore the release of amides using HMPO linker which was already applied with excellent results for the release of amine and phenol-based drugs. In this case, Linezolid **(21)**, Enzalutamide **(24)**, Tasimelteon **(26)** and *p*-Toluensulfonamide **(27)** were chosen as payloads. Tasimelteon is a drug developed for the treatment of non-24-h sleep wake rhythm disorder [239] while *p*-Toluensulfonamide mimics the behaviour of primary amides. Thus, for all drugs the amide moieties were deprotonated with KHMDS and treated with activated HMPO **28**:

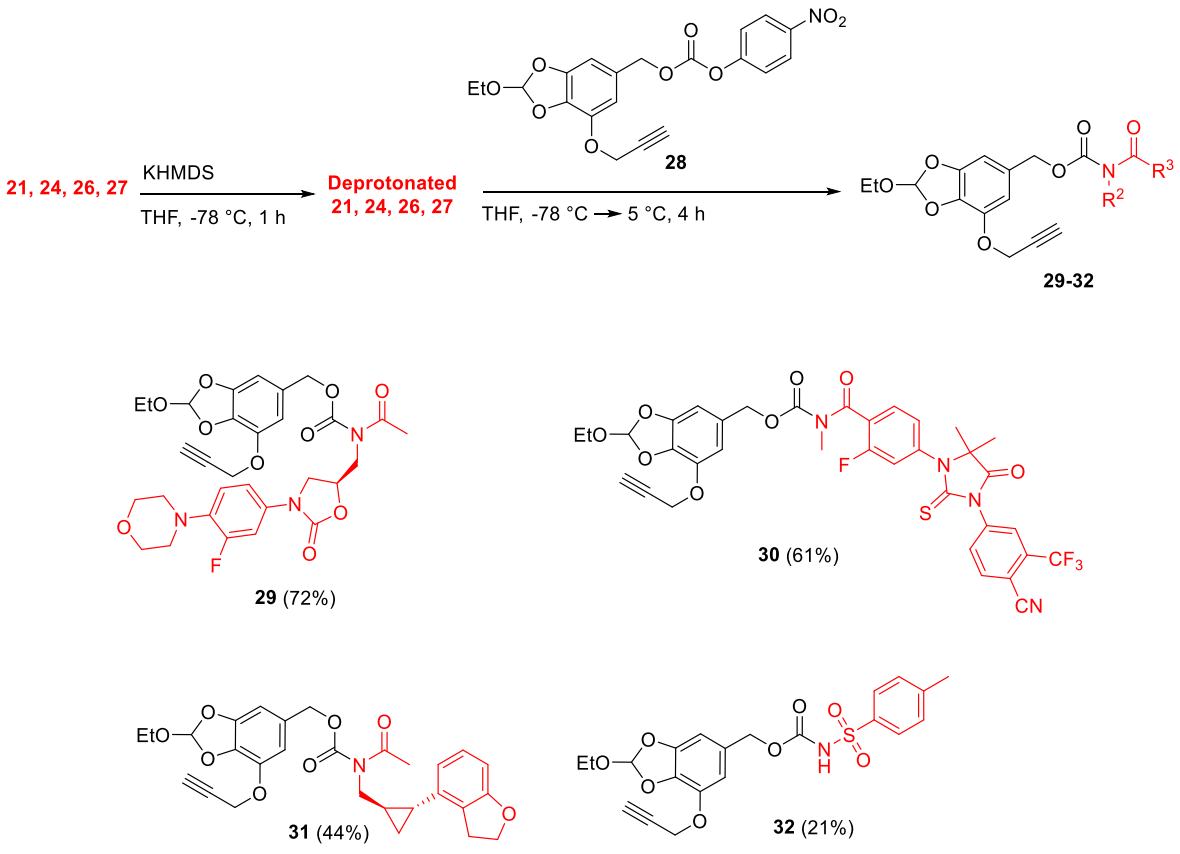

Scheme 12

Compounds **29-32** were obtained in good to acceptable yields. Only compound **32** was recovered in low yield due to a lot of unreacted starting material and purification issues.

Stability tests of products **29-32** show that they were stable in human plasma and in PBS at pH 7.4:

Cmp.	H_2O, [a] $t_{1/2}$ [b]	pH 7.4, [a] $t_{1/2}$ [b]	Plasma, [a] $t_{1/2}$ [b]
29	>99%, >48 h	94%, >48 h	95%, >24 h
30	>99%, >48 h	95%, >48 h	89%, >24 h
31	>99%, >48 h	95%, >48 h	89%, >24 h
32	>99%, >48 h	92%, >48 h	84%, >24 h

Table 4- a) Value expressed as percentage of unmodified compound after 48 h (water and PBS solution) or 24 h (plasma) of incubation; b) half-life ($t_{1/2}$) expressed as the amount of time it takes before half of the drug is degraded.

Hydrolysis kinetics of compounds **29-32** at pH 5.5 were check through HPLC-MS analysis as reported in the following figure:

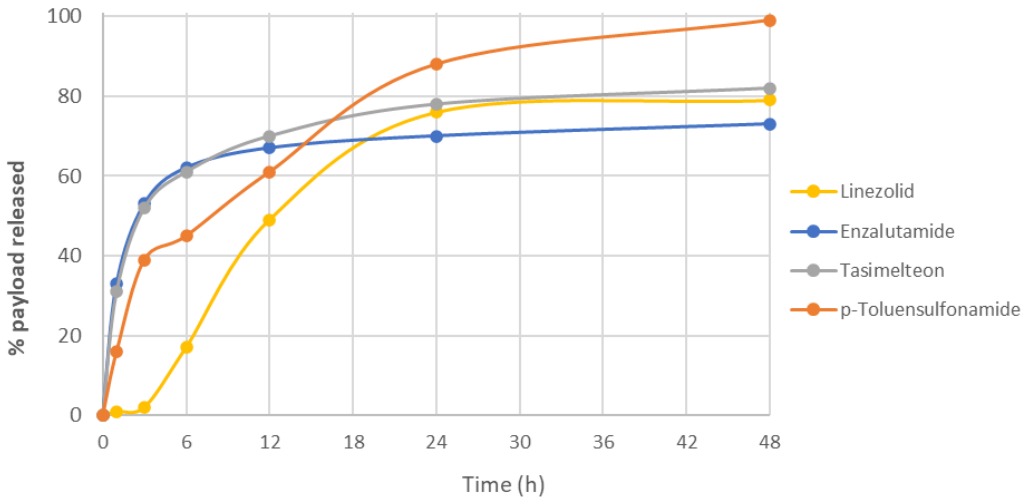

Figure 76- Hydrolysis kinetics of compounds 29-32 at pH 5.5. All the tests were carried out by using 10mM DMSO solution and incubated with the respective buffer at 37 °C as described in the experimental part.

After 48 hours, about 70-80% of Linezolid, Enzalutamide and Tasimelteon were released. In the case of the more acidic *p*-Toluensulfonamide derivative, complete release (100%) was achieved after 48 h.

Once again, the HMPO platform showed to be suitable for the release of different types of drugs, including the most challenging amides.

2.2.2 Antibody-drug-conjugates charged with Cyclopamine

2.2.2.1 Synthesis of linker-payload systems

Cyclopamine was the first SMO inhibitor discovered but problems such as low solubility in water and acid lability prevent its use in clinic. Over the years, several derivatives have been developed (*e.g.* Saridegib, Sonidegib, Galsdegib, Vismodegib, Taladegib) but for some of these products the problem related to drug resistance still remains. For this reason, our goal was to synthesize new ADCs charged with Cyclopamine using different linker technologies. As linkers, we thought about the possibility to use the orthoester pH-sensitive linker which was previously described and another non-cleavable linker based on maleimido derivatives. In the first case, the orthoester **4** was activated with 4-nitrophenyl chloroformate to give **28**. Further reaction of **28** with Cyclopamine gave the desired product **33** (Scheme 13).

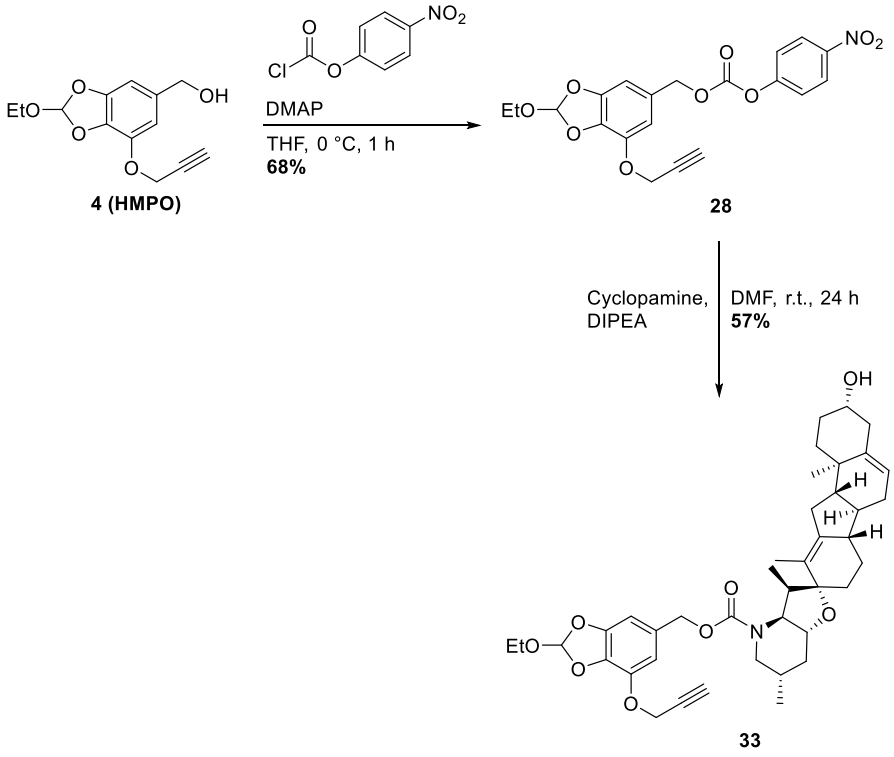

Scheme 13

The difficult step was the isolation of carbonate **28**, as it was unstable in silica gel when purified through chromatography. Nevertheless, a quick separation of **28** by flash chromatography allowed the further reaction with Cyclopamine which gave product **33** in good yield, even if sometimes contaminated with *p*-nitrophenol.

Linker-payload system **33** was treated with compound **12** in the same manner described for Doxorubicin and Combretastatin-A4; this click reaction allowed the insertion of carboxylic acid moiety which is required for bioconjugation with Cetuximab:

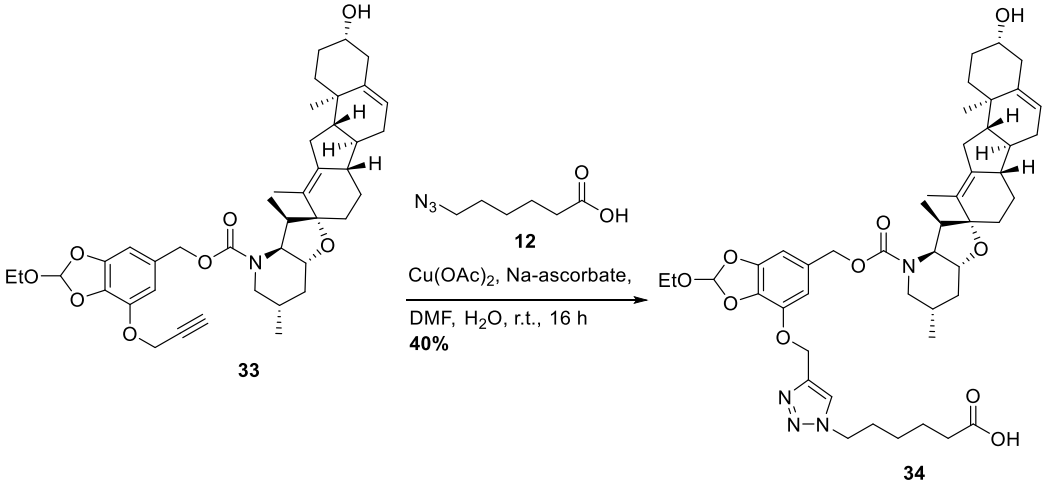

Scheme 14

Once the synthesis of compound **34** was achieved, our focus was on development of another type of linker that would allow for a different mechanism of release. Maleimido group is quite different from the orthoester. Indeed, it is stable in an acidic environment and, depending on the chemistry of the linker, releases the payload after complete degradation of the ADC or retro-Michael reaction. [103,240]

For the synthesis of non-cleavable linker, the first step was the reaction between maleic anhydride and propargyl amine which gave the intermediate **35** (Scheme 15). Then, the cyclization with Ac_2O in the presence of AcONa led to product **36**:

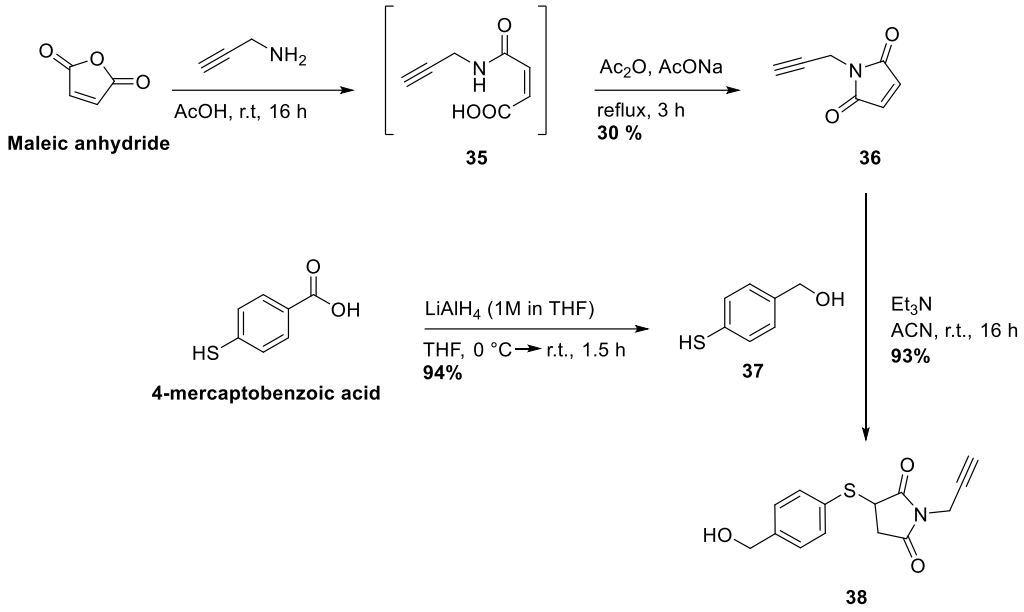

Scheme 15

At the same time, 4-mercaptobenzoic acid was reduced with $LiAlH_4$ (1M in THF) and the corresponding product **37** was treated with **36** to obtain compound **38** in good yield. There were two critical points in this synthesis: first the intramolecular condensation of intermediate **35** and second the handling of compound **37**. For the condensation, it was essential to remove all the acetic acid derived from the first step to push the reaction towards the formation of product **36**. Indeed, CH_3CO_2H was also the side-product of the cyclization and its excess slowed down the reaction and limited the yield of compound **36**. The second critical point was the handling of compound **37** which easily reoxidized to give the starting material 4-mercaptobenzoic acid. Thus, product **37** was used immediately after its synthesis or kept in the freezer for a few weeks.

Product **38** has a benzylic alcohol which needs to be activated for the reaction with $-NH_2$ group of Cyclopamine. Therefore, the activation was carried out with 4-nitrophenyl chloroformate and the resulting product treated with Cyclopamine:

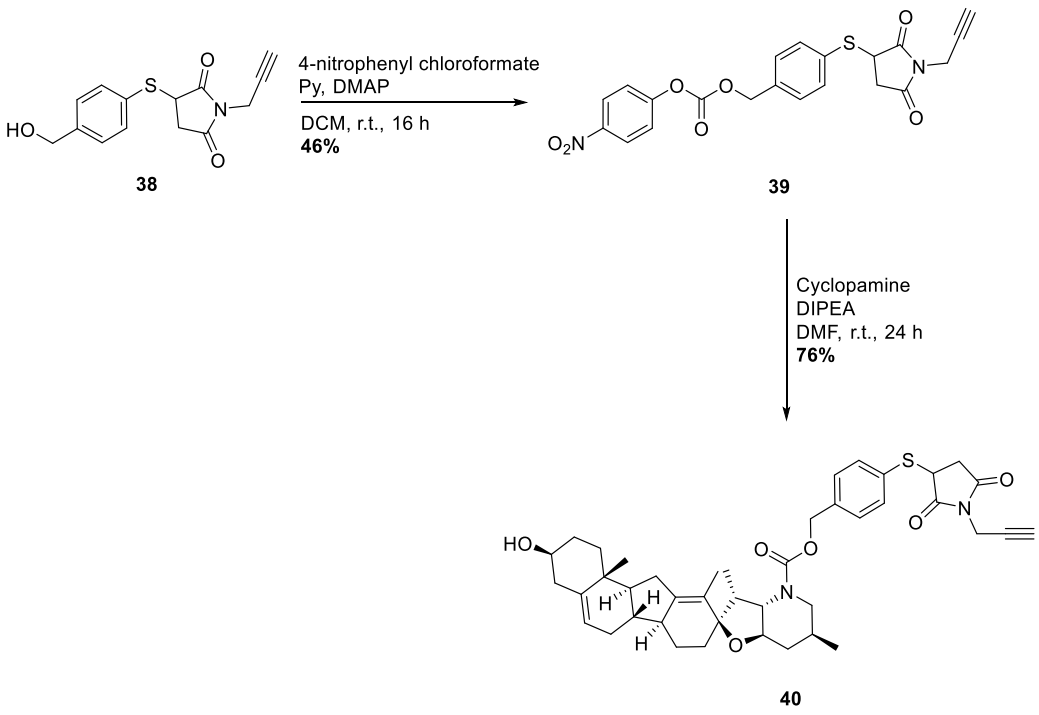

Scheme 16

Similarly to the orthoester linker, product **40** was subjected to a click reaction for the insertion of the carboxylic acid moiety (Scheme 17).

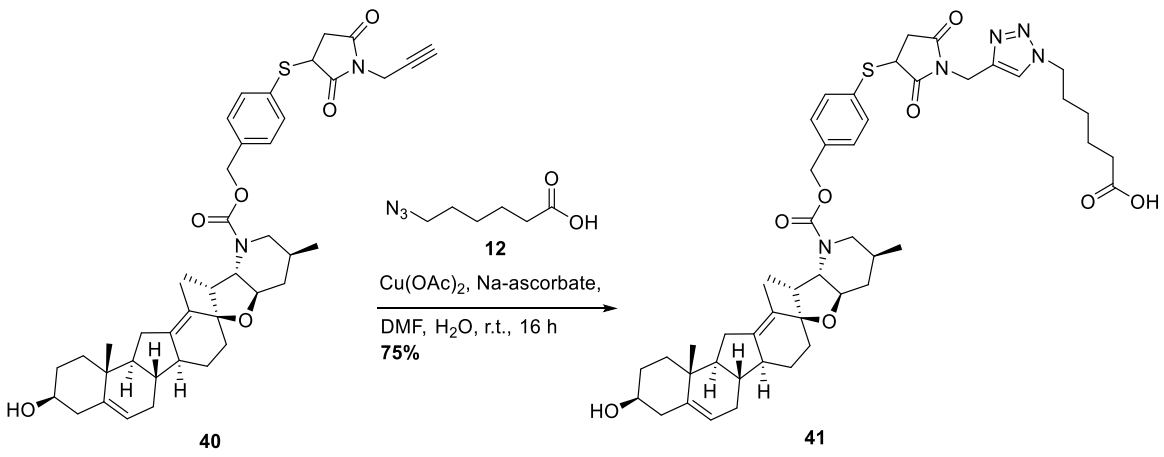

Scheme 17

Once compounds **34** and **41** were obtained, we explored the bioconjugation with mAb Cetuximab.

2.2.2.2 Bioconjugation of linker-payload systems 34 and 41 with Cetuximab

Bioconjugation of compounds **34** and **41** with Cetuximab was explored using two different methods:

- Bioconjugation with lysines of Cetuximab;
- bioconjugation with functionalized Cetuximab.

In the first case, we activated the carboxylic acid moiety of our products with NHS or S-NHS and then bioconjugated them with lysines of mAb.
In the other case, we treated both the antibody and our compounds in a chemical manner to insert specific linkers which allowed the bioconjugation through a click chemistry reaction in buffer solution.

2.2.2.2.1 Bioconjugation with lysines of Cetuximab

Linker-payload systems **34** and **41** were activated with NHS:

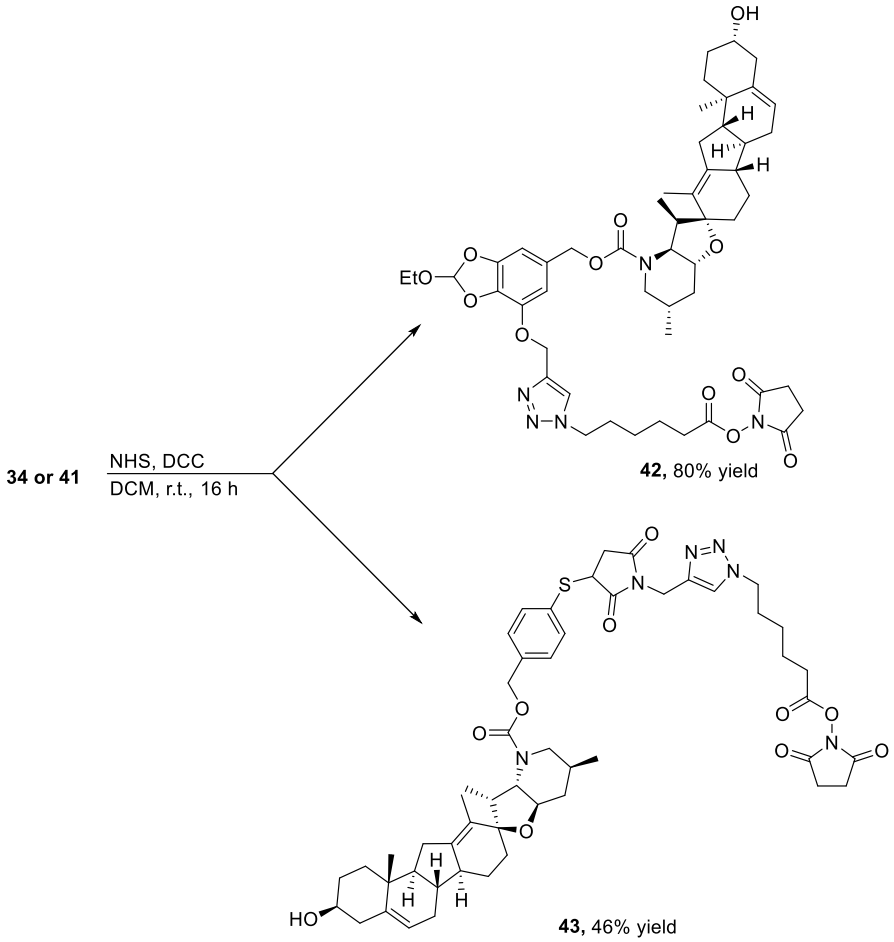

Scheme 18

For compound **42,** the bioconjugation with Cetuximab was tried in PBS (phosphate buffered-saline) or EPPS (*N*-(2-Hydroxyethyl)piperazine-*N*′-(3-propanesulfonic acid)) buffer solutions at different pH values, as reported in the following Table:

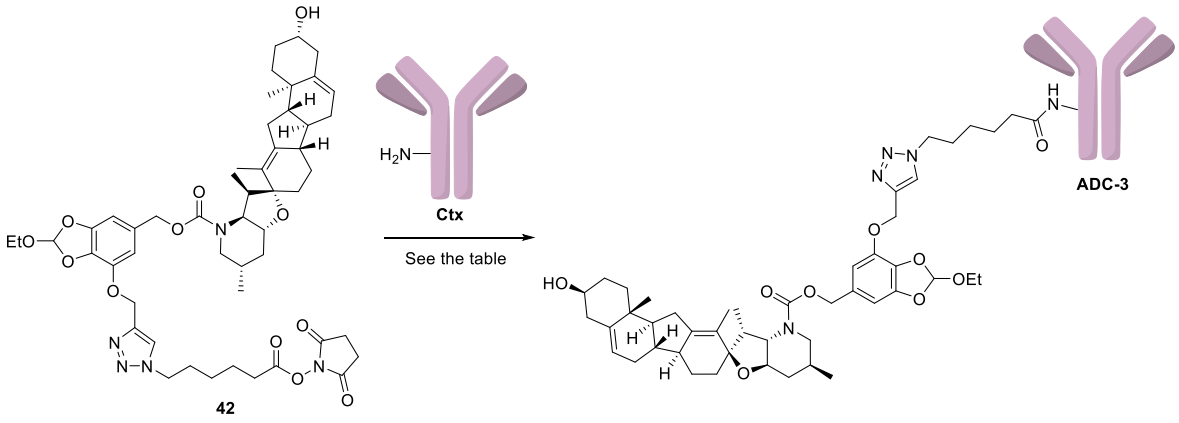

Entry	Buffer	Ratio (linker-payload: mAb)	DAR
1	PBS pH 7.4	20:1	0.5
2	EPPS pH 8	20:1	0.6
3	EPPS pH 8	40:1	0.7
4	EPPS pH 8	80:1	0.4

Table 5

In entry 1 (Table 5), using PBS buffer solution at pH 7.4 we obtained a low DAR. Although pH 7.4 is an optimal value of pH for the stability of Cetuximab, in our case only a little amount of product **42** reacted with amino groups of Cetuximab.

The use of EPPS buffer solution at pH 8 (entries 2-4, Table 5) needs more explanation. This idea arose from the need to replace the PBS pH 7.4 with something that would increase the reactivity of both linker-payload system and the amino moieties of monoclonal antibody. The use of EPPS was already described in literature and successfully applied in the case of Camptothecin (which is also a hydrophobic payload), even if at pH 7.4. [241] In addition, the reactivity of NHS-ester is well known, and the optimal range is between pH 7-9. [242] By combining this information with the greater reactivity of lysines at higher pHs (because they are less protonated) we thought of EPPS at pH 8. EPPS is an acidic compound and pH 8 buffer solution was achieved by treatment with NaOH.

However, only a slight improvement was observed in our case (entries 2-3, Table 5) along with worse results when the ratio was increased from 40:1 to 80:1, maybe due to the presence of antibody aggregates. Excellent results were obtained when compound **34** was activated *in situ* with S-NHS and bioconjugated with Cetuximab:

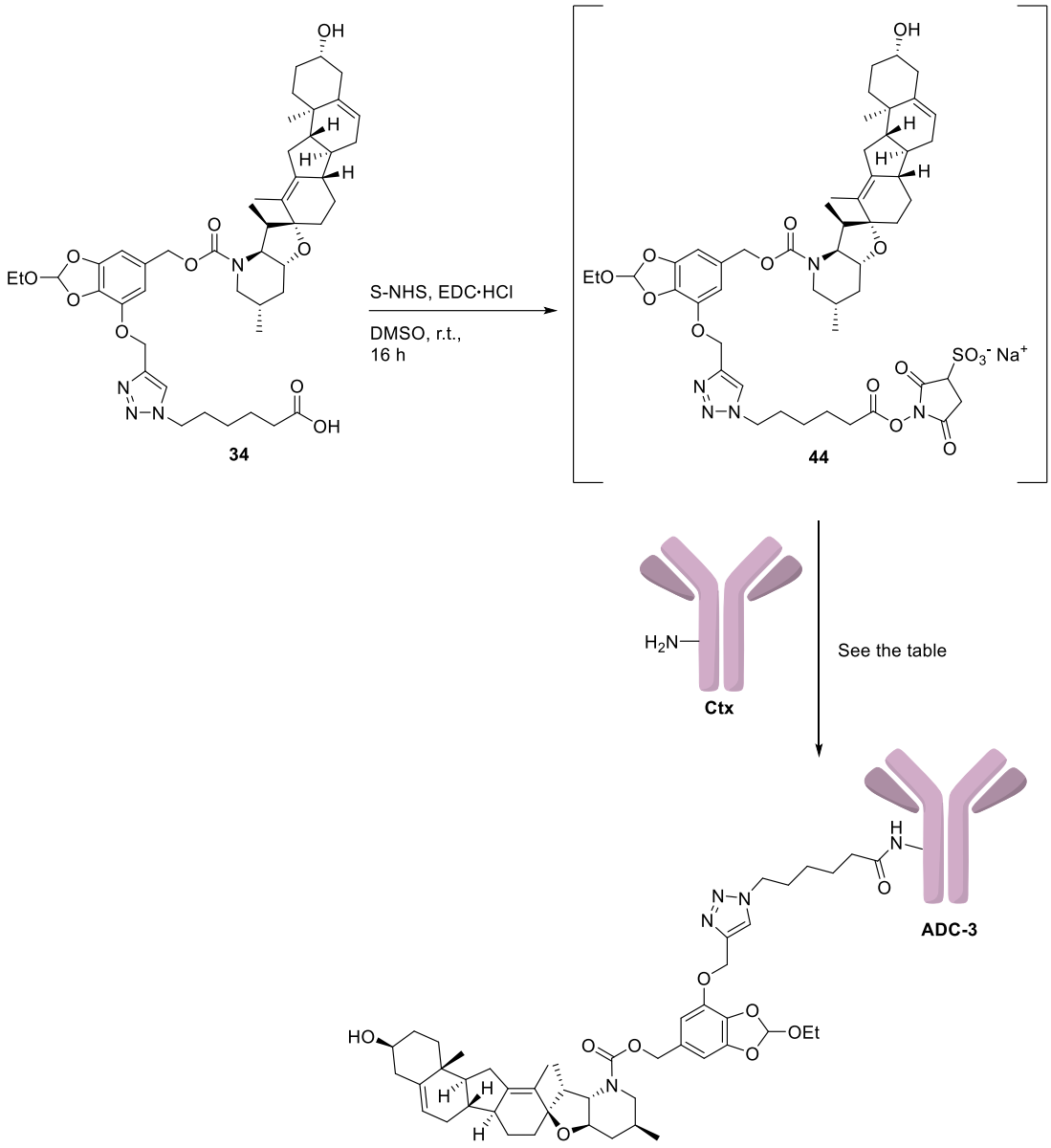

Entry	Buffer	Ratio (linker-payload: mAb)	DAR
1	EPPS pH 8	10:1	-
2	EPPS pH 8	20:1	7
3	EPPS pH 8	40:1	10

Table 6

While using 10:1 (linker-payload: mAb) stoichiometric ratio did not lead to good results (entries 1-2, Table 6), MALDI analysis of **ADC-3** made with 20:1 or 40:1 ratios showed optimal DARs (entries 2-3, Table 6). Thus, these ADCs were sent to ISPRO (Istituto per lo

Studio, la Prevenzione e la Rete Oncologica) in Florence for a further investigation of biological activity on various melanoma cell lines. In this case, by using S-NHS instead of NHS better results were obtained, perhaps due to the higher solubility of activated intermediate **44** which contained -SO_3^- Na^+ moiety.

For the bioconjugation of product **43** with non-cleavable linker, the same approach was investigated. First attempts by using the succinimide ester **43** gave good results when a 80:1 (linker-payload: mAb) stoichiometric ratio was used (entry 4, Table 7):

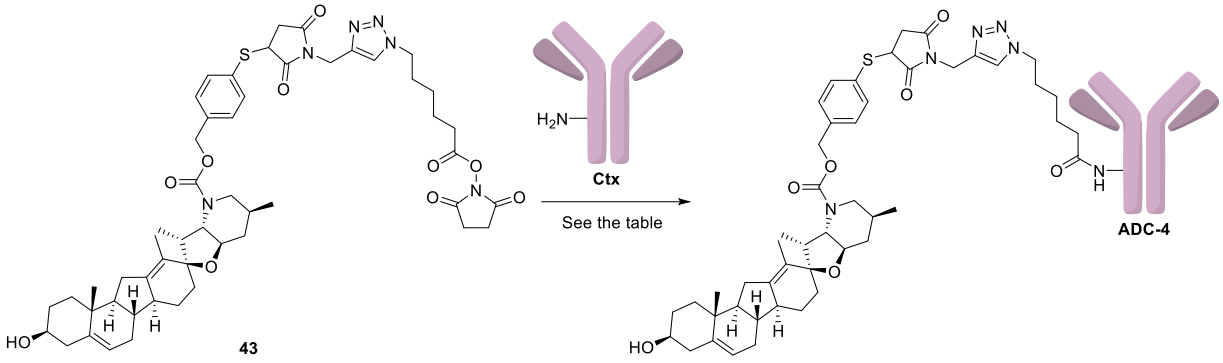

Entry	Buffer	Ratio (linker-payload: mAb)	DAR
1	PBS pH 7.4	20:1	0.3
2	PBS pH 7.4	40:1	0.2
3	EPPS pH 8	40:1	-
4	PBS pH 7.4	80:1	2

Table 7

In an opposite way to what had been observed with the orthoester linker, in this case PBS buffer solution at pH 7.4 seems to be the best choice for the bioconjugation process. Moreover, an 80:1 stoichiometric ratio was required to obtain a good DAR (2) for the evaluation of biological activity. Other tests by reducing the amount of linker-payload system were carried out but with poor results (entries 1-3, Table 7).

The in situ activation and bioconjugation of compound **41** with Cetuximab was also explored but with worse DAR values:

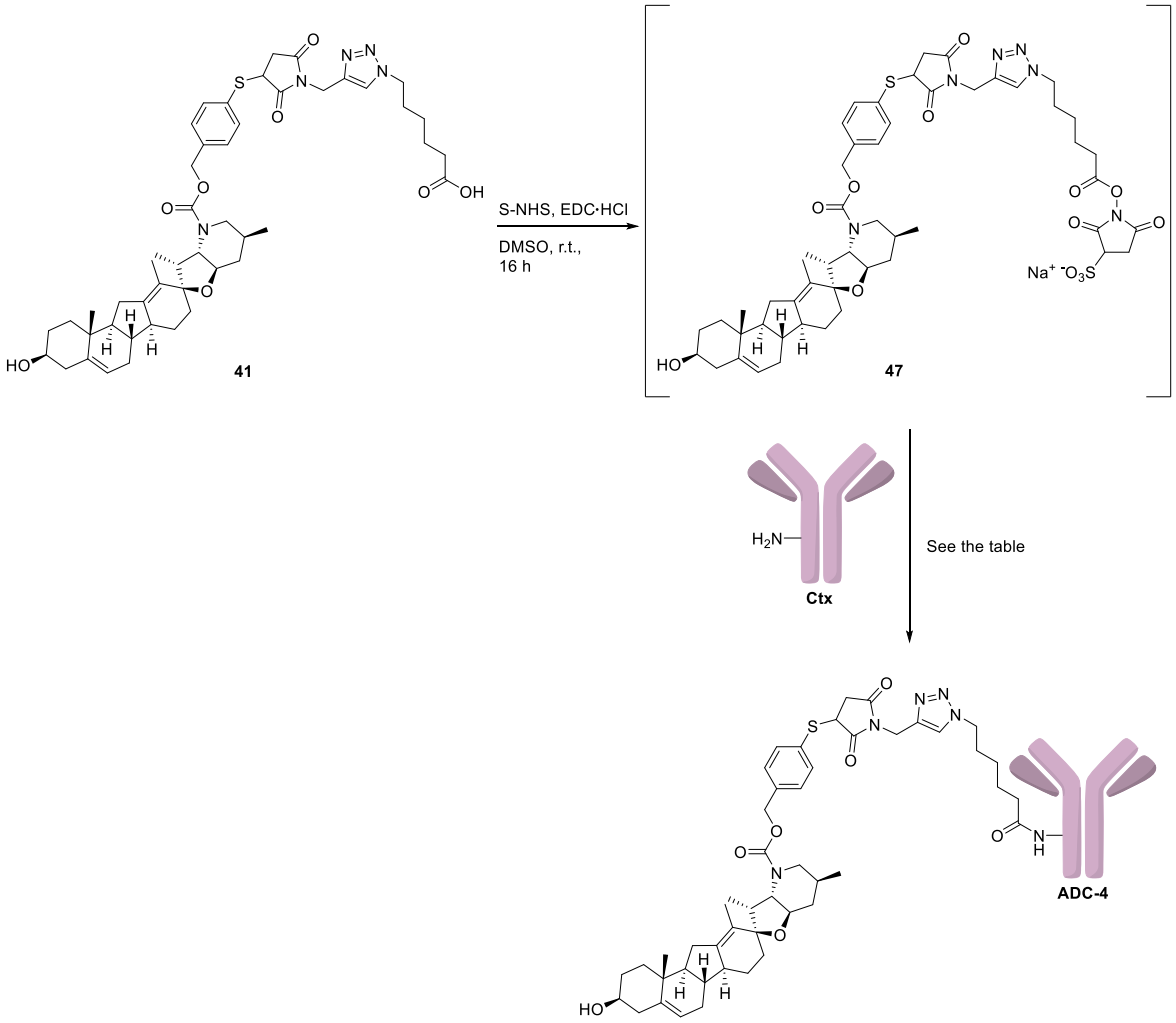

Entry	Buffer	Ratio (linker-payload: mAb)	DAR
1	PBS pH 7.4	20:1	0.1
2	PBS pH 7.4	80:1	0.7

Table 8

However, for the bioconjugation of compound **47** only PBS pH 7.4 has been explored as a buffer solution and further optimization of bioconjugation conditions (*i.e.* using EPPS pH 8) is underway.

Nevertheless, after all the tests we had in our hands some ADCs with good DAR values (**ADC-3** with DAR of 7 or 10 and **ADC-4** with a DAR of 2) and suitable for the evaluation of biological activity.

2.2.2.2.2 Bioconjugation with functionalized Cetuximab

The other strategy involved the functionalization of both Cetuximab and linker-payload systems to achieve a Copper-free click chemistry in buffer solution:

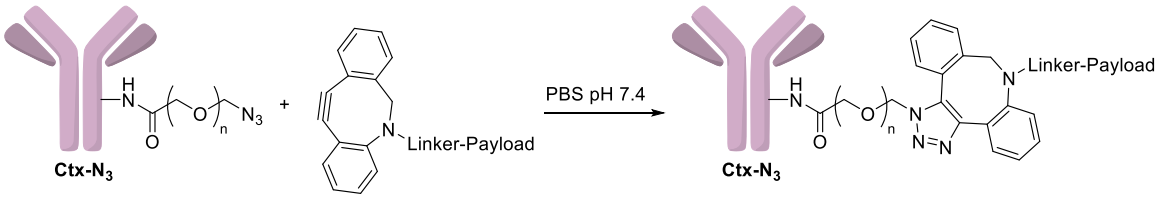

Scheme 19- General strategy for bioconjugation of the linker-payload system with functionalized Cetuximab.

The use of this method leads to some considerations:

- The insertion of PEG (polyethylene glycol) chain could improve the stability of the final product, especially in the case of hydrophobic payloads such as Cyclopamine or high DARs;

- the presence of dibenzocyclooctyne (DBCO) allows for a strain-promoted alkyne azide cycloaddition (SPAAC) with the azido groups of Cetuximab without the use of copper catalysts. Therefore, this method avoids the problems related to the possible presence of copper in the final product such as cytotoxicity on cells;

- the functionalization of Cetuximab leads to greater distance between mAb and Cyclopamine, thus reducing the interactions and allowing for a more efficient bioconjugation process;

- another consideration is that through this method a more controlled DAR can be obtained. Indeed, the linker-payload system can react only with azido groups and the DAR depends solely on the number of azido groups on the antibody.

Based on literature data, we found an interesting work made by Anderson and co-workers in which they used SPAAC cycloaddition for bioconjugation of cross-bridged macrocyclic chelators with Cetuximab. [243] Thus, we adapted the experimental conditions to our case. To

explore this bioconjugation protocol and have an idea of the efficiency of the process we started from activated NHS-ester compound **43** which had the non-cleavable linker.

A stock solution of linker-payload system (10 mM in DMSO) was treated with dibenzocyclooctyne-amine (DBCO-NH_2, 10 mM in DMSO) in 1:1 stoichiometric ratio:

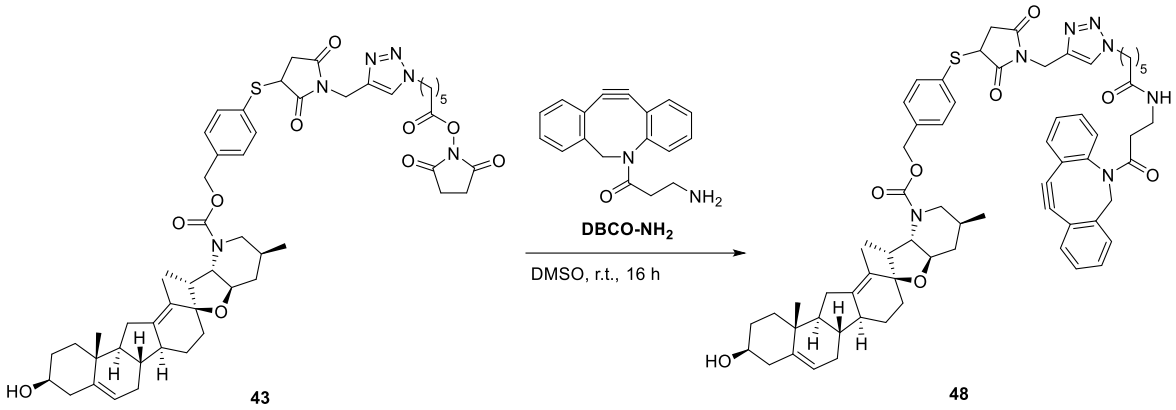

Scheme 20

The intermediate **48** was not isolated, but the resulting solution was directly used for bioconjugation with functionalized Cetuximab. However, the presence of compound **48** was confirmed by MS analysis which also provided some information for the disappearance of starting materials **43** and DBCO-NH_2.

The insertion of PEG chain on Cetuximab was achieved starting from azido-PEG4-acid which was activated with NHS:

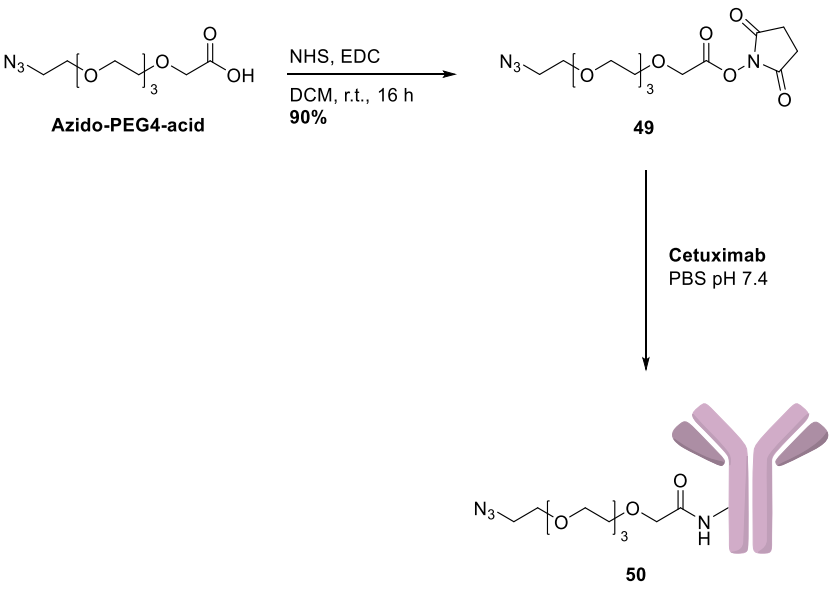

Scheme 21

Compound **49** was bioconjugate with lysines of Cetuximab and the results are reported in the following Table:

Entry	Buffer	Ratio (cmp. 49: mAb)	DAR
1	PBS pH 7.4	20:1	0.5
2	PBS pH 7.4	40:1	1.7
3	EPPS pH 8	20:1	0.9

Table 9

In entries 1 and 3 (Table 9) a 20:1 stoichiometric ratio was used in different buffers but with low DARs. In entry 2 (Table 9), 40:1 ratio gave the desired product with a good DAR value. Product **50** was used in the next step for SPAAC with compound **48** (Table 10):

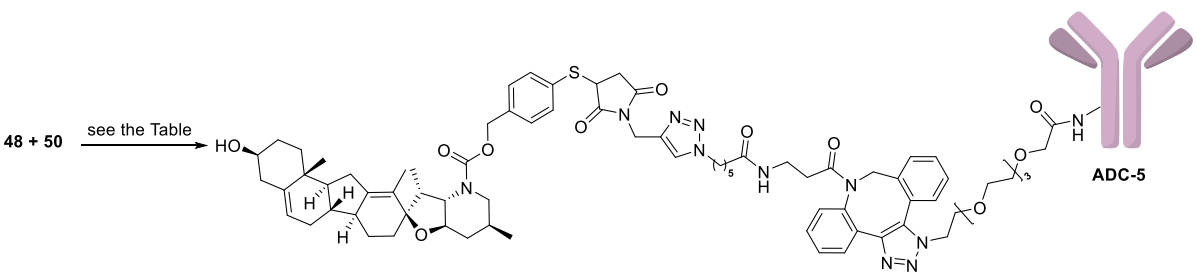

Entry	Buffer	Ratio (cmp. 48: 50)	DAR
1	PBS pH 7.4	20:1	0.6
2	PBS pH 7.4	40:1	0.7
3	PBS pH 7.4	80:1	1

Table 10

SPAAC cycloaddition required 80:1 stoichiometric ratio (cmp **48**: cmp. **50**) and long reaction time (16 hours at 0 °C). However, these conditions are in line with literature data, [243] and we successfully obtained the final **ADC-5** with DAR=1. As for the other compounds, **ADC-5** was sent to ISPRO in Florence for the evaluation of biological activity.

2.2.2.2.3 Biological tests of **ADC-3**, **ADC-4** and **ADC-5**

For the evaluation of biological activity of our products **ADC-3**, **ADC-4** and **ADC-5**, two melanoma cell lines were chosen: A375 and SKMEL5. Both express the EGFR receptor (which is the target antigen of Cetuximab) and some proteins involved in Hedgehog pathways such as Hsp90, GLI1 and GLI2 (Figure 77).

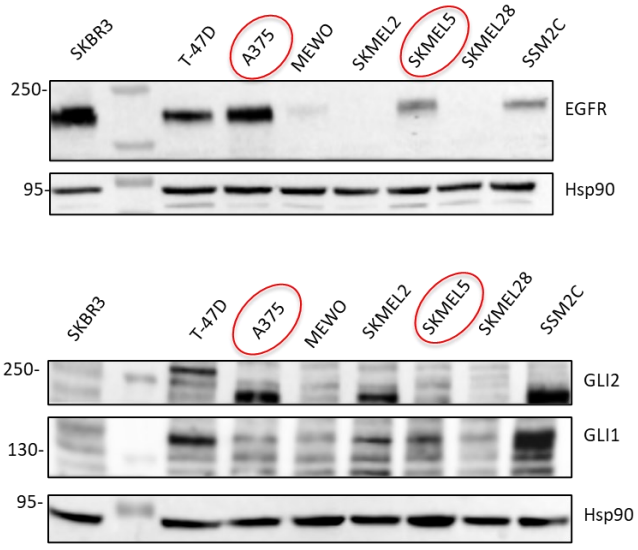

Figure 77- Western blot analysis for the evaluation of EGFR, Hsp90, GLI1 and GLI2.

Therefore, MTT assay on A375 and SKMEL5 were performed for all ADCs with different DAR values and the results are reported in the following Figure:

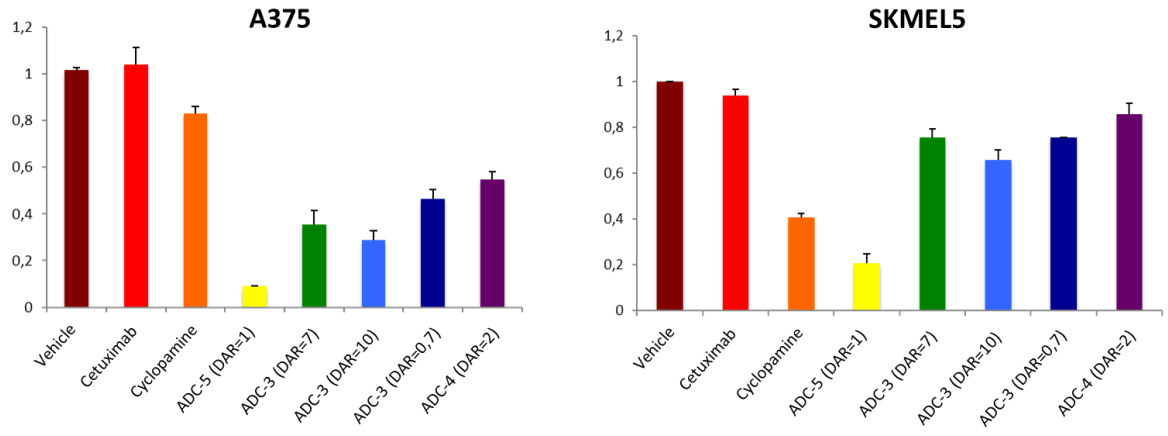

Figure 78- MTT assay of ADCs 3-5 on A375 (after 96 hours) and SKMEL (after 72 hours) cell lines. In the ordinate axis is the % of live cells. The study was carried out with a concentration of ADCs 3-5 of 1 µg/mL (7nM).

Interestingly, in both A375 and SKMEL5, our **ADCs 3-5** showed a stronger antiproliferative effect if compared to the reference drug Cyclopamine. For A375 cell line, after the treatment with Cyclopamine, about 80% of cells survived while in the case of our ADCs the percentage dropped to less than 20% for **ADC-5** (Figure 78). A similar outcome was observed in SKMEL5 where again **ADC-5** proved to be the most effective (Figure 78). Western blot analysis was performed to investigate the targets of HH and EGFR signaling pathways after treatment of cells with Cyclopamine and our **ADCs 3-5**:

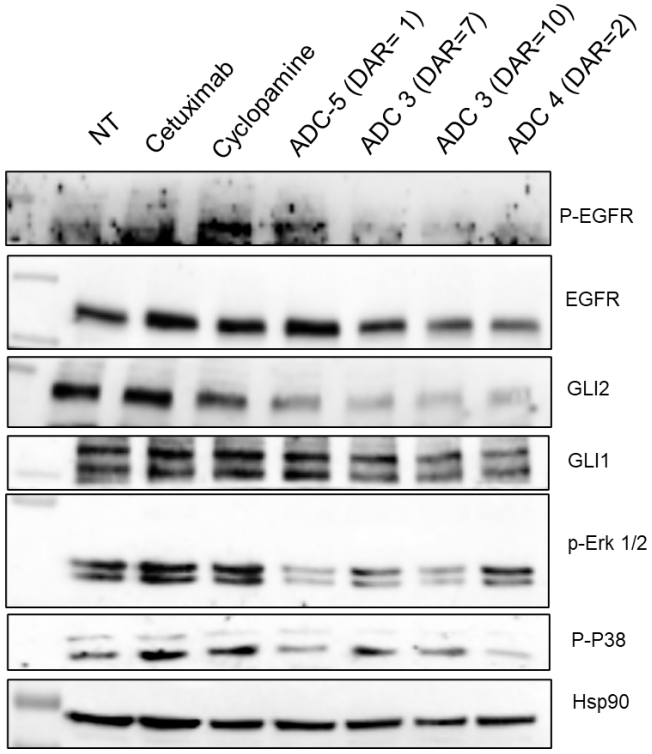

Figure 79

To conclude this part of the work we can say that for A375 and SKMEL5 cell lines, **ADC-5** was the most effective among all the bioconjugate products. **ADC-3** and **ADC-4** showed good activity on A375 but were less effective than Cyclopamine on SKMEL5 cell line.

2.3 ADCs for the treatment of viral infections

The idea behind this part of the work comes from the need to explore new therapies against viral infections. After the recent pandemic of SARS-CoV-2 we decided to select this Coronavirus as a model to study new ADCs against viral infections. The concept is almost the same: we select a specific mAb (J08) which has high affinity for spike protein of SARS-CoV-2 [244] and payloads that have antiviral activity.

Doxorubicin and Niclosamide were chosen as payloads as recent studies suggest a possible use of these two drugs against SARS-CoV-2. [185,245] The linkers used for this scope were the pH-sensitive linker based on the orthoester and a non-cleavable linker based on the maleimide group, both already described in the previous paragraphs.

2.3.1 Synthesis of linker-payload systems charged with Doxorubicin and Niclosamide

The synthesis of pH-sensitive orthoester linker charged with Doxorubicin was described in paragraph 2.1.4. In the case of non-cleavable linker, the activated compound **39** was treated with Doxorubicin in the presence of DIPEA and DMAP to give product **51**. A further CuAAC of **51** with **12** gave the desired product **52** (Scheme 22).

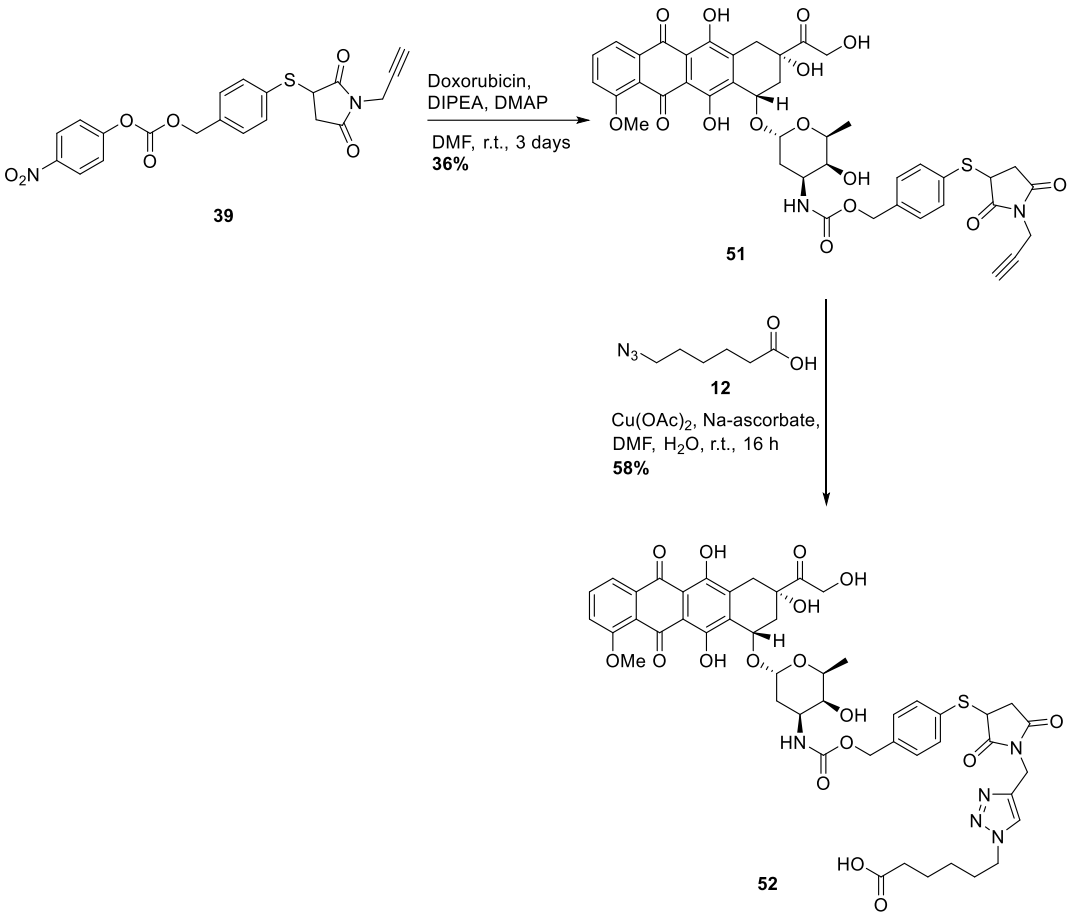

Scheme 22

To charge Niclosamide on our linkers, first we treated compound **38** with PBr_3 and then a nucleophilic substitution with deprotonated Niclosamide gave compound **54**:

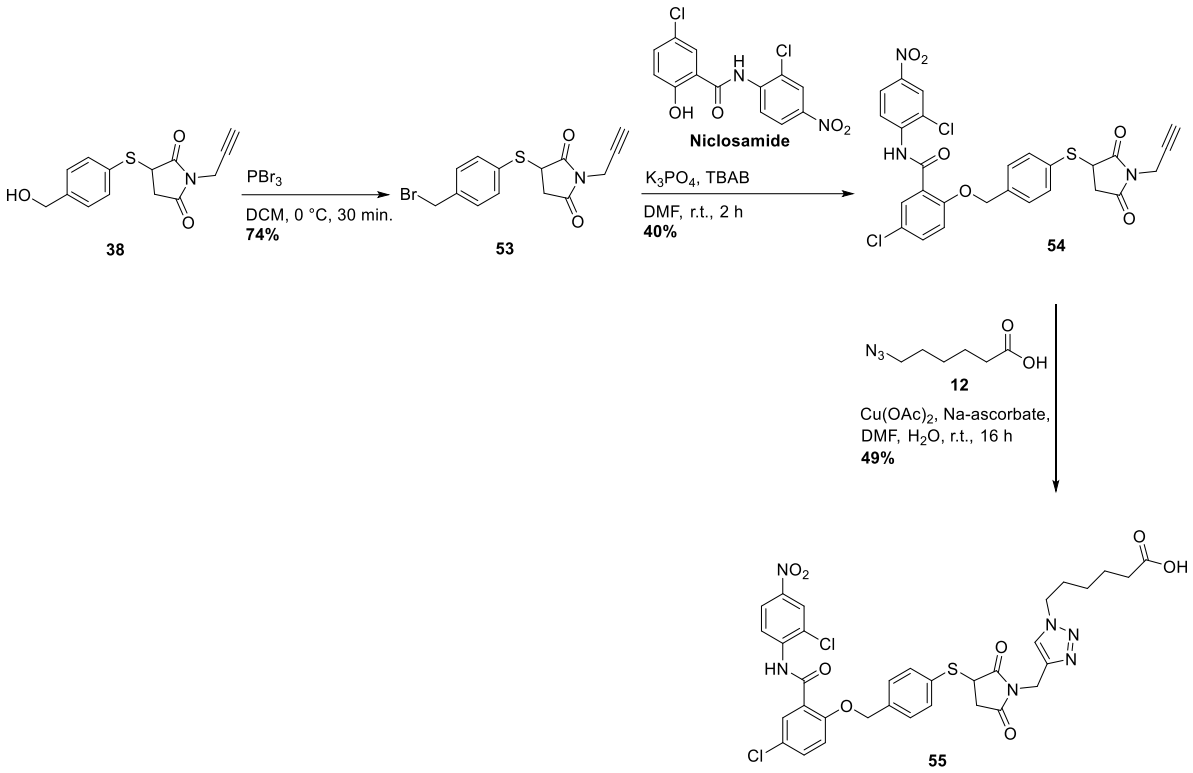

Scheme 23

Click reaction of **54** with azide **12** gave the final product **55**, ready for bioconjugation with J08 (Scheme 23). In the case of orthoester linker, the reaction with Niclosamide was quite challenging and various conditions were tried as reported in the following Table:

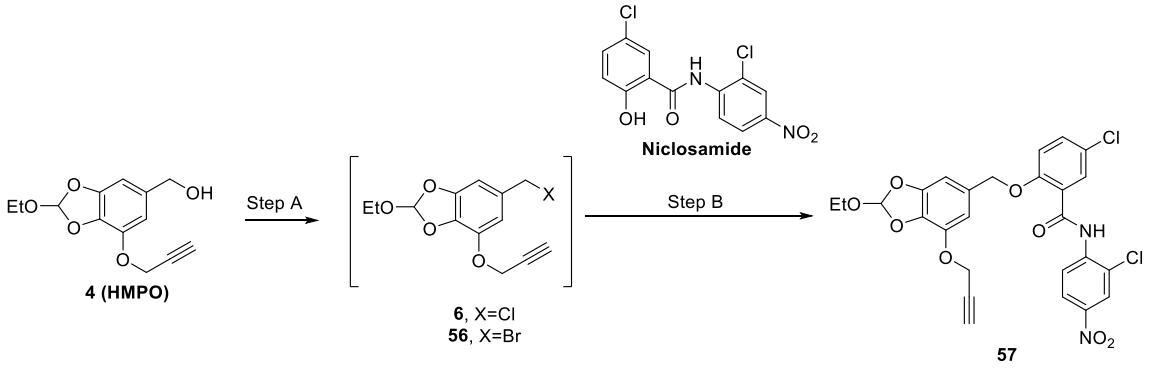

Entry	Step A	Step B	Yield% (57)
1	$SOCl_2$, Et_3N, DCM, 0 °C, 30 min.	NaOH, MeOH, r.t., 16 h	-
2	$SOCl_2$, Et_3N, DCM, 0 °C, 30 min.	NaH, THF, DMF, r.t., 16 h	-

3	$SOCl_2$, Et_3N, DCM, 0 °C, 30 min.	K_3PO_4, TBAB, DMF, r.t., 16 h	-
4	PBr_3, Et_3N, DCM, 0 °C, 1 h	K_3PO_4, TBAB, DMF, r.t., 16 h	traces
5	PBr_3, DIPEA, DCM, 0 °C, 1 h	K_3PO_4, TBAB, DMF, 75 °C, 16 h	7%

Table 11

Intermediates **6** and **56** have never been isolated due to their instability and a telescopic reaction with Niclosamide was carried out. However, in all cases (entries 1-5, Table 11) the desired product was not recovered in sufficient amounts to perform the subsequent step of cycloaddition with azide **12**. In particular, a lot of side products were observed when intermediates **6** and **56** were treated with a solution of deprotonated Niclosamide. Further studies are ongoing to find the best conditions to perform this reaction.

Despite this, we finally had three products available for bioconjugation with mAb J08 (Figure 80).

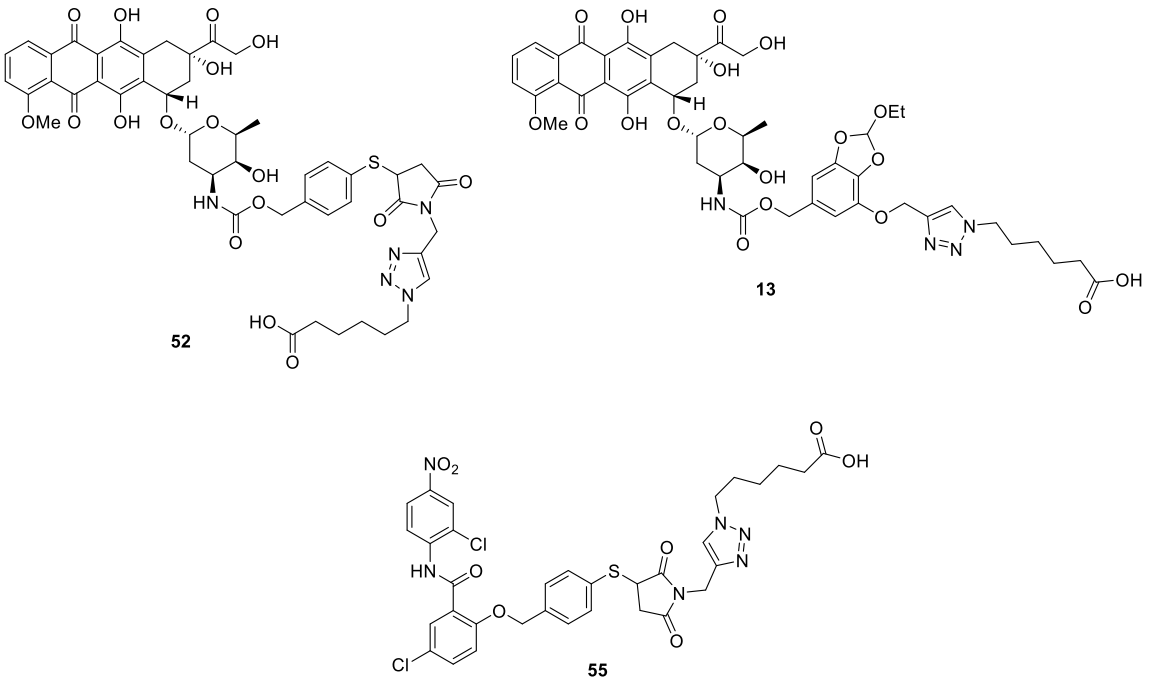

Figure 80

2.3.1 Bioconjugation of compounds **13**, **52** and **55** with J08

The mAb J08 was kindly provided by Toscana Life Sciences (TLS) to investigate the bioconjugation process on this antibody. Compounds **13**, **52** and **55** were activated with S-NHS and bioconjugate with both Cetuximab and J08:

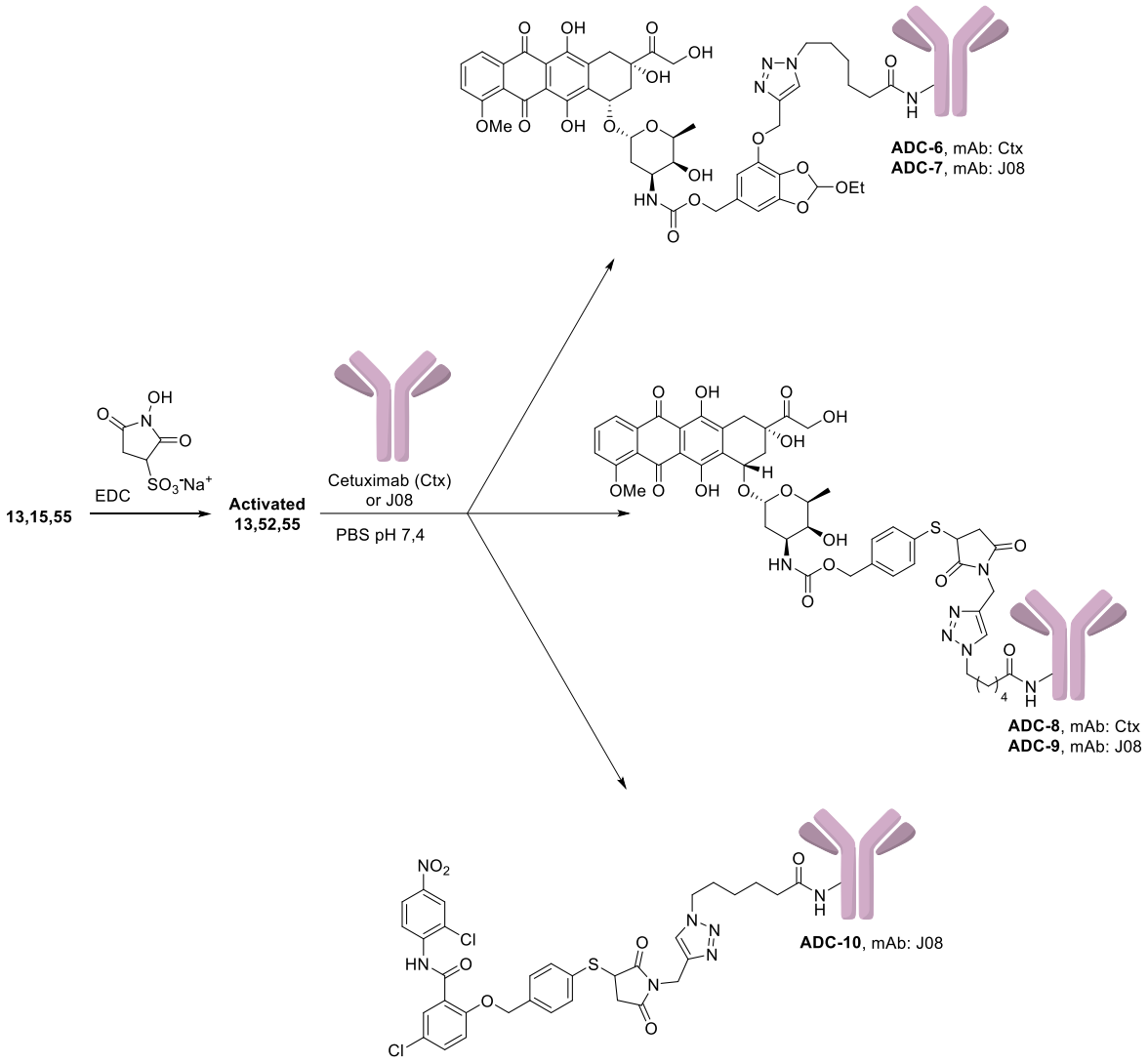

Entry	Cmp.	Ratio (cmp.: mAb)	mAb	ADC	DAR
1	**13**	40:1	Ctx	ADC-6	0.3
2	**13**	80:1	Ctx	ADC-6	1.7
3	**13**	40:1	J08	ADC-7	3.4
4	**52**	40:1	Ctx	ADC-8	0.7
5	**52**	80:1	Ctx	ADC-8	1.1
6	**52**	40:1	J08	ADC-9	1.2

7	**55**	40:1	J08	ADC-10	3.8

Table 12

Bioconjugations with Cetuximab were also explored to have a reference and check if there were any differences in terms of DAR. Surprisingly, bioconjugations with J08 (entries 3, 6, 7, Table 12) were better than those with Cetuximab (entries 1, 2, 4, 5, Table 12) and the respective ADCs were sent to TLS for a further investigation of the activity on SARS-CoV-2. In addition, 40:1 stoichiometric ratio was enough to obtain ADCs (**ADC-7**, **ADC-9**, **ADC-10**) with good DAR values.

CHAPTER 3- Conclusions

3.1 A new pH sensitive linker for drug targeting delivery

In this part of the work, our focus was developed a pH sensitive crosslinker which releases amine- or phenol- based drugs through 1,6-elimination mechanism. The synthesis of the HMPO platform was very easy and this linker can be obtained starting from Gallic acid in four steps. HMPO contains a benzylic alcohol which can be functionalized to charge different primary and secondary amine-, alcohol- and phenol containing molecules through formation of carbamates, carbonates or ethers. Moreover, the alkyne moiety allows the bioconjugation with mAb or in general with a carrier.

To investigate the behaviour of HMPO at various pHs, two model systems with Tryptamine or phenol **7** were synthesized. HPLC analysis showed that both payloads were released at pH 5.5 after 6 hours and the respective linker-payload systems were stable at pH 6.5, 7.4 and in water for 48 hours. Similar results were observed when Doxorubicin and Combretastatin-A4 were chosen as payloads. In this case, the complete release of Doxorubicin and Combretastatin-A4 were achieved after 6 hours or 12 hours, respectively. Stability in plasma was also investigated with great results. The final ADCs (**ADC-1** and **ADC-2**, Figure 81) showed a strong antiproliferative activity (MTT assay) on A431 and A459 cancer cell lines, confirming the efficiency of ADCs based on HMPO linker.

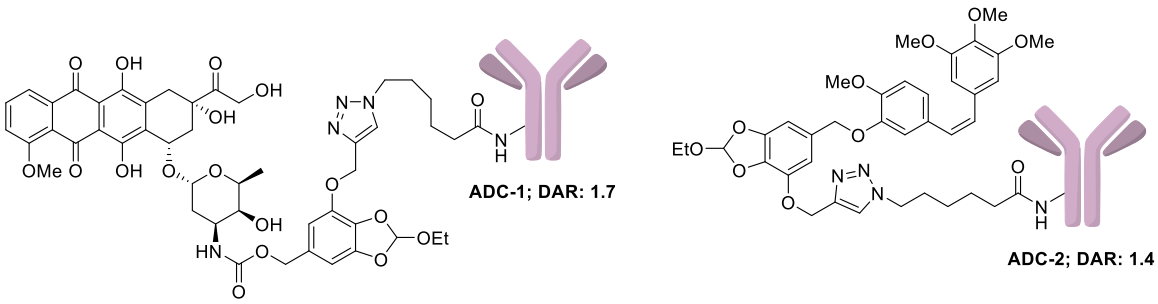

Figure 81

3.2 ADCs charged with unconventional payloads and exploration of new protocols for bioconjugation

Usually, ADCs are charged with high cytotoxic agents. However, the research group where I did this thesis project recently demonstrated that to have an effective ADC is not mandatory to charge the mAb with very cytotoxic agents. [166] This finding opened to the application of ADCs in different diseases beyond cancer.

In the first part of this work, we explored the possibility of making linker-payloads systems charged with various amide-based payloads suitable for ADCs or other drug delivery systems. After a first investigation, the HMPO platform demonstrated to be the best choice for the release of amides in an acidic environment. Therefore, four molecules were synthesized (Figure 82), and the release of the respective payloads was checked by HPLC analysis. In all cases, from 70% to 100% of drugs were release but only after 48 hours, confirming that the release of amides is very challenging.

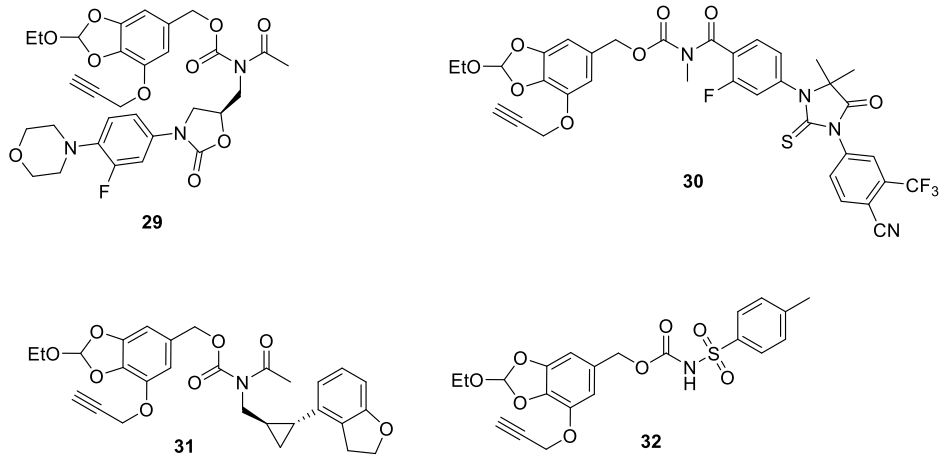

Figure 82

The second part was focused on ADCs charged with Cyclopamine, a natural alkaloid with excellent anticancer activity but poor pharmacokinetic properties. The inclusion of Cyclopamine in ADCs can overcome the problematic pharmacokinetic and allows a more selective therapy. For this purpose, HMPO linker and another non-cleavable linker based on maleimide moiety were chosen and the final systems were bioconjugated with Cetuximab (**ADC-3**, **ADC-4**, Figure 83). In addition, several conditions for bioconjugation along with the use of functionalized Cetuximab were explored leading to a new ADC with excellent *in vitro* activity (**ADC-5**, Figure 83).

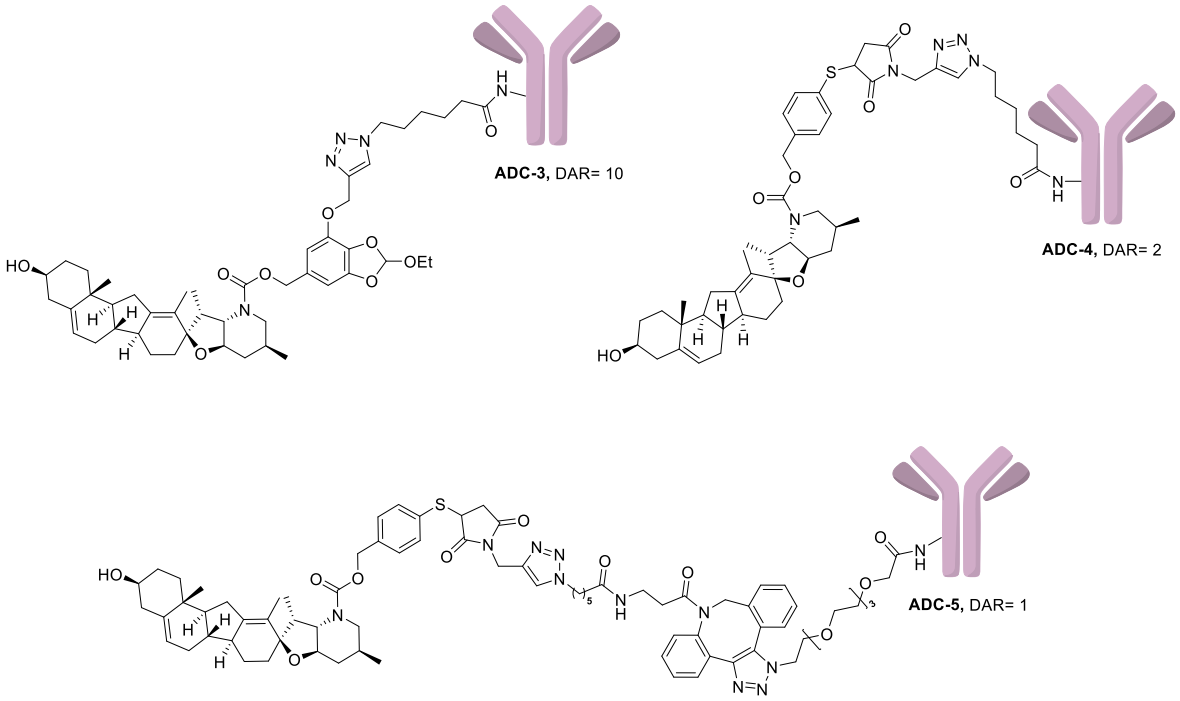

Figure 83- ADCs charged with Cyclopamine.

In the last part of this work, the aim was to synthesize ADCs against SARS-Cov-2 which represent a model system to study the applicability of our ADCs in viral infections. Doxorubicin and Niclosamide that show antiviral activities against SARS-CoV-2 were chosen as payloads, while the mAb J08 gave the selectivity to our ADCs. Taking advantage of the linkers described above, we synthesized the following ADCs:

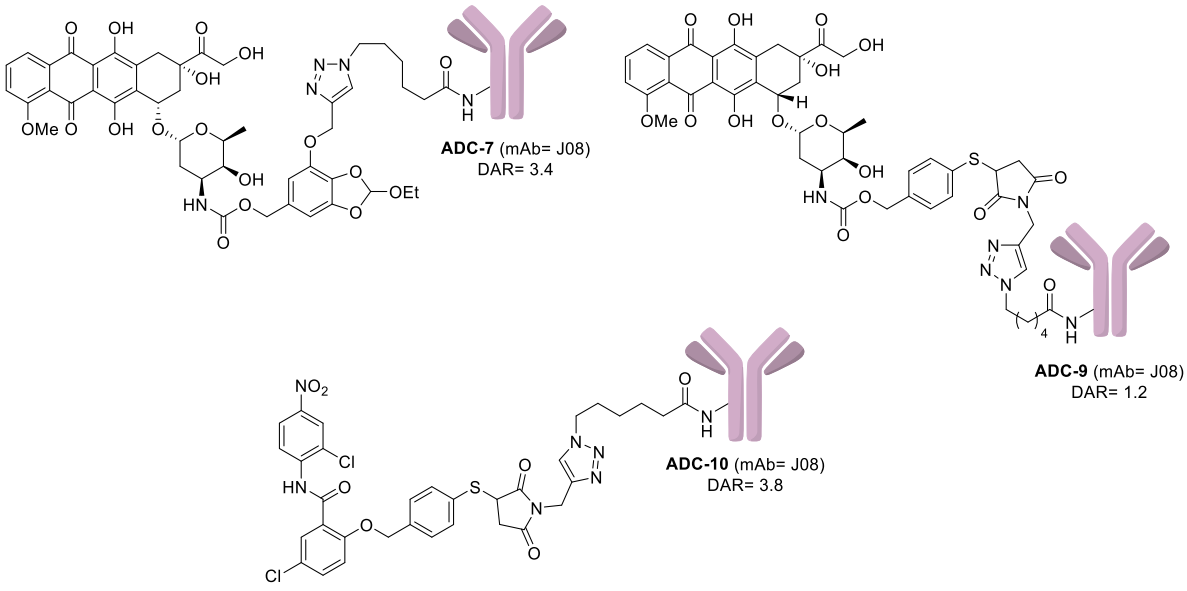

Figure 84- ADCs against SARS-CoV-2.

ADC-7, **ADC-9** and **ADC-10** were sent to TLS for a further investigation of the activity on SARS-CoV-2.

CHAPTER 4- Experimental part

4.1 A new pH sensitive linker for drug targeting delivery

4.1.1 General experimental procedures, materials and instruments

All reagents were used as purchased from commercial suppliers without further purification. The reactions were carried out in oven dried vessels. Solvents were dried and purified by conventional methods prior use or, if available, purchased in anhydrous form.

Flash column chromatography was performed with Merck silica gel Å 60, 0.040-0.063 mm (230-400 mesh).

MPLC Syncore® Büchi on highly resistant PP cartridges Normal Phase silica gel NP 40 – 63 μm particle size and 60 Å pore size (Si60) withstand a maximum pressure of 10 bar (145 psi) column with PE (Eluent A) and EtOAc (Eluent B) as mobile phase.

Merck aluminum backed plates pre-coated with silica gel 60 (UV254) were used for analytical thin layer chromatography and were visualized by staining with a $KMnO_4$ or Ninidrine solution.

NMR spectra were recorded at 25 °C or at 37 °C with 400 or 600 MHz for ^{1}H and 101 or 151 MHz for ^{13}C Brücker Advance NMR spectrometers. The solvent is specified for each spectrum. Splitting patterns are designated as s, singlet; d, doublet; t, triplet; q, quartet; m, multiplet; bs, broad singlet. Chemical shifts (d) are given in ppm relative to the resonance of their respective residual solvent peaks.

High and low resolution mass spectroscopy analyses were recorded by electrospray ionization with a mass spectrometer Q-exactive Plus.

HPLC analyses were performed on a LC/MSD system InfinityLab LC/MSD iQ, Method: Column: InfinityLab PoroShell 120 EC-C18 2.1 x 50mm x 2.7µm. Flow: 0.4 mL/min. Eluent A/B: H_2O/MeCN. Gradient: 5% B to 95% B in 10 minutes, 4 minutes at 95 % B and 3 minutes of re-equilibration. Detection: 254 nm and 210 nm.

MALDI analyses were performed with the MALDI-TOF in linear mode set at 83% of laser intensity. The m/z range was from 30 kDa to 200 kDa.

4.1.2 Synthetic procedures

Ethyl 3,4,5-trihydroxybenzoate (1)

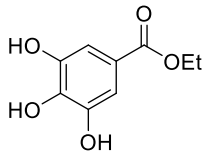

The product was prepared according to the literature. [246]

Gallic acid (1 g, 5.88 mmol) was suspended in EtOH (40 mL) in a 250 mL round-bottomed flask. A catalytic amount of H_2SO_4 conc. (600 µL) was added at r.t. and was heated under reflux with continuous stirring for 16 h. The reaction mixture was cooled to r.t. and the solvent was evaporated under reduced pressure. The residue was dissolved in EtOAc (50 mL) and washed with a $NaHCO_{3\ SS}$ (2 x 100 mL) and $NaCl_{SS}$ (30 mL). The organic phase was dried over anhydrous Na_2SO_4, filtered, and evaporated under vacuum to obtain the esterified compound **1** (1.10 g, 5.59 mmol, 95% yield) as a white solid. mp: 153-155 °C (lit. mp 148–149). Spectral data coherent with the literature. [246]

^{1}H NMR (400 MHz, CD_3OD, δ ppm, J Hz): δ 7.04 (s, 2H), δ 4.86 (bs, 3H), δ 4.26 (q, J = 7.1 Hz, 2H), δ 1.33 (t, J = 7.1 Hz, 3H).

Ethyl 2-ethoxy-7-hydroxybenzo[d][1,3]dioxole-5-carboxylate (2)

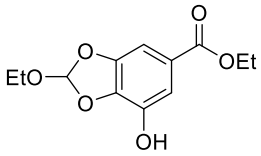

Under N_2 atmosphere, Amberlyst® 15 (62 mg) was suspended in toluene dry (80 mL). After 30 minutes, compound **1** (1 g, 5.05 mmol) and triethyl orthoformate (2.5 mL, 15.10 mmol) were added at r.t. and then the mixture was heated to reflux for 16 h. The reaction mixture was cooled to room temperature, filtered on Celite pad and toluene was evaporated under reduced pressure. The product **2** was purified by chromatography on silica gel with MPLC Syncore® Büchi eluting 0-30 % gradient of EtOAc in petroleum ether, as a white solid (1.06 g, 4.19 mmol, 83% of yield).

^{1}H NMR (600 MHz, $CDCl_3$, δ ppm, J Hz): δ 7.43 (s, 1H), 7.15 (s, 1H), 6.92 (s, 1H), 6.46 (bs, 1H), 4.33 (q, J = 7.1 Hz, 2H), 3.72 (q, J = 7.3Hz, 2H), 1.35 (t, J = 7.1 Hz, 3H), 1.23 (t, J = 7.2 Hz, 3H).

^{13}C NMR (151 MHz, $CDCl_3$, δ ppm): δ 166.84, 147.19, 139.08, 137.23, 124.21, 119.98, 114.11, 102.48, 61.47, 59.65, 14.74, 14.19.

ESI: m/z 255 $[M+H]^+$; 277 $[M+Na]^+$.

Ethyl 2-ethoxy-7-(prop-2-yn-1-yloxy)benzo[d][1,3]dioxole-5-carboxylate (3)

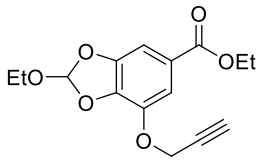

Under N_2, compound **2** (1.34 g, 5.27 mmol), K_2CO_3 (2.188 g, 15.83 mmol) and KI (875 mg, 5.27mmol) in dry acetone (80 mL) were mixed for 20 minutes. Then propargyl bromide (1.41mL, 15.83 mmol) was added and the reaction was carried out to reflux for 16 h. Acetone was evaporated and the crude was solubilized in EtOAc (50 mL), washed with H_2O (2 x 25 mL) and brine (25 mL) and the organic phases dried over anhydrous Na_2SO_4, filtered, and evaporated under reduce pressure. The alkylated product **3** was triturated in Et_2O (7 mL), filtrated and washed with Et_2O (5 mL). The resulting compound was purified by

chromatography on silica gel with MPLC Syncore® Büchi eluting 0-20 % gradient of EtOAc in petroleum ether (1.35 g, 4.64 mmol, 88% yield) and obtained as a white solid.

^{1}H NMR (600 MHz, $CDCl_3$, δ ppm, J Hz): δ 7.46 (s, 1H), 7.29 (s, 1H), 6.96 (s, 1H), 4.84 (s, 2H), 4.34 (q, J = 7.1 Hz, 2H), 3.75 (q, J = 7.1 Hz, 2H), 2.54 (s, 1H), 1.37 (t, J = 7.1 Hz, 3H), 1.27 (t, J = 7.1 Hz, 3H).

^{13}C NMR (151 MHz, $CDCl_3$, δ ppm): δ 165.72, 147.33, 140.23, 138.48, 124.69, 120.12, 112.32, 104.19, 77.87, 76.30, 61.02, 59.59, 57.37, 14.77, 14.32.

ESI: m/z 315 $[M+Na]^+$.

(2-Ethoxy-7-(prop-2-yn-1-yloxy)benzo[d][1,3]dioxol-5-yl)methanol (4, HMPO)

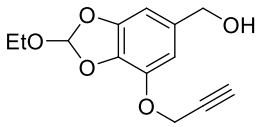

Under N_2, compound **3** (1.07 g, 3.85 mmol) was solubilized in THF dry (60 mL) and mixture was cooled to 0 °C. Then a solution of $LiAlH_4$ 1M in THF (11.55 mL) was added slowly and mixture were carried out at room temperature for 1 h. Then HCl 0.5 N was added until pH 7-8 and the mixture was extracted with EtOAc (50 mL). The organic phase was separated and washed with H_2O (25 mL) and brine (25 mL) and dried over anhydrous Na_2SO_4, filtered and evaporated under reduce pressure. Compound **4** was recovered as a white solid (915 mg, 3.66 mmol, 95% yield). The analytical sample was crystallized from heptane.

^{1}H NMR (600 MHz, $CDCl_3$, δ ppm, J Hz): δ 6.89 (s, 1H), 6.67 (s, 1H), 6.63 (s, 1H), 4.81 (s, 2H), 4.58 (s, 2H), 3.75 (q, J = 7.1 Hz, 2H), 2.52 (s, 1H), 1.26 (t, J = 7.1 Hz, 3H).

^{13}C NMR (151 MHz, $CDCl_3$, δ ppm): δ 147.68, 140.58, 135.42, 133.89, 119.50, 108.82, 101.75, 78.39, 75.94, 65.23, 59.37, 57.39, 14.82.

ESI: m/z 273 $[M+Na]^+$.

Elemental Analysis calcd. for $C_{12}H_{14}O_6$: C, 56.69; H, 5.55; found C, 56.82; H, 5.65.

General procedures for the synthesis of carbamates

The activated linker (0.4 mmol) was solubilized in THF dry (5 mL) at r.t under N_2. At 0 ° C *p*-nitrophenyl chloroformate (89 mg, 0.44 mmol) and DMAP (98 mg, 0.8 mmol) were added, and the reaction was carried out for 30 minutes at 0 °C. The formation of the activated

compound was checked by TLC and the solution was dropped into a solution of the desired amine (0.6 mmol) and DIPEA (209 μL, 1.2 mmol) at 0 °C and the reaction was stirred at r.t. for 0.15 h-16 h. The solvent was evaporated under reduced pressure. The residue was dissolved in EtOAc (10 mL) and washed with H_2O (5 mL) and brine (5 mL). The organic phase was dried over anhydrous Na_2SO_4, filtered, and evaporated under vacuum.

(2-Ethoxy-7-(prop-2-yn-1-yloxy)benzo[d][1,3]dioxol-5-yl)methyl(2-(1H-indol-2-yl)ethyl)carbamate (5)

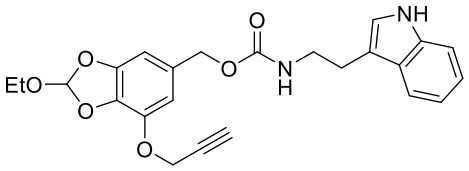

The compound **5** was purified by flash chromatography on silica gel with MPLC Syncore® Büchi eluting 0-40 % gradient of EtOAc in petroleum ether (139 mg, 0.32 mmol, 81% yield).
^{1}H NMR (600 MHz, $CDCl_3$, δ ppm, J Hz): δ 8.16 (bs, 1H), 8.13 (d, J = 8.4 Hz, 1H), 7.60 (d, J = 7.9 Hz, 1H), 7.37 (d, J = 8.1 Hz, 1H), 7.21 (t, J = 7.7 Hz, 1H), 7.12 (t, J = 7.5 Hz, 1H), 6.98 (s, 1H), 6.89 (s, 1H), 6.65 (s, 1H), 6.62 (s, 1H), 5.00 (s, 2H), 4.88 (bs, 1H), 4.80 (s, 2H), 3.76 (q, J = 7.2 Hz, 2H), 3.54 (t, J = 6.6 Hz, 2H), 2.99 (t, J = 6.8 Hz, 2H), 2.51 (s, 1H), 1.27 (t, J = 7.0 Hz, 3H).
^{13}C NMR (151 MHz, $CDCl_3$, δ ppm): δ 162.65, 156.45, 147.60, 140.51, 136.44, 134.28, 130.92, 126.19, 122.23, 119.51, 118.71, 115.67, 112.66, 111.30, 110.26, 102.92, 76.08, 66.52, 59.58, 57.47, 41.29, 29.73, 25.65, 14.83.
ESI: m/z 459 $[M+Na]^+$.
HRMS (EI) calcd. for $C_{24}H_{24}N_2O_6Na$ $[M+Na]^+$ 459.1532, found 459.1529.

(2-Ethoxy-7-(prop-2-yn-1-yloxy)benzo[*d*][1,3]dioxol-5-yl)methyl ((2*S*,3*S*,4*S*,6*R*)-3-hydroxy-2-methyl-6-(((1*S*,3*S*)-3,5,12-trihydroxy-3-(2-hydroxyacetyl)-10-methoxy-6,11- dioxo-1,2,3,4,6,11-hexahydrotetracen-1-yl)oxy)tetrahydro-2*H*-pyran-4-yl)carbamate (11)

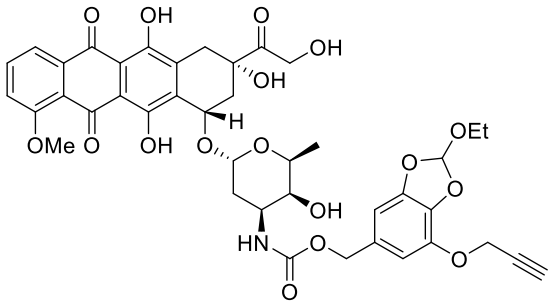

Compound **11** was purified with flash chromatography on silica gel eluting 0-10 % gradient of MeOH in CH_2Cl_2 (237 mg, 0.29 mmol, 73% yield).

^{1}H NMR (600 MHz, $CDCl_3$, δ ppm, J Hz): δ 13.98 (s, 1H), 13.24 (s, 1H), 8.04 (d, J = 7.7 Hz, 1H), 7.79 (t, J = 8.0 Hz, 1H), 7.39 (d, J = 8.4 Hz, 1H), 6.87 (s, 1H), 6.62 (s, 1H), 6.58 (s, 1H), 5.51 (d, J = 4.2 Hz, 1H), 5.30 (s, 1H), 5.13 (dd, J = 5.7 Hz, 1H), 4.93 (s, 2H), 4.77 (s, 2H), 4.55 (s, 1H), 4.08 (s, 3H), 3.87 (bs, 1H), 3.77 – 3.60 (m, 3H), 3.15 (dd, J = 15.6, 8.4 Hz, 2H), 2.51 (s, 1H), 2.26 (dd, J = 6.8, 4.5 Hz, 2H), 1.98 – 1.74 (m, 4H), 1.62 (s, 2H), 1.35 – 1.11 (m, 6H).

^{13}C NMR (151 MHz, $CDCl_3$, δ ppm): δ 213.86, 187.13, 186.73, 161.09, 156.19, 155.67, 155.42, 147.59, 140.44, 135.80, 135.53, 134.35, 133.60, 133.53, 130.60, 120.90, 119.88, 119.56, 118.47, 111.64, 111.46, 110.29, 102.95, 100.70, 76.65, 76.03, 69.70, 69.59, 67.27, 66.67, 65.56, 59.34, 57.41, 56.69, 47.03, 35.66, 34.04, 30.20, 29.71, 16.84, 14.78.

ESI: m/z 842 $[M+Na]^+$.

HRMS (EI) calcd. for $C_{41}H_{41}NO_{17}Na$ $[M+Na]^+$ 842.2273, found 842.2278.

6-(Chloromethyl)-2-ethoxy-4-(prop-2-yn-1-yloxy)benzo[d][1,3]dioxole (6)

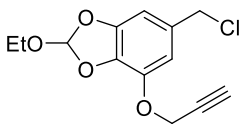

Compound **4** (100 mg, 0.4 mmol) was solubilized in CH_2Cl_2 dry (6 mL) at 0 °C and $SOCl_2$ and Et_3N, both freshly distilled, were added carefully. The reaction was carried out at 0 °C for 30 minutes. The mixture was concentrated under N_2 and quickly filtrated on a pad of silica gel using PE:EtOAc 1:1. Filtrate was concentrated under reduced pressure and was immediately used for the next step.

Methyl 4-hydroxy-3,5-dimethoxybenzoate (7)

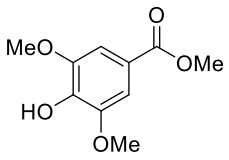

The product was prepared according to literature. [247]

Syringic acid (3 g, 15.14 mmol) was dissolved in MeOH (30 mL), and a catalytic amount of H_2SO_4 conc. was added. The reaction mixture was stirred at reflux for 4 h. The resulting mixture was concentrated under reduced pressure and the residue dissolved in EtOAc (50 mL). The solution was transferred into a separating funnel, washed with $NaHCO_3$ $_{SS}$ (100 mL) and NaCl $_{SS}$ (30 mL). The organic layer was dried over anhydrous Na_2SO_4, filtered, and concentrated to give the methyl ester **7** in good yield (3.03 g, 14.38 mmol, 95% yield).

^{1}H NMR (600 MHz, $CDCl_3$, δ ppm, J Hz): δ 7.30 (s, 2H), 3.91 (s, 6H), 3.88 (s, 3H).

^{13}C NMR (151 MHz, $CDCl_3$, δ ppm): δ 166.87, 146.67, 139.27, 121.05, 106.67, 56.40, 52.07.

ESI: m/z 211 $[M-H]^+$.

Methyl 4-((2-ethoxy-7-(prop-2-yn-1-yloxy)benzo[d][1,3]dioxol-5-yl)methoxy)-3,5-dimethoxybenzoate (8)

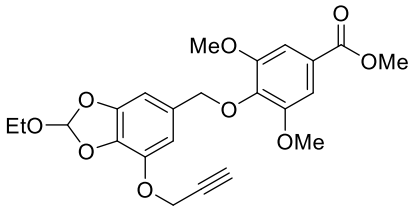

Compound **7** (100 mg, 0.47 mmol) was solubilized in dry acetone (10 mL) and K_2CO_3 an. (195 mg, 1.41 mmol) was added to the mixture at r.t. under Ar. After 10 minutes a solution of benzyl chloride **6** (377 mg, 1.41 mmol) in dry acetone (10 mL) was added under Ar and the reaction was stirred for 30 min at r.t. The mixture was filtered and the filtrated concentrated under reduced pressure. EtOAc (20 mL) was added, washed with H_2O (10 mL)

and brine (5 mL). The organic phases were dried over anhydrous Na_2SO_4, filtered and evaporated under reduce pressure. The product was purified by flash chromatography on silica gel eluting 0-40% gradient of EtOAc in petroleum ether (168 mg, 0.38 mmol, 81% yield).

^{1}H NMR (600 MHz, $CDCl_3$, δ ppm, J Hz): δ 7.29 (s, 2H), 6.90 (s, 1H), 6.79 (s, 1H), 6.78 (s, 1H), 4.99 (s, 2H), 4.80 (s, 2H), 3.91 (s, 3H), 3.90 (s, 6H), 3.73 (q, J = 7.1 Hz, 2H), 2.51 (s, 1H), 1.25 (t, J = 7.0 Hz, 3H).

^{13}C NMR (151 MHz, $CDCl_3$, δ ppm): δ 166.74, 153.21, 147.41, 140.78, 140.25, 134.32, 131.79, 129.39, 125.38, 110.46, 110.13, 106.84, 105.44, 103.27, 75.84, 74.84, 59.13, 57.38, 56.23, 52.24, 29.71, 14.83.

ESI: m/z 445 $[M+H]^+$; 467 $[M+Na]^+$.

HRMS (EI) calcd. for $C_{23}H_{25}O_9$ $[M+H]^+$ 445.1499, found 445.1501.

(Z)-2-Ethoxy-6-((2-methoxy-5-(3,4,5-trimethoxystyryl)phenoxy)methyl)-4-(prop-2-yn-1- yloxy)benzo[d][1,3]dioxole (14)

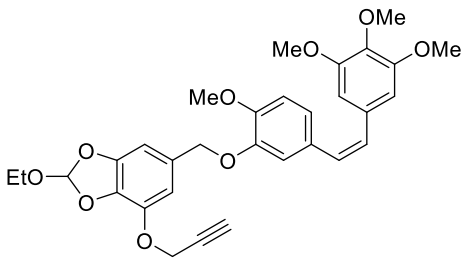

Combretastatin-A4 (100 mg, 0.32 mmol) was solubilized in DMF dry (3 mL) and was added into a DMF dry (2 mL) solution of previously washed NaH 60% (25 mg, 0.64 mmol) under Ar at 0 °C. The mixture was stirred for 10 minutes and the activated linker **6** (257 mg, 0.96 mmol) solubilized in 3 mL of dry DMF was dropped slowly at 0 ° C. The reaction was carried out at r.t. for 16 h and at the end H_2O (5 mL) was added to quench the excess of NaH. The crude was extracted with EtOAc (10 mL), the organic phase was dried over anhydrous Na_2SO_4, filtered, and evaporated under reduce pressure. The product **14** was purified by chromatography on silica gel with MPLC Syncore® Büchi eluting 0-30 % gradient of EtOAc in petroleum ether (170 mg, 1.31 mmol, 98% yield).

^{1}H NMR (600 MHz, $CDCl_3$, δ ppm, J Hz): δ 6.91 – 6.85 (m, 3H), 6.78 (d, J = 7.8 Hz, 1H), 6.64 (s, 1H), 6.61 (s, 1H), 6.51 (s, 2H), 6.49 – 6.39 (m, 2H), 4.81 (s, 2H), 4.79 (s, 2H), 3.86 (s, 3H), 3.83 (s, 3H), 3.77 – 3.68 (m, 8H), 2.49 (s, 1H), 1.26 (t, J = 6.7 Hz, 3H).
^{13}C NMR (151 MHz, $CDCl_3$, δ ppm): δ 153.01, 148.94, 147.68, 147.53, 140.51, 137.15, 134.13, 132.96, 131.29, 129.81, 129.62, 128.88, 122.60, 119.53, 114.68, 111.41, 109.39, 105.99, 102.16, 75.93, 70.81, 60.92, 59.29, 57.41, 55.97, 29.71, 14.82.
ESI: m/z 571 $[M+Na]^+$.
HRMS (EI) calcd. for $C_{31}H_{32}O_9Na$ $[M+Na]^+$ 571.1944, found 571.1946.

6-Azidohexanoic acid (12)

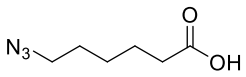

The product was prepared according to literature. [248]
6-bromohexanoic acid (700 mg, 3.6 mmol) was solubilized in dry DMF (5 mL) and NaN_3 (1.17 g, 18 mmol) was added at the mixture at r.t. The reaction was stirred for 16 h at 100 °C. EtOAc (100 mL) was added at the crude filtered on Büchner. The organic phase was washed with $KHSO_4$ 1 M (2 x 50 mL), H_2O (2 x 30 mL) and $NaCl_{SS}$ (30 mL). The organic phase was dried over anhydrous Na_2SO_4, filtered, and evaporated under reduce pressure. The product **12** was obtained as yellow oil (289 mg, 1.84 mmol, 51% yield).
^{1}H NMR (400 MHz, $CDCl_3$, δ ppm, J Hz): δ 10.93 (bs, 1H), 3.19 (t, J = 6.8 Hz, 2H), 2.28 (t, J = 7.4 Hz, 2H), 1.60-1.56 (m, 4H), 1.44 – 1.26 (m, 2H).
NMR data are coherent with the literature. [248]

General procedure for CuAAC cycloaddition

The desired alkyne (0.07 mmol) and the compound **11** (9 mg, 0.056 mmol) were dissolved in DMF dry (2 mL) under Ar. The solution was degassed with three cycles of argon/vacuum. To this solution, a freshly prepared aqueous mixture (2 mL) of $Cu(OAc)_2$ (4 mg, 0.021 mmol) and Na ascorbate (8 mg, 0.042 mmol), previously degassed by argon/vacuum cycles, was added dropwise. The reaction mixture was degassed and left to stir under Ar. at r.t. for

16 h. The solvent was evaporated and the crude was purified by silica gel flash chromatography eluting 0-10 % gradient of MeOH in CH_2Cl_2 provide the desired product.

6-(5-(((2-Ethoxy-6-(((((2S,3S,4S,6R)-3-hydroxy-2-methyl-6-(((1S,3S)-3,5,12-trihydroxy-3-(2 hydroxyacetyl)-10-methoxy-6,11-dioxo-1,2,3,4,6,11 hexahydrotetracen-1-yl)oxy)tetrahydro- 2H pyran-4-yl)carbamoyl)oxy)methyl)benzo[d][1,3]dioxol-4-yl)oxy)methyl)-1H-1,2,3-triazol- 1-yl)hexanoic acid (13)

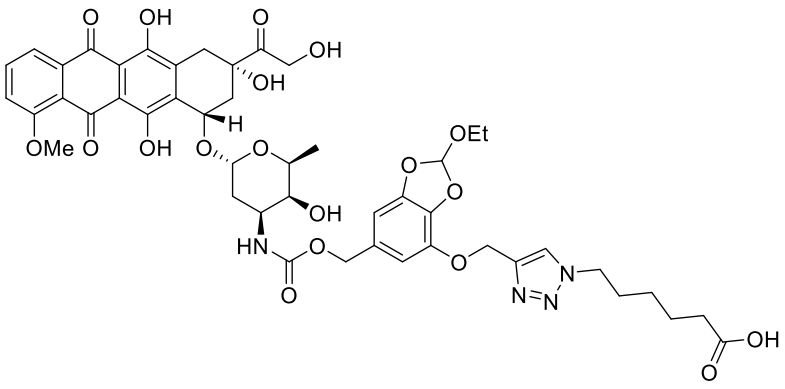

Obtained 39 mg, 0.04 mmol, 64% yield.

^{1}H NMR (600 MHz, dmso-d_6, δ ppm, J Hz): δ 14.02 (bs, 1H), 13.26 (bs, 1H), 11.83 (bs, 1H), 8.16 (s, 1H), 7.91 (t, J = 8.0 Hz, 1H), 7.64 (d, J = 7.5 Hz, 1H), 7.04 (s, 1H), 6.82 – 6.71 (m, 2H), 6.62 (s, 1H), 5.40 (s, 1H), 5.23 (s, 1H), 5.17 (s, 2H), 4.97 (s, 1H), 4.85 (s, 2H), 4.75 (bs, 1H), 4.56 (s, 2H), 4.32 (t, J = 7.1 Hz, 2H), 4.14 (d, J = 6.6 Hz, 1H), 3.98 (s, 3H), 3.75-3.70 (m, 1H), 3.64 (q, J = 6.9 Hz, 2H), 3.46 (s, 1H), 2.98 (s, 2H), 2.25 – 2.10 (m, 4H), 1.87-1.77 (m, 3H), 1.50 (p, J = 7.4 Hz, 3H), 1.23 (q, J = 7.8 Hz, 3H), 1.15-1.10 (m, 6H).

^{13}C NMR (151 MHz, dmso-d_6, δ ppm): δ 187.13, 187.01, 174.74, 161.37, 156.60, 155.72, 155.02, 147.17, 142.68, 141.55, 136.69, 136.10, 135.28, 134.65, 133.59, 131.94, 124.98, 120.69, 120.33, 119.54, 111.38, 111.24, 109.81, 102.32, 100.72, 90.71, 80.65, 75.54, 70.37, 68.54, 67.22, 65.60, 64.12, 62.96, 60.07, 57.12, 49.73, 47.64, 37.26, 33.92, 32.68, 30.36, 29.86, 25.88, 24.32, 17.47, 15.22.

ESI: m/z 999 $[M+Na]^+$.

HRMS (EI) calcd. for $C_{47}H_{52}N_4O_{19}Na$ $[M+Na]^+$ 999.3124 (100%), 1000.3158 (51%) found 999.3127 (100%), 1000.3161 (51%).

(Z)-6-(5-(((2-Ethoxy-6-((2-methoxy-5-(3,4,5 trimethoxystyryl) phenoxy)methyl)benzo[d][1,3]- dioxol-4-yl)oxy)methyl)-1H-1,2,3-triazol-1-yl)hexanoic acid (15)

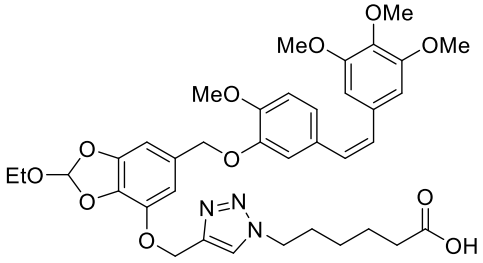

Obtained 21 mg, 0.03 mmol, 75% yield.

^{1}H NMR (600 MHz, $CDCl_3$, δ ppm, J Hz): δ 7.65 (s, 1H), 6.90 – 6.86 (m, 3H), 6.79 (d, J = 8.1 Hz, 1H), 6.66 (s, 1H), 6.59 (s, 1H), 6.51 (s, 2H), 6.49 – 6.40 (m, 2H), 5.32 (s, 2H), 4.80 (s, 2H), 4.36 (t, J = 7.0 Hz, 2H), 3.86 (s, 3H), 3.83 (s, 3H), 3.76 – 3.70 (m, 8H), 2.35 (t, J = 7.2 Hz, 3H), 1.96-1.92 (m, J = 7.7 Hz, 2H), 1.69-1.65 (m, 2H), 1.40-1.35 (m, 2H), 1.26 (t, J = 6.7 Hz, 3H).

^{13}C NMR (151 MHz, $CDCl_3$, δ ppm): δ 177.29, 152.99, 148.90, 147.56, 147.51, 141.34, 137.11, 133.87, 132.99, 131.46, 129.82, 129.62, 128.91, 122.59, 119.48, 114.65, 111.41, 109.08, 106.00, 101.88, 70.81, 63.52, 60.93, 59.55, 55.98, 50.08, 33.33, 29.86, 29.72, 25.80, 23.91, 14.84.

ESI: m/z 707 $[M+H]^+$; 729 $[M+Na]^+$. HRMS (EI) calcd. for $C_{37}H_{44}N_3O_{11}$ $[M+H]^+$ 706.2976, found 706.2979.

4.1.3 General procedure for the preparation of ADC-1 and ADC-2

The proper carboxylic acid (28 μL, 10 mM in DMSO) was activated by adding S-NHS (5 μL, 100 mM in H_2O) and EDC·HCl (5 μL, 100 mM in H_2O). The reaction was mixed (600 rpm) for 16 h at r.t. PBS at pH 7.4 (35 μL) and Cetuximab freshly dialyzed using a 10 kDa cutoff dialysis membrane (100 μL, 5 mg/mL in PBS pH 7.4) were added to the activated carboxylic acid solution. The reaction was mixed in a shaker (650 rpm) at r.t. and after 1 h quenched with a 20 mM glycine aqueous solution (27 μL). The final ADCs were purified using PD SpinTrapTM G-25 column removing the unreacted excess of small molecules. DAR was detected by MALDI analysis.

4.1.4 MALDI analysis of ADCs 1-2

Samples preparation: the matrix solutions were prepared at two different concentrations, and both were used in parallel. 20.0 mg or 25 mg of Super DHB were dissolved in a solution of MeCN (150 µL), H_2O (350 µL) and TFA (0.05 µL) and deposited in a stainless-steel target placed in a termoblock set at 39 °C. When the sample was dried, 1.65 µL of matrix solution was added and once completely dried and crystalized, the target plate was removed from the termoblock. The target plate was analyzed with MALDI-TOF set in linear mode at 83% of laser intensity. The m/z range was from 30 kDa to 200 kDa. For each sample spot, 10 shots were acquired to improve the spectra quality and mass accuracy.
DAR was calculated as follows: (M.W. ADC – M.W. mAb)/ M.W. linker-payload.

MALDI spectra

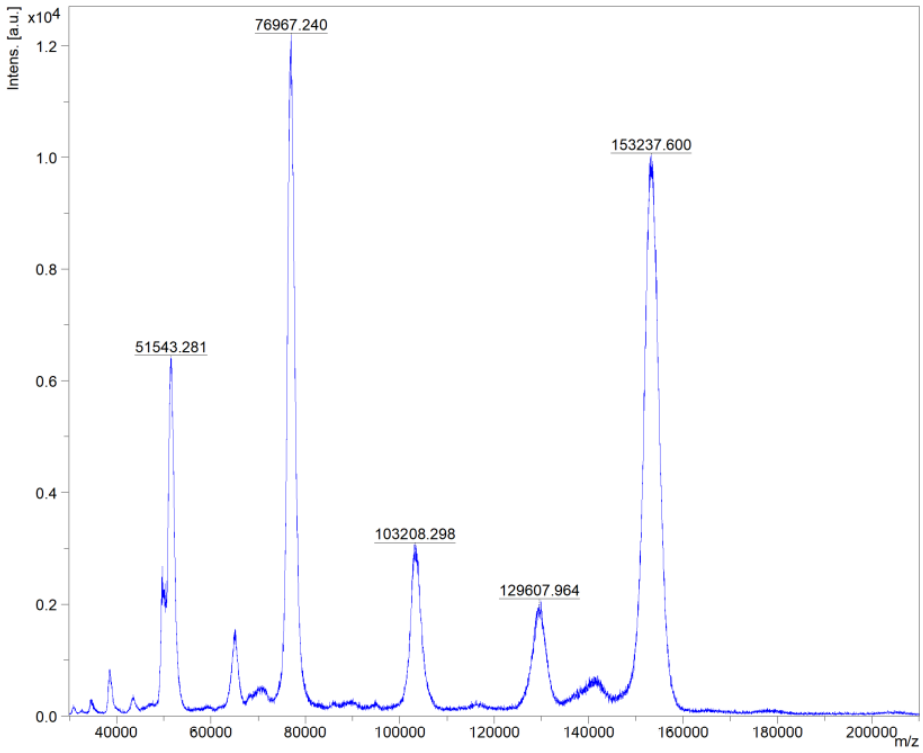

Figure 85- MALDI of ADC-1.

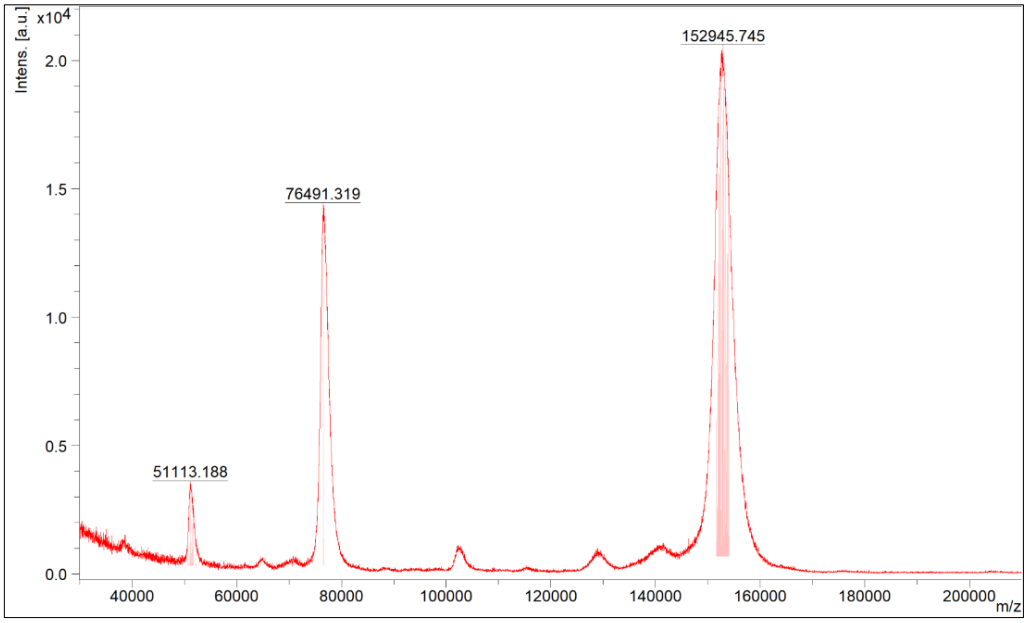

Figure 86- MALDI of ADC-2.

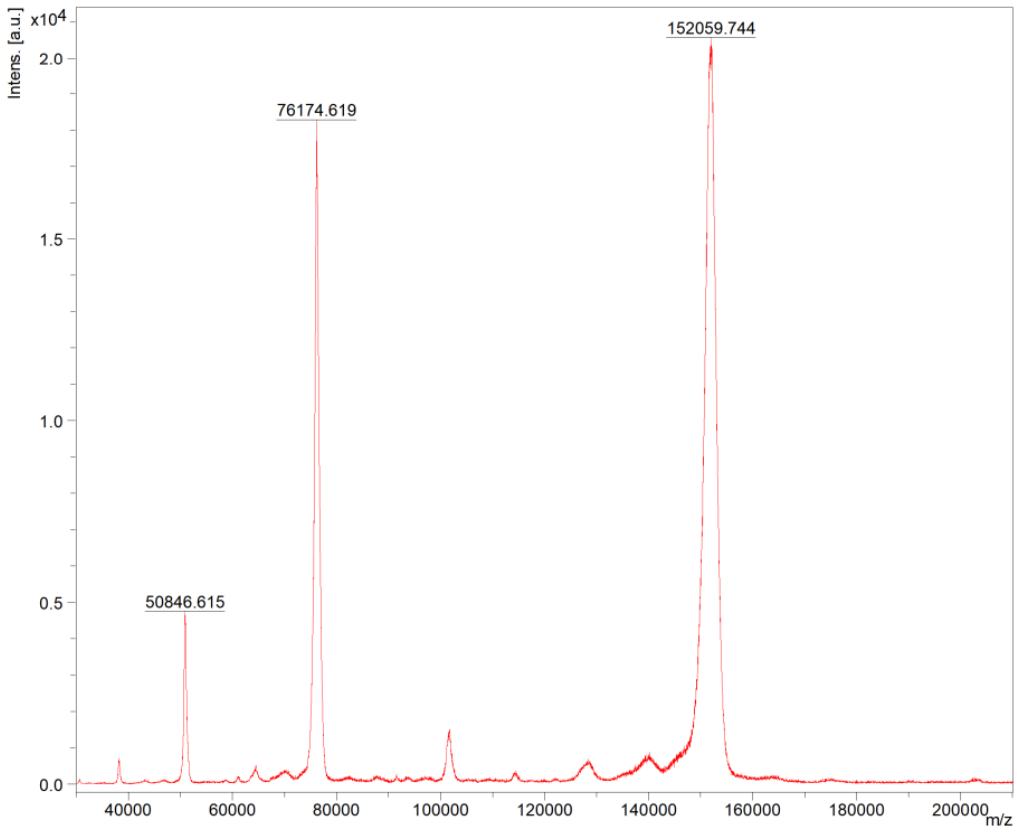

Figure 87- MALDI of Cetuximab.

4.1.5 HPLC methods for hydrolysis

Samples were prepared according to the literature. [83]

A 10 mM solution of the desired compound (**5**, **8**, **11**, **14**) was prepared in DMSO and diluted in H_2O or in the corresponding buffer to obtain a final 1 mM solution of the compound. For pH 7.4, 6.5, 5.5, phosphate buffers 0.1 M was used (KH_2PO_4/K_2HPO_4). Each solution was analyzed by analytical HPLC. Reaction was performed at 25 °C, incubated at 37 °C and the crude was injected every 1 h up to 48 hours. All data were recorded in triplicate. HPLC analyses were performed on a LC/MSD system InfinityLab LC/MSD iQ, Column: InfinityLab PoroShell 120 EC-C18 2.1 x 50mm x 2.7µm. Flow: 0.4 mL/min. Eluent A/B: H_2O/MeCN. Gradient: 5% B to 95% B in 10 min., 4 min. at 95 % B and 3 min. of reequilibration. Detection: 254 nm and 260 nm.

4.1.6 ^{1}H NMR studies for the release mechanism of HMPO

The products **8** and **7** ($4.8 \cdot 10^{-6}$ mol) were solubilized in acetonitrile-d_3 (160 µL) and added to a previously prepared deuterated buffer at pH 5.5 (50 mM, 640 µL) or D_2O (640 µL). The NMR tubes were incubated at 37 °C, and the FID was recorded every 30 minutes at 37 °C using 600 MHz Brücker Advance NMR spectrometer.

NMR spectra

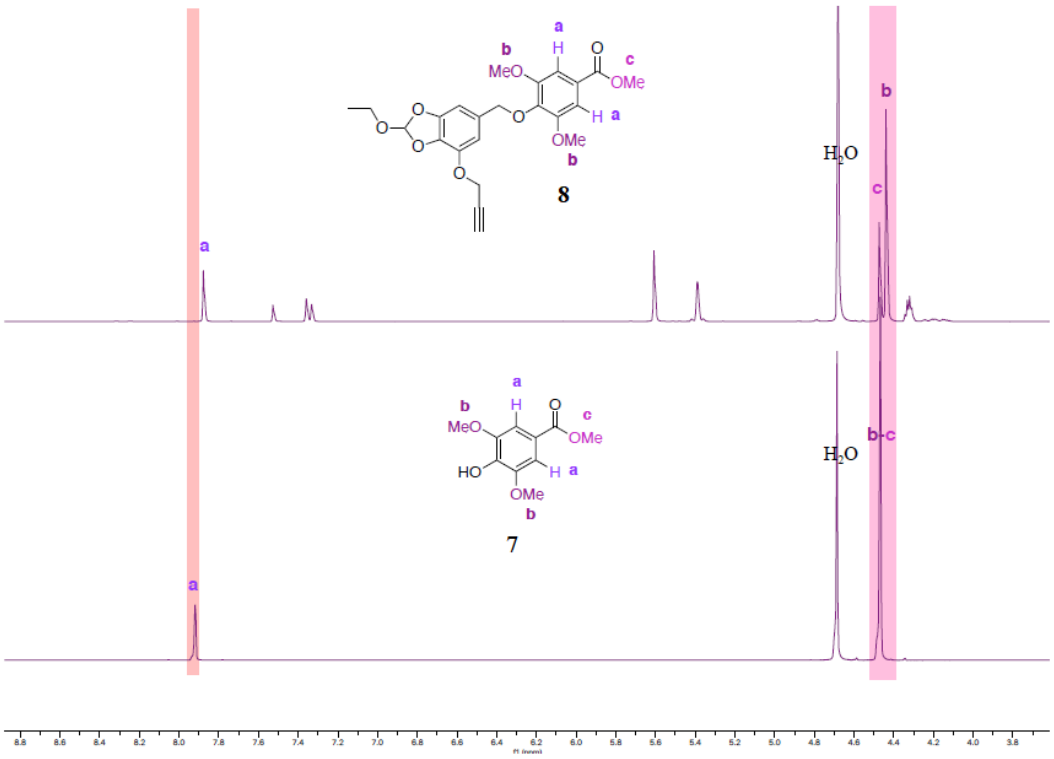

Figure 88- ^{1}H NMR of reference compounds 7 and 8 in D_2O and acetonitrile-d_3 at 37 °C.

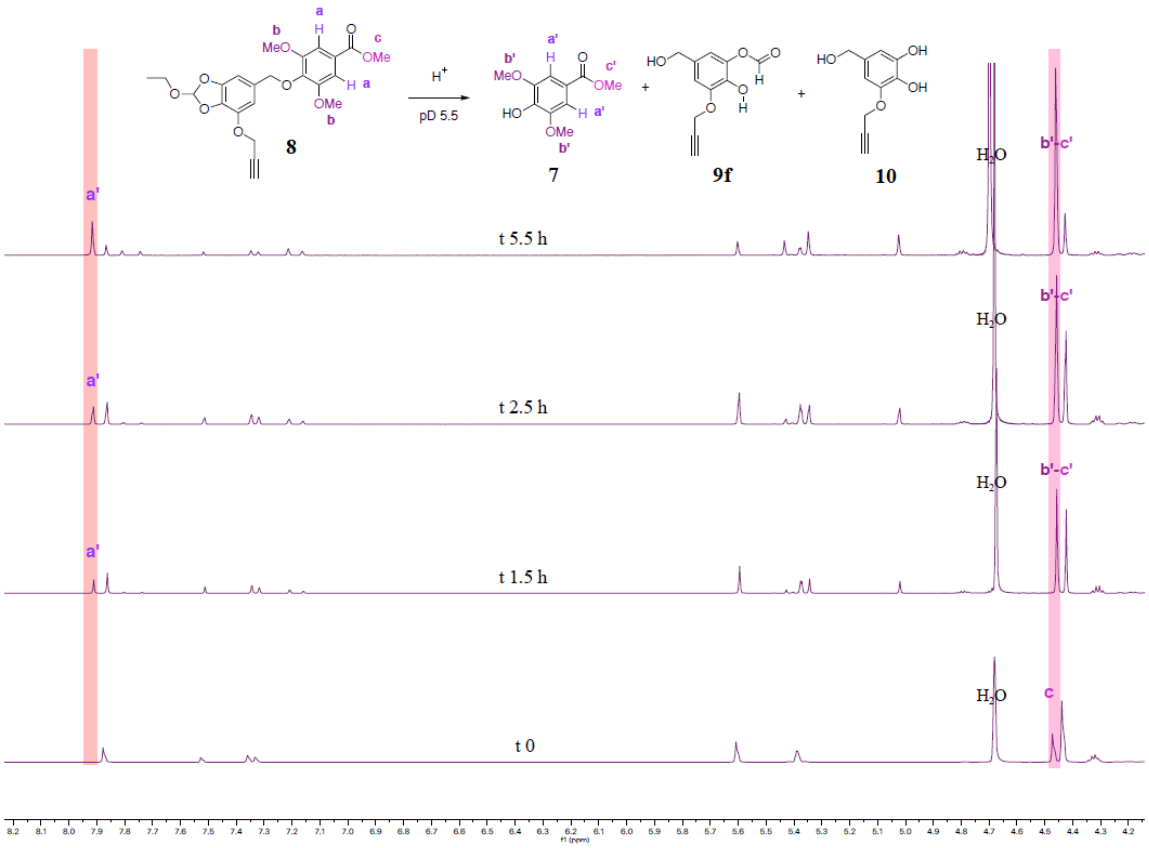

Figure 89- ^{1}H NMR of 8 monitored during the hydrolysis in deuterated buffer pH 5.5 at 37 °C.

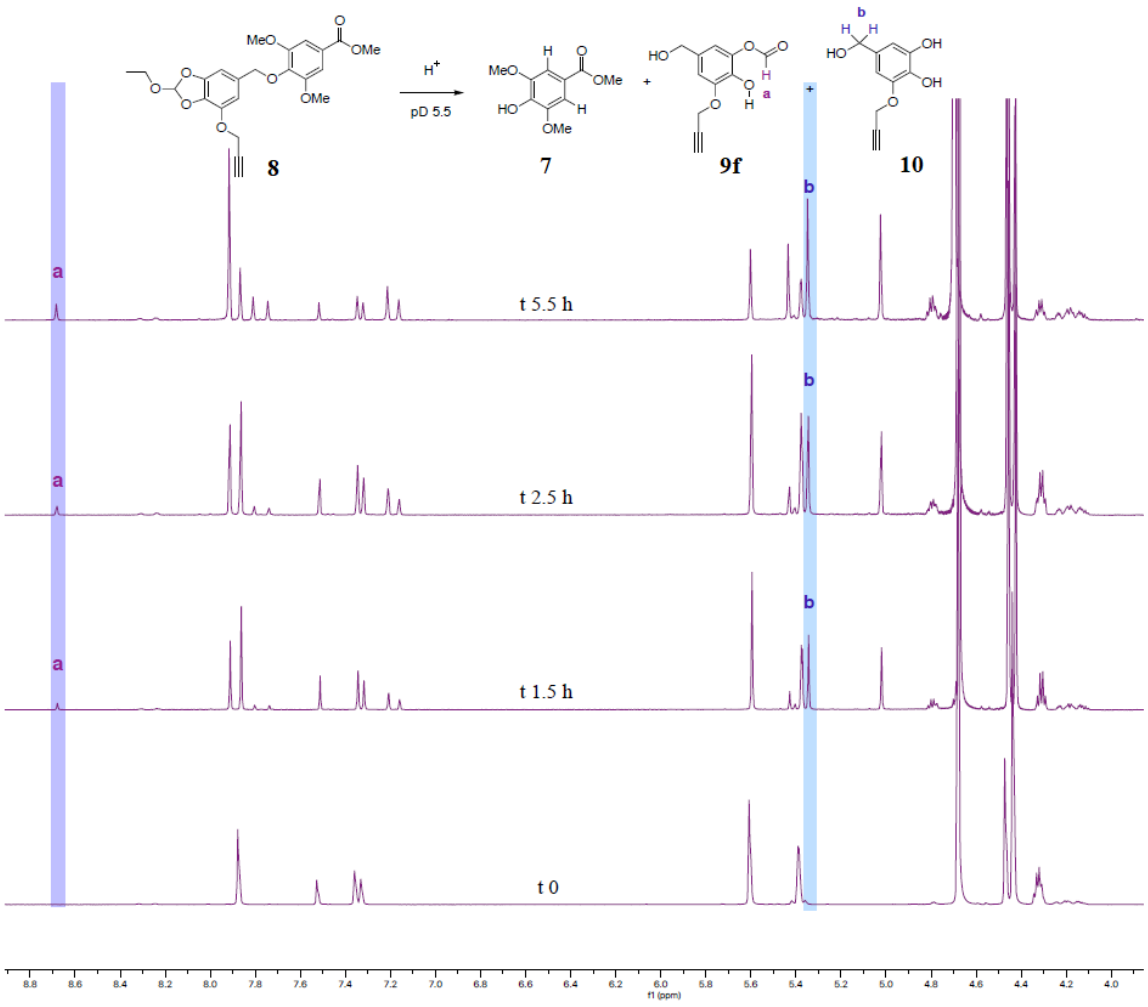

Figure 90- ^{1}H NMR of 8 monitored during the hydrolysis in deuterated buffer pH 5.5 at 37 °C.

4.1.7 Stability in human plasma of HMPO derivatives

Pooled human plasma (0.9 mL, 55.7 µg protein/mL), [249] hepes buffer (1.0 mL, 25 mM, NaCl 140 mM, pH 7.4) and tested compound dissolved in DMSO (100 µL, 2.0 mM) were mixed in a test tube that was incubated at 37 °C under continuous mechanical agitation. At set time points (0.0, 0.25, 0.50, 1.0, 3.0, 5.0, 8.0, and 24.0 h), samples of 100 µL were taken, mixed with 400 µL of cold MeCN and centrifuged at 5000 rpm for 15 min. [250] The supernatant was collected and analysed by UV/LC-MS to monitor the amount of unmodified compound. For each product, the determination was performed in three independent experiments. UV/LC-MS methods LC analyses of plasma stability tests were performed by using Agilent 1100 LC/MSD VL system (G1946C) (Agilent Technologies, Palo Alto, CA) constituted by a vacuum solvent degassing unit, a binary high-pressure gradient pump, an 1100 series UV

detector, and an 1100 MSD model VL benchtop mass spectrometer. MSD single-quadrupole instrument was equipped with the orthogonal spray API-ES (Agilent Technologies, Palo Alto, CA). The pressure of the nebulizing gas and the flow of the drying gas (nitrogen used for both) were set at 40 psi, 9 L/min, respectively. The capillary voltage, the fragmentor voltage, and the vaporization temperature were 3000 V, 10 V, and 350 °C, respectively. MSD was used in the positive and negative ion mode. Spectra were acquired over the scan range m/z 100-2000 using a step size of 0.1. Chromatographic analyses were performed using a Phenomenex Kinetex EVO C18-100Å (150 x 4.6 mm, 5 μm particle size) at r.t., at flow rate of 0.6 mL/min, and injection volume of 10 μL, operating with a gradient elution of A: water (H_2O) and B: MeCN. Both solvents were acidified with 0.1% v/v of HCOOH. UV detection was monitored at 254 nm. The analysis started with 0% of B, then B was increased to 80% (from t = 0 to t = 20 min.), then kept at 80% (from t = 20 to t = 25 min.) and finally return to 0% of eluent B in 5.0 min.

4.1.8 MTT assay of ADC-1 and ADC-2

Cell culture: A431 epidermoid carcinoma cells and A549 lung carcinoma cells (ATCC, Rockville, MD, USA) were cultured in DMEM (Euroclone) supplemented with 10% fetal bovine serum (FBS, Euroclone), 100 U/ml penicillin/streptomycin (Euroclone), and 4 mM Lglutamine (Euroclone). All cell lines were grown at 37°C and 5% CO_2.
MTT: 2.5 x 103 cells/well were seeded in 96-multiwell plates in medium 10% FBS. After adherence, cells were incubated in fresh medium with increasing concentrations of Doxorubicin (0.05-50 μM), Combretastatin A4 (0.1-100 μM), Cetuximab (0.1-10 μg/ml), ADC-1 (0.1-10 μg/ml related to the DAR value) and ADC-2 (0.1-10 μg/ml related to the DAR value). At the indicated time (48, 72 and 96 h) the medium was removed, and cells were incubated for 4h with fresh medium in the presence of 1.2 mM MTT (3-(4,5-dimethylthiazol-2-yl)-2,5-diphenyltetrazolium bromide) (Sigma-Aldrich). The MTT solution was then removed and 50 μL of DMSO were added to the each well to dissolve the blue formazan crystals. The absorbance of the formazan dye was measured at 570 nm with a microplate reader (EnVision, PerkinElmer, Waltham, MA, USA). Data were expressed as a percentage of the basal control.

4.2 ADCs charged with unconventional payloads and exploration of new protocols for bioconjugation

4.2.1 Amide-based drugs

4.2.1.1 General experimental procedures, materials and instruments

All reagents were used as purchased from commercial suppliers without further purification. The reactions were carried out in oven dried vessels. Solvents were dried and purified by conventional methods prior use or, if available, purchased in anhydrous form.

Flash column chromatography was performed with Merck silica gel Å 60, 0.040-0.063 mm (230-400 mesh).

MPLC Syncore® Büchi or MPLC Isolera Prime Biotage on highly resistant PP cartridges Normal Phase silica gel NP 40 – 63 μm particle size and 60 Å pore size (Si60) withstand a maximum pressure of 10 bar (145 psi) column column with petroleum ether (eluent A) and Ethyl Acetate (Eluent B) as mobile phase.

Merck aluminum backed plates pre-coated with silica gel 60 (UV254) were used for analytical thin layer chromatography and were visualized by staining with a $KMnO_4$ or Ninidrine solution.

NMR spectra were recorded at 25 °C or at 37 °C with 400 for ^{1}H and 101 for ^{13}C Brücker Advance NMR spectrometers. The solvent is specified for each spectrum. Splitting patterns are designated as s, singlet; d, doublet; t, triplet; q, quartet; m, multiplet; bs, broad singlet. Chemical shifts (d) are given in ppm relative to the resonance of their respective residual solvent peaks.

High and low resolution mass spectroscopy analyses were recorded by electrospray ionization with a mass spectrometer Q-exactive Plus.

HPLC analyses were performed on the chromatographic system JASCO LC-Net II/ ADC connected with UV detector (254 nm) using an Intersil ODS-3V C18 column (5 μm, 4.6 x 250mm), flow 0.8 mL/min, eluent A/B: H_2O/MeCN Gradient 20% B to 80% B in 45 minutes, 15 minutes at 95 % B.

HPLC/MS analyses were performed on a InfinityLab LC/MSD iQ apparatus. Method: column: InfinityLab PoroShell 120 EC-C18 4.6 x 100 mm x 2.7μm; flow: 1.5 mL/min; eluent A/B: H_2O/MeCN, gradient: 5% B to 95% B in 10 minutes, 4 minutes at 95 % B and 3 minutes of re-equilibration; detection: 254 nm and 210 nm.

4.2.1.2 Synthetic procedures

3-Hydroxy-4-(methoxymethoxy)benzaldehyde (17a)

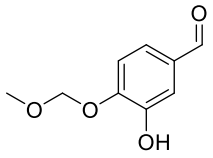

The product was prepared according to literature. [251]

Under N_2 atmosphere, 3,4-dihydroxybenzaldehyde (700 mg, 5.07 mmol) was suspended in CH_3CN dry (25 mL) and K_2CO_3 (2.1 g, 15.20 mmol) was added. The mixture was stirred for 30 min at r.t. and chloromethyl methyl ether (0.300 mL, 2.1 M in toluene, 6.30 mmol) was added. After stirring 16 h at r.t., NaOH 10% (25 mL) and EtOAc (3 x 25 mL) were added and the aqueous phase extracted, neutralized with HCl 1N until pH 9 and extracted again with EtOAc (2 x 25 mL). The organic phases were collected and washed with Na_2CO_3 (1 x 25 mL), brine (1 x 25 mL), dried over anhydrous Na_2SO_4, filtered, and evaporated under reduced pressure. The final crude product (593 mg, 64 % yield) was obtained as a yellow oil.

^{1}H NMR (400 MHz, $CDCl_3$): δ 9.75 (s, 1H), 7.38 (s, 1H), 7.31 (d, J = 8.2 Hz, 1H), 7.13 (d, J = 8.3 Hz, 1H), 5.75-6.5 (bs, 1H), 5.22 (s, 2H), 3.43 (s, 3H).

^{13}C NMR (101 MHz, $CDCl_3$) δ 191.5, 149.9, 146.7, 131.3, 124.3, 114.9, 114.3, 95.1, 56.6.

ESI-MS: m/z 205 $[M+ Na]^+$.

4-(Methoxymethoxy)-3-(prop-2-yn-1-yloxy)benzaldehyde (18a)

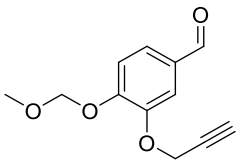

Compound **17a** (500 mg, 2.75 mmol) was solubilized in dry acetone (15 mL) under N_2 atmosphere and mixed with K_2CO_3 (1.13 g, 8.24 mmol) and KI (457 mg, 2.75 mmol). After 10 minutes, propargyl bromide (981 mg of a 30% solution in toluene, 8.24 mmol) was added and the reaction refluxed for 16 h. Acetone was evaporated and the crude was solubilized in

$CHCl_3$ (50 mL), washed with H_2O (2 x 25 mL) and brine (25 mL) and the organic phase dried over anhydrous Na_2SO_4, filtered, and evaporated under reduced pressure. The product was purified by chromatography on silica gel with MPLC (Medium Pressure Liquid Chromatography), 0-50 % gradient of EtOAc in petroleum ether to obtain the product **18a** as a pale-yellow oil (417 mg, 68% yield).

^{1}H NMR (400 MHz, $CDCl_3$): δ 9.73 (s, 1H), 7.44 (d, J = 1.1 Hz, 1H), 7.35 (dd, J = 8.3, 1.1 Hz, 1H), 7.15 (d, J = 8.3 Hz, 1H), 5.18 (s, 2H), 4.70 (d, J = 1.9 Hz, 2H), 3.38 (s, 3H), 2.53 – 2.44 (m, 1H).

^{13}C NMR (101 MHz, $CDCl_3$) δ 190.8, 152.5, 147.8, 130.9, 126.8, 115.2, 112.7, 95.04, 77.7, 76.4, 56.6, 56.6.

ESI-MS: m/z 243 $[M+Na]^+$. HRMS calcd for $C_{12}H_{12}NaO_4$ $[M+Na]^+$ 243.0633; found 243.0631.

(4-(Methoxymethoxy)-3-(prop-2-yn-1-yloxy)phenyl)methanol (19a)

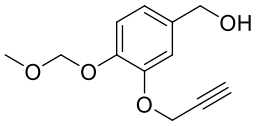

$NaBH_4$ (373 mg, 9.86 mmol) was suspended in dry MeOH (11 mL) under N_2 atmosphere and cooled at 0 °C. Then, a solution of compound **18a** (542 mg, 2.46 mmol) in dry CH_2Cl_2 (30 mL) was slowly added and the reaction mixture stirred for 2 h at 0 °C. Water was added until a white suspension appeared and the mixture was extracted with CH_2Cl_2 (3 x 25 mL). The organic phases were washed with H_2O (25 mL) and brine (25 mL), dried over anhydrous Na_2SO_4, filtered, and evaporated under reduced pressure. The product was purified by silica gel MPLC, 0-60 % gradient of EtOAc in petroleum ether to obtain the product (466 mg, 85% yield).

^{1}H NMR (400 MHz, $CDCl_3$): δ 7.10 (d, J = 8.2 Hz, 1H), 7.06 (d, J = 1.7 Hz, 1H), 6.91 (dd, J = 8.2, 1.7 Hz, 1H), 5.18 (s, 2H), 4.75 (s, 2H), 4.60 (d, J = 2.4 Hz, 2H), 3.48 (s, 3H), 2.48 (t, J = 2.4 Hz, 1H), 1.62 (bs, 1H).

^{13}C NMR (101 MHz, $CDCl_3$): δ 147.4, 146.1, 135.0, 120.3, 116.6, 113.3, 95.2, 78.1, 75.4, 64.5, 56.4, 55.8.

ESI-MS: m/z 245 $[M+Na]^+$. Anal. calcd. for $C_{12}H_{14}O_4$ C 64.85, H 6.35, O 28.80; found C 64.81, H 6.33.

4-(Methoxymethoxy)-3-(prop-2-yn-1-yloxy)benzyl (4-nitrophenyl) carbonate (20a)

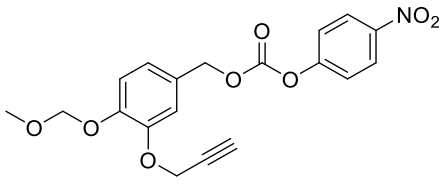

Compound **19a** (78 mg, 0.35 mmol) was solubilized in dry THF (8 mL) and cooled at 0 °C. DMAP (4 mg, 0.035 mmol), 4-nitrophenyl chloroformate (142 mg, 0.7 mmol) and pyridine (57 µL, 0.7 mmol) were added and the reaction was stirred at r.t. for 16 h. THF was evaporated and the crude was dissolved in EtOAc (20 mL) and washed with H_2O (10 mL), brine (10 mL), dried over anhydrous Na_2SO_4, filtered, and evaporated under reduced pressure. The product was purified by silica gel MPLC, 0-30 % gradient of EtOAc in petroleum ether to obtain the product **20a** (112 mg, 82% yield).

^{1}H NMR (400 MHz, $CDCl_3$) δ 8.24 (d, J = 9.2 Hz, 2H), 7.35 (d, J = 9.2 Hz, 2H), 7.15 (d, J = 8.3 Hz, 1H), 7.11 (d, J = 1.9 Hz, 1H), 7.02 (dd, J = 8.3, 1.9 Hz, 1H), 5.21 (s, 4H), 4.76 (d, J = 2.4 Hz, 2H), 3.49 (s, 2H), 2.48 (t, J = 2.4 Hz, 1H).

HRMS calcd for $C_{19}H_{17}NNaO_8$ $[M+Na]^+$ 410.0852, found 410.0850.

3-Hydroxy-4-((2-methoxyethoxy)methoxy)benzaldehyde (17b)

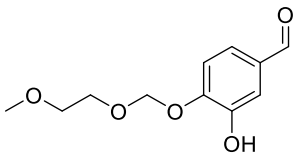

Obtained as previously described for **17a**. Obtained 711 mg of a pale yellow oil, 83% yield.

^{1}H NMR (400 MHz, $CDCl_3$): δ 9.82 (s, 1H), 7.42 (d, J = 1.9 Hz, 1H), 7.35 (dd, J = 8.3, 2.0 Hz, 1H), 7.17 (d, J = 8.3 Hz, 1H), 6.5-6.0 (bs, 1H), 5.34 (s, 2H), 3.84 (dd, J = 5.2, 3.7 Hz, 2H), 3.55 (dd, J = 5.4, 3.5 Hz, 2H), 3.36 (s, 3H).

^{13}C NMR (101 MHz, $CDCl_3$) δ 191.2, 149.9, 147.1, 131.7, 124.0, 115.2 115.0, 94.8, 71.5, 68.8, 59.0.

ESI-MS: m/z 249 $[M+Na]^+$ HRMS calcd for $C_{11}H_{14}NaO_5$ $[M+Na]^+$ 249.0739, found 249.0737.

4-((2-Methoxyethoxy)methoxy)-3-(prop-2-yn-1-yloxy)benzaldehyde (18b)

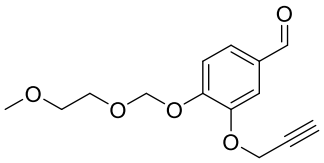

Obtained as previously described for **18a**. MPLC 0- 60 % gradient of EtOAc in petroleum ether gave the product **18b** as a yellow oil (335 mg, 80% yield).

^{1}H NMR (400 MHz, $CDCl_3$): δ 9.70 (s, 1H), 7.40 (s, 1H), 7.33 (d, J = 8.2 Hz, 1H), 7.17 (d, J = 8.3 Hz, 1H), 5.24 (s, 2H), 4.67 (d, J = 2.1 Hz, 2H), 3.72 (d, J = 4.3 Hz, 2H), 3.40 (d, J = 4.5 Hz, 2H), 3.19 (s, 3H), 2.48 (s, 1H).

^{13}C NMR (101 MHz, $CDCl_3$): δ 190.7, 152.4, 147.8, 130.8, 126.8, 115.5, 112.5, 93.9, 77.8, 76.5, 71.4, 68.2, 58.9, 56.6.

ESI-MS: m/z 287 $[M+Na]^+$. HRMS calcd for $C_{14}H_{16}NaO_5$ $[M+Na]^+$ 287.0895, found 287.0893.

(4-((2-Methoxyethoxy)methoxy)-3-(prop-2-yn-1-yloxy)-phenyl)methanol (19b)

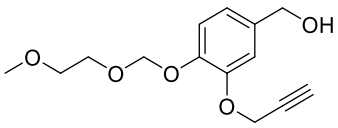

Obtained as previously described for **19a**. MPLC 0-70 % gradient of EtOAc in petroleum ether gave product **19b** as a colourless oil (162 mg, 78% yield).

^{1}H NMR (400 MHz, $CDCl_3$): δ 7.07 (d, J = 8.2 Hz, 1H), 6.97 (s, 1H), 6.83 (d, J = 8.2 Hz, 1H), 5.19 (s, 2H), 4.66 (s, 2H), 4.50 (s, 2H), 3.83 – 3.73 (m, 2H), 3.49 – 3.43 (m, 2H), 3.28 (s, 3H), 2.56 (s, 1H), 2.45 (s, 1H).

^{13}C NMR (101 MHz, $CDCl_3$): δ 147.3, 146.1, 135.1, 120.3, 116.7, 113.2, 94.2, 78.1, 75.4, 71.1, 67.4, 64.3, 58.5, 56.3.

ESI-MS: m/z 289 $[M+Na]^+$. HRMS calcd for $C_{14}H_{18}NaO_5$ $[M+Na]^+$ 289.1052, found 289.1054.

4-((2-Methoxyethoxy)methoxy)-3-(prop-2-yn-1-yloxy)benzyl (4-nitrophenyl) carbonate (20b)

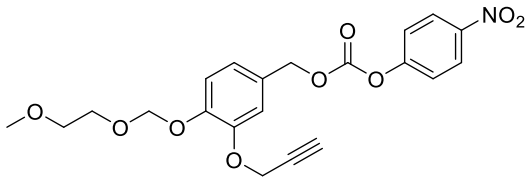

Obtained as previously described for **20a**. MPLC 0-50 % gradient of EtOAc in petroleum ether gave product **20b** as a colourless oil (198 mg, 82% yield).

^{1}H NMR (400 MHz, $CDCl_3$): δ 8.20 (d, J = 9.0 Hz, 2H), 7.32 (d, J = 9.0 Hz, 2H), 7.17 (d, J = 8.3 Hz, 1H), 7.08 (s, 1H), 6.99 (d, J = 8.3 Hz, 1H), 5.27 (s, 2H), 5.18 (s, 2H), 4.73 (d, J = 2.2 Hz, 2H), 3.85 – 3.78 (m, 2H), 3.54 – 3.48 (m, 2H), 3.32 (d, J = 3.7 Hz, 3H), 2.48 (t, J = 2.0 Hz, 1H).

ESI-MS: m/z 432 $[M+H]^+$. HRMS calcd for $C_{21}H_{22}NO_9$ $[M+H]^+$. 432.1295, found 431.1297

General procedure for the synthesis of carbamates

The amide (50 mg, 0.15 mmol) was solubilized in dry THF (0,8 mL) under N_2 atmosphere in a Schlenk tube and the mixture was cooled at - 78 °C. Then KHMDS (0.15 mL of a 0,5 M solution in toluene, 0.13 mmol) was added and the reaction was stirred -78 °C for 1 h. A solution of carbonate (52 mg, 0.13 mmol) in 0,8 mL of dry THF was slowly added, the temperature was raised from -78 °C to -5 °C and the mixture stirred at this temperature for 1.5-16 h. Then EtOAc (15 mL) was added, the mixture heated to r.t. and the organic phase washed with NH_4Cl (10 mL), H_2O (10 mL) and brine (10 mL) The organic layer was dried over anhydrous Na_2SO_4, filtered, and evaporated under reduced pressure. The product was purified through silica gel MPLC.

{[3-(3- Fluoro-4-morpholinophenyl)-2-oxo-1,3-oxazolidin-5- yl]methyl}acetylamino-{4-[(2-methoxyethoxy)methoxy]-3-(2- propynyloxy)-phenyl}methylformylate (23b)

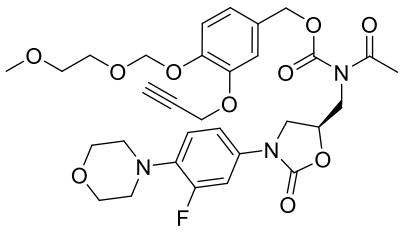

Compound **23b** was prepared according to general procedure. Time reaction: 4 h. The compound was purified through silica gel MPLC, 0-70 % gradient of EtOAc in petroleum ether (42 mg, 59% yield). **^{1}H NMR** (400 MHz, $CDCl_3$): δ 7.35 (d, J = 14.3 Hz, 1H), 7.15 (dd, J = 8.2, 2.1 Hz, 1H), 7.07 (s, 1H), 7.02 (d, J = 8.8 Hz, 1H), 6.96 (d, J = 8.2 Hz, 1H), 6.89 (dd, J = 12.7, 5.4 Hz, 1H), 5.30 – 5.09 (m, 4H), 4.73 (s, 3H), 4.22 – 3.94 (m, 4H), 3.83 (d, J = 3.3 Hz, 6H), 3.67 – 3.58 (m, 1H), 3.54 – 3.50 (m, 2H), 3.33 (d, J = 2.2 Hz, 2H), 3.05 – 2.95 (m, 4H), 2.52 (d, J = 2.1 Hz, 3H), 2.46 (d, J = 2.3 Hz, 1H).

^{13}C NMR (101 MHz, $CDCl_3$): δ 172.9, 156.3, 153.9, 153.6, 147.3, 136.1, 132.6, 128.2, 122.6, 118.4, 116.5, 114.9, 113.5, 107.2, 106.9, 94.1, 78.0, 75.4, 71.1, 70.1, 68.8, 67.5, 66.5, 58.5, 56.4, 50.6, 48.0, 46.3, 26.2.

ESI-MS: m/z 630 $[M+H]^+$, 652 $[M+ Na]^+$. Anal calcd. for $C_{31}H_{36}FN_3O_{10}$: C 59.13, F 3.02, H 5.76, N 6.67, O, 25.41; found C 59.10, H 5.74, N 6.69.

4-(Methoxymethoxy)-3-(prop-2-yn-1-yloxy)benzyl (R)- acetyl((3-(3-fluoro-4 morpholino-phenyl)-2-oxooxazolidin-5-yl)methyl)carbamate (23a)

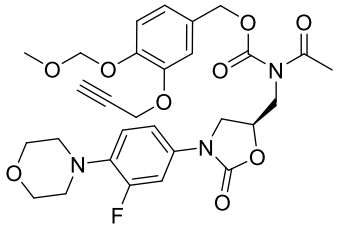

Compound **23a** was prepared according to general procedure. Time reaction: 4 h. The compound was purified through silica gel MPLC, 0-70 % gradient of EtOAc in petroleum ether (51 mg, 88% yield). **^{1}H NMR** (400 MHz, $CDCl_3$): δ 7.34 (dd, J = 14.3, 2.5 Hz, 1H), 7.09 (dd, J = 10.9, 5.0 Hz, 2H), 6.99 (ddd, J = 10.1, 8.5, 2.1 Hz, 2H), 6.88 (t, J = 9.1 Hz, 1H), 5.28 – 5.06 (m, 4H), 4.71-4.80 (m, 3H), 4.13 (dd, J = 14.2, 7.6 Hz, 1H), 4.08 – 3.92 (m, 2H),

3.88 – 3.79 (m, 4H), 3.61 (dd, J = 9.1, 5.7 Hz, 1H), 3.46 (d, J = 6.1 Hz, 3H), 3.12 – 2.96 (m, 4H), 2.51 (s, 3H), 2.46 (s, 1H).

^{13}C NMR (101 MHz, $CDCl_3$): δ 172.8, 156.2, 153.8, 153.5, 153.4, 147.3, 136.0, 132.7, 132.6, 128.1, 122.5, 118.4, 116.48, 115.0, 113.5, 107.1, 106.9, 95.0, 78.0, 75.5, 70.1, 67.5, 66.4, 56.4, 55.8, 50.5, 47.9, 46.2, 26.1.

ESI-MS: m/z 586 $[M+H]^+$; 608 $[M+Na]^+$; 624 $[M+K]^+$. Anal calcd. for $C_{29}H_{32}FN_3O_9$ C 59.48; F 3.24; H 5.51; N 7.18; O 24.59; found C 59.39, H 5.49, N 7.16

4-(Methoxymethoxy)-3-(prop-2-yn-1-yloxy)benzyl (4-(3-(4- cyano-3 (trifluoromethyl)phenyl)-5,5-dimethyl-4-oxo-2- thioxoimidazolidin-1-yl)-2 fluorobenzoyl)(methyl)carbamate (25a)

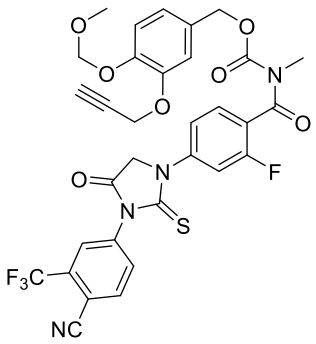

Compound **25a** was prepared according to general procedure for synthesis of carbamates. Time reaction: 4 h. The compound was purified through silica gel MPLC, 0-50 % gradient of EtOAc in petroleum ether (46 mg, 64% yield).

^{1}H NMR (400 MHz, $CDCl_3$): δ 7.96 (s, 1H), 7.93 (d, J = 5.5 Hz, 1H), 7.80 (dd, J = 8.3, 1.8 Hz, 1H), 7.59 (t, J = 7.8 Hz, 1H), 7.14 (dd, J = 8.2, 1.7 Hz, 1H), 7.06 (d, J = 8.3 Hz, 1H), 6.98 (dd, J = 10.0, 1.7 Hz, 1H), 6.95 (d, J = 1.9 Hz, 1H), 6.81 (dd, J = 8.3, 1.9 Hz, 1H), 5.17 (d, J = 2.3 Hz, 2H), 5.02 (s, 2H), 4.71 (d, J = 2.4 Hz, 2H), 3.47 (s, 3H), 3.37 (s, 3H), 2.47 (t, J = 2.3 Hz, 1H), 1.56 (s, 6H).

^{13}C NMR (101 MHz, $CDCl_3$): δ 179.7, 174.5, 166.8, 159.9, 157.4, 153.9, 147.7, 147.5, 138.0, 137.9, 136.9, 135.3, 133.8, 133.5, 132.1, 130.2, 128.6, 127.4, 127.3, 127.1, 127.0, 125.7, 123.2, 122.9, 120.5, 117.3, 117.0, 116.7, 115.5, 114.7, 110.4, 95.4, 75.9, 68.7, 66.6, 57.0, 56.3, 32.1, 29.7, 23.8.

ESI-MS: m/z 713 $[M+H]^+$; 735 $[M+Na]^+$. Anal calcd. for $C_{34}H_{28}F_4N_4O_7S$: C 57.30, F 10.66, H 3.96, N 7.86, O 15.71, S 4.50; found C 57.27, H, 3.95, N 7.88.

2-Ethoxy-6-[(p-nitrophenoxycarbonyloxy)methyl]-4-(2- propynyloxy)-2H-1,3-benzodioxole (28)

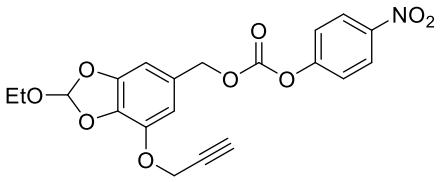

Obtained as previously described for **20a**. MPLC, 0-50 % gradient of EtOAc in petroleum ether gave 28 as a colourless oil (101 mg, 70% yield).

^{1}H NMR (400 MHz, $CDCl_3$) δ 8.24 (d, J = 8.9 Hz, 2H), 7.35 (d, J = 8.9 Hz, 2H), 6.89 (s, 1H), 6.73 (s, 1H), 6.68 (s, 1H), 5.16 (s, 2H), 4.80 (s, 2H), 3.74 (q, J = 7.0 Hz, 2H), 2.51 (s, 1H), 1.24 (t, J = 7.0 Hz, 3H).

ESI-MS: m/z 438 $[M+Na]^+$. HRMS calcd for $C_{20}H_{17}NNaO_9$ 438.0801; found 438.0802.

(2-Ethoxy-7-(prop-2-yn-1-yloxy)benzo[d][1,3]dioxol-5- yl)methyl acetyl(((R)-3-(3-fluoro-4-morpholinophenyl)-2- oxooxazolidin-5-yl)methyl)carbamate (29)

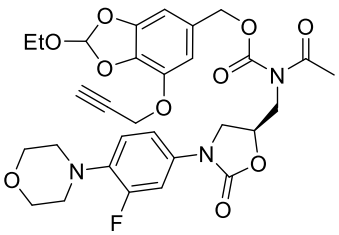

Compound **29** was prepared according to the general procedure. Time reaction: 1.5 h. The compound was purified by silica gel MPLC, 0-70 % gradient of EtOAc in petroleum ether (44 mg, 72% yield).

^{1}H NMR (400 MHz, $CDCl_3$): δ 7.40 – 7.30 (m, 1H), 7.01 (t, J = 7.5 Hz, 1H), 6.91 – 6.83 (m, 2H), 6.69 (s, 1H), 6.64 (d, J = 4.0 Hz, 1H), 5.12 (m, 2H), 4.78 (s, 2H), 4.12 (m, 1H),

4.00 (m, 2H), 3.89 – 3.79 (m, 4H), 3.71 (dt, J = 13.8, 7.0 Hz, 2H), 3.66 – 3.57 (m, 1H), 3.04 – 2.97 (m, 4H), 2.51 (s, 3H), 2.48 (d, J = 1.1 Hz, 1H), 1.59 (s, 1H), 1.27 – 1.18 (m, 3H).

^{13}C NMR (101 MHz, $CDCl_3$): δ 172.9, 156.3, 153.9, 153.6, 147.3, 140.2, 136.0, 134.5, 132.8, 128.2, 119.4, 118.5, 113.5, 110.7, 107.3, 103.2, 77.8, 75.6, 70.0, 68.9, 66.5, 59.2, 57.0, 50.6, 48.0, 46.3, 26.2, 14.3.

ESI-MS: m/z 614 $[M+H]^+$; 636 $[M+Na]^+$. Anal calcd. for $C_{30}H_{32}FN_3O_{10}$: C 58.72, F 3.10, H 5.26, N 6.85, O 26.08; found: C 58.70, H 5.25, N 6.87.

(2-Ethoxy-7-(prop-2-yn-1-yloxy)benzo[d][1,3]dioxol-5- yl)methyl (4-(3-(4-cyano-3-(trifluoromethyl)phenyl)-5,5- dimethyl-4-oxo-2-thioxoimidazolidin-1-yl)-2-fluorobenzoyl)(methyl)carbamate (30)

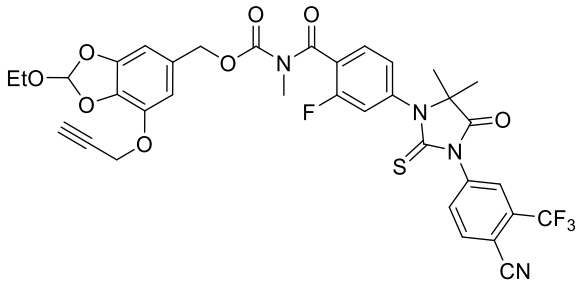

Compound **30** was prepared according to the general procedure. Time reaction: 3 h. The compound was purified by silica gel MPLC 0-60 % gradient of EtOAc in petroleum ether (44 mg, 61% yield).

^{1}H NMR (400 MHz, $CDCl_3$): δ 7.96 (s, 1H), 7.93 (d, J = 4.8 Hz, 1H), 7.80 (d, J = 8.3 Hz, 1H), 7.60 (t, J = 7.7 Hz, 1H), 7.15 (d, J = 8.1 Hz, 1H), 7.00 (d, J = 10.0 Hz, 1H), 6.83 (s, 1H), 6.55 (s, 1H), 6.48 (s, 1H), 4.97 (s, 2H), 4.76 (d, J = 1.1 Hz, 2H), 3.71 (q, J = 7.0 Hz, 2H), 3.37 (s, 3H), 2.48 (d, J = 2.2 Hz, 1H), 1.56 (s, 6H), 1.22 (t, J = 7.1 Hz, 3H).

^{13}C NMR (101 MHz, $CDCl_3$): 179.7, 174.5, 166.8, 159.9, 157.4, 153.8, 147.6, 140.4, 138.1, 138.0, 136.9, 135.3, 134.7, 132.1, 130.2, 128.7, 127.3, 127.2, 127.1, 127.0, 125.7, 119.7, 117.3, 117.1, 114.7, 111.1, 110.3, 103.4, 76.1, 68.8, 66.6, 59.8, 57.5, 32.1, 23.8, 14.8.

ESI-MS: m/z 741 $[M+H]^+$, 764 $[M+Na]^+$. Anal calcd. for $C_{35}H_{28}F_4N_4O_8S$: C 56.75, F 10.26, H 3.81, N 7.56, O 17.28, S 4.33; found C 56.71, H 3.78, N 7.59.

(2-Ethoxy-7-(prop-2-yn-1-yloxy)benzo[d][1,3]dioxol-5-yl)methyl(((1R,2R)-2-(2,3-dihydrobenzofuran-4-yl)cyclopropyl)-methyl)(propionyl)carbamate (31)

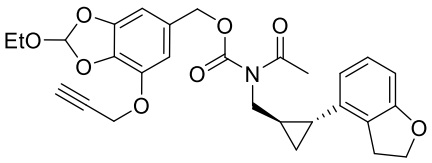

Compound **31** was prepared according to the general procedure. Time reaction: 3.5 h. The compound was purified by silica gel MPLC, 0-30 % gradient of EtOAc in petroleum ether (23 mg, 44% yield).

^{1}H NMR (400 MHz, $CDCl_3$): δ 6.95 (t, J = 7.8 Hz, 1H), 6.86 (s, 1H), 6.66 (s, 1H), 6.61 (s, 1H), 6.55 (d, J = 7.9 Hz, 1H), 6.23 (dd, J = 7.7, 2.7 Hz, 1H), 5.10 (s, 2H), 4.74 (d, J = 1.1 Hz, 2H), 4.51 (t, J = 8.7 Hz, 2H), 3.87 – 3.70 (m, 4H), 3.16 – 2.99 (m, 2H), 2.88 (q, J = 7.2 Hz, 2H), 2.44 (m, 1H), 1.79 (m, 1H), 1.55 (m, 2H), 1.41 – 1.34 (m, 1H), 1.28 – 1.20 (m, 3H), 1.11 (dd, J = 7.6, 6.9 Hz, 3H), 0.88 (td, J = 12.9, 5.0 Hz, 2H).

^{13}C NMR (101 MHz, $CDCl_3$): δ 176.9, 159.5, 154.4, 147.7, 140.6, 139.0, 129.2, 128.1, 126.1, 119.7, 115.9, 115.9, 110.9, 106.7, 103.3, 71.0, 68.3, 59.7, 57.4, 47.7, 31.8, 29.7, 28.5, 21.4, 19.9, 14.8, 14.1, 13.3, 9.3.

ESI-MS: m/z 544 $[M+ Na]^+$, 560 $[M+K]^+$. Anal calcd. for $C_{30}H_{33}NO_7$: C 69.35, H 6.40, N 2.70, O 21.55; found C 69.31, H 6.37, N 2.73.

(2-Ethoxy-7-(prop-2-yn-1-yloxy)benzo[d][1,3]dioxol-5-yl)methyl tosylcarbamate (32)

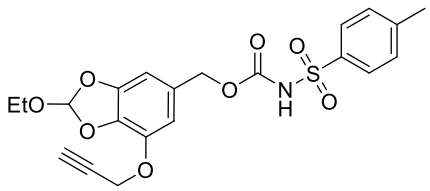

Compound **32** was prepared according to the general procedure. Time reaction: 16 h. The compound was purified through chromatography on silica gel with MPLC 0-60 % gradient of EtOAc in petroleum ether (13 mg, 21% yield).

^{1}H NMR (400 MHz, $CDCl_3$) δ 7.85 (d, J = 8.3 Hz, 2H), 7.28 (d, J = 8.1 Hz, 2H), 6.85 (s, 1H), 6.55 (s, 1H), 6.45 (s, 1H), 4.94 (s, 2H), 4.74 (s, 2H), 3.71 (q, J = 7.1 Hz, 2H), 2.49 (t, J = 2.3 Hz, 1H), 2.41 (s, 3H), 1.23 (q, J = 9.0, 5.1 Hz, 3H).

^{13}C NMR (101 MHz, $CDCl_3$): δ 150.1, 147.6, 145.2, 140.5, 135.3, 129.7, 129.6, 129.2, 128.5, 128.4, 126.5, 119.7, 110.8, 103.3, 68.5, 59.6, 57.4, 29.7, 21.7, 14.8.
ESI-MS: m/z 448 $[M+H]^+$, 479 $[M+Na]^+$. HRMS calcd. for $C_{21}H_{22}NO_8S$: 448.1066; found 448.1065.

4.2.1.3 General procedure for release experiments

10 mM stock solution of compounds **23a**, **23b**, **25**, **29**, **31** and **32** was prepared in DMSO and diluted in the corresponding buffers to obtain a 1 mM solution. In the case of compound **30**, the 10 mM stock solution was diluted in the corresponding buffer and additionally diluted with DMSO to obtain a final 0.67 mM solution in buffer/H_2O/DMSO. For analysis at pH 7.4, and 6, phosphate buffers 0.1 M were used (KH_2PO_4/K_2HPO_4). For pH 5.5 and 4.5 acetate buffer 0.1 M was used (CH_3COONa/ CH_3COOH). All compounds were mixed with the buffers at 25 °C and further incubated at 37 °C. HPLC analyses were carried out following the method reported in general experimental procedure every 1-3 h up to 6 h and every 6 h up to 48 h.

4.2.1.4 Stability in plasma experiments

Pooled human plasma, purchased from Merck (0.9 mL, 55.7 μg protein/mL), hepes buffer (1.0 mL, 25 mM, NaCl 140 mM, pH 7.4) and tested compound dissolved in DMSO (100 μL, 2.0 mM) were mixed in a test tube incubated at 37 °C under continuous mechanical agitation. At set time points (0.0, 0.25, 0.50, 1.0, 3.0, 5.0, 8.0, and 24.0 h), samples of 100 μL were taken, mixed with 400 μL of cold acetonitrile and centrifuged at 5000 rpm for 15 min. The supernatant was collected and analysed by UV/LC-MS to monitor the amount of unmodified compound. LC analyses of plasma stability tests were performed by using Agilent 1100 LC/MSD VL system (G1946C) (Agilent Technologies, Palo Alto, CA) constituted by a vacuum solvent degassing unit, a binary high-pressure gradient pump, an 1100 series UV detector, and an 1100 MSD model VL benchtop mass spectrometer. MSD single-quadrupole instrument was equipped with the orthogonal spray API-ES (Agilent Technologies, Palo Alto, CA). The pressure of the nebulizing gas and the flow of the drying gas (nitrogen used for both) were set at 40 psi, 9 L/min, respectively. The capillary voltage, the fragmentation voltage, and the vaporization temperature were 3000 V, 10 V, and 350 °C, respectively.

MSD was used in the positive and negative ion mode. Spectra were acquired over the scan range m/z 100-2000 using a step size of 0.1. Chromatographic analyses were performed using a Phenomenex Kinetex EVO C18-100Å (150 x 4.6 mm, 5 μm particle size) at room temperature, at flow rate of 0.6 mL/min, and injection volume of 10 μL, operating with a gradient elution of A: water (H_2O) and B: acetonitrile (ACN). Both solvents were acidified with 0.1% v/v of formic acid. UV detection was monitored at 254 nm. The analysis started with 0% of B, then B was increased to 80% (from t = 0 to t = 20 min), then kept at 80% (from t = 20 to t = 25 min) and finally return to 0% of eluent B in 5.0 min.

4.2.2 ADCs charged with Cyclopamine

4.2.2.1 General experimental procedures, materials and instruments

All reagents were used as purchased from commercial suppliers without further purification. The reactions were carried out in oven dried vessels. Solvents were dried and purified by conventional methods prior use or, if available, purchased in anhydrous form.
Flash column chromatography was performed with Merck silica gel Å 60, 0.040-0.063 mm (230-400 mesh).
MPLC Syncore® Büchi or MPLC Isolera Prime Biotage on highly resistant PP cartridges Normal Phase silica gel NP 40 – 63 μm particle size and 60 Å pore size (Si60) withstand a maximum pressure of 10 bar (145 psi) column column with petroleum ether (eluent A) and Ethyl Acetate (Eluent B) as mobile phase.
Merck aluminum backed plates pre-coated with silica gel 60 (UV254) were used for analytical thin layer chromatography and were visualized by staining with a $KMnO_4$ or Ninidrine solution.
NMR spectra were recorded at 25 °C or at 37 °C with 400 for ^{1}H and 101 for ^{13}C Brücker Advance NMR spectrometers. The solvent is specified for each spectrum. Splitting patterns are designated as s, singlet; d, doublet; t, triplet; q, quartet; m, multiplet; bs, broad singlet. Chemical shifts (d) are given in ppm relative to the resonance of their respective residual solvent peaks.
High and low resolution mass spectroscopy analyses were recorded by electrospray ionization with a mass spectrometer Q-exactive Plus.

MALDI analysis were performed with the MALDI-TOF in linear mode set at 83% of laser intensity. The m/z range was from 30 kDa to 200 kDa.

4.2.2.2 Synthetic procedures

(2-ethoxy-7-(prop-2-yn-1-yloxy)benzo[d][1,3]dioxol-5-yl)methyl (3S,3'R,3a'S,6aS,6bS,6'S,7a'R,9R,11aS,11bR)-3-hydroxy-3',6',10,11b-tetramethyl 1,2,3,3',3a',4,5',6,6a,6b,6',7,7',7a',8,11,11a,11b-octadecahydro-4'H-spiro[benzo[a]fluorene-9,2' furo[3,2-b]pyridine]-4'-carboxylate (33)

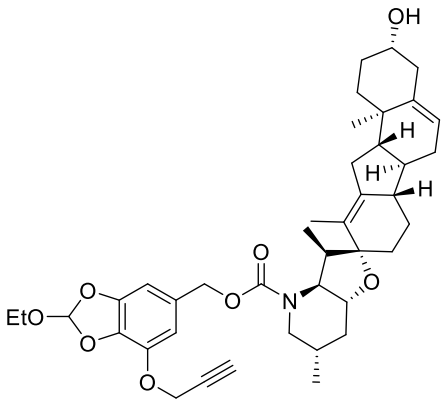

Cyclopamine (954 mg, 3.20 mmol) and DIPEA (1.21 mL, 6.96 mmol) were solubilized in dry DMF (8 mL) and cooled at 0 °C. Then, a solution of carbonate **28** (481 mg, 1.16 mmol) in DMF dry (2 mL) was added and the reaction stirred at r.t. for 24 h. DMF was evaporated and the crude was purified by silica gel MPLC, 0-5 % gradient of MeOH in CH_2Cl_2 to obtain the product **33** (453 mg, 0.66 mmol, 57% yield).

1-(prop-2-yn-1-yl)-1H-pyrrole-2,5-dione (36)

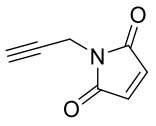

The product was prepared according to the literature. [252]

Maleic anhydride (3 g, 30.50 mmol) and propargylamine (2.16 mL, 33.65 mmol) were dissolved in glacial acetic acid (15 mL) and stirred at r.t. for 16 h. The reaction mixture was concentrated under reduced pressure to remove all the acetic acid. The residue was suspended in acetic anhydride (20 mL) and NaOAc (1.25 g, 15.29 mmol) was added. The reaction vessel was heated to reflux for 3 h. After cooling to r.t., the reaction mixture was diluted in H_2O (70 mL) and extracted with Et_2O (3 × 100 mL). The combined organic phases were dried over Na_2SO_4, filtered, and evaporated under vacuum. The compound was purified by chromatography on silica gel with MPLC Syncore® Büchi eluting 0-50 % gradient of EtAOc in petroleum ether to obtain the desired product as a transparent oil (1.24 g, 9.15 mmol, 30% yield).

^{1}H NMR (400 MHz, $CDCl_3$, δ ppm, J Hz) δ 6.66 (s, 2H), 4.12 (s, 2H), 2.13 (s, 1H).

(4-mercaptophenyl)methanol (37)

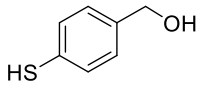

The product was prepared in according to the literature. [166]

4-mercaptobenzoic acid (1.4 g, 9.08 mmol) was solubilized in THF dry (25 mL) and cooled to 0 °C. Then, a solution of $LiAlH_4$ (27 mL, 27.24 mmol, 1M in THF) was slowly added and the reaction heated to r.t. and stirred for 1.5 h. At the end of the reaction, HCl 1N was added until pH 2. H_2O (20 mL) and EtOAc (50 mL) were added and the layers were separated. EtOAc and washed with H_2O (20 mL), brine (20 mL), dried over anhydrous Na_2SO_4, filtered, and evaporated under reduced pressure to obtain the product as a yellow oil (1.19 g, 94% yield).

^{1}H NMR (400 MHz, $CDCl_3$, δ ppm, J Hz): δ 7.23 (d, J = 8.1 Hz, 2H), 7.19 (d, J = 8.2 Hz, 2H), 4.60 (s, 2H).

3-((4-(hydroxymethyl)phenyl)thio)-1-(prop-2-yn-1-yl)pyrrolidine-2,5-dione (38)

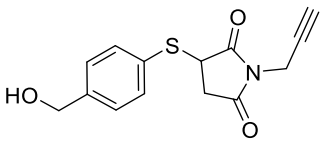

The compound **36** (1.11 mg, 8.22 mmol) and the thiol **37** (678 mg, 4.84 mmol) were solubilized in MeCN (40 mL) and a catalytic amount of Et_3N (33 μL, 0.24 mmol) was added. The reaction was stirred at r.t. for 16 h and after the crude was concentrated in vacuo. The product was purified by chromatography on silica gel with MPLC Syncore® Büchi eluting 0-100 % gradient of EtAOc in petroleum ether, obtaining the product as a transparent oil (1.24 g, 4.50 mmol, 93% yield).

^{1}H NMR (400 MHz, $CDCl_3$, δ ppm, J Hz): δ 7.47 (d, J = 7.9 Hz, 2H), 7.30 (d, J = 7.7 Hz, 2H), 4.66 (s, 2H), 4.15 (s, 2H), 3.99 (dd, J = 9.2, 4.1 Hz, 1H), 3.14 (dd, J = 18.8, 9.2 Hz, 1H), 2.67 (dd, J = 18.8, 4.2 Hz, 1H), 2.13 (s, 1H).

ESI: m/z 276 $[M+H]^+$, 298 $[M+Na]^+$.

4-((2,5-dioxo-1-(prop-2-yn-1-yl)pyrrolidin-3-yl)thio)benzyl (3S,3'R,3a'S,6aS,6bS,6'S,7a'R,9R,11aS,11bR)-3-hydroxy-3',6',10,11b-tetramethyl 1,2,3,3',3a',4,5',6,6a,6b,6',7,7',7a',8,11,11a,11b-octadecahydro-4'H-spiro[benzo[a]fluorene 9,2'-furo[3,2-b]pyridine]-4'-carboxylate (40)

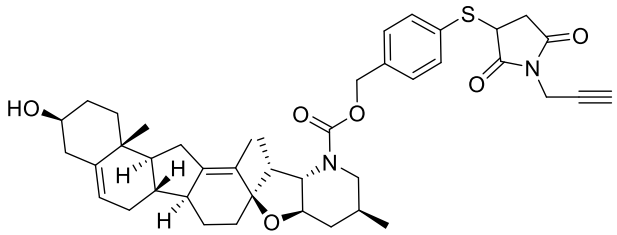

Compound **38** (100 mg, 0.36 mmol) was solubilized in DCM dry (5 mL) and cooled to 0 °C under N_2. Then, pyridine (58 mL, 0.72 mmol), DMAP (4 mg, 0.036 mmol) and 4-nitrophenyl chloroformate (145 mg, 0.72 mmol) were added and the reaction mixture stirred at r.t. for 16 h. DCM was evaporated and the product was purified by silica gel MPLC, 0-65 % gradient of EtOAc in petroleum ether to obtain the carbonate **39** (75 mg, 46% yield). Product **39** was confirmed by ESI-MS analysis and immediately used for the next step.

Cyclopamine (140 mg, 0.34 mmol) and DIPEA (0.18 mL, 1.02 mmol) were solubilized in dry DMF (5 mL) and cooled at 0 °C. Then, a solution of carbonate **39** (75 mg, 0.17 mmol) in DMF dry (2 mL) was added and the reaction stirred at r.t. for 24 h. DMF was evaporated

and the crude was purified by silica gel MPLC, 0-5 % gradient of MeOH in CH_2Cl_2 to obtain the product **40** (93 mg, 76% yield).

General procedure for CuAAC reaction

The desired alkyne (0.07 mmol) and the azide **12** (9 mg, 0.056 mmol) were dissolved in dry DMF (2 mL) under Ar. The solution was degassed with three cycles of argon/vacuum. To this solution, a freshly prepared aqueous mixture (2 mL) of $Cu(OAc)_2$ (4 mg, 0.021 mmol) and Na-ascorbate (8 mg, 0.042 mmol), previously degassed by argon/vacuum cycles, was added dropwise. The reaction mixture was degassed and left to stir under Ar. at r.t. for 16 h. The solvent was evaporated and the crude was purified by silica gel flash chromatography eluting 0-10 % gradient of MeOH in CH_2Cl_2 to obtain the desired compound.

6-(4-(((2-ethoxy-6-((((3S,3'R,3a'S,6aS,6bS,6'S,7a'R,9R,11aS,11bR)-3-hydroxy-3',6',10,11b tetramethyl-1,2,3,3a',4,4',5',6,6a,6b,6',7,7',7a',8,11,11a,11b-octadecahydro-3'H spiro[benzo[a]fluorene-9,2'-furo[3,2-b]pyridine]-4'-carbonyl)oxy)methyl)benzo[d][1,3]dioxol-4 yl)oxy)methyl)-1H-1,2,3-triazol-1-yl)hexanoic acid (34)

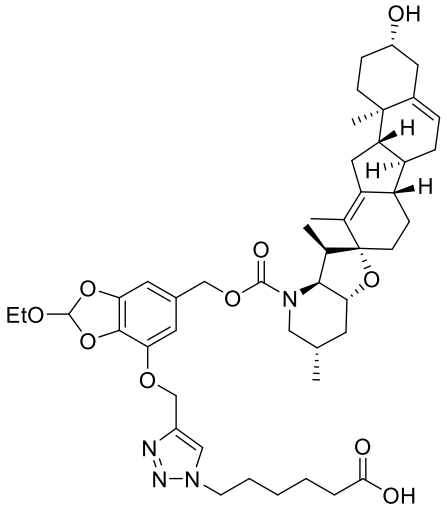

Compound **34** was synthesized in according to the general procedure for CuAAC. Obtained 19 mg, 0.022 mmol, yield 40%.

^{1}H NMR (400 MHz, DMSO, δ ppm, J Hz) δ 8.19 (s, 1H), 7.06 (s, 1H), 6.80 (d, J = 15.7 Hz,

1H), 6.63 (d, J = 11.7 Hz, 1H), 5.72 (s, 1H), 5.16 (d, J = 12.6 Hz, 2H), 4.95 (s, 2H), 3.63 (q, J = 7.0 Hz, 2H), 3.51 – 3.43 (m, 3H), 3.07 (t, J = 7.2 Hz, 1H), 2.92 – 2.79 (m, 1H), 2.63 (dd, J = 14.4, 7.4 Hz, 1H), 2.18 – 2.02 (m, 5H), 1.98 (dd, J = 22.8, 11.6 Hz, 3H), 1.84 – 1.66 (m, 5H), 1.60 (dd, J = 26.8, 11.8 Hz, 4H), 1.51 – 1.38 (m, 6H), 1.25 – 1.16 (m, 4H), 1.11 – 1.02 (m, 4H), 0.95 – 0.81 (m, 8H).

ES-MS: m/z 868 $[M+H]^+$, 884 $[M+Na]^+$.

6-(4-((3-((4-((((3S,3'R,3a'S,6aS,6bS,6'S,7a'R,9R,11aS,11bR)-3-hydroxy-3',6',10,11b tetramethyl-1,2,3,3a',4,4',5',6,6a,6b,6',7,7',7a',8,11,11a,11b-octadecahydro-3'H spiro[benzo[a]fluorene-9,2'-furo[3,2-b]pyridine]-4'-carbonyl)oxy)methyl)phenyl)thio)-2,5 dioxopyrrolidin-1-yl)methyl)-1H-1,2,3-triazol-1-yl)hexanoic acid (41)

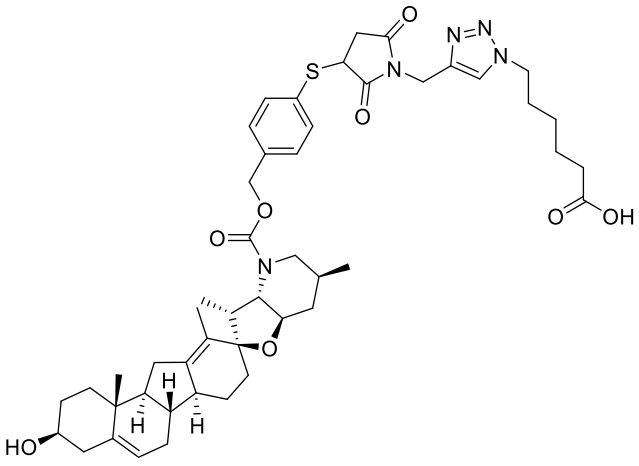

Compound **41** was synthesized in according to the general procedure for CuAAC. Obtained 37 mg, 0.042 mmol, yield 75%.

^{1}H NMR (400 MHz, $CDCl_3$, δ ppm, J Hz): δ 7.51 (s, 1H), 7.46 (d, J = 6.0 Hz, 2H), 7.29 (d, J = 6.0 Hz, 1H), 5.37 (s, 1H), 5.30 (s, 1H), 4.73 (m, 2H), 5.12 (s, 2H), 4.34 – 4.31 (m, 2H), 4.10 – 4.08 (m, 1H), 3.64 (d, J = 6.0 Hz, 1H), 3.56 – 3.54 (m, 2H), 3.23 – 3.17 (m, 2H), 2.96 – 2.93 (m, 1H), 2.84 – 2.80 (m, 1H), 2.69 (dd, J = 1.61 Hz, 1H), 2.38 – 2.34 (m, 3H), 2.27 – 2.15 (m, 5H), 1.92 – 1.89 (m, 5H), 1.87 – 1.82 (m, 2H), 1.80 – 1.68 (m, 9H), 1.66 – 1.64 (m, 2H), 1.54 – 1.26 (m, 6H), 1.19 – 1.17 (m, 1H), 1.10 – 1.07 (m, 1H), 1.01 (d, J = 6.06 Hz, 3H), 0.93 (s, 3H), 0.89 – 0.88 (m, 3H).

ES-MS: m/z 892 $[M+Na]^+$.

General procedure for the activation of the linker with NHS

The linker (0.2 mmol) was solubilized in DCM dry (5 mL) under Ar and cooled to 0 °C. Then, NHS (0.24 mmol) and DCC (0.24 mmol) were added and the reaction mixture was heated to r.t. and stirred for 16 h. DCM was evaporated and the product was purified by silica gel flash chromatography eluting 0-5% gradient of MeOH in CH_2Cl_2.

14-Azido-3,6,9,12-tetraoxatetradecanoic acid NHS ester (49)

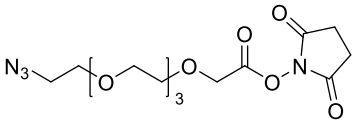

Compound **49** was synthesized in according to the general procedure for the activation of the linker with NHS. EDC instead of DCC was used. Obtained 0.18 mmol, 90% yield.
ESI-MS: m/z 375 $[M+H]^+$.

Activated linker-NHS ester (42)

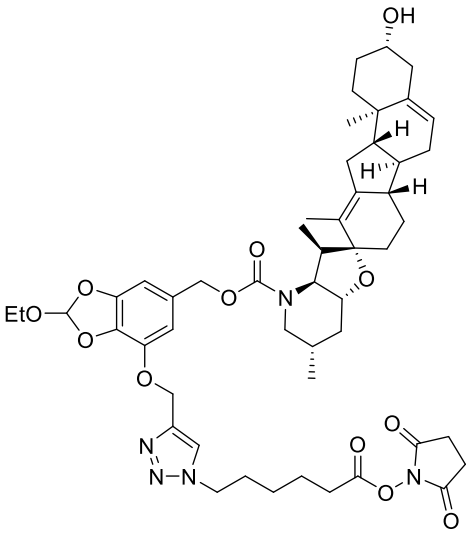

Compound **42** was synthesized in according to the general procedure for the activation of the linker with NHS. Obtained 0.16 mmol, 80% yield.

ESI-MS: m/z 943 $[M+H]^+$.

Activated linker-NHS ester (43)

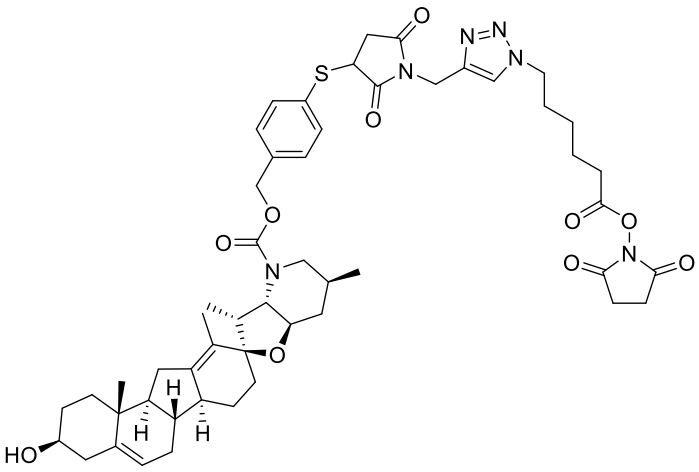

Compound **43** was synthesized in according to the general procedure for the activation of the linker with NHS. Obtained 0.09 mmol, 46% yield.
ESI-MS: m/z 968 $[M+H]^+$.

4.2.2.3 Bioconjugation

General procedure for bioconjugation with activated linker as NHS-ester

To a solution of activated linker (10 mM in DMSO) was added a solution Cetuximab (50 µL, 10 mg/mL) in PBS pH 7.4 or EPPS pH 8 and the reaction was mixed at 650 rpm for 1 h. Then, a solution of glycine (20 mM in H_2O) was added and the mixture stirred at 650 rpm for 10 minutes. The final ADC was purified through centrifugation at 3000 rpm for 2 minutes by using PD spintrapTM G-25 previously washed with water (3 x 400 µL, 3000 rpm 1 min.). The product was collected in Eppendorf and sent for MALDI analysis and biological activity.
Linker: mAb stoichiometric ratios:

- 20:1 = 6.5 µL of activated linker (10mM in DMSO), 3.25 µL of glycine (20 mM in H_2O) and 50 µL of Cetuximab (50 µL, 10 mg/mL) in PBS pH 7.4 or EPPS pH 8;

- 40:1 = 13 µL of activated linker (10mM in DMSO), 6.5 µL of glycine (20 mM in H_2O) and 50 µL of Cetuximab (50 µL, 10 mg/mL) in PBS pH 7.4 or EPPS pH 8;

- 80:1 = 26 µL of activated linker (10mM in DMSO), 13 µL of glycine (20 mM in H_2O) and 50 µL of Cetuximab (50 µL, 10 mg/mL) in PBS pH 7.4 or EPPS pH 8;

General procedure for bioconjugation with *in situ* activated linker as S-NHS-ester

For 80:1 (linker: mAb) stoichiometric ratio:
To a solution of activated linker (28 µL, 10 mM in DMSO) was added a solution of S-NHS (5 µL, 100 mM in H_2O) and EDC·HCl (5 µL, 100 mM in H_2O) and the mixture stirred at 700 rpm for 16 h. Then, PBS pH 7.4 or EPPS pH 8 (35 µL) and Cetuximab (100 µL, 10 mg/mL) in PBS pH 7.4 or EPPS pH 8 were added and the reaction was mixed at 650 rpm for 1 h. Then, a solution of glycine (14 µL, 20 mM in H_2O) was added and the mixture stirred at 650 rpm for 10 minutes. The final ADC was purified through centrifugation at 3000 rpm for 2 minutes by using PD spintrapTM G-25 previously washed with water (3 x 400 µL, 3000 rpm 1 min.). The product was collected in Eppendorf and sent for MALDI analysis and biological activity.
For 40:1 and 20:1 stoichiometric ratios, 14 µL or 7 µL of payload were used, respectively.

General procedure for bioconjugation with DBCO linker and functionalized Cetuximab

Functionalized Cetuximab **50** was obtained by using general procedure for bioconjugation with activated linker as NHS-ester (40:1 stoichiometric ratio, DAR= 1.7).
DBCO linker **48** was obtained by mixing the activated NHS-ester **43** (20 µL, 10 mM in DMSO) with DBCO-NH_2 (20 µL, 10 mM in DMSO) at 700 rpm for 16 h.
To a solution of functionalized Cetuximab **50** (400 µL, 6.4 mg/mL in H_2O), H_2O (50 µL) and DBCO linker **48** (89 µL, 15 mM) were added and the mixture stirred at 650 rpm for 30 minutes. Then, the solution was cooled to 4 °C and stirred for 16 h at 650 rpm. The final ADC was purified through centrifugation at 3000 rpm for 2 minutes by using PD spintrapTM G-25 previously washed with water (3 x 400 µL, 3000 rpm 1 min.). The product was collected in Eppendorf and sent for MALDI analysis and biological activity.

4.2.2.3 MALDI analysis of ADCs 3-5

Samples preparation: the matrix solutions were prepared at two different concentrations, and both were used in parallel. 20.0 mg or 25 mg of Super DHB were dissolved in a solution of MeCN (150 µL), H_2O (350 µL) and TFA (0.05 µL) and deposited in a stainless-steel target placed in a termoblock set at 39 °C. When the sample was dried, 1.65 µL of matrix solution was added and once completely dried and crystalized, the target plate was removed from the termoblock. The target plate was analyzed with MALDI-TOF set in linear mode at 83% of laser intensity. The m/z range was from 30 kDa to 200 kDa. For each sample spot, 10 shots were acquired to improve the spectra quality and mass accuracy.
DAR was calculated as follows: (M.W. ADC – M.W. mAb)/ M.W. linker-payload.

MALDI spectra

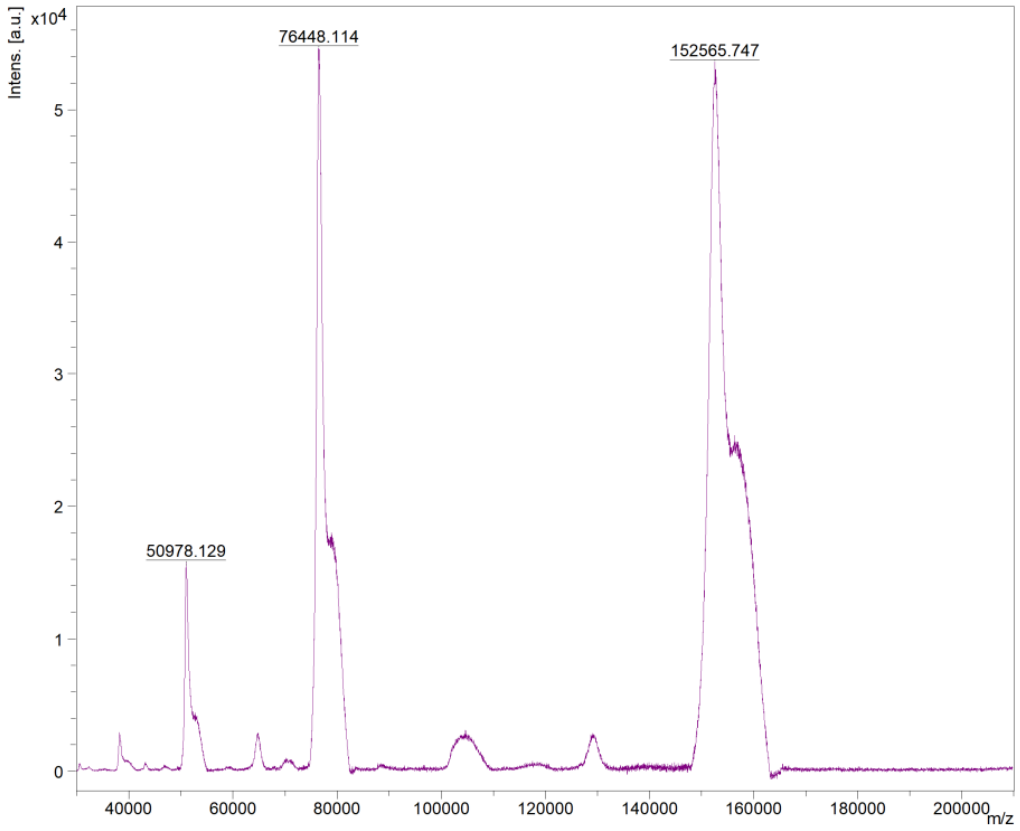

Figure 91- MALDI of ADC-3 (DAR= 7).

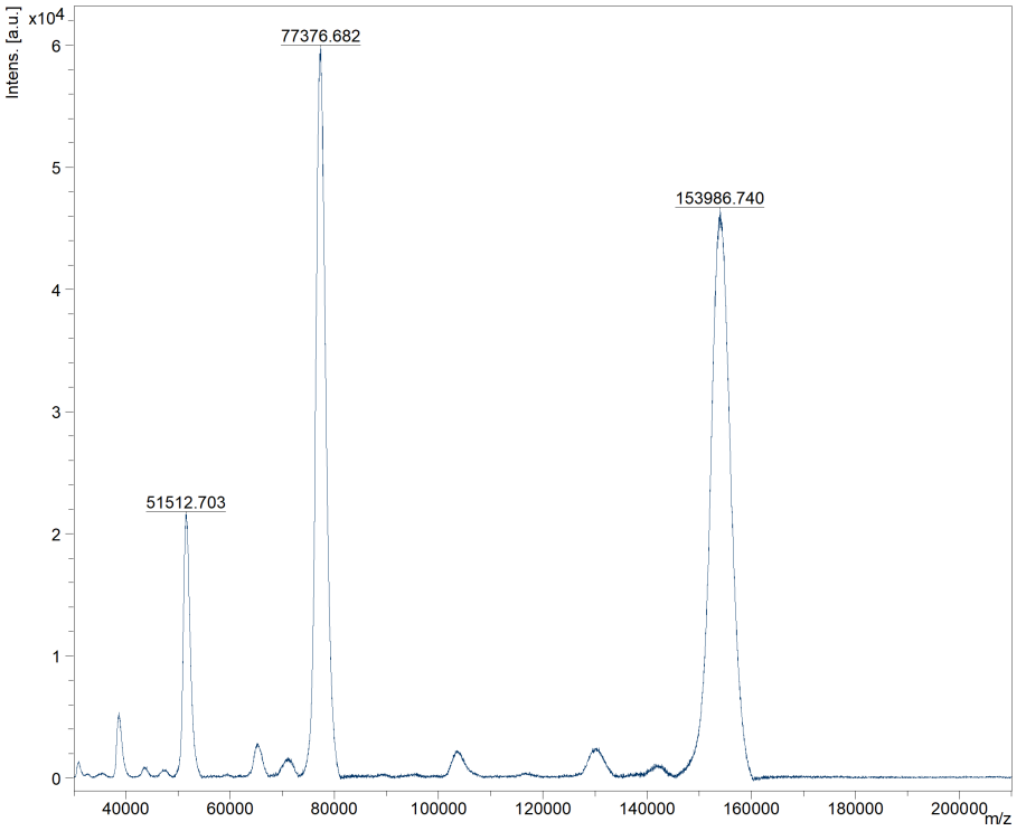

Figure 92- MALDI of ADC-4 (DAR= 2).

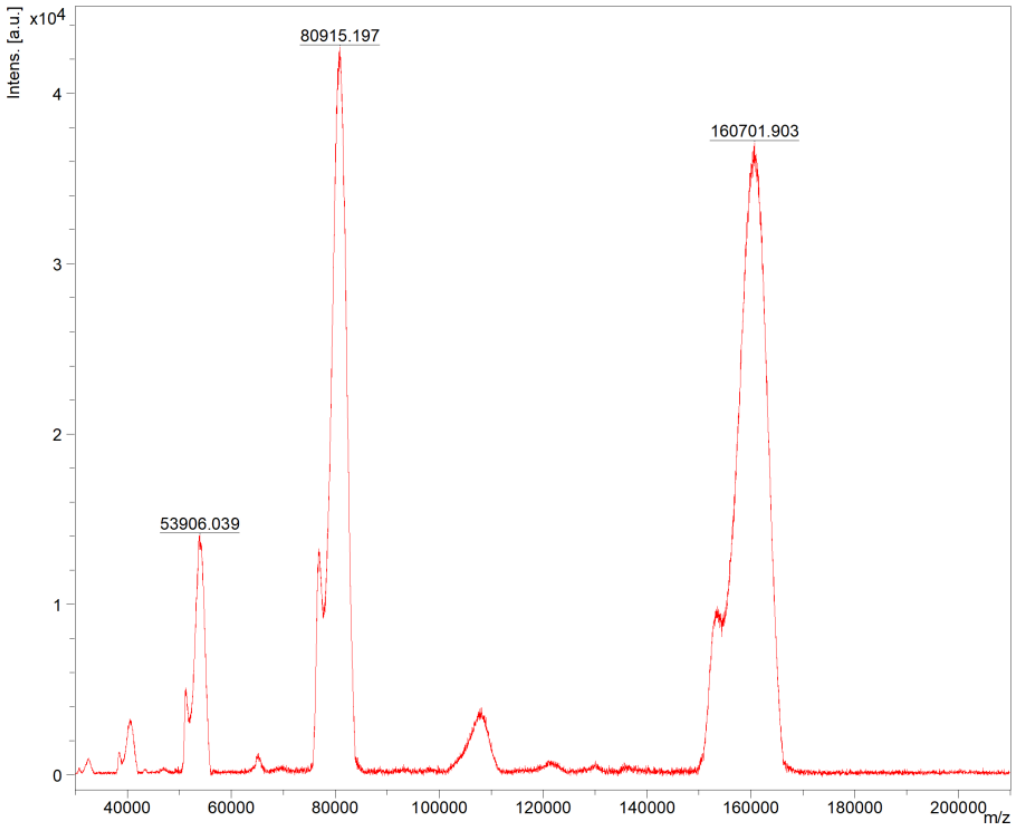

Figure 93- MALDI analysis of ADC-3 (DAR= 10).

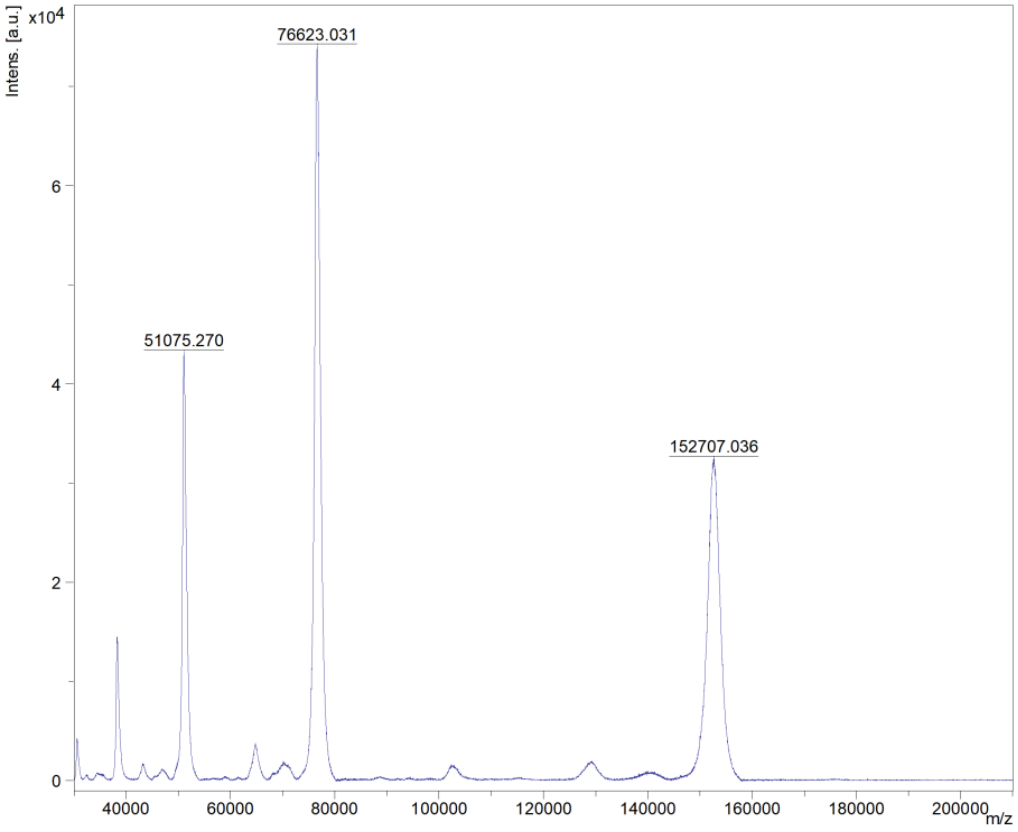

Figure 94- MALDI of functionalized Cetuximab 50 (DAR= 1.7).

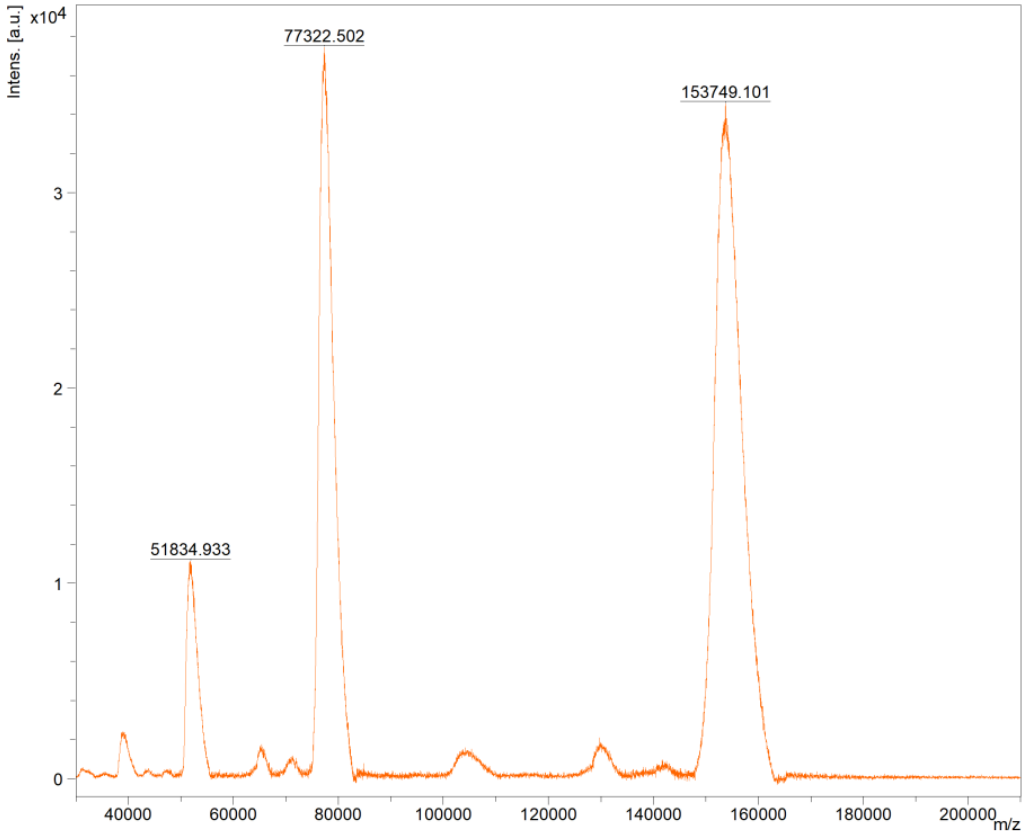

Figure 95- MALDI of ADC-5 (DAR= 1).

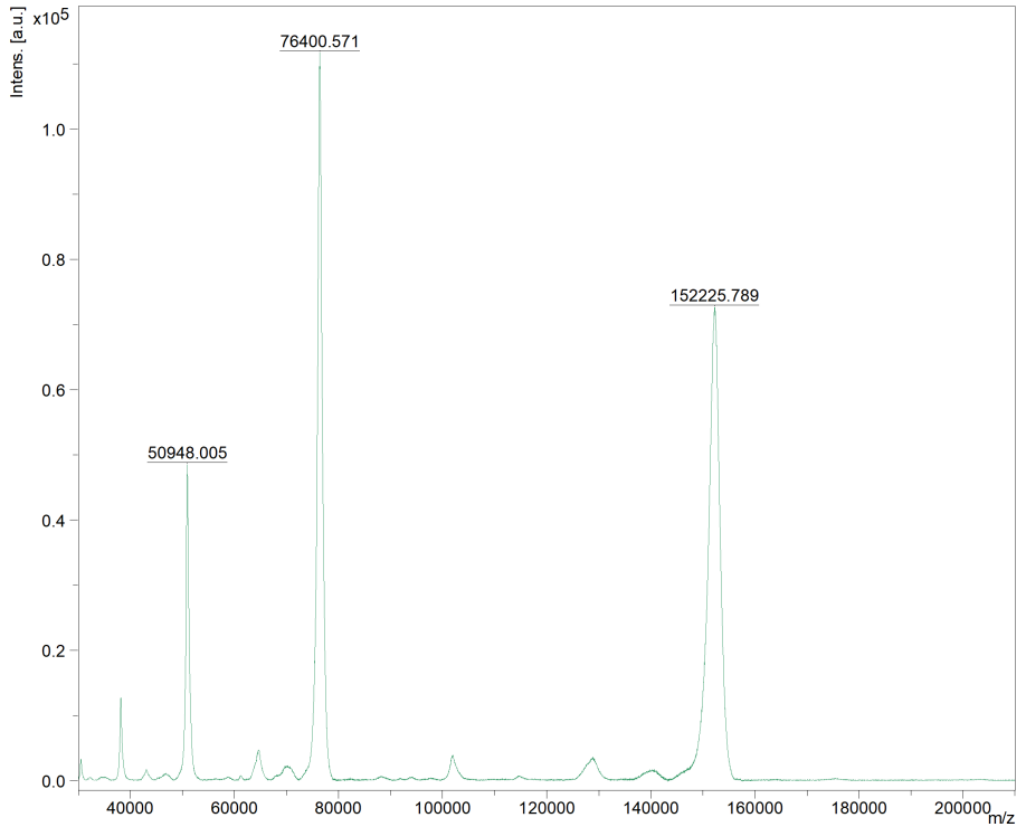

Figure 96- MALDI of Cetuximab (reference).

4.2.3 ADCs for the treatment of viral infections

4.2.3.1 General experimental procedures, materials and instruments

All reagents were used as purchased from commercial suppliers without further purification. The reactions were carried out in oven dried vessels. Solvents were dried and purified by conventional methods prior use or, if available, purchased in anhydrous form.

Flash column chromatography was performed with Merck silica gel Å 60, 0.040-0.063 mm (230-400 mesh).

MPLC Syncore® Büchi or MPLC Isolera Prime Biotage on highly resistant PP cartridges Normal Phase silica gel NP 40 – 63 µm particle size and 60 Å pore size (Si60) withstand a maximum pressure of 10 bar (145 psi) column column with petroleum ether (eluent A) and Ethyl Acetate (Eluent B) as mobile phase.

Merck aluminum backed plates pre-coated with silica gel 60 (UV254) were used for analytical thin layer chromatography and were visualized by staining with a $KMnO_4$ or Ninidrine solution.

NMR spectra were recorded at 25 °C or at 37 °C with 400 or 600 MHz for ^{1}H and 101 or 151 MHz for ^{13}C Brücker Advance NMR spectrometers. The solvent is specified for each spectrum. Splitting patterns are designated as s, singlet; d, doublet; t, triplet; q, quartet; m, multiplet; bs, broad singlet. Chemical shifts (d) are given in ppm relative to the resonance of their respective residual solvent peaks.

High and low resolution mass spectroscopy analyses were recorded by electrospray ionization with a mass spectrometer Q-exactive Plus.

MALDI analysis were performed with the MALDI-TOF in linear mode set at 83% of laser intensity. The m/z range was from 30 kDa to 200 kDa.

4.2.3.2 Synthetic procedures

4-((2,5-dioxo-1-(prop-2-yn-1-yl)pyrrolidin-3-yl)thio)benzyl ((2S,3S,4S,6R)-3-hydroxy 2-methyl-6-(((1S,3S)-3,5,12-trihydroxy-3-(2-hydroxyacetyl)-10-methoxy-6,11-dioxo 1,2,3,4,6,11-hexahydrotetracen-1-yl)oxy)tetrahydro-2H-pyran-4-yl)carbamate (51)

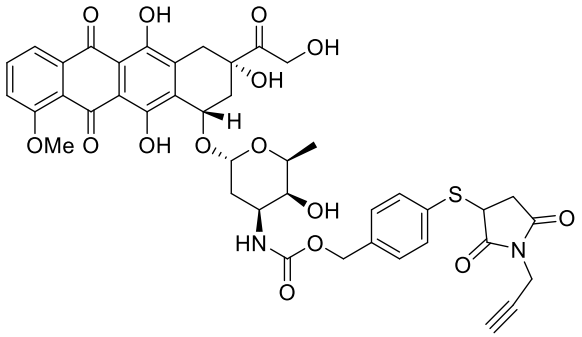

Doxorubicine (450 mg, 0.78 mmol), DMAP (10 mg, 0.08 mmol) and DIPEA (0.26 mL, 1.53 mmol) were solubilized in DMF dry (5 mL) at r.t. Then, a solution of carbonate **39** (230 mg, 0.51 mmol) in DMF dry (2 mL) was added and the reaction stirred for 3 days at r.t EtOAc (25 mL) was added and washed with H_2O (3 x 10 mL), brine (10 mL), dried over anhydrous

Na_2SO_4, filtered, and evaporated under reduced pressure. The product was purified by silica gel MPLC, 0-5 % gradient of MeOH in DCM to obtain the desired product as a red solid (155 mg, 0.18 mmol, 30% yield).

^{1}H NMR: (400 MHz, $CDCl_3$) δ 8.01 (d, J = 7.7 Hz, 1H), 7.76 (t, J = 8.1 Hz, 1H), 7.44 (d, J = 7.7 Hz, 2H), 7.37 (d, J = 8.5 Hz, 1H), 7.26 – 7.20 (m, 2H), 5.48 (d, J = 3.1 Hz, 1H), 5.27 (s, 1H), 5.13 (d, J = 8.6 Hz, 1H), 4.99 (d, J = 3.7 Hz, 2H), 4.74 (s, 2H), 4.52 (s, 1H), 4.14 (d, J = 2.5 Hz, 2H), 4.06 (s, 3H), 3.99 (d, J = 5.4 Hz, 1H), 3.84 (s, 1H), 3.65 (s, 1H), 3.47 (s, 2H), 3.26 (d, J = 19.4 Hz, 1H), 3.17 – 3.10 (m, 1H), 3.01 (d, J = 18.8 Hz, 2H), 2.68 – 2.63 (m, 1H), 2.32 (d, J = 15.0 Hz, 1H), 2.17 – 2.15 (m, 2H), 2.08 – 1.66 (m, 4H), 1.27 (d, J = 6.6 Hz, 3H).

ESI: m/z 868 $[M+Na]^+$.

3-((4-(bromomethyl)phenyl)thio)-1-(prop-2-yn-1-yl)pyrrolidine-2,5-dione (53)

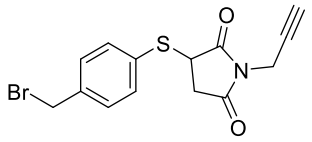

Compound **38** (100 mg, 0.36 mmol) was solubilized in DCM dry (5 mL) and cooled to 0 °C under N_2. PBr_3 (51 µL, 0.54 mmol) was added and the reaction stirred for 30 min. Then, DCM was evaporated and the product was purified by silica gel MPLC, 0-50 % gradient of EtOAc in PE to obtain the desired product as a yellow oil (90 mg, 0.27 mmol, 74% yield) and immediately used for the next step.

ESI: m/z 338 $[M+H]^+$.

5-chloro-N-(2-chloro-4-nitrophenyl)-2-((4-((2,5-dioxo-1-(prop-2-yn-1-yl)pyrrolidin-3-yl)thio)benzyl)oxy)benzamide (54)

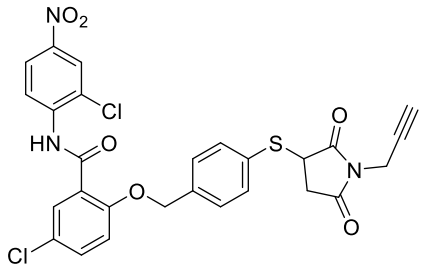

Niclosamide (118 mg, 0.36 mmol), il K_3PO_4 (114 mg, 0.54 mmol) and TBAB (58 mg, 0.18 mmol) were suspended in DMF dry (2 mL) at r.t. and under N_2. A solution of compound **53** (146 mg, 0.43 mmol) in DMF dry (1 mL) was added and the reaction mixture stirred for 2 h. EtOAc (25 mL) was added and washed with H_2O (3 x 10 mL), brine (10 mL), dried over anhydrous Na_2SO_4, filtered, and evaporated under reduced pressure. The product was purified by silica gel MPLC, 0-60 % gradient of EtOAc in PE to obtain the desired product as a yellow solid (84 mg, 0.14 mmol, 40% yield).
ESI: m/z 587 $[M+Na]^+$.

General procedure for CuAAC reaction

The desired alkyne (0.07 mmol) and the azide **12** (9 mg, 0.056 mmol) were dissolved in dry DMF (2 mL) under Ar. The solution was degassed with three cycles of argon/vacuum. To this solution, a freshly prepared aqueous mixture (2 mL) of $Cu(OAc)_2$ (4 mg, 0.021 mmol) and Na-ascorbate (8 mg, 0.042 mmol), previously degassed by argon/vacuum cycles, was added dropwise. The reaction mixture was degassed and left to stir under Ar. at r.t. for 16 h. The solvent was evaporated and the crude was purified by silica gel flash chromatography eluting 0-10 % gradient of MeOH in CH_2Cl_2 to obtain the desired compound.

6-(4-((3-((4-(((((2S,3S,4S,6R)-3-hydroxy-2-methyl-6-(((1S,3S)-3,5,12-trihydroxy-3-(2-hydroxyacetyl)-10-methoxy-6,11-dioxo-1,2,3,4,6,11-hexahydrotetracen-1 yl)oxy)tetrahydro-2H-pyran-4-yl)carbamoyl)oxy)methyl)phenyl)thio)-2,5-dioxopyrrolidin 1-yl)methyl)-1H-1,2,3-triazol-1-yl)hexanoic acid (52)

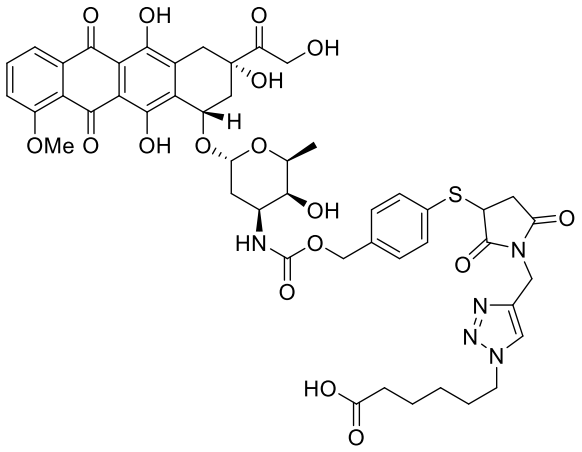

Compound **52** was synthetized in according to the general procedure for CuAAC cycloaddition. Product was purified by silica gel MPLC, 0-5 % gradient of MeOH in DCM to obtain the desired product as a red solid (32.5 mg, 0.032 mmol, 58% yield).

ESI: m/z 1003 $[M+H]^+$.

6-(4-((3-((4-((4-chloro-2-((2-chloro-4 nitrophenyl) carbamoyl)phenoxy)methyl)phenyl)thio)-2,5-dioxopyrrolidin-1-yl)methyl) 1H-1,2,3-triazol-1-yl)hexanoic acid (55)

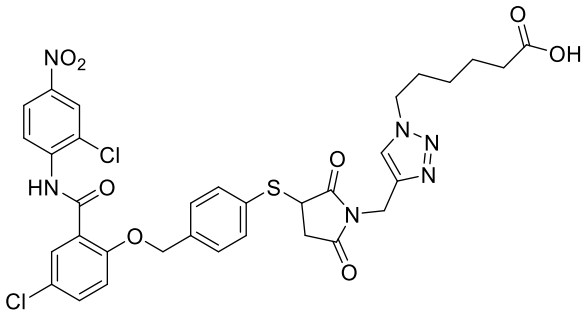

Compound **55** was synthetized in according to the general procedure for CuAAC cycloaddition. Product was purified by silica gel MPLC, 0-5 % gradient of MeOH in DCM to obtain the desired product as a red solid (20 mg, 0.027 mmol, 49% yield).

^{1}H NMR: (600 MHz, $CDCl_3$) δ 10.61 (s, 1H), 8.91 (d, J = 6.0 Hz, 1H), 8.28 (s, 1H), 8.21 (d, J = 12.00 Hz, 2H), 7.54 (s, 1H), 7.47 (d, J = 12.00 Hz, 2H), 7.39 (s, 1H), 7.03 (d, J = 6.00

Hz, 2H), 5.36 (s, 2H), 4.79 (s, 2H), 4.44 – 4.38 (m, 2H), 4.20 – 4.16 (, 1H), 3.30 – 3.28 (m, 2H), 3.01 (s, 1H), 2.39 – 2.34 (m, 2H), 1.69 – 1.63 (m, 4H), 1.36 – 1.26 (m, 2H).
ESI: m/z 741 $[M+H]^+$.

4.2.3.3 Bioconjugation

General procedure for bioconjugation with *in situ* activated linker as S-NHS-ester

For 80:1 (linker: mAb) stoichiometric ratio:
To a solution of activated linker (28 µL, 10 mM in DMSO) was added a solution of S-NHS (5 µL, 100 mM in H_2O) and EDC·HCl (5 µL, 100 mM in H_2O) and the mixture stirred at 700 rpm for 16 h. Then, PBS pH 7.4 or EPPS pH 8 (35 µL) and Cetuximab (100 µL, 10 mg/mL) in PBS pH 7.4 or EPPS pH 8 were added and the reaction was mixed at 650 rpm for 1 h. Then, a solution of glycine (14 µL, 20 mM in H_2O) was added and the mixture stirred at 650 rpm for 10 minutes. The final ADC was purified through centrifugation at 3000 rpm for 2 minutes by using PD spintrapTM G-25 previously washed with water (3 x 400 µL, 3000 rpm 1 min.). The product was collected in Eppendorf and sent for MALDI analysis and biological activity.
For 40:1 and 20:1 stoichiometric ratios, 14 µL or 7 µL of payload were used, respectively.

4.2.3.4 MALDI analysis of ADCs 7-10

Samples preparation: the matrix solutions were prepared at two different concentrations, and both were used in parallel. 20.0 mg or 25 mg of Super DHB were dissolved in a solution of MeCN (150 µL), H_2O (350 µL) and TFA (0.05 µL) and deposited in a stainless-steel target placed in a termoblock set at 39 °C. When the sample was dried, 1.65 µL of matrix solution was added and once completely dried and crystalized, the target plate was removed from the termoblock. The target plate was analyzed with MALDI-TOF set in linear mode at 83% of laser intensity. The m/z range was from 30 kDa to 200 kDa. For each sample spot, 10 shots were acquired to improve the spectra quality and mass accuracy.
DAR was calculated as follows: (M.W. ADC – M.W. mAb)/ M.W. linker-payload.

MALDI spectra

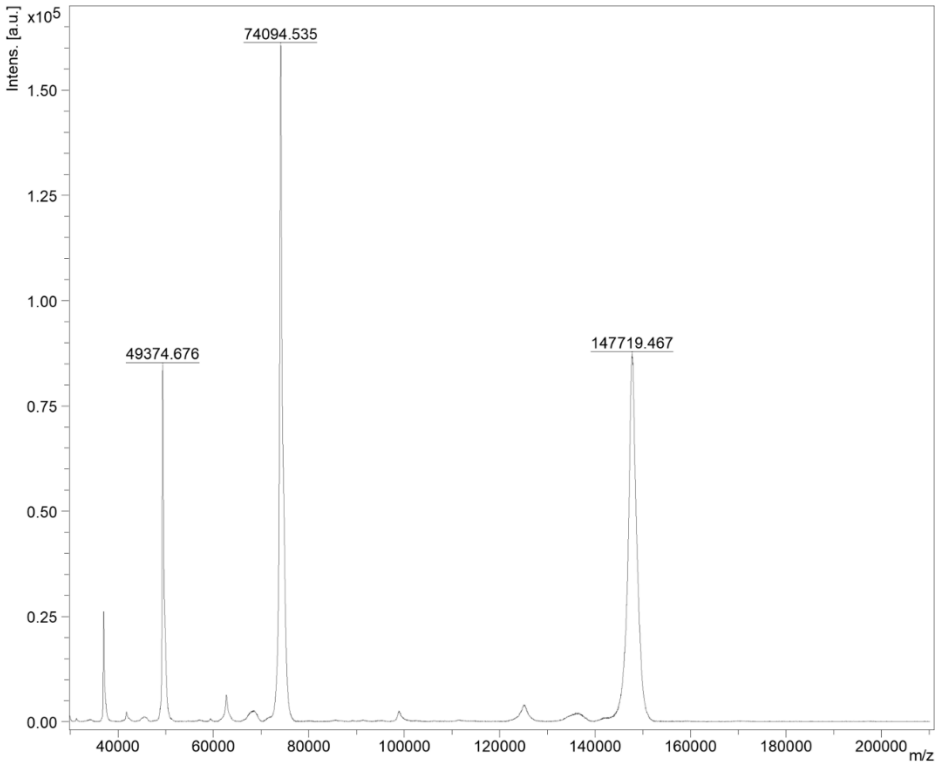

Figure 97- MALDI of J08 (reference)

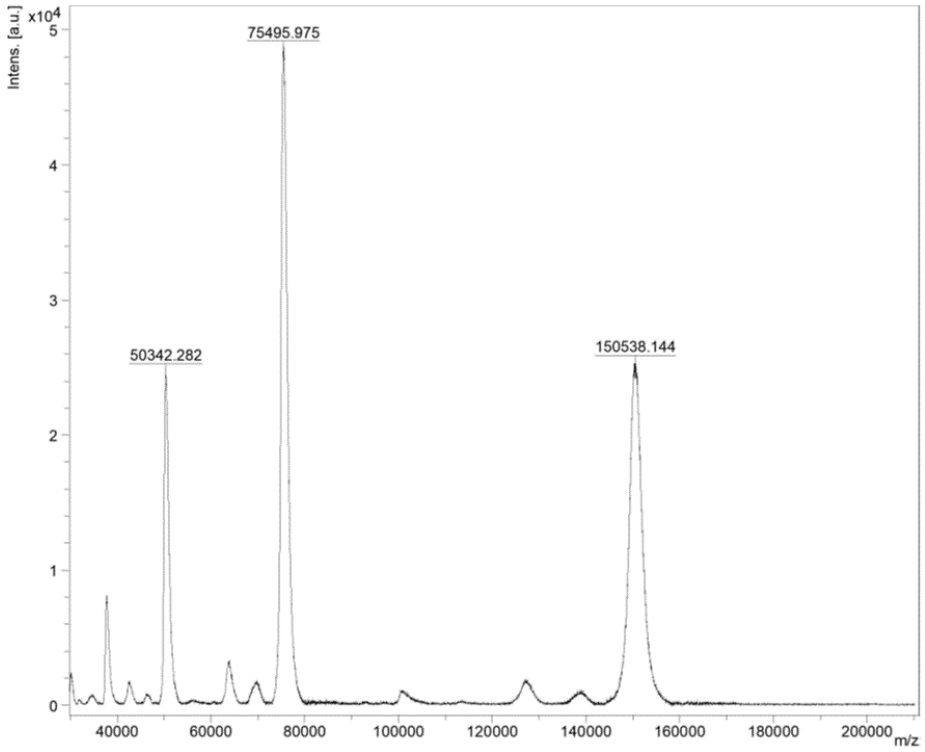

Figure 98- MALDI of ADC-7 (DAR= 3.4).

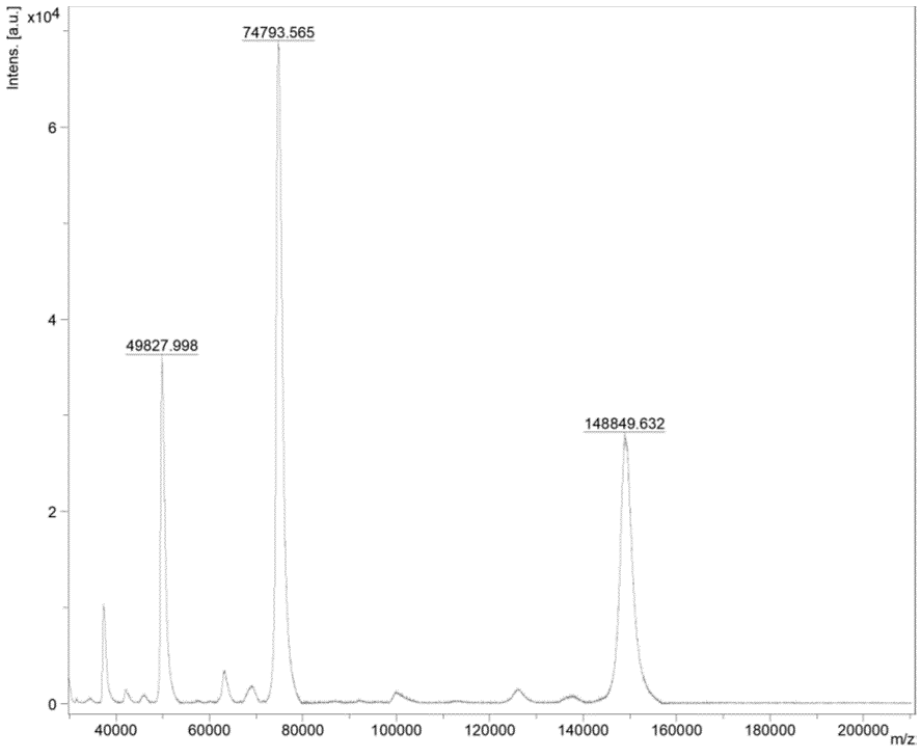

Figure 99-MALDI of ADC-9 (DAR= 1.2).

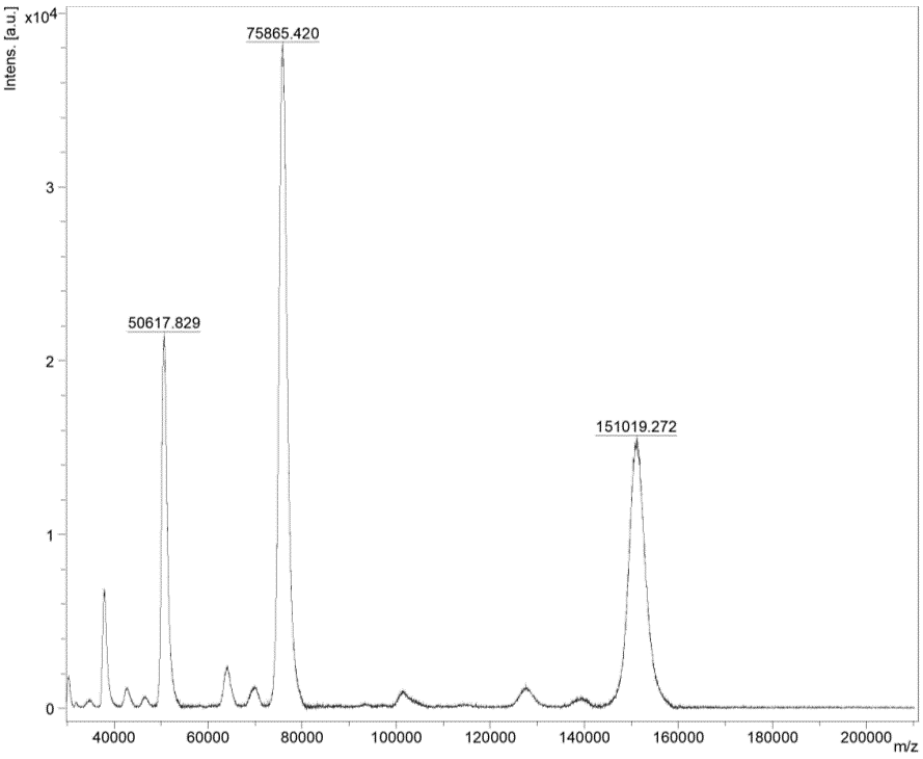

Figure 100- MALDI of ADC-10 (DAR =3.8).

SECTION B

Preparation of intermediates useful for the synthesis of biological active compounds

Chapter 1- Introduction

This part of the work was made in collaboration with a leading Italian pharmaceutical company focused on the research and development of new active pharmaceutical ingredients (APIs) for various disease. [253] The project essentially consisted of two tasks:

- development of asymmetric Biginelli reactions to synthesize API starting materials;
- C-N functionalization of Heteroaryl scaffolds;

Below is reported the state of art on the different methodologies that can be applied to our cases.

1.1 Biginelli reaction

Multicomponent reactions (MCRs) are one of the most useful strategies to make heterocycles. As the resulting product contains the features of all starting materials, the major advantage is obtaining when a molecular diversity is desired. [254] Among MCRs, the Biginelli reaction is a straightforward method to synthesize dihydropyrimidinones (DHPMs) scaffold. This reaction was discovered by Pietro Biginelli in 1983 and involves easily accessible materials such as ethyl acetoacetate, benzaldehyde and urea (or thiourea) to give the desired DHPM adduct (Scheme 24). [255]

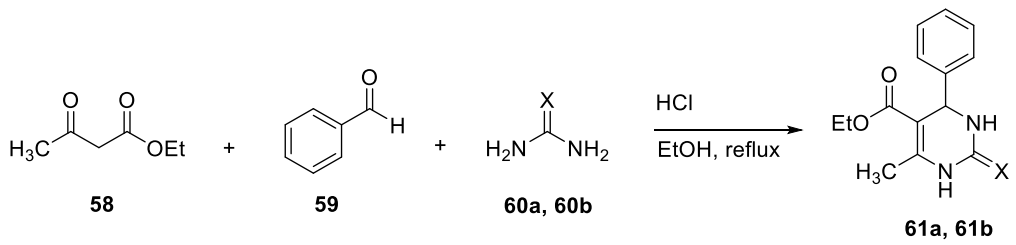

Scheme 24-Biginelli reaction. 60a, 61a: X= O; 60b, 61b: X= S.

The first Biginelli reaction was carried out in EtOH with a catalytic amount of aqueous HCl and the product isolated after precipitation at room temperature. The interest in Biginelli

reaction gained huge popularity in the 1990s when the biological activity of DHPMs became the subject of investigations Indeed, DHPM scaffolds can be found in molecules with pharmacological activities such as antivirals, antitumourals, antibacterials, anti-inflammatory agents, antimalarials, antituberculars, antidiabetics and many others. [256–262] Since the first Biginelli reaction, some improvements have been implemented to obtain DHPMs with specific properties through asymmetric or solid-phase synthesis. [263,264]

1.1.1 Proposed mechanisms for Biginelli reaction

The mechanism of this reaction has sparked a lot of interest and debate and three alternatives have been proposed. First, in 1933 Folkers and Johnson suggested that urea **60** can react with either benzaldehyde **59** or ethyl acetoacetate **58** to form benzal-bisurea **62** or β-carbamidocrotonate **63** respectively (Scheme 25): [265]

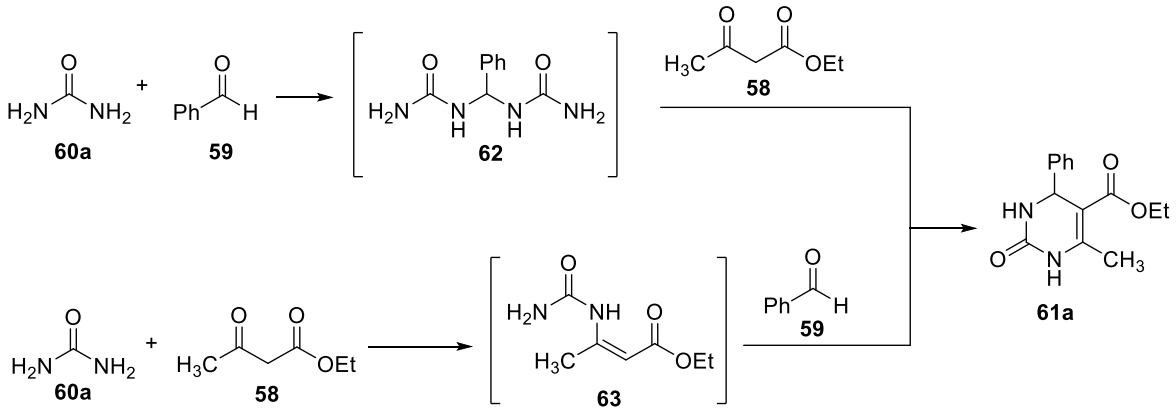

Scheme 25- Mechanisms proposed by Folkers and Johnson.

Then, intermediates **62** and **63** undergo cyclization with ethyl acetoacetate **58** or benzaldehyde **59** to obtain the DHPM **61a**.

In 1973, Fissekis and Sweet hypothesized a Knoevenagel route in which a carbenium ion formed from the condensation between benzaldehyde **59** and ethyl acetoacetate **58** in acidic conditions (Scheme 26). [266] Subsequently, the carbenium ion is captured by the urea **60a** to give the product **61a**.

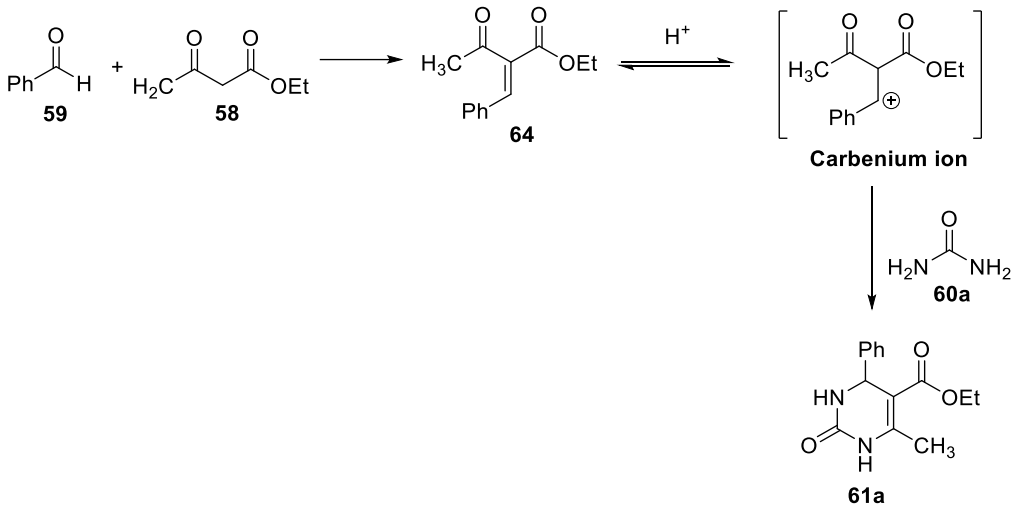

Scheme 26- Mechanism proposed by Sweet and Fissekis.

However, the Knoevenagel pathway was refuted by Kappe in 1997 when he published his paper on the re-examination of the Biginelli reaction mechanisms based on NMR studies. [267] In particular, he did not observe the presence of the aldol product **64** when aldehyde **59** and ethyl acetoacetate **58** were mixed in CD_3OH/HCl, but instead he found the bisureide **62** by mixing **59** and **60a** (Scheme 27).

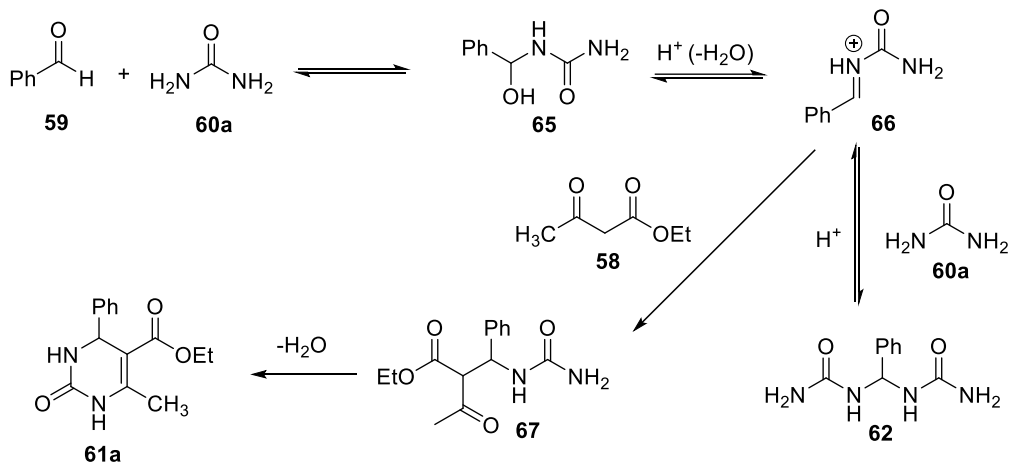

Scheme 27- Two pathways described by Kappe.

When ethyl acetoacetate **58** was added to the mixture, only DHPM **61a** was detected. This suggests that the reaction between **59** and **60a** leads to hemiaminal **65** which is unstable in acidic conditions. The N-acyliminium ion **66** can either undergo a reversible reaction with urea **60a** to give **62,** or react with ethyl acetoacetate **58** in an irreversible manner to afford

61a after cyclization. Furthermore, the presence of carbenium ion seems unlikely if we considered the reaction between the intermediate **64** and thiourea or methylthiourea, also described by Kappe (Scheme 28). [267]

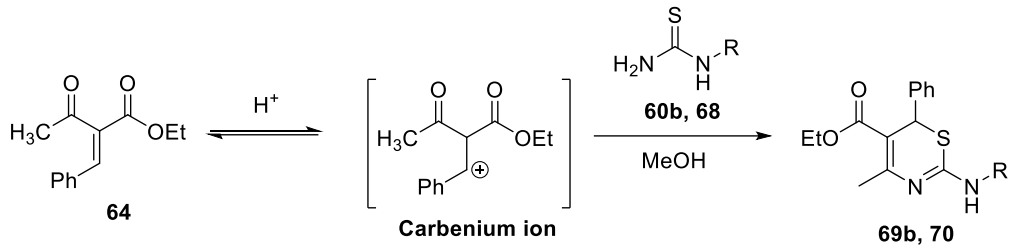

Scheme 28- Reaction between carbenium ion and thiourea. 60b: R= H; 68: R= -CH$_3$; 69b: R= H; 70: R= -CH$_3$.

In that case, 2-amino-1,3-thiazines **69b** and **70** were found as products instead of the expected DHPM. All these observations, confirm the iminium route as the most plausible. This theory was also supported by De Souza and co-workers when they studied the mechanism of Biginelli reaction through density functional theory (DFT) and ESI-MS. [268] They found that the Knoevenagel route gave a very little contribution to the reaction and several intermediates associated with the iminium mechanism were detected by MS. Over the time, other studies based on NMR, DFT and ESI-MS analysis gave further increased the confidence in the iminium route as the most likely reaction mechanism. [269,270] Interestingly, the reaction seems to be catalysed by urea which stabilize the iminium intermediate *via* hydrogen bonding.

1.1.2 Some pharmacological activities of DHPMs

Pharmacological properties of DHPMs are the main reason for the growth of synthetic methods in this field. As mentioned before, a lot of biological activities associated to DHPM scaffolds have been discovered, but the most relevant of them include calcium channel inhibitors, anticancer, anti-inflammatory, antimicrobial and antioxidant activities.

1.1.2.1 Calcium channel inhibitors

In 1978, Khanina reported a β-aminoethyl ester based on DHPM scaffold that have moderate hypotensive activity and coronary dilatory properties (compound **71**, Figure 101). [271] Then,

in the 1980s, the interest focused on compounds that mimic dihydropyridine (DHP) scaffold where the most famous was nifedipine (Figure 101). [272,273] Some notable improvements were achieved when Atwal et. al performed studies on structure-activity relationship. [274,275] They found that the thio-adducts (*i.e.* compound **72**, Figure 101) were the most potent when compared to the oxo- and aza- analogues (*i.e*. compound **73**, **74**, Figure 101).

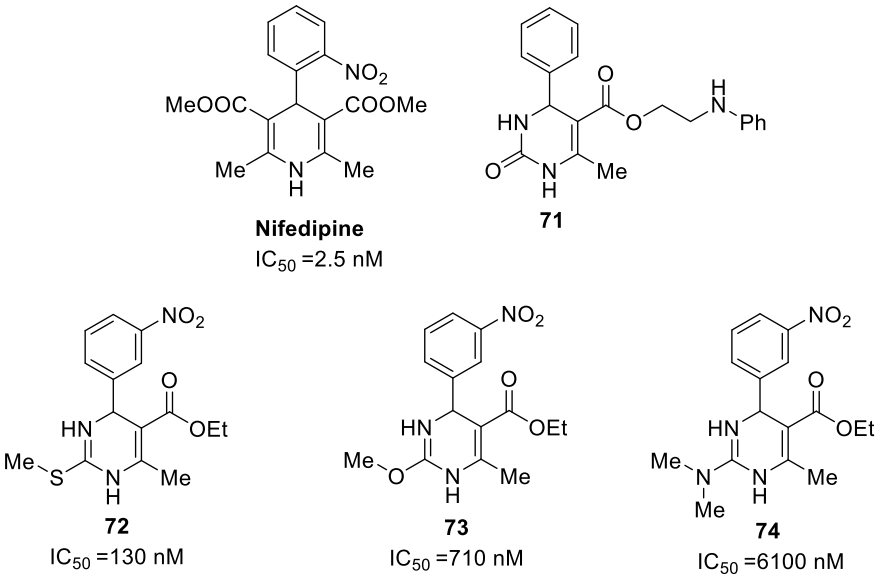

Figure 101-Nifedipine and other compounds that show inhibition of calcium channels. IC_{50} refers to the vasorelaxant potency based on strips of K^+-depolarized rabbit thoracic aortae.

Other important features that helped increasing the vasorelaxant activity were the presence of a -NO_2 group on the aromatic ring and an isopropyl ester on C5 which afforded compounds that were more potent than the ethyl- or methyl ester analogues. [274] Atwal and co-workers continued their studies by modifying the group on N3. They obtained a series of compounds with a promising *in vitro* activity (Figure 102). [276]

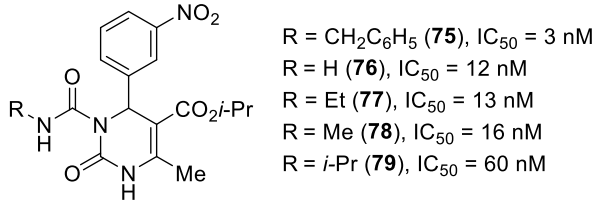

Figure 102- Structures obtained by some modification on N3 on DHPM scaffold.

Another aspect to be considered is the stereocenter on C4. In 1992, Rovnyak et al. described two enantiomers of N3 substituted compounds bearing 1-(phenylmethyl)-4-piperidinyl carbamate of which the (*R*)-enantiomer was significantly more potent than the (*S*)-enantiomer (Figure 103). [272]

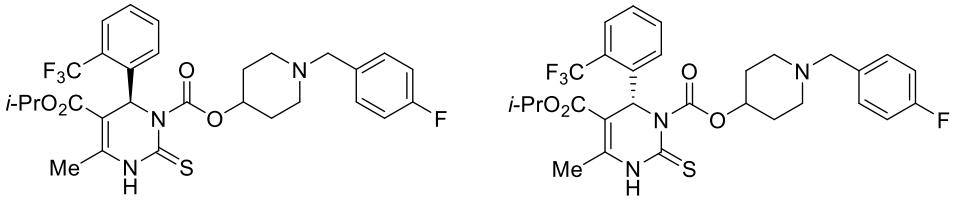

(*R*)-80
IC_{50}= 15 nM

(*S*)-80
IC_{50}> 1000 nM

Figure 103

Moreover, the CF_3 group in *ortho* position on the aromatic ring enhances the activity of these molecules while the presence of fluorine on the side chain decreases the rate of metabolization in rat cells compared to the reference drug amlodipine. [272]

1.1.2.2 Antitumor activity

The anticancer activity of Biginelli adducts has been explored since the discovery of Monastrol as antimitotic agent (Figure 104). [277] In particular, Monastrol inhibits the kinesin Eg5 that is a mitotic spindle protein involved in spindle bipolarity formation. [278]Among various analogues, Piperastrol (Figure 104) was identified as the best anticancer agent due to its activity on some cell lines such as MCF-7 breast (1.9 µg mL^{-1}), 786-0 kidney (2.0 µg mL^{-1}), HT-29 colon (2.5 µg mL^{-1}), UACC.62 melanoma (6.0 µg mL^{-1}) and OVCAR03 ovarian (6.6 µg mL^{-1}). [279]

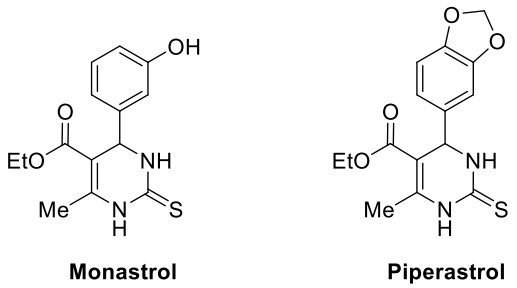

Figure 104- Structure of Monastrol and Piperastrol.

The substituent on C4 has a great influence on the antitumoral activity. Compounds bearing cinnamoyl, pyridin-4-yl or furan-2-yl groups showed significant cytotoxic effects against the MCF-7 breast cancer cell line. [280] Over the years, other structural modifications of Biginelli adducts have been explored, leading to compounds with both antiproliferative and radical scavenging activities. [281]

More interesting, hybrid Biginelli adducts have attracted a lot of interest as antiproliferative agents; in these compounds, the central DHPM core is maintained while different chains (peptoids, cumarins and sugars) have been introduced. [282–284]

In 2015, novel hybrids DHPM-fatty acids with *in vitro* activity against glioma cell growth were reported. [285] Two compounds (**81**, **82**, Figure 105) derived from palmitic and oleic acids were proved to be promising candidates for the treatment of glioma.

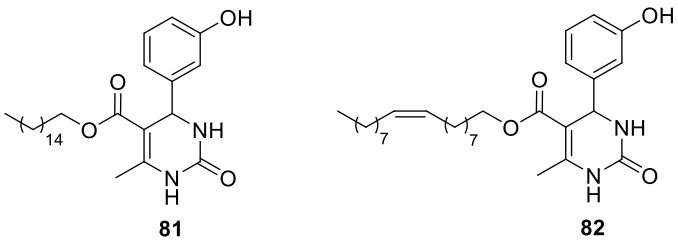

Figure 105- Compound 81: hybrid DHPM-palmitic acid; compound 82: hybrid DHPM-oleic acid.

All these examples show the interest in using DHPMs for hybrid and multifunctional drugs, a growing field for the development of new pharmaceutical products. [286–288]

1.1.2.3 Anti-inflammatory activity

The inflammation process involves several factors such as proinflammatory cytokines (i.e. TNF-α and IL-6), prostaglandin E_2, nitric oxide synthase (iNOS), cyclooxygenase-2 (COX-2) and others. Many of these have been targeted by Biginelli adducts, exploiting their anti-inflammatory activity. [289–293] As an example, some compounds bearing the propanoic acids moiety (compounds **83-87**, Figure 106) show an interesting anti-inflammatory activity on Albino rats paw edema compared to Diclofenac as a reference drug. [294,295]

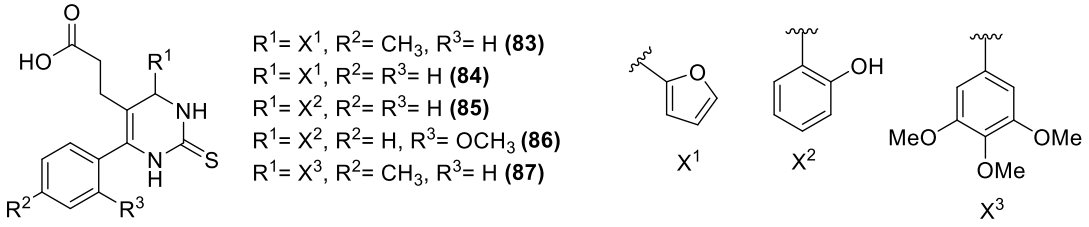

Figure 106- DHPMs bearing propionic acid with anti-inflammatory activity.

Other DHPMs such as compound **88** (Figure 107) were proven to reduce inflammation mediated by TNF-α and IL-6 in THP-1 cells at a concentration of 10 μM, [293] while compounds **89-92** (Figure 107) inhibit hyaluronidase which is an enzyme involved in chronic inflammation. [289] Compound **93** (Figure 107) is one of the most potent inhibitors of prostaglandin E_2 and iNOS and COX-2 gene expression. [290]

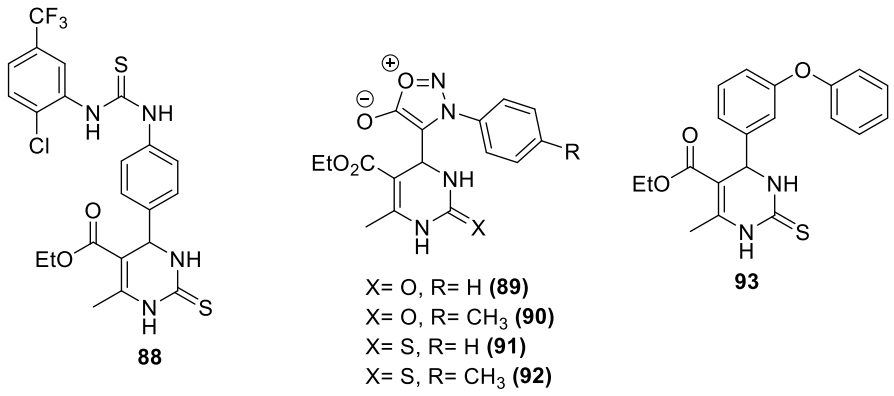

Figure 107- Biginelli adducts that inhibit TNF-α, IL-6 and hyaluronidase.

Also in this case, the substituent in position C4 has a greater impact on the activity of DHPMs. Beside the substituent, sometimes only one enantiomer is effective as the case of transient receptor potential A1 (TRPA1) inhibitors. [291] Furthermore, from the examples

reported in literature, thio-adducts seem to be more effective than oxo-adducts in reducing the inflammation process.

1.1.2.4 Antibacterial and antiviral activities

DHPMs are effective against different types of bacteria such as *Mycobacterium tuberculosis*, *Escherichia coli*, *Klebsiella pneumonia*, *Pseudomonas aeruginosa*, *Salmonella typhi* and *Staphylococcus aureus*. [296]Antimicrobial activity of Biginelli compounds is also correlated to the substituent on C4. As examples, compounds **94** and **95** (Figure 108) containing imidazole moiety show some interesting value of minimal inhibition concentration (MIC) against *Mycobacterium tuberculosis*. [297,298] Compounds **96** and **97** (Figure 108), containing -NO_2 and -F moieties in *para* position on the aromatic ring, exhibit MIC of 12.5 μg mL^{-1} and 12.5-25 μg mL^{-1} respectively against *E. coli*, *K. pneumonia*, *P. aeruginosa*, *S. typhi* and *S. aureus* resulting more potent than the standard drug Ciprofloxacine. [296] The same compounds also have higher antifungal activity than Amphotericin B against *C. albicans*, *A. flavus*, *Rhizopus* and *Mucor*, resulting in a broad spectrum of action. [296]

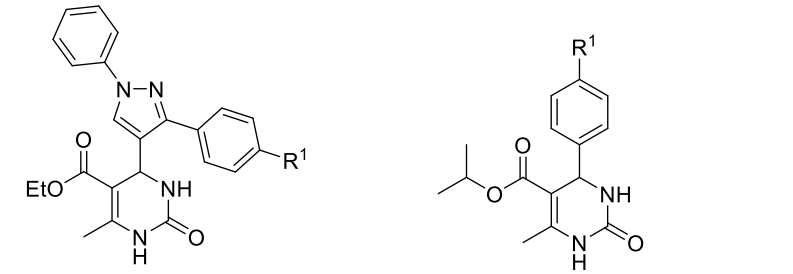

94, R^1= F; MIC= 20 ng mL^{-1}
95, R^1= NO_2; MIC= 20 ng mL^{-1}
96, R^2= NO_2; MIC= 12.5 μg mL^{-1}
97, R^2= F; MIC= 12.5-25 μg mL^{-1}

Figure 108- Some DHPMs with antimicrobial activity.

Recently, Sethiya et al. synthesized new pyrimidine derivatives in an eco-friendly way using Vitamin B_1 as organocatalyst. [299] They found the compound **101** (Scheme 29) as the most active in their docking studies using *S. aureus* dihydropteroate synthase (DHPS), (6CLV) and DNA gyrase (1KZN) proteins.

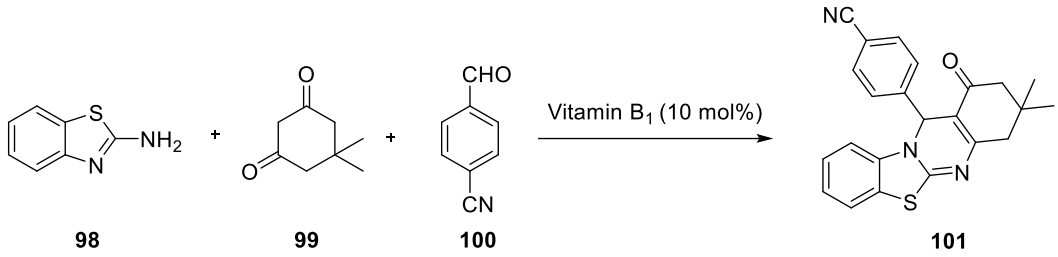

Scheme 29

Many other DHPMs have been developed as antibacterial drugs even if the detailed description is out of our scope. Marinescu in her recent review, describes all the Biginelli compounds with antibacterial activity discovered in the last ten years. [300]

Regarding the antiviral activity, some examples of DHPMs against HIV-1, herpex simplex virus (HSV) and SARS-Cov have been reported. [301–304] In 2012, Kim et al. synthesized a series of compounds that exhibit inhibitory activity against HIV replication at low micromolar concentration, representing the first application of DHPMs in this field. [303] Interestingly, they selected a few molecules as promising candidates but only (*S*)-enantiomers were active. Moreover, starting from compound **102** (Figure 109) which appears to be the most effective, the same research group developed a bioisostere analogue **103** (Figure 109) with an improved metabolic stability. [302]

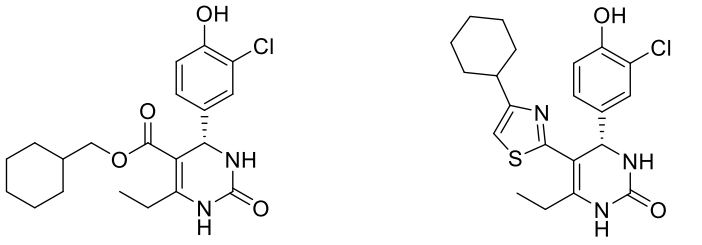

Figure 109- Compound 102 and bioisostere 103. HLM= human liver microsomes; RLM= rat liver microsomes.

In the same year, other Biginelli adducts were reported for their activity against the HSV. [301] Compound **104** (Figure 110) was found as the most effective based on its inhibitory activity (IC_{50} = 0.9 μM) and negligible toxicity on mammalian cells. [301] Some DHPMs have been

explored also as SARS-CoV 3CL protease inhibitors; among all, the compound **105** (Figure 110) was the most promising. [304]

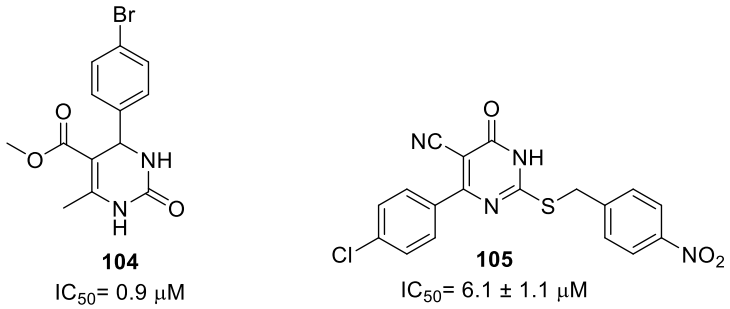

Figure 110

1.1.2.5 Antioxidant activity

The first study on antioxidant activity of DHPMs was reported in 2006 when Stefani et al. synthesized a series of DHPMs using ultrasounds in the presence of NH_4Cl as catalyst. [305] The resulting compounds were tested in vitro; **106** and **107** (Figure 111) exhibited a strong activity against lipid peroxidation induced by Fe + EDTA, while compounds **106** and **108** (Figure 111) were effective in reducing ROS levels. [305]

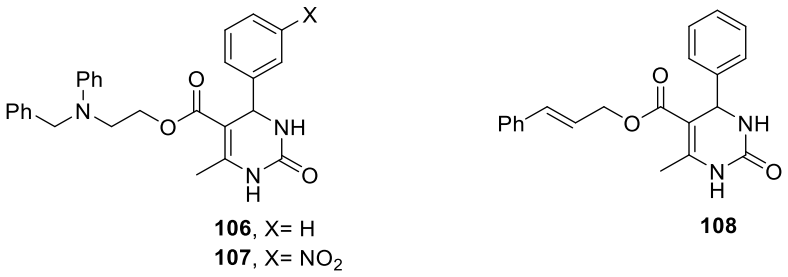

Figure 111

Another work described the activity of simple thio-products **109** and **110** (Figure 112) regarding the scavenging of 2,2-diphenyl-1-picrylhydrazyl (DPPH) radicals. [306] Compound **111** (Figure 112) was described as the most promising for the scavenging of RNS/ROS compared to resveratrol. [281]

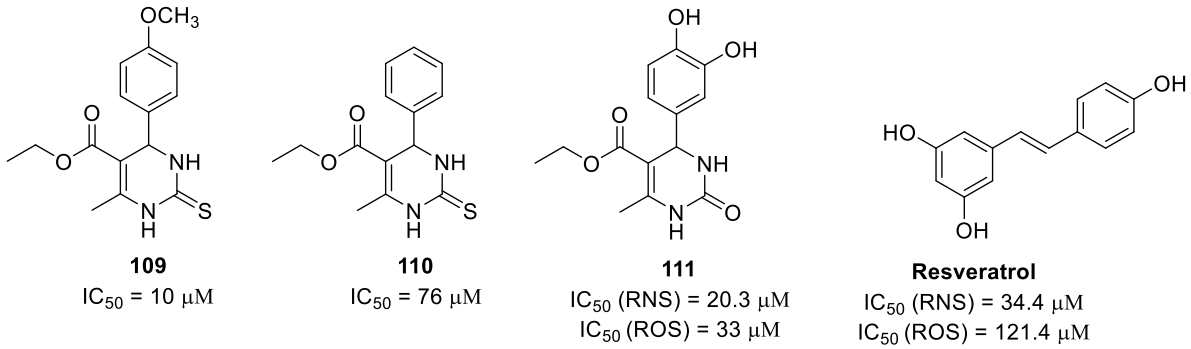

Figure 112- Some DHMPs that act as DPPH, ROS and RNS scavengers.

Other adducts have been reported as DPPH scavengers but the activity was lower than the reference compound Gallic acid. [307]

1.1.3 Asymmetric Biginelli reaction

From the example discussed above, we can notice that DHPMs are hardly used as racemic mixture. Usually, only one enantiomer is the most effective while the other is less active or has an opposite effect. Thus, an efficient method for the purification of resulting enantiomers is needed. The classic approach relies on the resolution of the racemic mixture by forming the respective diastereomers in a chemical or enzymatic manner. An elegant method, which has seen a growing number of applications in recent years, involves the asymmetric Biginelli reaction using chiral catalysts. In particular, advances in organocatalysis have led to the development of organic molecules that are very effective for this scope. The most useful methods described in literature to obtain optically pure DHPMs are reported in the following paragraphs.

1.1.2.6 Chiral resolution of racemic DHPMs

1.1.2.6.1 Chemical approach

Chiral resolution using optically pure reagents, is one of the most reliable methods, even if it has a negative impact on the efficiency of the synthesis. This approach allows the conversion of the racemic mixture to the corresponding diastereomers that can then be separated. In 1991, Atwal and co-workers reported the resolution of compound **116** after the

treatment of starting material **112** with (*R*)-(α)-benzylmethylamine (**113**) and further recrystallization to separate the diastereomers (Scheme 30). [276] Then compound **115** was treated with CF_3CO_2H to give (*R*)-**116**.

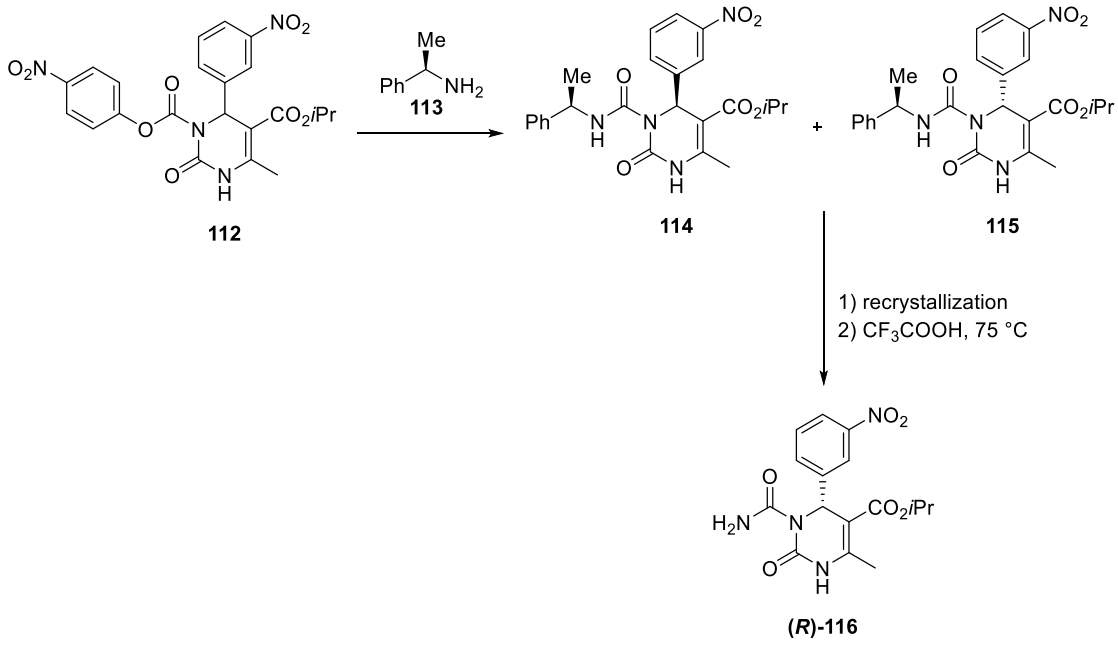

Scheme 30

Another example reported in literature by Dondoni is the resolution of racemic monastrol. [308] First, protected racemic monastrol (**117**) was transformed into the correspondent diastereoisomeric N-glycosil amides **119** and **120** which are then treated with NaOEt to obtain the resulting (*S*)- and (*R*)-monastrol (Scheme 31).

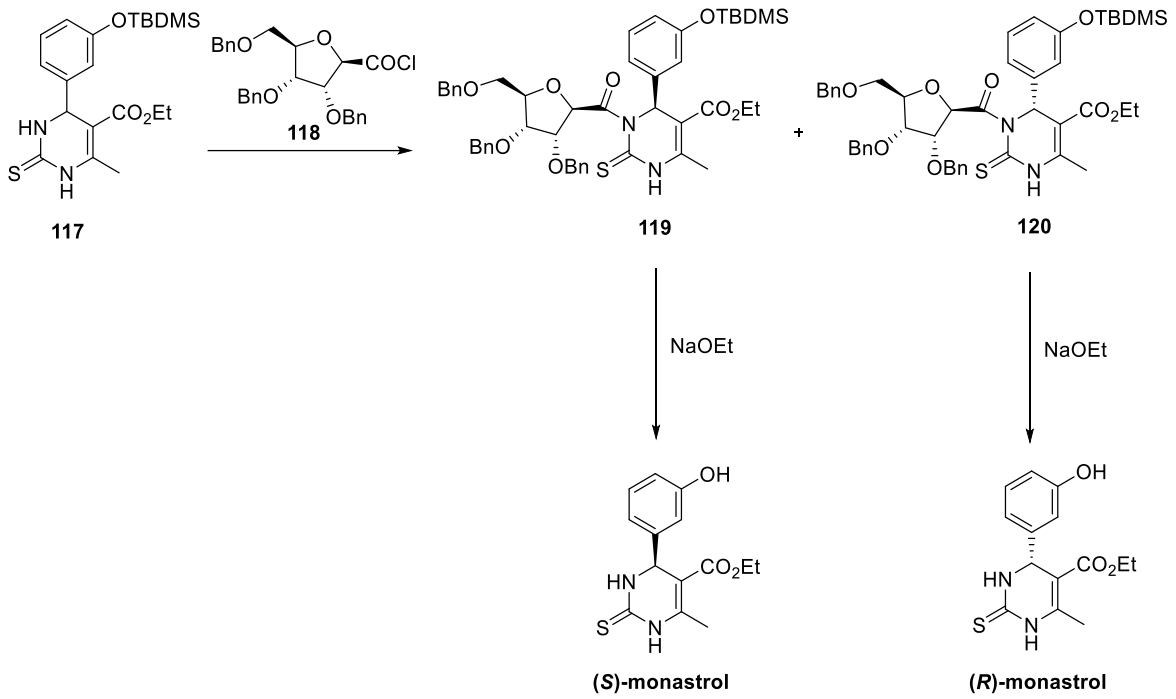

Scheme 31

The procedure reported by Dondoni was the first method for preparative scale resolution of racemic monastrol (ca. 100 mg), which allows the recovery of isomers in sufficient amount for biological evaluation. [308]

1.1.2.6.2 Enzymatic resolution

This approach relies on the use of specific enzymes that promote the enantioselective transformation of chemical groups of starting materials. In 2002, Sidler reported an enzymatic resolution of compound **121** (Scheme 32) using Subtilisin. [309] The right enantiomer **122** was recovered as ester while the unwanted (*R*)-enantiomer was converted to acid **123**.

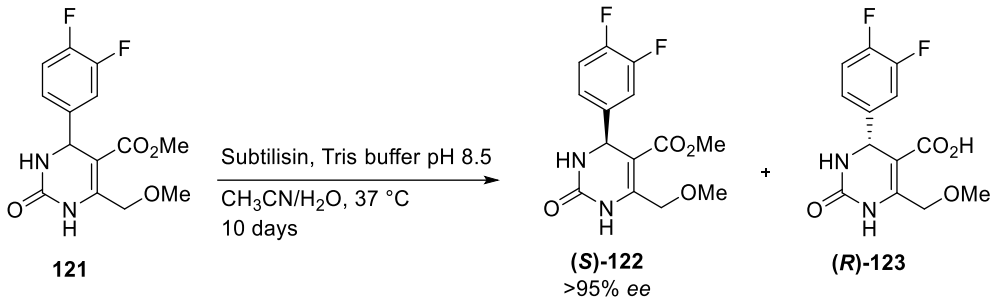

Scheme 32

Subtilisin was found after enzyme screening, where several esterases and lipases tested were ineffective. [309]

The precursor of compound **116** described above can be also prepared by the treatment of **124** with *Thermomyces lanuginosus* lipase, which converts only one enantiomer to the respective alcohol while leaving the other unmodified (Scheme 33). [310]

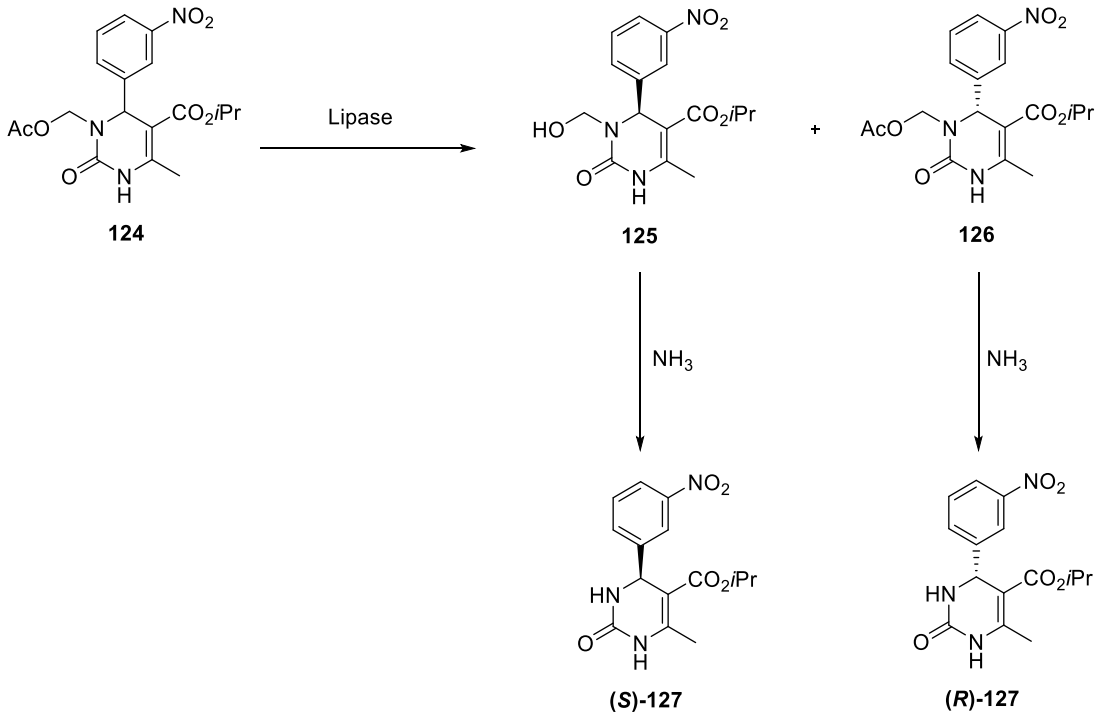

Scheme 33

Further treatment of **125** and **126** with NH_3 gave (*S*)- and (*R*)-**127**.

Enzymatic resolution is a useful method for the separation of racemic mixture due to the high specificity of enzymes. However, the choice of the right enzyme can be a limitation for this approach and usually a screening of these is required.

1.1.2.7 Asymmetric catalytic Biginelli reaction

From the synthetic point of view, having a process in which optically active DHPMs are obtained directly from the starting materials, avoiding the separation of enantiomers, can be advantageous. However, the difficulty in developing an enantioselective Biginelli reaction lies in finding the right catalyst which leads to the desired enantiomer in high yield and enantiomeric excess. In general, the asymmetric catalytic Biginelli reaction can be achieved using:

- chiral metal complexes;
- organocatalysis.

1.1.2.7.1 Chiral metal complexes

One of the first examples of the use of chiral metal complexes for Biginelli reaction was reported by Muñoz in 2003. [311] He described the use of chiral amine **129** in combination with $CeCl_3$ or $InCl_3$ to obtain the compound **130** in an enantioselective manner (Scheme 34).

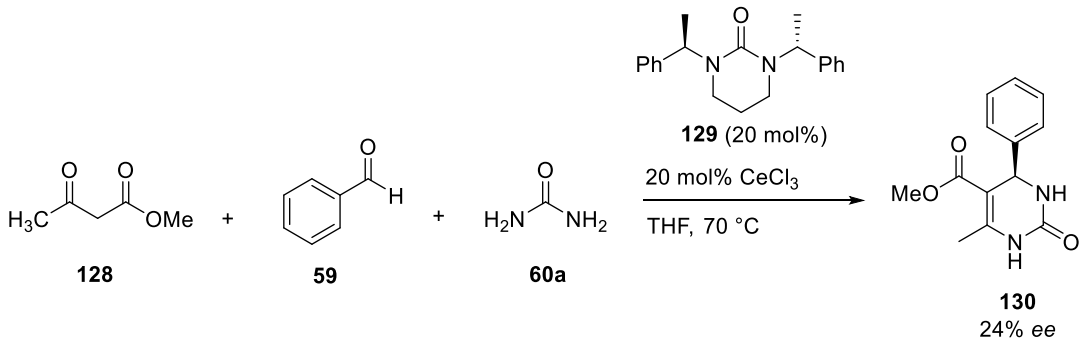

Scheme 34

However, even if $CeCl_3$ gave the best results in terms of yield, the enantiomeric excess (*ee*) remained low. [311] Moreover, to increase the *ee* of product **130**, Muñoz and co-workers tried to decrease the temperature, thus obtaining 40% of *ee* but with a very low yield. [311]

Zhu et al. reported a new ytterbium catalyst for asymmetric synthesis of DHPMs (Scheme 35). [312]

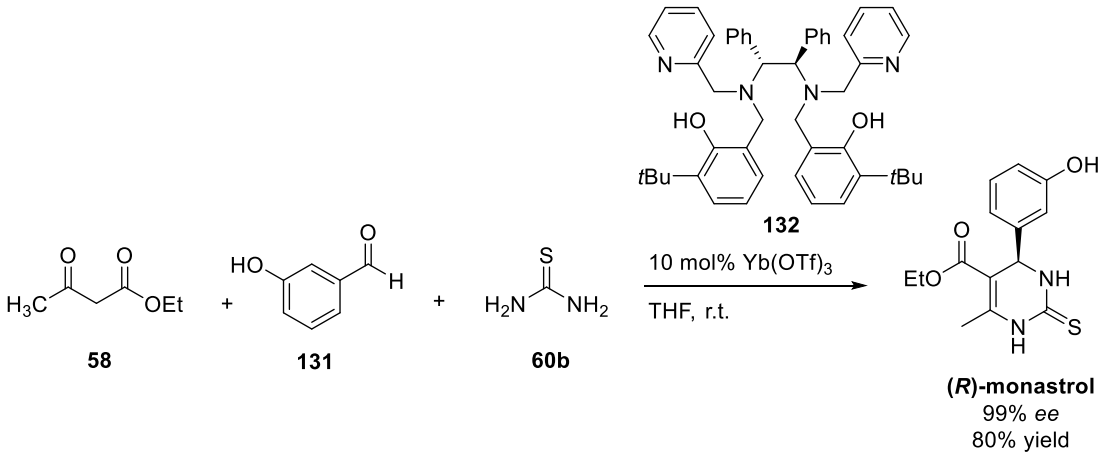

Scheme 35- An example reported by Zhu for the enantioselective synthesis of (*R*)-monastrol. [312]

To form the chiral catalyst, $Yb(OTf)_3$ was treated with the hexadentate ligand **132** for 15 minutes and then the other compounds were added. [312] This catalyst was very effective for the synthesis of (*R*)-monastrol, as well as many other chiral products which can be obtained by changing the substituent on the aldehyde or acetoacetate. In all cases the products were obtained with good to excellent *ee* (80-99%). [312] Interestingly, the authors also described the possibility to recycle and reuse the catalyst several times *via* pH-controlled extraction.

Another work, described the use of chiral copper complex **135** by mixing $Cu(OAc)_2$, (*S*)-1-phenylethylamine **134** and benzaldehyde **133** (Scheme 36). [313]

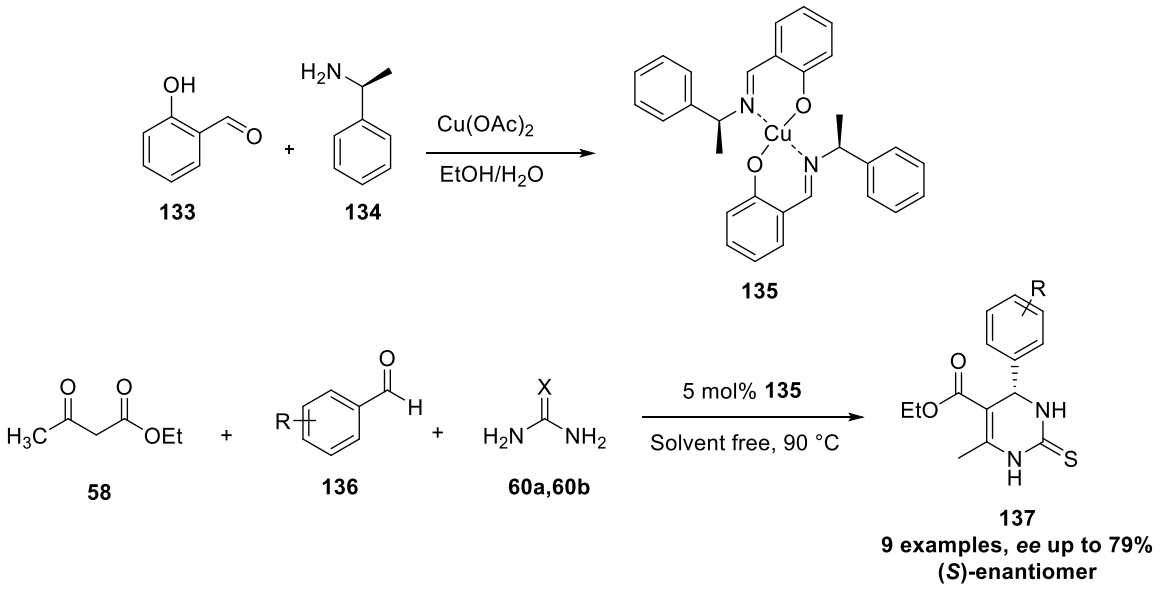

Scheme 36- Synthesis of chiral catalyst and its application. 60a: X= O; 60b: X= S. R= H, 2-Cl, 2-OH, 3-MeO, 3-NO_2, 3-OH.

Various aromatic aldehydes, both activated and deactivated, were used with very good results in all cases. The catalyst **135** can be recycled for three consecutive runs without significant loss of activity. [313]

In 2016, Titova and co-workers reported the asymmetric Biginelli reaction in the presence of compound **138** as chiral inducer and silicon, titanium or aluminium oxides as heterogeneous catalysts (Scheme 37). [314] Metal oxides seem to possess active centers that can act as co-catalysts and promote the chiral induction. [315]

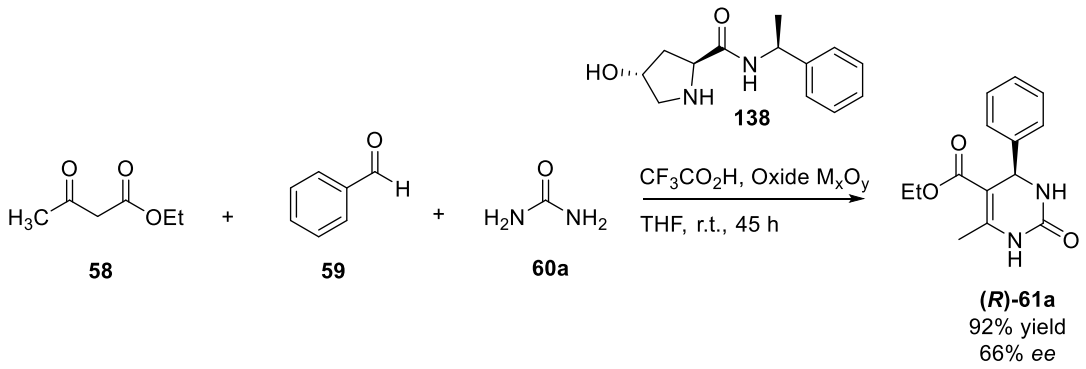

Scheme 37- M= Al, Ti, Si.

This reaction is sensitive to various parameters such as the nature of oxides (Al, Ti, Si), their dimension (nanosized or bulk) and the order of mixing of reagents. [314] In addition, the

amount of water has a great influence on the reaction as it can be adsorbed on the oxide surface and give additional active sites. Regarding the mechanism of action, they confirmed the iminium route hypothesized by Kappe (see paraghraph 1.1.1); both the imine (formed between **59** and **60a**) and the complex between acetoacetate **58** and chiral inducer **138** were adsorbed on metal surface which acts as catalyst and promote an additional steric control of the reaction. [314]

1.1.2.7.2 Enantioselective Organocatalytic Biginelli reaction

Along with chiral metal complexes, the use of organocatalysts in enantioselective Biginelli reactions represent a straightforward approach. However, the critical point is the evaluation and synthesis of chiral catalyst to promote an efficient process. Usually, both Lewis and Brønsted acids can be used to activate the iminium intermediate **139**, but these catalysts should be water-compatible due to the generation of two molecules of water during the reaction (Scheme 38). [316]

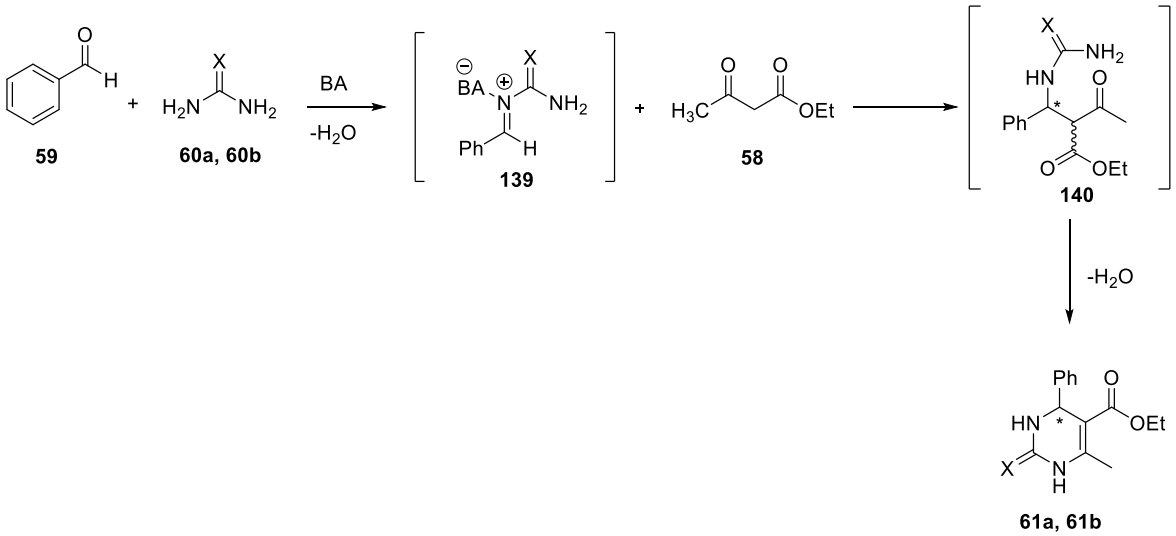

Scheme 38- Mechanism of Brønsted acids-catalyzed reaction. 60a, 61a: X= O; 60b, 61b: X= S.

The use of Brønsted acids as chiral catalyst was explored in 1992 by Kappe who used (*R*,*R*)-tartaric acid to catalyzed Biginelli reaction, but without obtaining the desired enantioselectivity. [317] Since that, a lot of progress have been made and different chiral catalysts have been developed.

Chiral phosphoric acids have been used for enantioselective activation of imine and then also applied to Biginelli reactions.[318,319] In 2006, Gong and co-workers developed a series of chiral phosphoric acids based on binol- or H_8-binol scaffolds (Figure 113). [319]

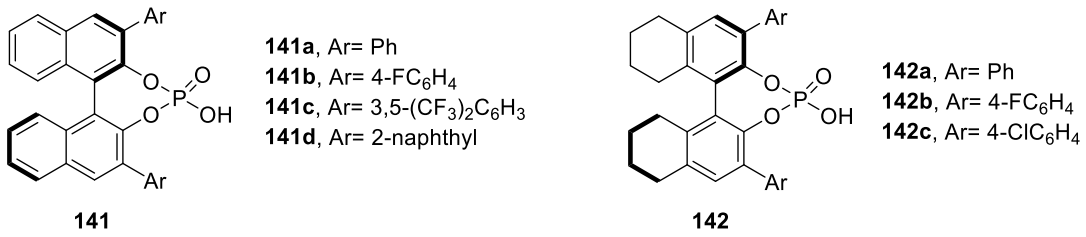

Figure 113- Chiral phosphoric acids based on binol- (141) or H_8-binol (142) scaffolds.

3,3'-disubstituents of chiral catalysts have an important impact on the Biginelli reaction. In contrast to the other works, [318,320,321] by increasing the size of the substituent there is a decrease of both the yield and enantioselectivity of the reaction. An interesting effect was obtained with **141c** as the configuration of products were reverse respect to the other catalysts. [319] Among of all of them, **142a** was proven to be the most effective catalyst and various substituent on the aldehyde and β-keto ester were well tolerated (Scheme 39).

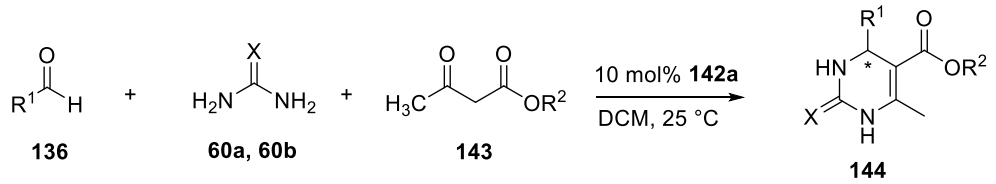

Scheme 39- Organocatalytic enantioselective Biginelli reaction with phosphoric acid 142a. 60a: X= O; 60b: X= S. For R^1 and R^2 see Gong et al. [319]

The presence of water, generated during the reaction, seems not have an impact on the reaction as the addition of molecular sieves (5 Å) didn't increase the yield. [319] Moreover, with the high temperatures the yield remained almost the same but the enantioselective was slightly lower.

In 2009, the same research group discovered other catalysts by tuning the 3,3'-disubstituents on chiral phosphoric acids. [322] Since they noticed that the size of these substituents controls the stereochemistry (but also the conversion) of the reaction, Gong and co-workers developed a number of compounds bearing bulky 3,3'-disubstituents. Compound **145** was

the most effective in catalyzed the Biginelli reaction and in reversing the stereochemistry if compared to compound **142a** (Scheme 40). [322]

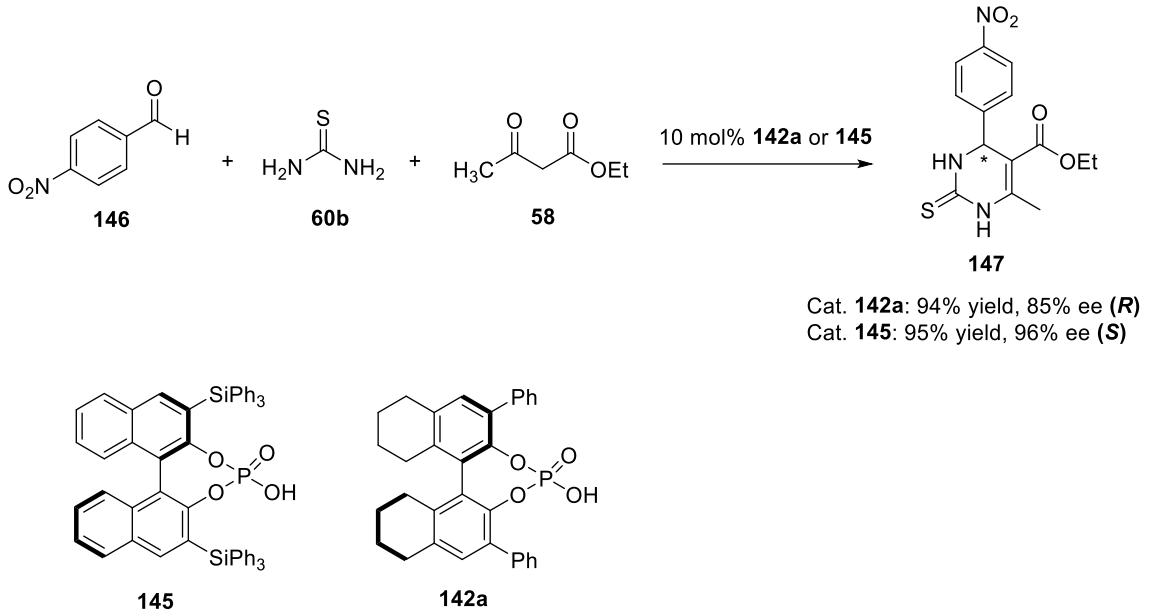

Scheme 40

Beside the classic reaction, catalyst **145** was also applied in Biginelli-like reaction which means the use of enolizable ketones instead of β-keto esters. Indeed, ketones are less enolizable than β-keto esters and thus less reactive, requiring the use of strong Lewis or Brønsted acids. However, with catalyst **145** the Biginelli-like reactions appear to be effective using both cyclic and acyclic ketones, also replacing thiourea **60b** with benzylthiourea. [322] In the same paper, Gong et al. described a possible reaction mechanism for classic Biginelli or Biginelli-like reactions, catalyzed by phosphoric acids, based on DFT studies and other works reported in literature (Scheme 41). [322]

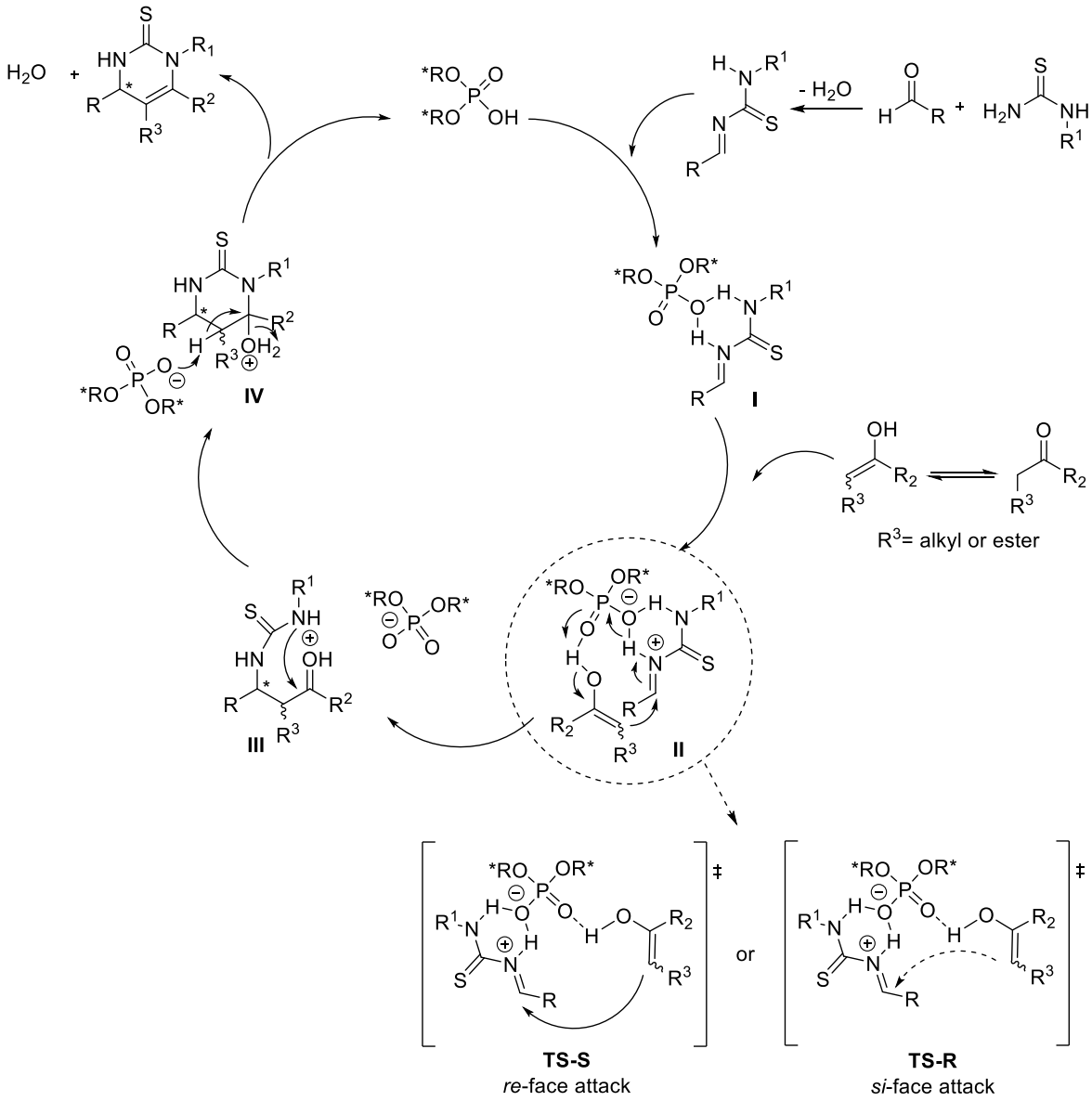

Scheme 41- Biginelli and Biginelli like reactions catalyzed by chiral phosphoric acids. TS= transition state.

A key point for the stereochemistry of the reaction is the intermediate **II**. The chiral phosphoric acid activates the imine, which is then attacked by the β-keto ester or the enolizable ketone to undergo an enantioselective Mannich reaction. At this point, two transition states are possible in which the enol can attack the *re*-face or *si*-face of the imine. This process depends mainly on the type of catalyst and the strength of hydrogen bonds formed in the transition states (TSs); with **142a** the *si*-face attack is favoured while with **145** the preferred attack is on the *re*-face of the imine and thereby gave the enantiomer *S*. [322]

These studies on chiral phosphoric acid catalysts led to the development of further protocols for the enantioselective Biginelli reaction. For example, a paper published in 2017 by Zou

et al. described the application of catalyst **148** (Figure 114) when aliphatic aldehydes were used instead of classic aromatic ones. [323] Moreover, double axially chiral bisphosphorylimides (Figure 114) were investigated as a possible catalyst leading to several chiral DHPMs with high yield (up to 96%) and enantioselectivities (up to 97%) in only 12 hours, thus overcoming the problem related to the long reaction time. [324]

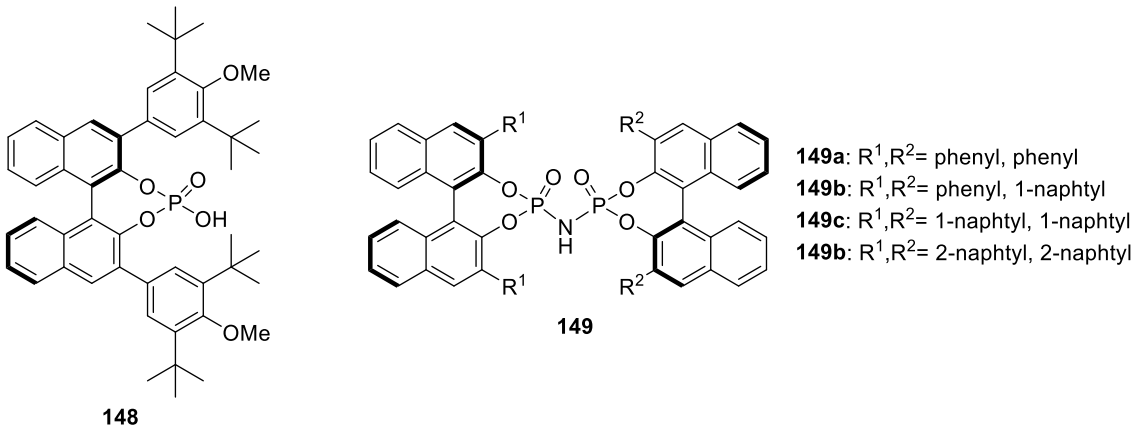

Figure 114

Although the products are obtained with high *ee*, one of the biggest disadvantages of the reactions catalyzed by chiral phosphoric acids is the long time required to afford acceptable yields. Except for bisphosphorylimides, in most cases the reaction time is between 4 and 10 days, representing a clear limit for these catalysts.

Since the acidic conditions seem to favour the reaction, other methods to perform enantioselective Biginelli reactions rely on the use of achiral Brønsted acids in combination with simple chiral amines. [325,326] An early example was reported by Feng and co-workers in which they described the use of trans-4-hydroxyproline-derived secondary amine (**152**) in combination with 2-chloro-4-nitrobenzoic acid (**151**) to obtain DHPMs with an excellent *ee*, even if with moderate yield under these mild conditions (Scheme 42). [325]

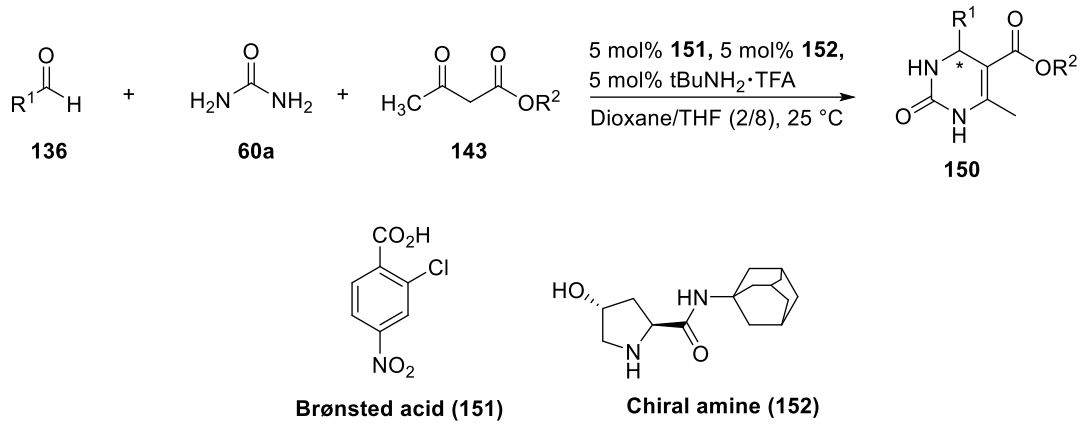

Scheme 42- Enantioselective Biginelli reaction catalyzed by achiral Brønsted acid and chiral secondary amine. For R^1 and R^2 see Feng et al. [325]

More interestingly, the catalytic cycle generated by the chiral amine **152** represents an example of dual-activation mechanism. [327] This means that catalyst **152** can activate both the nucleophile (int. **II**) and the electrophile (int. **III**) to promote the asymmetric synthesis (Scheme 43).

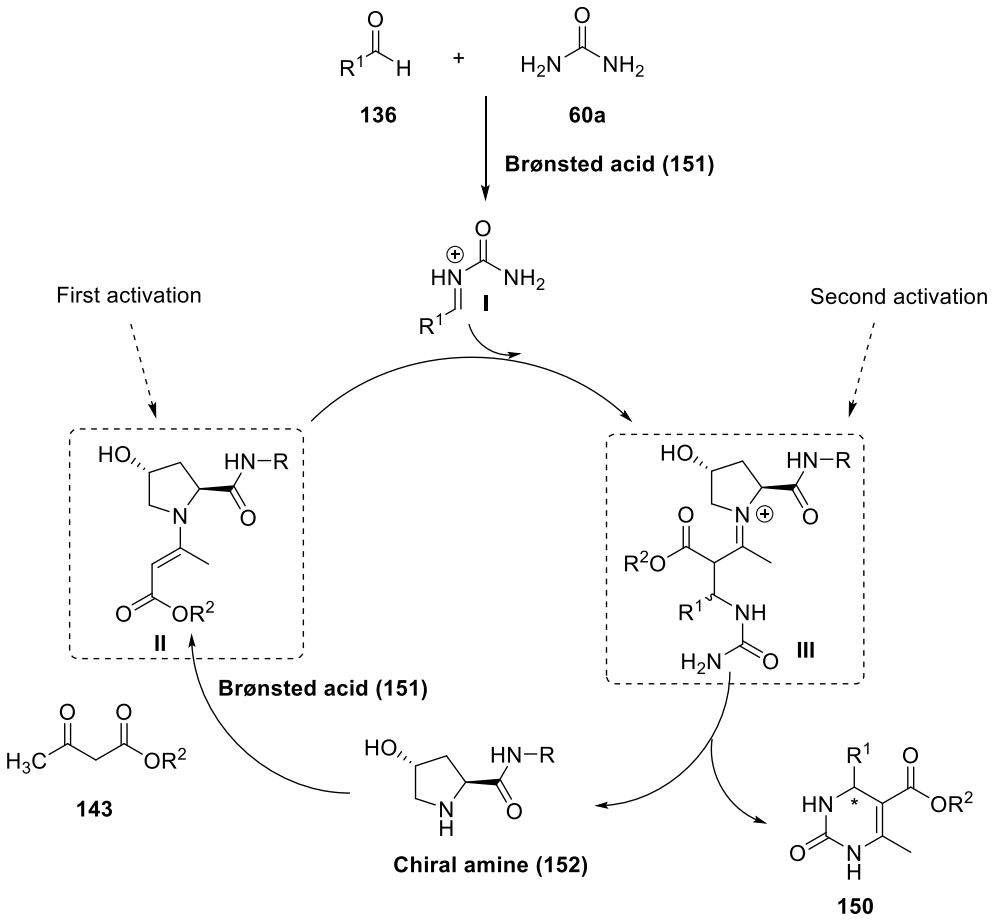

Scheme 43- Dual-activation pathway mediated by chiral amines.

As in the case of chiral phosphoric acids, also with chiral amines two transition states are possible, however the one with the lowest energy leads to the *R*-enantiomer. [325]

Another example reported in literature involves the use of bifunctional primary amine-pyridine (**153**, Figure 115) as catalysts associated with HCl. [326] Compared to the catalyst **152**, the picolinamide moiety of compound **153** has more sites for the formation of hydrogen bonding and thus influencing the structure of intermediates.

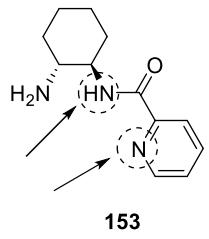

Figure 115- Bifunctional primary amine pyridine catalyst. Sites involved in hydrogen bonding are circled.

The amount of HCl is also crucial for the yield and enantioselectivity of the reaction. Less than 10 mol% of HCl has a negative impact on the yield, even if the *ee* remains high; in contrast, experiments with more than 10 mol% of HCl gave excellent yield but lower *ee*. [326] Most likely, high amounts of acid catalyzed both the iminium ion and the cyclization steps, replacing the activity of chiral amine.

In 2012, Frings et al. described for the first time the application of chiral sulfoximine-based thiourea in asymmetric Biginelli reaction. [328] They synthesized several chiral mono- or bis-thioureas bearing primary, secondary and tertiary amines able to form hydrogen bonds with the intermediates of Biginelli reaction. After a catalyst screening, the best was compound **154** even if 5 days were required to obtain good yields (Scheme 44). [328]

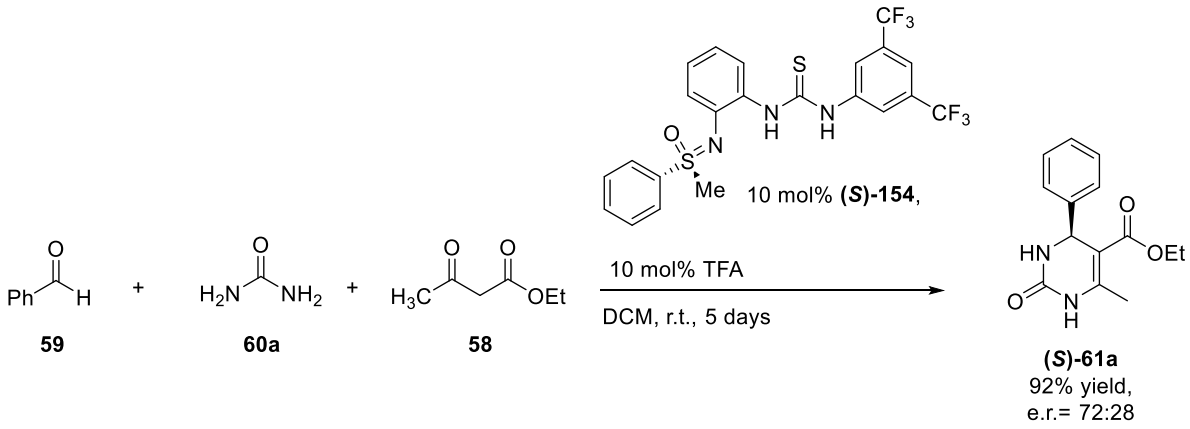

Scheme 44- Enantioselective biginelli reaction with thiourea 154 as catalyst. e.r.= enantiomeric ratio.

The concentration of the thiourea-based catalyst in the reaction was important for the enantioselectivity. Indeed, at high concentrations, thiourea can form less active aggregates, resulting in lower enantioselectivities. [329]

A green protocol for asymmetric Biginelli reaction using a chiral derivative of 1,2-benzenesulfonimide was reported by Barbera et al. (Scheme 45, example A). [330] The main advantages include the absence of solvent, complete catalyst recycling, mild reaction conditions and short reaction time if compared to the other methods. [330]

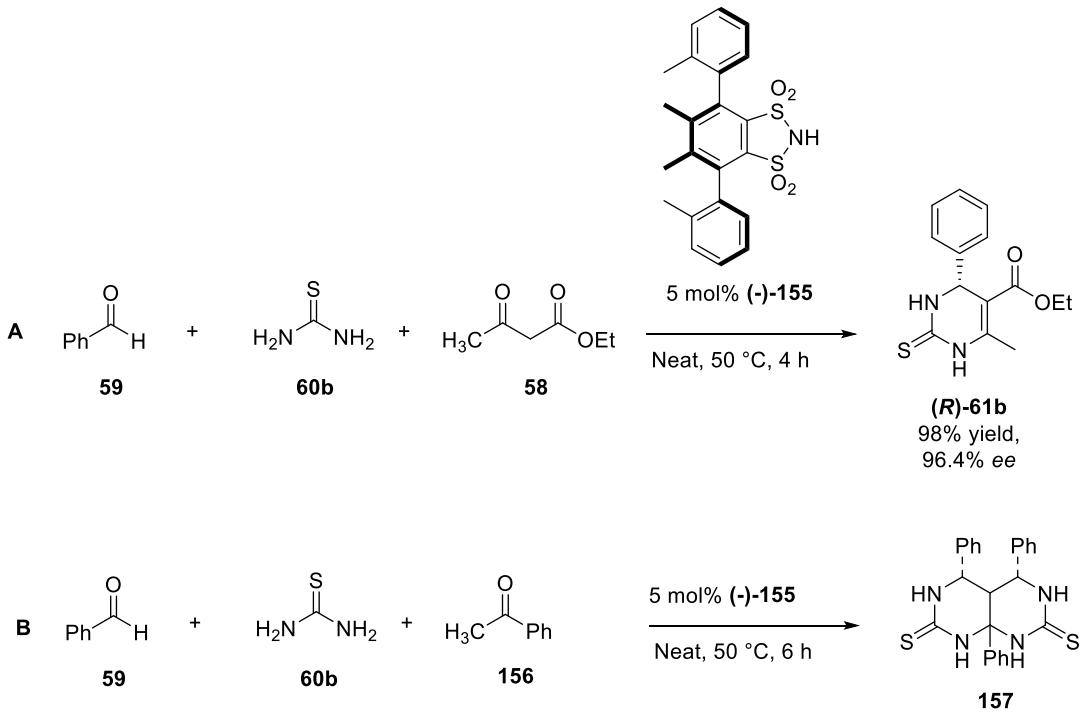

Scheme 45- Biginelli (A) and Biginelli like (B) reactions catalyzed by benzenesulfonimide 155.

Both electron-withdrawing and electron-donating groups on the aldehyde are well tolerated and excellent yields and enantioselectivities were achieved in all cases. They also investigated the possibility to perform Biginelli like reactions by replacing the β-ketoester with acetophenone (Scheme 45, example B). [330] However, instead of an expected chiral DHPM they obtained the product **157**. A possible mechanism which explained this alternative pathway was reported in literature and supported by DFT studies. [331] It seems that protic acids lower the activation energy of the bicyclic product and promotes an alternative mechanism, if compared to the reaction conducted in absence of protic acids. In addition, the *meso* form of product **157** was the most plausible as indicated by $[\alpha]_D$ and chiral HPLC analysis. [330]

An alternative approach to obtain chiral DHPMs and hexahydropyrimidinones (HHPMs) involve the use of organocatalysts displaying a network of cooperative hydrogen bonds (NCHB). [332] The most interesting part of this approach is the possibility to synthesized DHPMs or HHPMs by using acid or basic conditions respectively (Scheme 46).

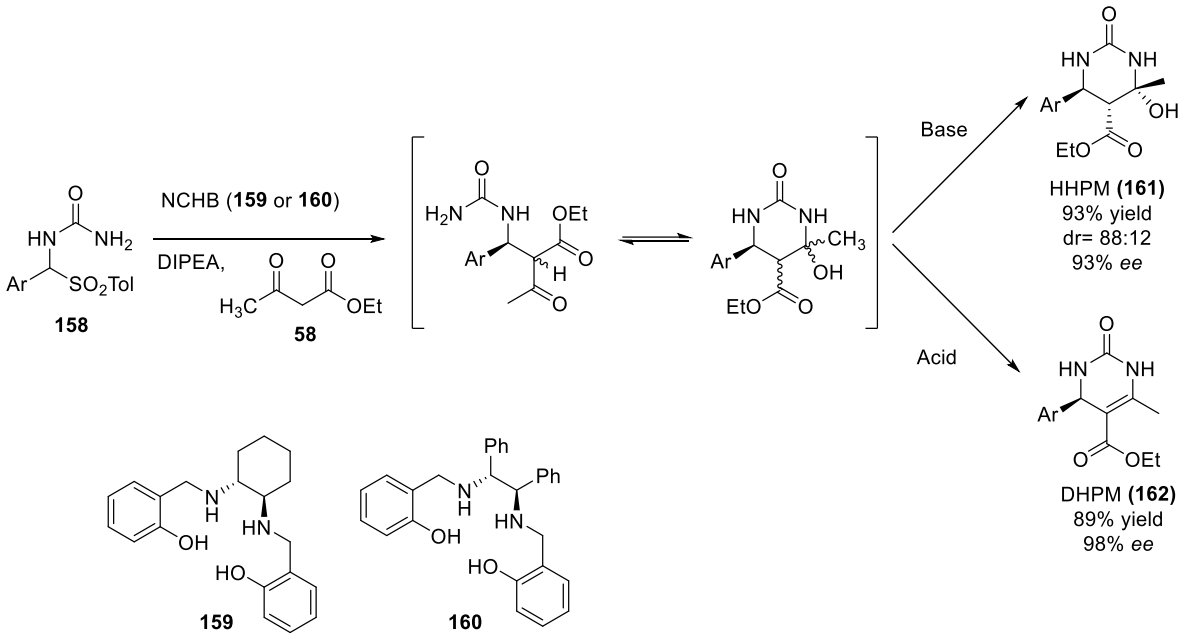

Scheme 46

Compared to the other Biginelli reactions, in this case α-ureidosulfone **158** was used as a surrogate of the classic N-acyliminium ion as starting material. Catalysts **159** and **160** were proven to be suitable to obtain one-pot highly enantioselective synthesis of DHPMs or highly enantioselective and diastereoselective synthesis of HHPMs, also varying the aryl substituent. [332] The choice of the base in the first step is fundamental, as bases stronger than diisopropylethylamine (DIPEA), such as diazabicyclo[5,4,0]undec-7-ene (DBU) and 1,1,3,3-tetramethylguanidine (TMG), gave racemic mixture. Moreover, the base can induce the retro-Mannich reaction of the intermediate, thus affecting the enantioselectivity of the process. [332]

Self-assembled methanoproline-thiourea catalysts for asymmetric Biginelli reaction have been developed to give the classic chiral DHPMs or 4-substitued unsaturated aryl DHPMs (Scheme 47). [333,334]

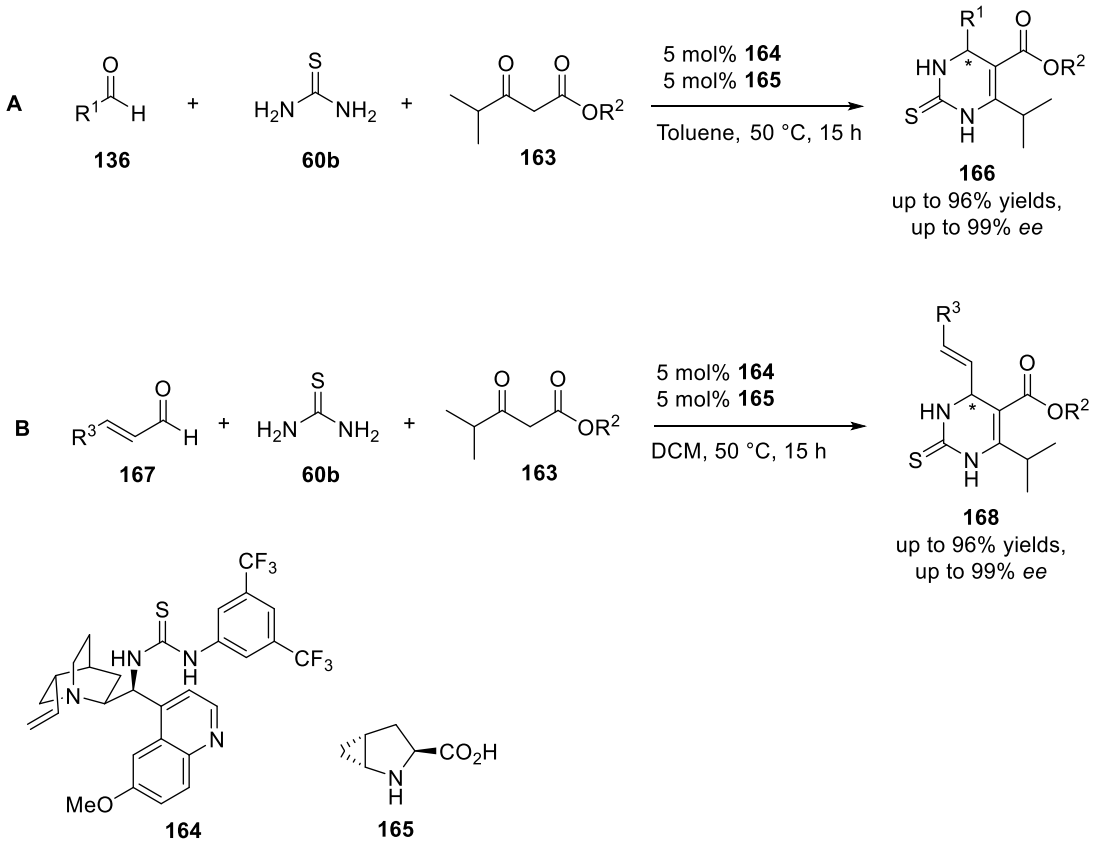

Scheme 47- Asymmetric Biginelli reaction catalyzed by methaproline-thiourea 164 and 165. Example A: asymmetric synthesis of chiral DHPMs; example B: asymmetric synthesis of 4-substitued unsaturated aryl DHPMs. For R^1, R^2 and R^3 see Han et al. [333,334]

The combination of the two catalysts **164** and **165** was much more effective than the single ones, and the mild conditions and relatively short reaction time represent an advantage of this reaction protocol. [333]

In addition to all the reported examples, other chiral organocatalysts, such as pyrrolidinyl tetrazole, [335] diazabicyclo derivatives, [336] calixarene-based proline [337] or nanocomposite, [338] have been reported.

1.2 C-N functionalization of Heteroaryl scaffolds

As the main focus on this part of the project was the synthesis of C-N bond involved heteroaryl scaffolds, the examples reported in the following paragraphs are limited to this scope. In general, the most common methodologies to make new C-N bonds include nucleophilic aromatic substitution (S_NAr), Ullmann and Buchwald-Hartwig coupling

reactions, the use of other transition metals (Rh, Fe, La, Ni, Ag) or reductive amination (Scheme 48). [339]

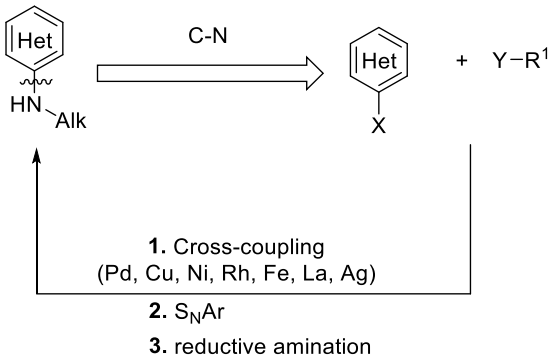

Scheme 48- C-N bond forming through cross-coupling reactions, S_NAr and reductive amination. X= Hal., -NH_2; Y= -NH_2, -C=O; R^1= alkyl, benzyl, aryl.

In this work, Ullmann cross-coupling along with S_NAr involved chloro-, bromo-, fluoro-heteroaryl derivatives and an alkyl amine as counterpart have been explored. Therefore, it is useful to make a brief description of some reaction protocols taking as examples the reactions between pyridines and benzylamine.

1.2.1 Ullmann coupling

Discovered by Ullmann in 1901, this reaction probably represents the earliest example of cross coupling protocol. [340] Although the classic Ullmann reaction involved the homocoupling between two aromatic rings, several modifications have been made to obtain the coupling with different nucleophiles such as ammines, alcohols, thiols and many others. [341] Nowadays, these reactions are known as Ullmann-type or hetero-Ullmann couplings (Scheme 49).

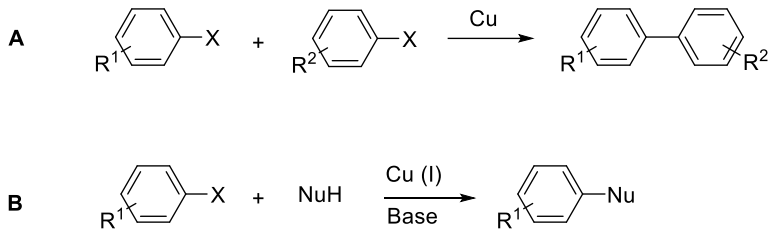

Scheme 49- Classic Ullmann (A) and Ullmann-type (B) reactions; X= Hal.

Despite the initial success and the broad scope of these reactions, harsh reaction conditions (generally T >200 °C) and low yields have limited its applicability especially in industrial field. The use of strong bases and a stoichiometric amount of copper reagents (Cu (0), Cu (I), Cu(II) as salts or oxides) are often required to improve the yield. [342] The mechanism of Ullmann reactions is still object of debate as the most troubling aspects are the activation of the aryl halide and the role of the ligand; recent studies also suggest the presence of Cu(III) as intermediate in the oxidative addition step. [343,344] In general, the order of reactivity for aryl halide is the opposite of that observed for S_NAr, with the aryl iodide and bromide being the most reactive substrates. The role of ligands (especially bidentate ligands), along with the use of inorganic bases, is important as they decrease the temperature (80-100°C), the time of the reaction and the amount of copper (5-10 mol%). [342] Common ligands in Ullmann-type reactions are *N*- and *O*-donor, even if sometimes also P-based ligands have been used but with poor results. [345]

Regarding the heteroaryl substrates, their coupling with aliphatic amines is generally less explored with some examples reported in literature. [346–352] In 2010, Liu et al. reported a ligand-free copper-catalyzed amination of heteroaryl halides with alkyl- and arylamines (Scheme 50). [346]

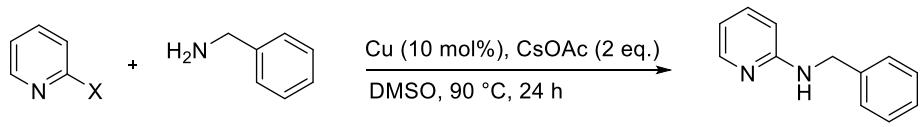

169a: X= I
169b: X= Br
169c: X= Cl
169d: X= F

170

171a, >95% yield
171b, 93% yield
171c, 30% yield
171d, 50% yield

Scheme 50- Example of coupling between heteroaryl halides and benzylamine.

In accordance with the order of reactivity of aryl halides in Ullmann reactions, heteroaryl iodide and bromide were the most reactive while the respective chloride gave lower yield. Interestingly, with the starting material **169d**, the product **171d** was obtained with moderate yield; probably in this case S_NAr was involved.

Another example reported the use of the oxime **172** as ligand, starting from the heteroaryl iodide **169a** (Scheme 51). [348]

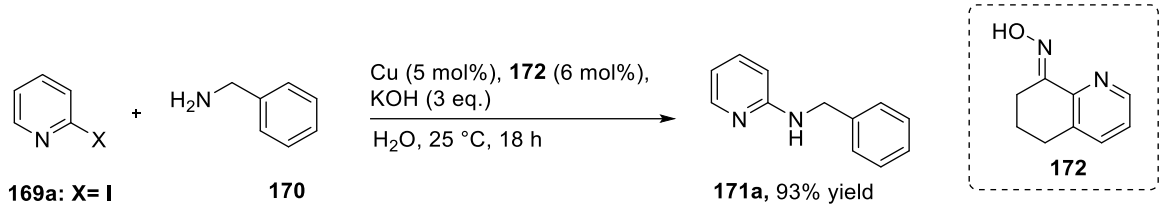

Scheme 51

The reaction was carried out in water at room temperature and excellent results were obtained.

For less reactive chloropyridine, specific ligands such as oxalamides or 2-aminopyridine oxides have been developed (Scheme 52). [349,352]

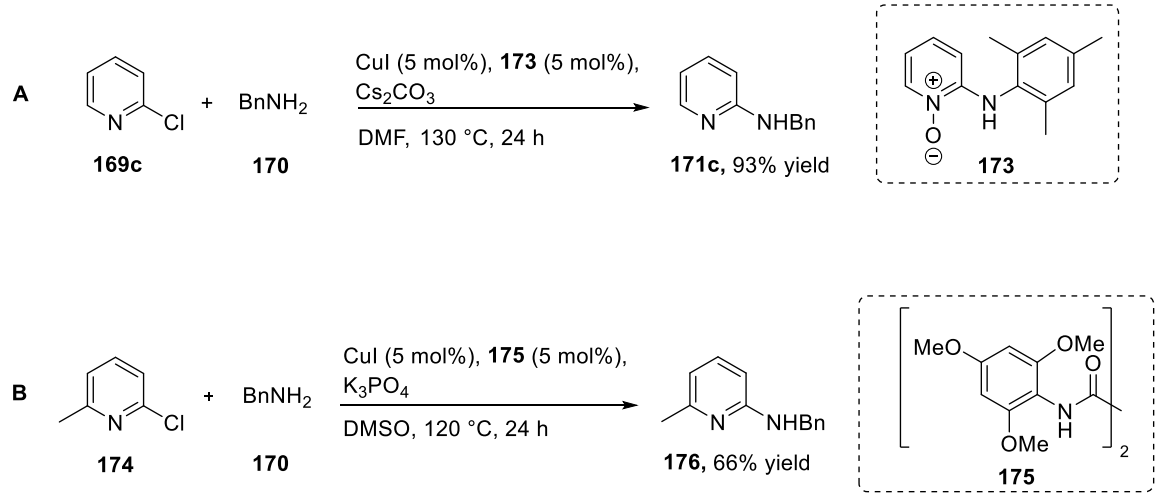

Scheme 52- Ullmann-type reaction using 2-aminopyridine 1-oxide (example A) or oxalamide (example B) ligands.

As we can notice from the examples, the Ullmann-type reaction can be carried with or without ligand in different conditions. Chloropyridine, as well as other aryl chloride, often required stronger reaction conditions with high temperatures and long reaction time. However, the advantages of Ullmann coupling lie in the low cost of both copper source and ligands and usually the catalytic system are not sensitive to moisture (as opposed to the Pd-catalyzed cross-coupling).

1.2.2 Buchwald-Hartwig cross-coupling

The Pd-catalyzed cross-coupling of amines and aryl halides is a widely used method to synthetize new C−N bonds. This is due to the large scope of these reactions along with many available ligands/precatalysts. As reported by Buchwald in his comprehensive review, C-N coupling reactions using Pd catalysts have been extensively applied in the field of Medicinal chemistry, Process chemistry, Natural products, Materials chemistry and Chemical biology. [353] However, also in this case the process still suffers from the substrate scope regarding the coupling between heteroaryl halides and primary amines. [354] A general catalytic cycle for C-N cross-coupling reactions is reported in Scheme 53.

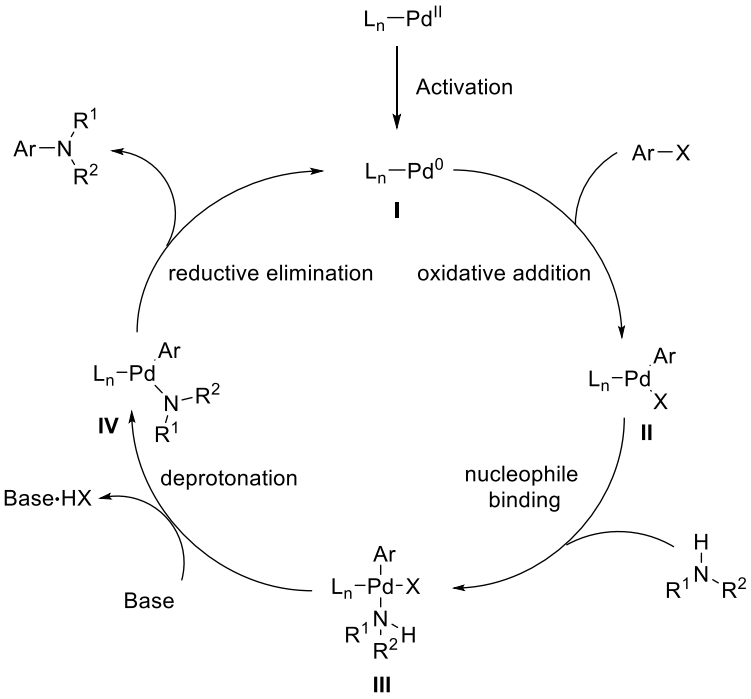

Scheme 53

Once activated, the complex **I** undergoes oxidative addition to an aryl halide to give **II**. Then, Pd^{II} acts as a Lewis acid to bind the amine giving the intermediate **III**. As the proton of the amine become more acidic, the base can promote the deprotonation step. The amido complex **IV** regenerate the active palladium catalyst **I** by reductive elimination with the release of the desired product. Each variable, such as ligand, Pd source, base, solvent and temperature, can affect the catalytic cycle lowering the yield and leading to the formation of side-products.
As example, Buchwald amination of chloropyridine and benzylamine was reported with the condition showed in Scheme 54: [354]

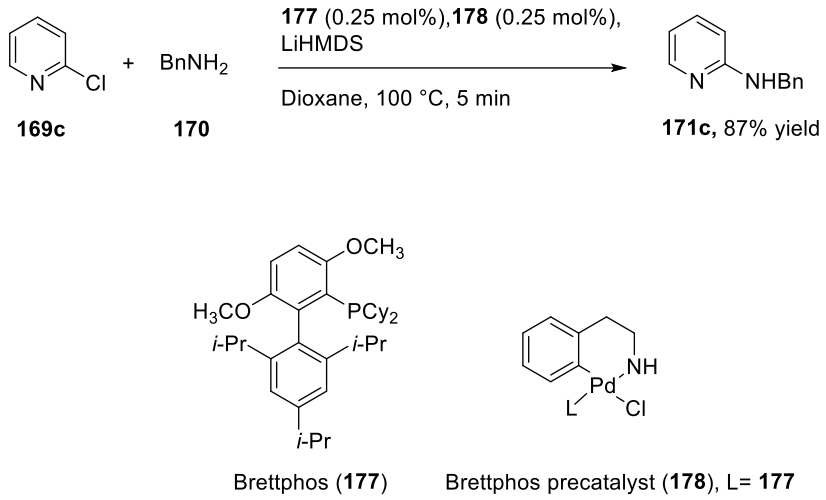

Scheme 54- Example of cross-coupling between chloropyridine and benzylamine reported by Buchwald.

Despite all the described advantages of Buchwald reactions (well-known mechanism, low catalyst loading, wider scope) [355–357] the cost of both palladium sources and their ligands remains the main drawback.

1.3 Aim of this research work

1.3.1 Enantioselective synthesis of Biginelli adducts

As we mentioned above, usually only one enantiomer of DHPMs is active towards the biological target. Although enantioselective syntheses of Biginelli adducts have been explored with various substituents on the aldehyde and β-ketoester, fewer papers report substituted (thio)ureas as possible building block. [358] The aim of this work is to use an asymmetric Biginelli reaction to directly obtain N1-substitued DHPMs in high yield and enantiomeric excess, thus avoiding the chiral resolution step (Scheme 55):

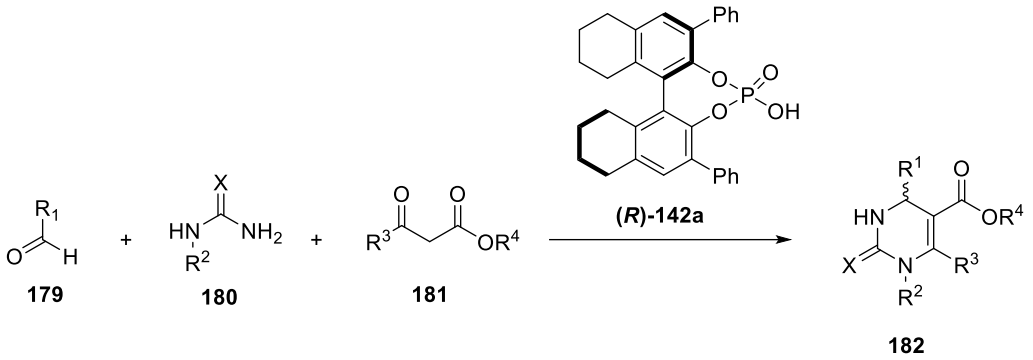

Scheme 55- Asymmetric Biginelli reaction. X, R^1,R^2, R^3 and R^4 cannot be disclosed due to IP protection.

Based on the data reported in literature, chiral phosphoric acid **142a** was chosen among the various catalysts, as the mechanism and the scope have been well explored. [319,322]

The product **182** is a useful intermediate in the synthesis of biologically active molecules. An alternative pathway involved the enantioselective Biginelli reaction using (thio)urea and further arylation of N1 of the resulting DHMP **183** to give the product of interest **185** (Scheme 56).

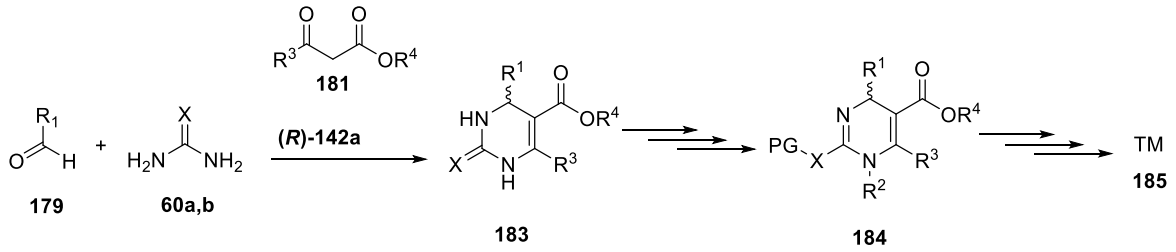

Scheme 56- Alternative pathway to obtain the product of interest 185.

1.3.2 Functionalization of Heteroaryl scaffolds

One of the main issues to solve is the functionalization of heteroaryl scaffold with an alkyl amine. The work reported in this thesis has mainly focused on two synthetic strategies shown in Scheme 57.

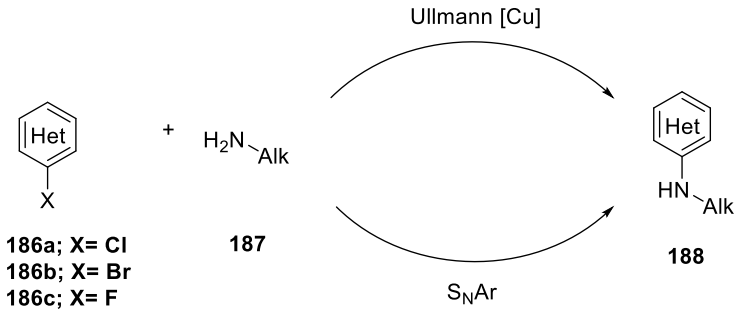

Scheme 57- Two possible strategies to make new C-N bond. Alk group cannot be disclosed due to IP protection.

Even if Buchwald reaction can be useful for this transformation, this cross-coupling was not considered in this thesis as one of the focus was to remove the use of precious metal catalyst. Some experiments using S_NAr on chloro-, bromo-, fluoroheteroaryl derivatives have been performed using different reaction conditions. For Ullmann reaction, a screening of several catalysts, ligands, solvents and temperatures was conducted in order to find the best conditions for our substrates.

Chapter 2- Results and discussion

2.1 Enantioselective synthesis of Biginelli adducts

One reported major issue is the chiral resolution of the Biginelli adduct **182** from the racemic mixture, which leads to the loss of half of the input material as the wrong enantiomer. Therefore, to achieve the final product **185** and overcome the chiral resolution, we hypothesized two synthetic routes (Scheme 58):

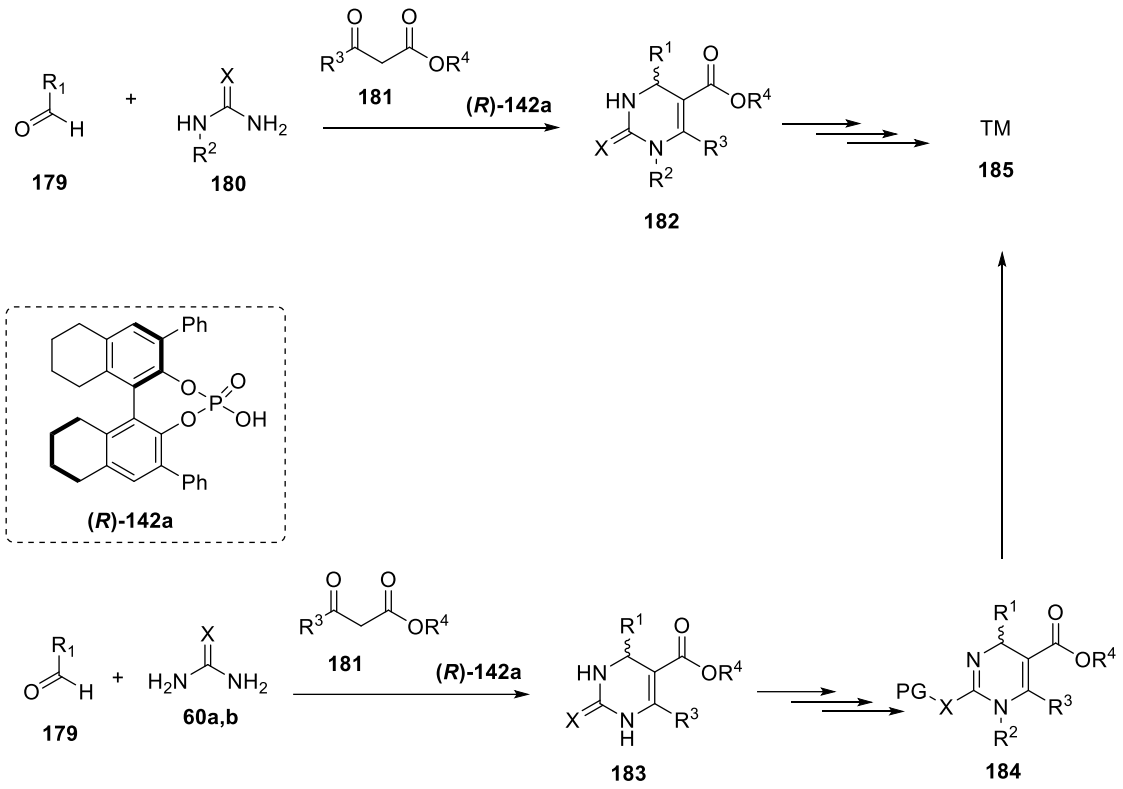

Scheme 58- Two possible synthetic pathways.

In the first case, we wanted to explore the use of chiral catalyst **(*R*)-142a** in the asymmetric Biginelli reaction applied to *N*-substitued (thio)ureas **180**, which can lead to the optically pure **182**. However, the difficulty of this approach relies in the use of substituted (thio)ureas which are explored only with methyl, ethyl or benzyl substituents in the asymmetric synthesis. [358] The other approach, involve the classic enantioselective Biginelli reaction to obtain **183** and then find a suitable synthesis to achieve the product **185**.
First of all, we need to synthesize the chiral phosphoric acid **(*R*)-142a**.

2.1.1 Synthesis of chiral catalyst

Based on the data reported in literature, [359,360] the synthesis of chiral phosphoric acid can be done as follows:

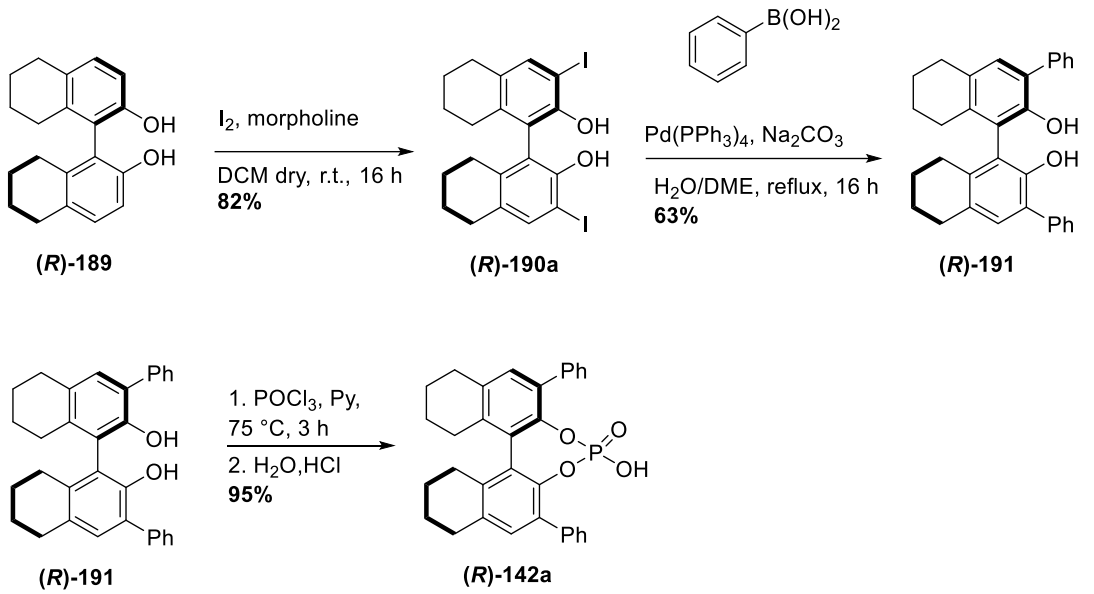

Scheme 59- Synthesis of chiral catalyst.

In the first step, the iodination of the aromatic rings was carried out with I_2 in the presence of morpholine to give the product **(*R*)-190a** in good yield. The subsequent Suzuki step was the most challenging, as the following side-products were identified:

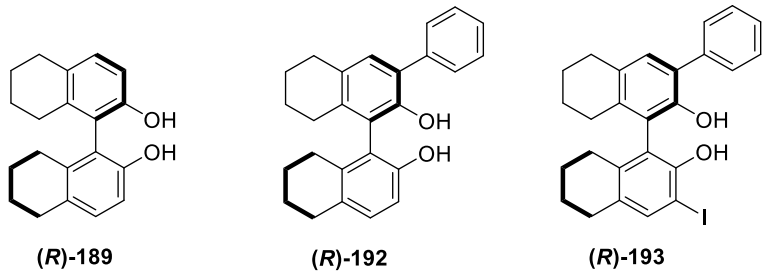

Figure 116- Side-products found in the Suzuki step.

The product **(*R*)-189** is the classic dehalogenated compound often found in this coupling reaction, while **(*R*)-192** and **(*R*)-193** are monoarylated side-products. To reduce the amount of impurities, a screening of different reaction conditions was done (Table 13).

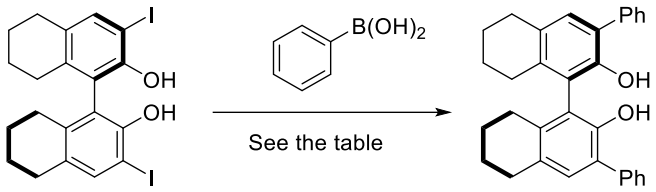

(*R*)-190a **(*R*)-191**

Entry	Solvent	Catalyst	Base	Temperature (°C)	Time (h)	Yield
1	H_2O/Dioxane (1,5:1)	1mol% Pd/C (10%)	Na_2CO_3 (2.5 eq.)	95 °C	16 h	-
2	H_2O/Dioxane (0,5:1)	1mol% Pd/C (10%)	Na_2CO_3 (2.5 eq.)	MW 110 °C	10 min	24%
3	H_2O/DMF (0,5:1)	3mol% $Pd(PPh_3)_2Cl_2$	K_2CO_3 (2.5 eq.)	80 °C	16 h	-
4	H_2O/DME (0,7:1)	5mol% $Pd(PPh_3)_4$	Na_2CO_3 (2.5 eq.)	Reflux	16 h	63%

Table 13

With Pd/C as catalyst (entries 1-2, Table 13), a very low yield of the desired product was obtained; in this case a significant amount of dehalogenation was detected. A similar outcome was observed with $Pd(PPh_3)_2Cl_2$, where dehalogenation along with side-products shown in Figure 116 were found. The best result was achieved with $Pd(PPh_3)_4$ (entry 4, Table 13), which gave the desired product in sufficient amount to conclude the synthesis. It is worth noting that the same conditions of Suzuki coupling were applied to the bromo derivative of compound **(*R*)-189**, obtaining similar results; however, the synthesis of **(*R*)-190b** using Br_2 gave lower yield:

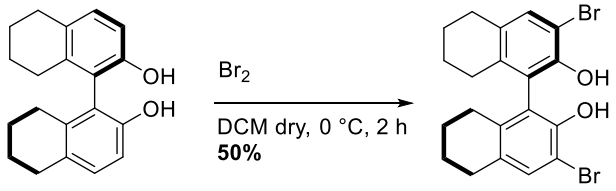

(*R*)-189 **(*R*)-190b**

Scheme 60

In the last step, **(*R*)-191** was treated with $POCl_3$ and then hydrolysed in aqueous conditions, to give **(*R*)-142a** in almost quantitative yield (Scheme 59).

2.1.2 Enantioselective Biginelli reaction using chiral catalyst **(*R*)-142a**

At this point, we performed the Biginelli reaction without the chiral catalyst to have the reference of racemic compound (Scheme 61).

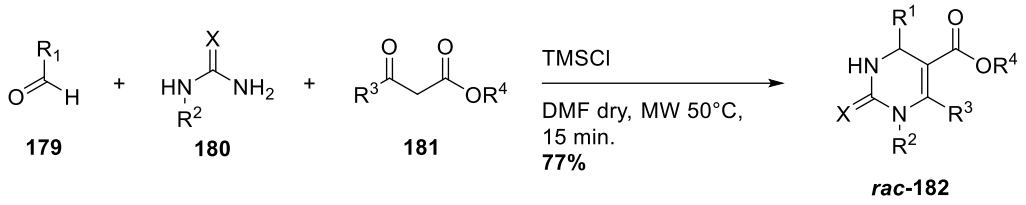

Scheme 61- Racemic Biginelli reaction.

Chlorotrimethylsilane (TMSCl) was used as a Lewis acid and gave good results with or without the use of microwaves. Indeed, the same reaction can be carried out through the conventional heating but required at least 6 h.

The next step was the asymmetric Biginelli reaction using chiral catalyst **(*R*)-142a** (Table 14).

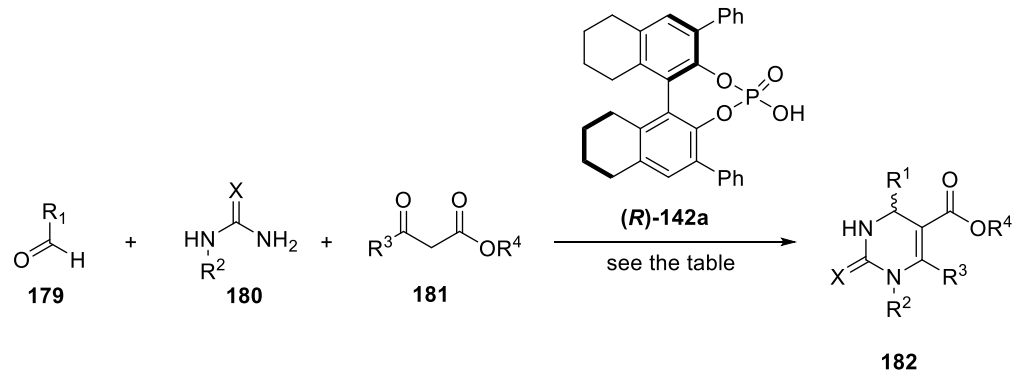

Entry	Catalyst	Solvent	Conditions	Outcome	*ee*
1	10mol% **(*R*)-142a**	DCM dry [a]	r.t., 6 days	trace of product	> 99%
2	10mol% **(*R*)-142a**	DMF dry	50 °C, 6 days	25% (HPLC)	> 99%
3	10mol% **(*R*)-142a** + TMSCl (> 2-4 eq.) [b]	DMF dry	MW 50 °C, 25 min.	75% (isolated yield)	racemic
4	10mol% **(*R*)-142a** + H_2SO_4 (0.1 eq.)	DMF dry	50 °C, 6 days	50% (HPLC)	racemic
5	10mol% **(*R*)-189** + H_2SO_4 (0.1 eq.)	DMF dry	50 °C, 6 days	37% (HPLC)	racemic

Table 14- a) aldehyde was slightly soluble in DCM; b) TMSCl was added after an initial stirring of the other components.

As we can notice from the Table 14, excellent enantiomeric excess was obtained but with very low conversion (entries 1-2). In particular, DMF proved to be better than DCM as more homogeneous mixture was observed. In entry 3, different amounts of TMSCl were added in combination with the chiral catalyst, however the resulting product was racemic in all cases. In the latest tests (entries 4-5, Table 14), H_2SO_4 was added as a co-catalyst with both **(*R*)-142a** and diol **(*R*)-189** to give an additional acidity and promote a synergistic effect. However, even in these cases the presence of racemic product indicates that the superior activity of H_2SO_4 overcame the effect of the chiral acid catalyst, leading to the racemic mixture.

Beside the excellent results in terms of enantioselectivity, the desired product was obtained in very low yield. Therefore, we considered the possibility of preforming a complex between the chiral catalyst **(*R*)-142a** and TMSCl:

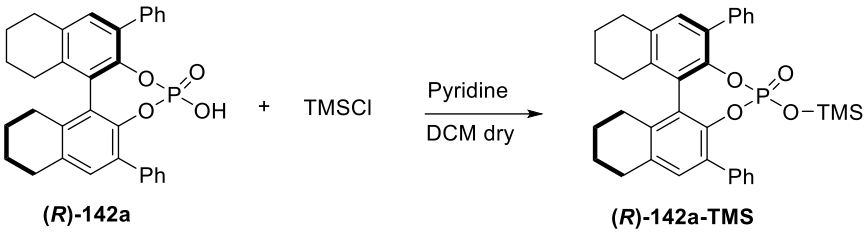

Scheme 62

This kind of complex is described in literature and applied to other types of reactions. [361] The presence of pyridine is mandatory to quench the HCl which can interfere with the activity of chiral catalyst. Indeed, experiments performed with complex **(*R*)-142a-TMS** or by simply adding TMSCl to the reaction mixture gave different results (Table 15).

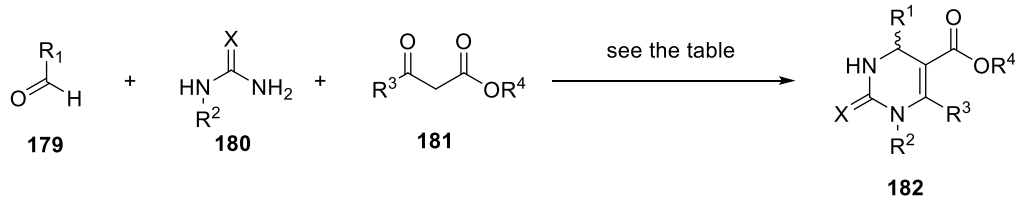

Entry	Catalyst	Solvent	Conditions	Outcome	*ee*
1	10mol% **(*R*)-142a-TMS**	DMF dry	50 °C, 6 days	20% (HPLC)	> 99%
2	10mol% **(*R*)-142a** + 0.1 eq TMSCl	DMF dry	50 °C, 6 days	50% (isolated yield)	racemic

Table 15

Although an excellent *ee* was observed (entry 1, Table 15), the conversion was still unsatisfactory. An interesting result was obtained using toluene as a solvent (Scheme 63). This protocol gave the product with 42% of yield but the *ee* was lower than the previous tests. In addition, a side-product was identified and characterized by ^{1}H NMR and MS analysis turned out to be an intermediate that did not undergo a cyclization. A similar result was obtained also by increasing the amount of catalyst from 10mol% to 20mol%.

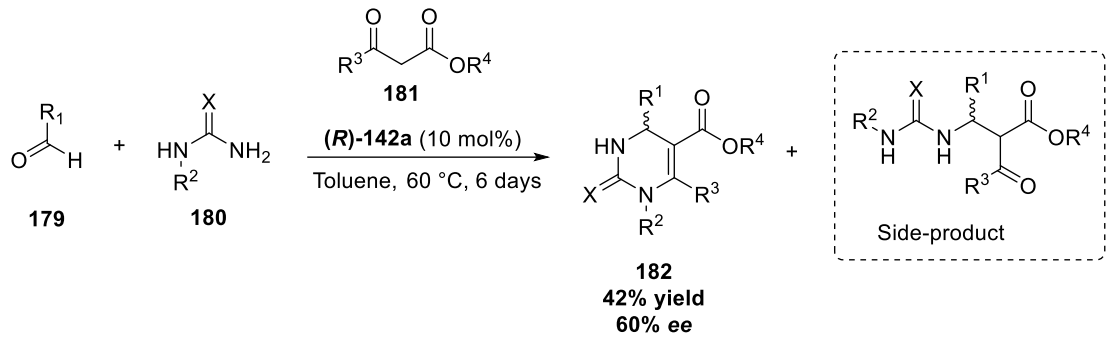

Scheme 63

All the experiments showed above were performed using the (*R*)-catalyst; to ensure we got the right enantiomer, we compared our products with the optically pure **182** provided by our industrial partner.

2.1.2.1 Some considerations on the asymmetric Biginelli reaction

The Brønsted acid **(*R*)-142a** seems to be ineffective in catalyzing the Biginelli reaction with *N*-substitued (thio)urea due to the lower acidity of this catalyst if compared to TMSCl. Indeed, TMSCl releases HCl after the activation of β-ketoester **181** (example A, Scheme 64), which competes with the chiral catalyst.

Another aspect to be considered is that TMSCl can promote the cyclization of intermediate **V** but also other steps as reported in literature (example B, Scheme 64). [362] This additional difference has a great impact on the yield; as shown in Scheme 63 (experiment in toluene) the side-product corresponding to the intermediate **V** (example B, Scheme 64) was detected, confirming that the chiral catalyst is less effective than TMSCl in the cyclization step.

The pre-complex **(*R*)-142a-TMS** could promote the activation of the aldehyde through an *O*-silylation and act as counteranion (example C, Scheme 64). This behaviour is described by List in his paper on asymmetric catalysis on disulfonimide motifs. [363] However, in our case the conversion remained low (entry 1, Table 15) and comparable to the activity of catalyst alone.

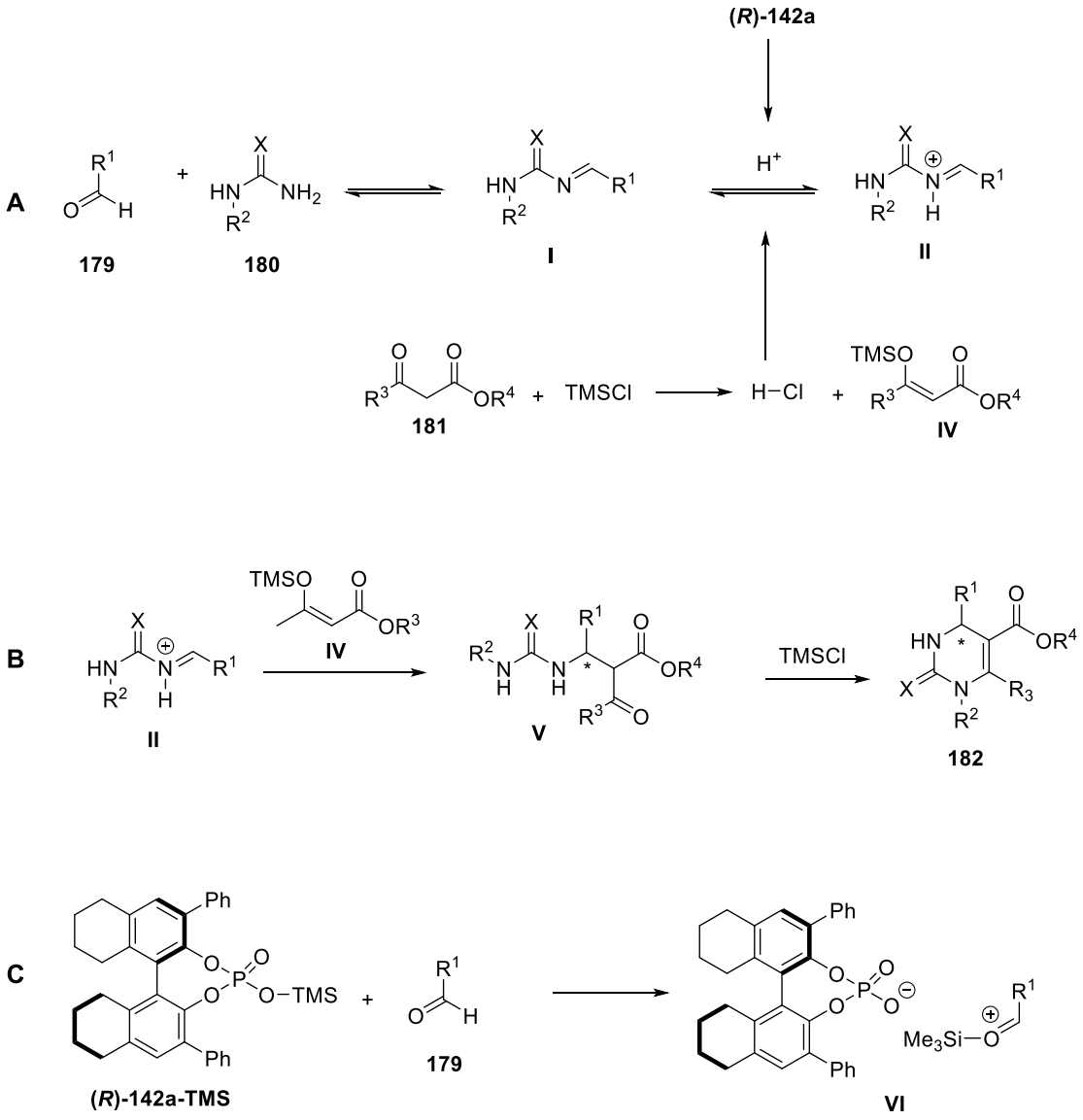

Scheme 64

2.1.3 Alternative synthetic pathways

From the various tests carried out starting from the *N*-substitued (thio)ureas, we realized that, beside the excellent *ee*, the low yields demonstrated that are no advantages using the synthesis described above. Therefore, we needed alternative strategies to overcome these difficulties. As a general idea, we started from the enantioselective Biginelli reaction using unsubstitued (thio)urea **60a,b**, and then we explored different synthetic routes to achieve intermediate **184** (Scheme 65).

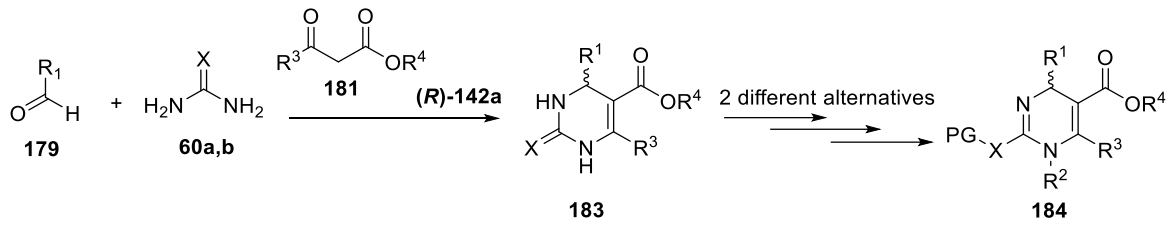

Scheme 65

2.1.3.1 First alternative synthetic route

The first synthetic route is shown in the Scheme 66. The starting point was the enantioselective Biginelli reaction using (thio)urea **60a,b** to obtain **183**. Then, a selective protection of N3 allowed the introduction of a substituent on the N1 of the DHPM scaffold. Deprotection of -Boc group using trifluoroacetic acid (TFA) gave the product **182** which is useful in the synthesis of this kind of biologically active molecules.

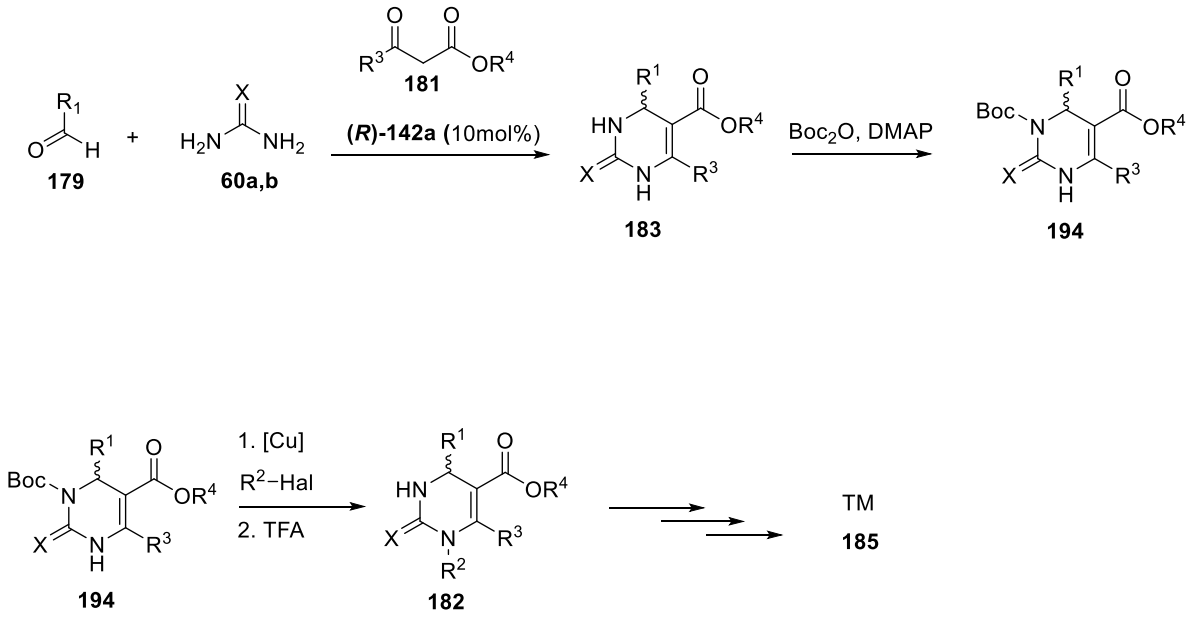

Scheme 66

For the asymmetric Biginelli reaction we explored several conditions, mainly changing the solvent and the temperature. First, we used DCM as a solvent (entries 1-2, Table 16), obtaining better results than tests with *N*-substitued (thio)ureas. The desired product was recovered in moderate yield and good enantiomeric excess. Interestingly, 5 equivalents of β-

ketoester **181** (instead of 3 eq.) slightly improved the yield without affecting the enantioselectivity of the process.

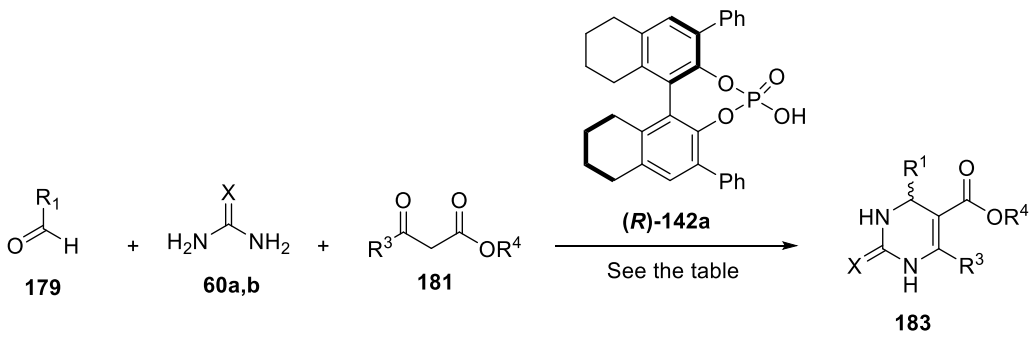

Entry	Catalyst	Solvent	Conditions	Yield	*ee*
1	10mol% **(*R*)-142a**	DCM dry	r.t., 6 days	42%	84%
2	10mol% **(*R*)-142a** + 5 eq. of **181**	DCM dry	r.t., 6 days	54%	84%
3	10mol% **(*R*)-142a**	Toluene dry	50 °C, 36 h	80%	90%

Table 16

The best result was obtained with toluene as a solvent and by heating the reaction to 50°C (entry 3, Table 16). Alongside the good results in both yield and enantioselectivity, the reaction time was decreased from 6 days to 36h.

In the subsequent step, compound **183** was treated with Boc_2O. Based on literature data, [364] the protection of N3 should be selective, thus affording only one isomer. As expected, in our case the product was obtained in good yield (Table 17), but some starting material was found along with the presence of the undesired isomer.

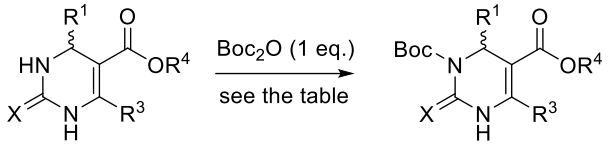

183 194

Entry	Base	Solvent	Conditions	Yield
1	NaH (60%), 1 eq.	DMF dry	r.t., 6 h	35%
2	DMAP (cat.)	ACN dry	r.t., 4.5 h	55%
3	DMAP (cat.)	ACN dry	r.t., 6 h	27%
4	DMAP (cat.)	ACN dry	r.t., 2.5 h	56%
5	DMAP (cat.)	ACN dry	r.t., 2 h	49%

Table 17

As shown in Table 5, while the use of NaH gave the product in low yield, a catalytic amount of 4-dimethylaminopyridine (DMAP) appears to be more effective (entries 2-5, Table 17). More interestingly, better results were obtained when the reaction time was between 2.5 and 4.5 hours, after which the formation of several impurities was observed. To confirm that the product **194** was the right isomer, we performed a series of analysis including ^{1}H NMR, ^{13}C NMR, NOESY and HETCOR; anyhow, after the arylation and deprotection steps (Scheme 66), we could compare our product **196** with a standard.

The next step involves the reaction between **194** and the halide **195** (Table 18):

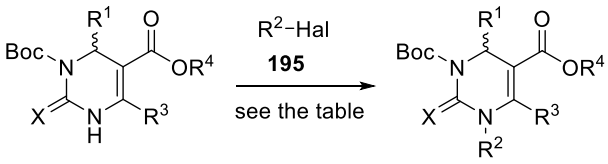

194 196

Entry	Catalyst/Ligand	Base	Solvent	Conditions	Yield
1	CuI (10-30%)	Cs_2CO_3	DMF dry	MW 120 °C, 40 min.	< 10%
2	CuI (10-30%)/1,10-phenantroline	Cs_2CO_3	DMF or DMA dry	70 °C, 16 h	< 10%

Table 18

In the first experiment (test 1, Table 18), we used different amounts of catalyst and the reaction mixture was irradiated with microwaves at 120 °C. In all cases, the desired product was obtained in a very low yield (< 10%) but, surprisingly, we identified compound **197** as the main product (Figure 117).

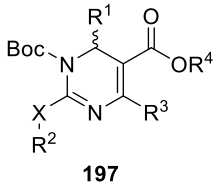

197

Figure 117

The same result was achieved when we added 1,10-phenantroline as the ligand or by replacing DMF with DMA (entry 2, Table 18). This side-product of X-arylation was also recovered in good yield in a Chan-Lam reaction using boronic acid **198**:

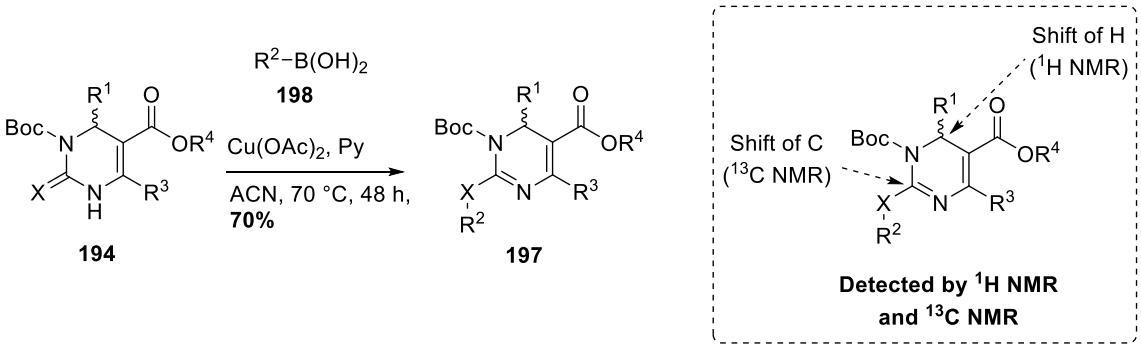

Scheme 67

The structural analysis of **197** was difficult as the ^{1}H NMR spectra was very similar to the desired product. The only shift detected was the proton on C4, which is affected by the presence of two internal double bond in the DHPM core. However, the main clue was the disappearance of C=X signal which is converted to C=N as showed by ^{13}C NMR spectra.
At this point, due to the difficulty in obtaining the right isomer, we needed to change the synthetic route.

2.1.3.3 Second alternative synthetic route

Starting from the chiral Biginelli adduct **183**, an alternative synthetic pathway is shown as follows:

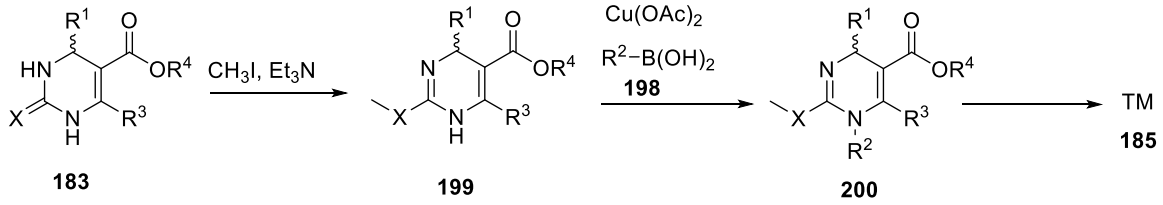

Scheme 68

We were interested in the first steps as the transformation on **200** was previously studied. [365] In the first step, compound **183** was treated with iodomethane in presence of Et_3N to obtain **199** in good yield (Scheme 69).

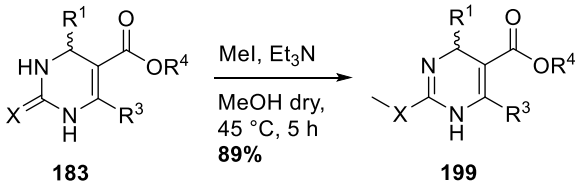

Scheme 69

Compound **199** has two different tautomers; indeed, tautomeric equilibrium has a great impact on which reaction product is the favoured one in the Chan-Lam reaction (Scheme 70).

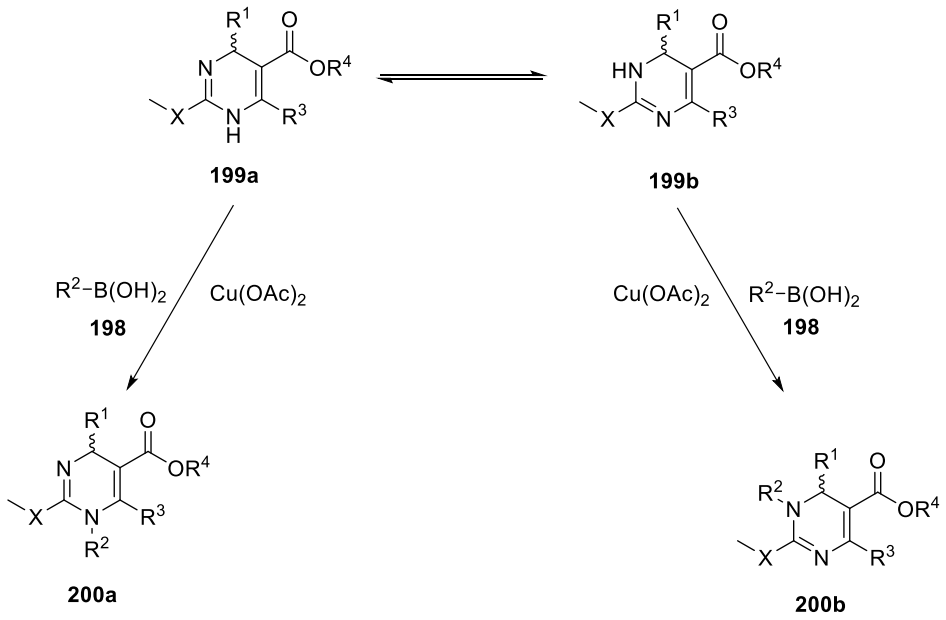

Scheme 70

From the literature data, at room temperature the major tautomer seems to be compound **199a**; however, with high temperatures or concentration, **199a** can be gradually converted into isomer **199b**. [364]

In our case, we needed a reference compound to see which isomer was formed from the Chan-Lam reaction. Therefore, we functionalized compound **199a** and performed the arylation on our substrate (Scheme 71).

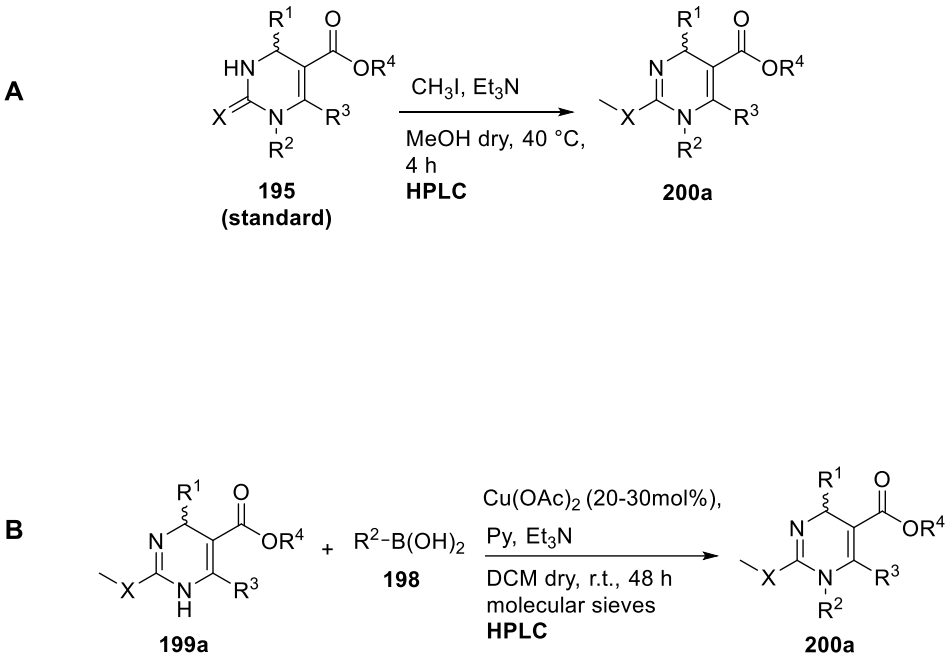

Scheme 71- A) synthesis of 200a to have a reference product; B) Chan-Lam reaction on our substrate. Each reaction was monitored by HPLC-MS.

From HPLC data, we confirmed that the obtained product corresponds to the right isomer (Figure 118); however, the reaction required a large amount of copper (between 20 and 30 mol%) and long reaction times.

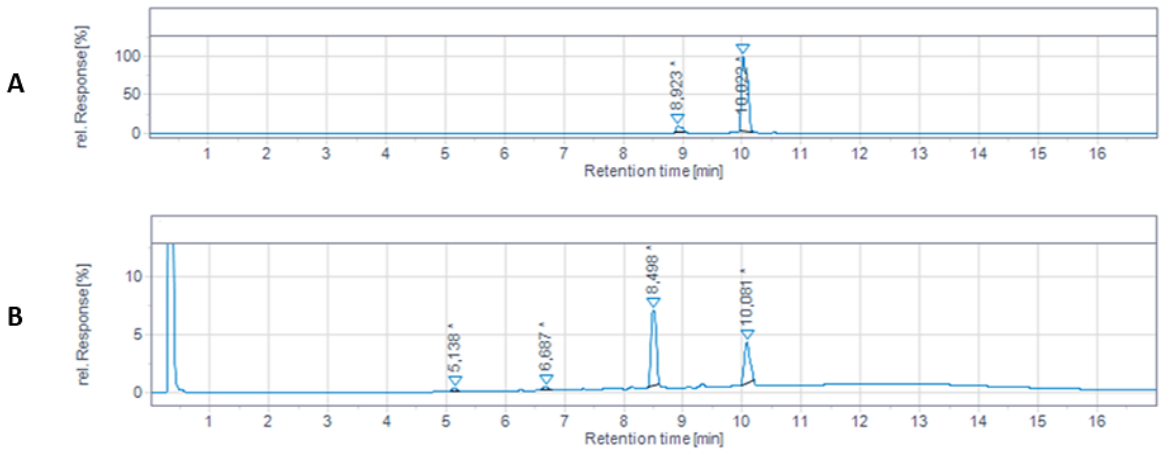

Figure 118- A) HPLC of reference product 200a: rt= 10.022; B) Crude of Chan-Lam reaction after 48 h: starting material 199a (rt= 5.138) and product 200a (rt= 10.081).

Moreover, a side product (rt: 8.498, Figure 118) which was difficult to purify by chromatography was found. Based on MS analysis, this by-product could result from an overoxidation of starting material **199a** catalyzed by copper:

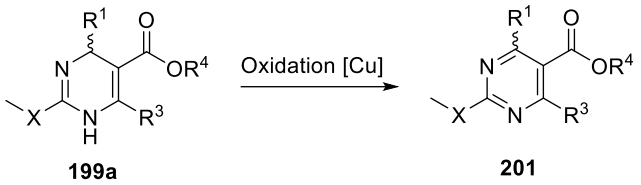

Scheme 72

Even if this synthetic pathway gave some interesting results, the presence of side products difficult to remove, the variable yields observed and the harsh and controlled conditions needed (strictly dry conditions, high reaction temperatures and catalyst loading along with long reaction times) limit the possibility to use this route for the synthesis of the desired intermediate.

2.2 Functionalization of Heteroaryl scaffolds

As introduced in the aim of this work, a key step for the synthesis of biologically active compounds is the coupling between **186a-c** and **187** to obtain product **188**:

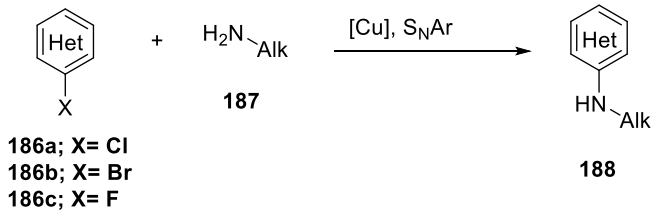

Scheme 73

First, we decided to explore the S_NAr to avoid the use of metal catalysts and then Ullmann protocol was applied to check if there was any difference in both yield and by-products formation.

2.2.1 S_NAr

To get some information on the reaction conditions, we decided to perform a first experiment starting from **186a**, which is a cheap material readily available on the market, and a generic amine as a model compound:

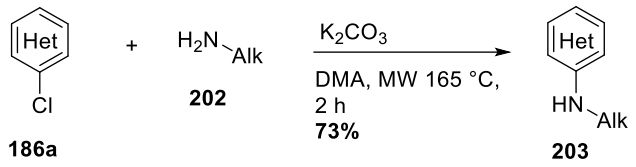

Scheme 74

The desired product was obtained in good yield despite the harsh conditions required. By replacing the microwaves with conventional heating (oil bath) and prolonging the reaction time to 24 h, the result was almost the same. Subsequently, we applied the same conditions to the alkyl amine **187** which has a sensitive group in both strongly acidic and basic environments (entry 1, Table 19).

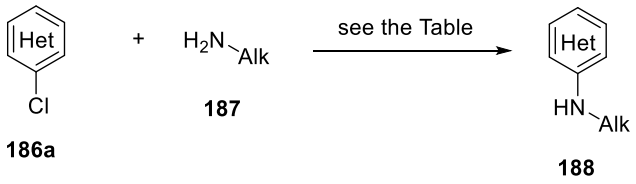

Entry	Base	Solvent	Conditions	Yield
1	K_2CO_3	DMA dry	MW 165 °C, 2 h	20%
2	K_2CO_3	DMA dry	reflux, 24 h	< 15%
3	DIPEA	2-PrOH	Reflux, 24 h	Product in traces

4	DIPEA	Isopropyl acetate	Reflux, 24 h	Product in traces and side products

Table 19

Product **188** was obtained in a very low yield and a lot of starting material remained unreacted. The use of organic base such as DIPEA, did not increase the yield but led to several side products (entries 3-4, Table 19). As the alkyl moiety on the amine seems to have a negative effect on the S_NAr reaction, we decided to increase the reactivity of the halo-heteroaryl partner by replacing the chlorine atom on **186a** with a fluorine. Indeed, fluorine promotes the addition step of amine **187** (which is the rate-determining step) and stabilizes the Mesenheimer complex through its inductive effect:

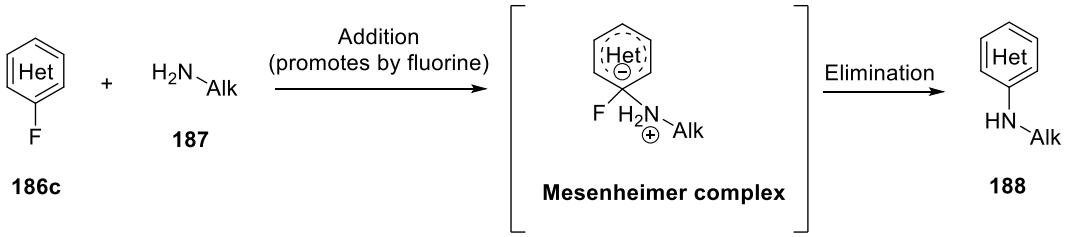

Scheme 75

A first attempt was made by treating **186a** with CsF and alkyl amine **187**, but with poor results (Scheme 76). In this case, the idea was to synthesize the fluoro-derivative *in situ*, which can undergo to S_NAr and give the desired product.

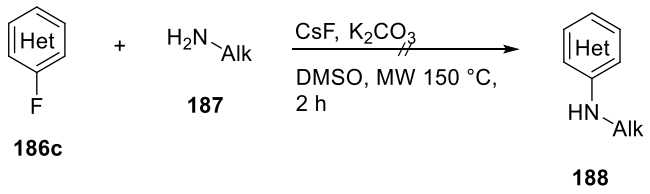

Scheme 76

Therefore, we decided to follow the conversion of **186a** into **186c** by HPLC and then added the alkyl amine **187** without isolating the fluorinated intermediate:

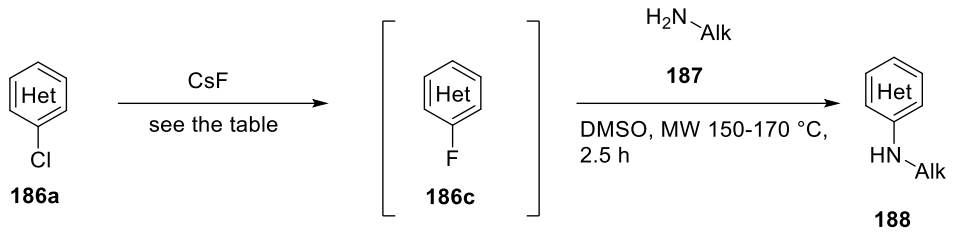

Entry	Base/catalyst	Solvent	Conditions	Yield (188)
1	-	DMSO	MW 100 °C, 1 h	27%
2	$Bu_4N^+Cl^-$	DMSO	MW 150 °C, 2 h	37%

Table 20

In both cases, we isolated the final product in moderate yield (entries 1-2, Table 20). Interestingly, during the first step, we observed the formation of a side product **186f** (rt= 20.2, Figure 119), which could result from the degradation of fluoro-derivative **186c**:

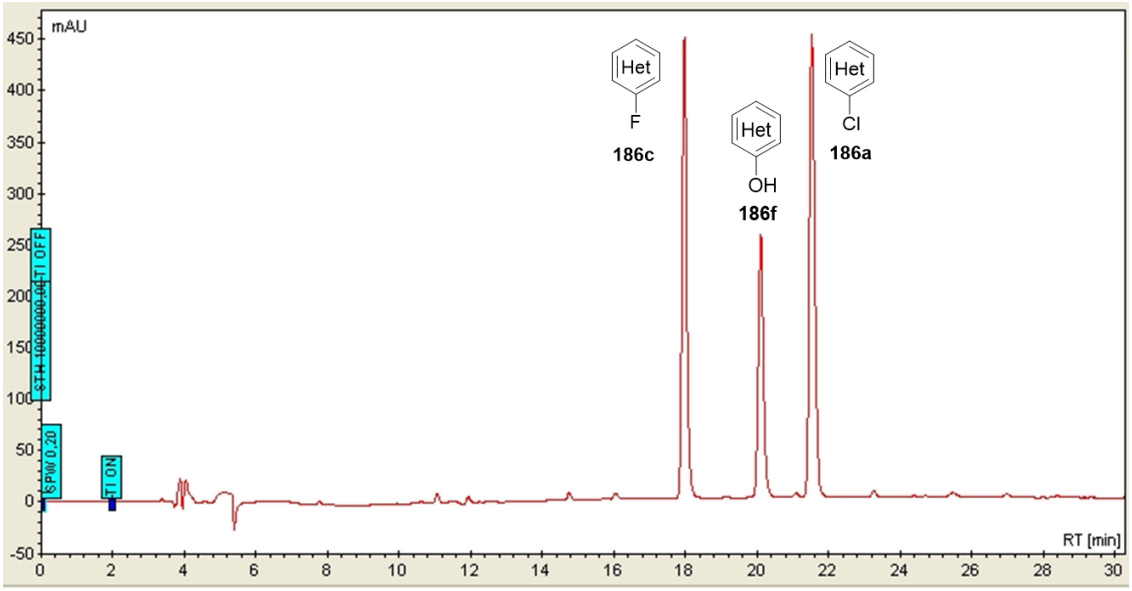

Figure 119- HPLC analysis of reaction mixture during fluorination step. Starting material 186a: rt= 21.7; product 186c: rt= 18; impurity 186f: rt= 20.1.

If on the one hand the phase-transfer catalyst $Bu_4N^+Cl^-$ promotes chlorine-fluorine exchange, on the other, being very hygroscopic, it brings water into the reaction thus favouring the product **186f**. When DMSO was replaced by DMF or DMA, similar results were observed. Because of the difficulty in obtaining the product **188** through S_NAr, we decided to explore the Ullmann-type or Buchwald cross-coupling reactions.

2.2.2 Ullmann-type reactions

Similarly to S_NAr, we obtained good results with Ullmann-type cross-coupling applied to the model system with alkyl amine **202**:

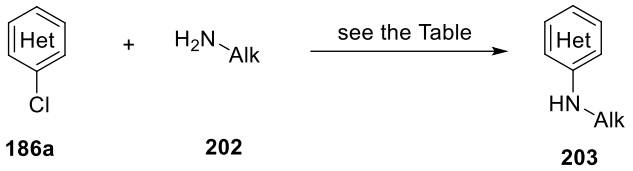

186a **202** **203**

Entry	Catalyst	Ligand	Base	Solvent	Conditions	Yield
1	CuI (10 mol%)	1,10-phenantroline	K_2CO_3	DMF dry	MW 160-180 °C, 1.5 h	58%
2	CuI (10 mol%)	1,10-phenantroline	K_2CO_3	DMA dry	MW 170-180 °C, 90 min	67%
3	CuI (10 mol%)	1,10-phenantroline	K_2CO_3	NMP	MW 170-180 °C, 90 min	63%
4	CuI (10 mol%)	-	K_2CO_3	DMA dry	MW 170-180 °C, 2.5 h	88%
5	CuI (10 mol%)	-	K_2CO_3	DMA dry	Reflux, 24 h	85%
6	CuI (10 mol%)	-	K_2CO_3	TPGS 2%/H_2O	MW 100 °C, 2.5 h	41%

Table 21

Entries 1-3 (Table 21) differ from each other only for the solvent; the lower yield observed with DMF was due to the side product **204** showed in Figure 120. The high temperature required for this cross-coupling, promotes the decarbonylation of DMF to give dimethylamine which can compete with the alkyl amine during the reaction.

An interesting result was obtained in entry 4 (Table 21), when the reaction was carried out without ligand; in this case the yield was increased from 67% to 88%. A similar result was obtained by replacing microwaves with conventional heating (entry 5, Table 21). To explore a greener protocol, we tried the Ullmann coupling in micellar conditions but with poor results (entry 6, Table 21). Indeed, side product **205** (Figure 120), which results from the oxidation of alkyl amine, was detected by GC-MS:

204 **205**

Figure 120- Side products observed during the Ullmann-type reaction.

Once the right conditions were found, we performed the reaction on our substrate with alkyl amine **187** (entry 1, Table 22):

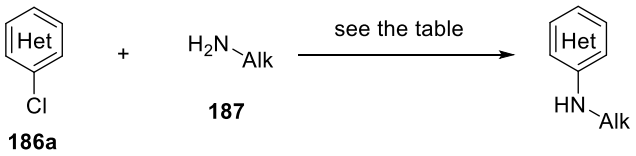

186a **187** **188**

Entry	Catalyst	Ligand	Base	Solvent	Conditions	Yield
1	CuI (10-20 mol%)	-	K_2CO_3	DMA dry	MW 170-180 °C, 2.5 h	16%
2	CuI (10-20 mol%)	-	Cs_2CO_3	DMA dry	MW 170-180 °C, 2.5 h	15%
3	CuI (20 mol%)	1,10-phenantroline	K_2CO_3	DMA dry	MW 170-180 °C, 2.5 h	Product in traces
4	CuI (10 mol%)	Ethylene glycol	K_2CO_3	2-PrOH	MW 100-150 °C, 2 h	-

5	CuI (10 mol%)	1,10-phenantroline	LiHMDS	DMA dry	MW 100-150 °C, 2.5 h	-
6	CuI (10 mol%)	DMCyDA*	K_2CO_3	DMA dry	MW 150 °C, 2 h	-

Table 22- *trans-*N,N*'-dimethylcyclohexane-1,2-diamine.

However, the low yield forced us to carry out a series of experiments (entries 2-6, Table 22) in which ligand, base and solvent were changed. In all cases, results were very poor and a lot of unreacted starting material along with degradation of alkyl amine **187** were observed. The amount of copper seems to have no influence on the outcome of the reaction as the increase from 10 to 20mol% gave the same results (entries 1-3, Table 22).
To raise the reactivity of the electrophile, bromo-heteroaryl derivative **186b** was chosen as starting material even if unsatisfactory results were obtained:

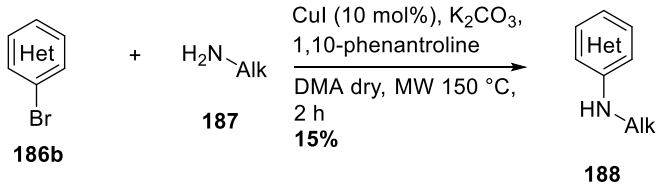

Scheme 77

In most of the reported examples, a degradation of product **187** (detected by TLC analysis) occurred perhaps due to the high temperatures applied (>150 °C). For this reason, a further optimization of this process is required to improve the yield of the reaction.

Chapter 3- Conclusions

3.1 Enantioselective synthesis of Biginelli adducts

In this part of the project, we achieve the synthesis of chiral catalyst **(*R*)-142a** and applied it to asymmetric Biginelli reaction using substrates to produce biologically active compounds of potential pharmacological interest. Regarding the Biginelli reaction exploiting *N*-

substitued (thio)ureas, we demonstrated that it is possible to obtain the desired product with excellent enantiomeric excess but only in a low yield:

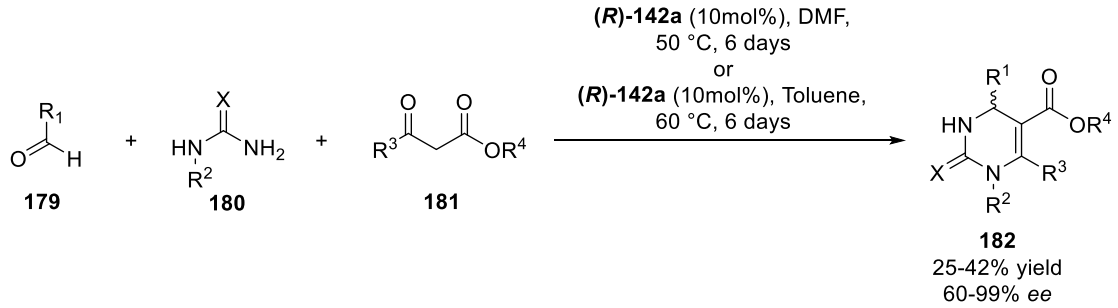

Scheme 78

We also carried out the enantioselective Biginelli reaction with urea/thiourea and then functionalized the resulting product through different synthetic routes (Scheme 79). In this case, harsh conditions and the formation of side products are the main issue of the synthesis.

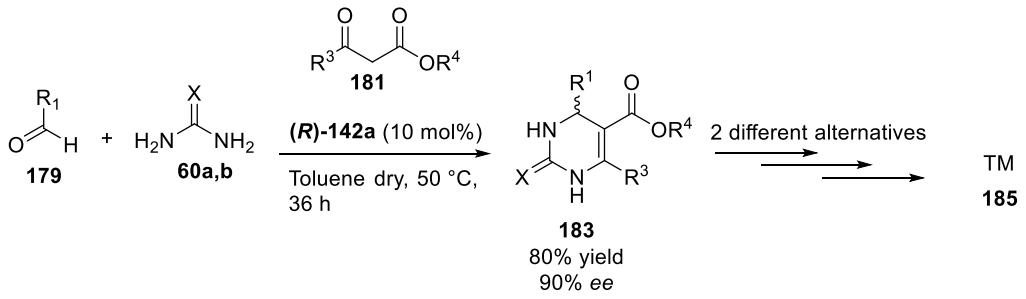

Scheme 79

3.2 Functionalization of Heteroaryl scaffolds

For the functionalization of pyridine with the alkyl amine of interest, we proposed two approaches: S_NAr and Ullmann-type cross-coupling reaction. Regarding the S_NAr, even if with the model system we obtained good results, with our substrates the yields were very low. Heteroaryl derivative **186c**, shows a higher reactivity but is difficult to synthesize:

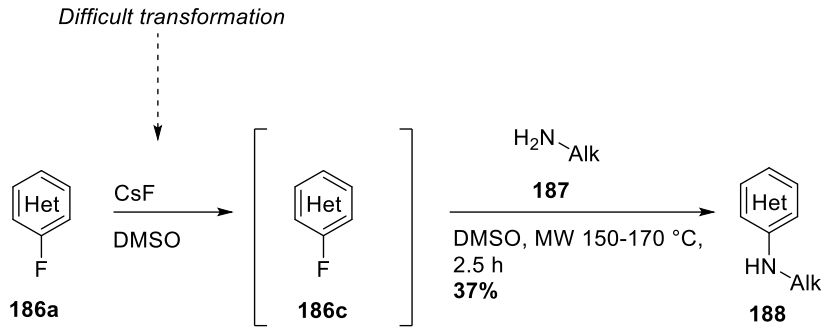

Scheme 80

The Ullmann-type protocol gave similar results with both chloro- and bromo-heteroaryl derivatives; by using CuI (10 mol%) as a catalyst and carrying out the reaction under microwave irradiation, the yield was about 16%.

Chapter 4- Experimental part

4.1 General experimental procedures, materials and instruments

All reagents were used as purchased from commercial suppliers without further purification. The reactions were carried out in oven dried vessels. Solvents were dried and purified by conventional methods prior use or, if available, purchased in anhydrous form.

Flash column chromatography was performed with Merck silica gel Å 60, 0.040-0.063 mm (230-400 mesh).

MPLC Isolera Prime Biotage on highly resistant PP cartridges Normal Phase silica gel NP 40 – 63 μm particle size and 60 A pore size (Si60) withstand a maximum pressure of 10 bar (145 psi) column with petroleum ether (eluent A) and Ethyl Acetate (Eluent B) as mobile phase.

Merck aluminum backed plates pre-coated with silica gel 60 (UV254) were used for analytical thin layer chromatography and were visualized by staining with a KMnO4 or Ninidrine solution.

NMR spectra were recorded at 25 °C or at 37 °C with 400 or 600 MHz for 1H and 101 or 151 MHz for 13C Bruker Advance NMR spectrometers. The solvent is specified for each spectrum. Splitting patterns are designated as s, singlet; d, doublet; t, triplet; q, quartet; m, multiplet; bs, broad singlet. Chemical shifts (d) are given in ppm relative to the resonance of their respective residual solvent peaks.

High and low resolution mass spectroscopy analyses were recorded by electrospray ionization with a mass spectrometer Q-exactive Plus.

HPLC analysis were performed on two instruments:

1. LC/MSD system InfinityLab LC/MSD iQ. Column: InfinityLab PoroShell 120 EC-C18 2.1 x 50 mm x 2.7µm. Flow: 0.4 mL/min. Eluent A/B: H_2O/MeCN. Gradient: 5% B to 95% B in 10 minutes, 4 minutes at 95 % B and 3 minutes of re-equilibration. Detection: 254 nm and 210 nm.
2. JASCO LC-Net II/ ADC connected with UV detector (254 nm) using an Intersil ODS-3V C18 column (5 µm, 4.6 x 250mm). Flow 0.8 mL/min. Eluent A/B: H_2O/MeCN. Gradient: 20% B to 80% B in 45 minutes, 15 minutes at 95 % B

Chiral HPLC analysis were performed using Chiralpak AD-H column (5µm 250 x 4.6mm). Flow: 1 mL/min. Eluent A/B: n-Hexane/2-PrOH. Gradient: 80% A and 20% B (isocratic) in 30 minutes.

Reactions carried out under MW dielectric heating were performed with CEM Discover (CEM, Corp., *Matthews*, NC) microwave oven equipped with 10 mL vials.

4.2 Synthetic procedures

4.2.1 Enantioselective Biginelli reaction

3,3'-diiodo-5,5',6,6',7,7',8,8'-octahydro-[1,1'-binaphthalene]-2,2'-diol (*R*)-190a

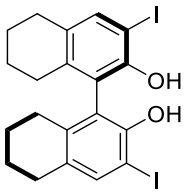

The synthesis of chiral catalyst was adapted from the literature data. [359,360,366]

To a solution of (*R*)-H_8-BINOL (200 mg, 0.68 mmol, 1.0 eq.) in dry DCM (5 mL) were added at room temperature, morpholine (0.38 mL, 4.42 mmol, 6.5 eq.) and I_2 (345 mg, 1.36 mmol, 2.0 eq.). The mixture was stirred at r.t. for 16 h and turned progressively red. Then DCM (10 mL) and HCl (1 N, 5 mL) was added, and the phases were separated. The aqueous layer was extracted with DCM (5 mL) and the combined organic layers were washed successively with a saturated sodium thiosulfate solution (3 × 5 mL) and Brine (5 mL), then

dried over Na_2SO_4, filtered and concentrated. The product was purified by chromatography on silica gel with MPLC Isolera Prime Biotage 0-10 % gradient of EtOAc in petroleum ether (PE) to obtain the product as a white solid (304 mg, 0.56 mmol, 82%).

^{1}H NMR (400 MHz, $CDCl_3$, δ ppm, J Hz): δ 7.48 (s, 2H), δ 4.94 (s, 2H), δ 2.70 (t, *J* = 5.6 Hz, 4H), δ 2,25 (m, 2H), δ 2.10 (m, 2H), δ 1.61-1.70 (m, 8H)

ESI: m/z 546 $[M+H]^+$; 545 $[M-H]^-$.

3,3'-diphenyl-5,5',6,6',7,7',8,8'-octahydro-[1,1'-binaphthalene]-2,2'-diol (*R*)-191

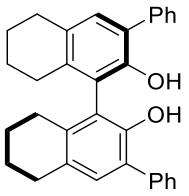

To a solution of **(*R*)-190a** (193 mg, 0.35 mmol, 1.0 eq.) in dry DME (1.5 mL) were added at r.t., phenylboronic acid (110 mg, 0.90 mmol, 2.6 eq.), $Pd(PPh_3)_4$ (20 mg, 0.017 mmol, 0.05 eq) and a solution of Na_2CO_3 (197 mg, 1.86 mmol, 5.3 eq) in H_2O (0.8 mL). The mixture was degassed under N_2 for 10 minutes and heated to reflux for 16 h. Then, HCl (1N, 10 mL) was added and the aqueous phase was extracted with DCM (3 x 10 mL). The combined organic layers were washed with Brine (5 mL) and dried over Na_2SO_4, filtered and concentrated. The product was purified by chromatography on silica gel with MPLC Isolera Prime Biotage 0-15 % gradient of EtOAc in PE to obtain the product as a white solid (99 mg, 0.22 mmol, 63%).

^{1}H NMR (400 MHz, DMSO-d_6, δ ppm, J Hz): δ 7.48 (t, *J* = 8.1 Hz, 3H), 7.34 (t, *J* = 7.7 Hz, 4H), 7.28 – 7.21 (m, 3H), 6.90 (d, *J* = 4.4 Hz, 2H), 2.68 (d, *J* = 6.3 Hz, 3H), 2.61 (m, 1H), 2.33 – 2.06 (m, 2H), 2.03 – 1.84 (m, 2H), 1.60 (m, 8H).

ESI: m/z 447 $[M+H]^+$; 445 $[M-H]^-$.

4-hydroxy-2,6-diphenyl-8,9,10,11,12,13,14,15-octahydrodinaphtho[2,1-d:1',2'-f][1,3,2]dioxaphosphepine 4-oxide (*R*)-142a

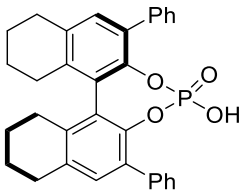

To a solution of **(*R*)-191** (50 mg, 0.112 mmol, 1.0 eq.) in dry Pyridine (0.3 mL) was added $POCl_3$ (21 µL, 0.22 mmol, 2.0 eq.) at 0 °C. Then the mixture was heated to 75 °C for 3.5 h. Water (3 mL) was slowly added at r.t. and the mixture was stirred for 2 h. DCM (15 mL) and HCl (1N, 10 mL) were added, the organic phase was separated and washed with Brine (5 mL), dried over Na_2SO_4, filtered and concentrated. The product was obtained as a white solid (54 mg, 0.106 mmol, 95%) and used without further purification.
Spectral data coherent with the literature. [366]
ESI: m/z 507 $[M-H]^-$.

General procedures for racemic and asymmetric Biginelli reaction

Compound *rac*-182

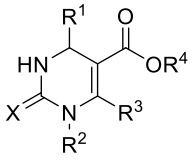

A generic aldehyde (0.2 mmol, 1 eq.), *N*-substitued (thio)ureas (0.2 mmol, 1 eq.) and β-ketoester (0.22 mmol, 1.1 eq.) were solubilized in dry DMF (0.5 mL) in a 10 mL vial and TMSCl (0.84 mmol, 4.2 eq.) was added at r.t. Then the mixture was irradiated at 50 °C for 15 minutes. EtOAc (10 mL) and H_2O (5 mL) were added, the phases were separated and the organic layer washed with H_2O (5 mL) and Brine (5 mL), dried over Na_2SO_4, filtered and concentrated. The resulting product was purified through chromatography on silica gel with MPLC Isolera Prime Biotage, with a gradient of EtOAc in PE.

Optically pure 182

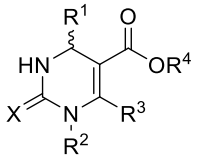

Method A: A generic aldehyde (0.2 mmol, 1 eq.), *N*-substitued (thio)ureas (0.24 mmol, 1.2 eq.) and chiral catalyst **(*R*)-142a** (0.02 mmol, 0.1 eq.) were suspended in dry DMF (0.5 mL) and stirred at r.t. for 2 h. Then β-ketoester (0.6 mmol, 3 eq.) was added and the mixture heated to 50 °C for 6 days. EtOAc (10 mL) and H_2O (5 mL) were added, the phases were separated and the organic layer washed with H_2O (5 mL) and Brine (5 mL), dried over Na_2SO_4, filtered and concentrated. The resulting product was purified through chromatography on silica gel with MPLC Isolera Prime Biotage, with a gradient of EtOAc in PE.

Method B: A generic aldehyde (0.2 mmol, 1 eq.), *N*-substitued (thio)ureas (0.24 mmol, 1.2 eq.) and chiral catalyst **(*R*)-142a** (0.02 mmol, 0.1 eq.) were suspended in dry Toluene (0.5 mL) and stirred at r.t. for 3.5 h. Then β-ketoester (0.6 mmol, 3 eq.) was added and the mixture heated to 60 °C for 6 days. Toluene was evaporated under reduced pressure and EtOAc (10 mL) and H_2O (5 mL) were added. The phases were separated, and the organic layer washed with H_2O (5 mL) and Brine (5 mL), dried over Na_2SO_4, filtered and concentrated. The resulting product was purified through chromatography on silica gel with MPLC Isolera Prime Biotage, with a gradient of EtOAc in PE.

Optically pure 183

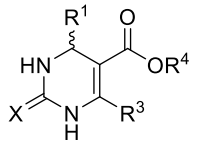

A generic aldehyde (0.2 mmol, 1 eq.), (thio)urea (0.24 mmol, 1.2 eq.) and chiral catalyst **(*R*)-142a** (0.02 mmol, 0.1 eq.) were suspended in dry Toluene (0.5 mL) and stirred at r.t. for 3 h. Then β-ketoester (0.6 mmol, 3 eq.) was added, and the mixture heated to 50 °C for 36 h. Toluene was evaporated under reduced pressure and EtOAc (10 mL) and H_2O (5 mL) were added. The phases were separated, and the organic layer washed with H_2O (5 mL) and

Brine (5 mL), dried over Na_2SO_4, filtered and concentrated. The resulting product was purified through chromatography on silica gel with MPLC Isolera Prime Biotage, with a gradient of EtOAc in PE.

General procedures for functionalization of DHPM scaffolds

Compound 194

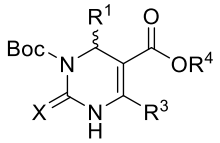

To a solution of **183** (0.5 mmol, 1 eq.) in dry ACN (5 mL) was added at r.t. and dropwise a solution of Boc_2O (0.75 mmol, 1.5 eq.) in dry ACN (2 mL). After 2.5 h, the solution turned orange and the solvent was removed under reduced pressure. Then, EtOAc (10 mL) and H_2O (5 mL) were added, and the phases were separated. The organic layer washed with H_2O (5 mL) and Brine (5 mL), dried over Na_2SO_4, filtered and concentrated. The resulting product was purified through chromatography on silica gel with MPLC Isolera Prime Biotage, with a gradient of EtOAc in PE.

Compound 197

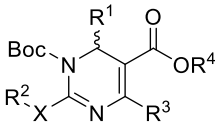

To a suspension of **194** (0.2 mmol, 1 eq.), phenylboronic acid **198** (0.24 mmol, 1.2 eq.), $Cu(OAc)_2 \cdot H_2O$ (0.04 mmol, 0.2 eq.) in ACN (2 mL) was added at r.t. Pyridine (0.4 mmol, 2 eq) and the mixture was heated to 70 °C for 48 h. Then the solvent was removed under reduced pressure, EtOAc (15 mL) and H_2O (7 mL) were added, and the phases were separated. The organic layer washed with H_2O (7 mL) and Brine (5 mL), dried over Na_2SO_4,

filtered and concentrated. The resulting product was purified through chromatography on silica gel with MPLC Isolera Prime Biotage, with a gradient of EtOAc in PE.

Compound 199

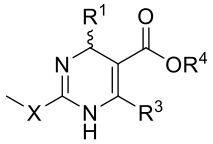

Compound **199** was prepared in according to the literature data. [364]
To a solution of **183** (0.5 mmol, 1 eq.) and Et_3N (5 mmol, 10 eq.) in dry MeOH (5 mL) was added at 0 °C CH_3I (5 mmol, 10 eq.). The mixture was heated to 45 °C and stirred for 5 h. Then the solvent was removed under reduced pressure, EtOAc (20 mL) and H_2O (10 mL) were added, and the phases were separated. The organic layer washed with H_2O (10 mL) and Brine (10 mL), dried over Na_2SO_4, filtered and concentrated. The resulting product was purified through chromatography on silica gel with MPLC Isolera Prime Biotage, with a gradient of EtOAc in PE.

Compound 200a

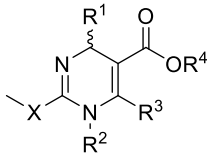

To a suspension of **199** (0.1 mmol, 1 eq.), phenylboronic acid **198** (0.25 mmol, 2.5 eq.), $Cu(OAc)_2$ (0.02 mmol, 0.2 eq.) and molecular sieves (3 Å) in dry DCM (2.5 mL), were added at 0 °C Pyridine (0.2 mmol, 2 eq) and Et_3N (0.2 mmol, 2 eq). The mixture was stirred at r.t. for 48 h and the reaction was followed by HPLC to check the formation of products and identified side products.

4.2.2 Functionalization of heteroaryl scaffolds

General procedures of S_NAr and Ullmann-type reactions

Compound 188

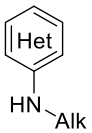

Method A (S_NAr): chloro-heteroaryl derivative **186a** (0.5 mmol, 1 eq.), CsF (2 mmol, 4 eq.) and $Bu_4N^+Cl^-$ (0.25 mmol, 0.5 eq.) were suspended in DMSO (1 mL) in a 10 mL vial and irradiated at 150 °C for 2 h. Then, alkyl amine **187** (0.75 mmol, 1.5 eq.) was added and the mixture irradiated at 150 °C for 2.5 h. EtOAc (10 mL) and H_2O (5 mL) were added, and the phases were separated. The organic layer washed with H_2O (2 x 5 mL) and Brine (5 mL), dried over Na_2SO_4, filtered and concentrated. The resulting product was purified through chromatography on silica gel with MPLC Isolera Prime Biotage, with a gradient of EtOAc in PE.

Method B (Ullmann-type): chloro-heteroaryl derivative **186a** (0.5 mmol, 1 eq.), K_2CO_3 (1 mmol, 2 eq.), CuI (0.05 mmol, 0.1 eq.) and alkyl amine **187** (0.75 mmol, 1.5 eq.) were suspended in dry DMA (1 mL) in a 10 mL vial and degassed under N_2 for 15 minutes. The mixture was irradiated at 150 °C for 2.5 h. Then, EtOAc (10 mL) and H_2O (5 mL) were added, and the phases were separated. The organic layer washed with H_2O (2 x 5 mL) and Brine (5 mL), dried over Na_2SO_4, filtered and concentrated. The resulting product was purified through chromatography on silica gel with MPLC Isolera Prime Biotage, with a gradient of EtOAc in PE.

4.3 Chiral HPLC

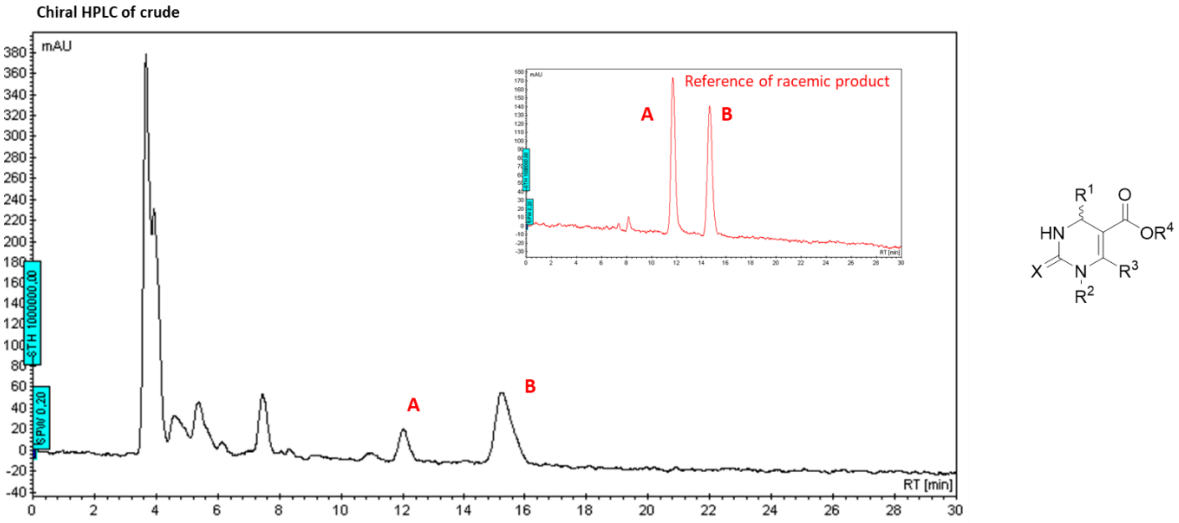

Figure 121- Chiral HPLC of crude of enantioselective Biginelli reaction with *N*-substitued(thio)urea. Enantiomer A (rt= 12): 20%; enantiomer B (rt= 15): 80%.

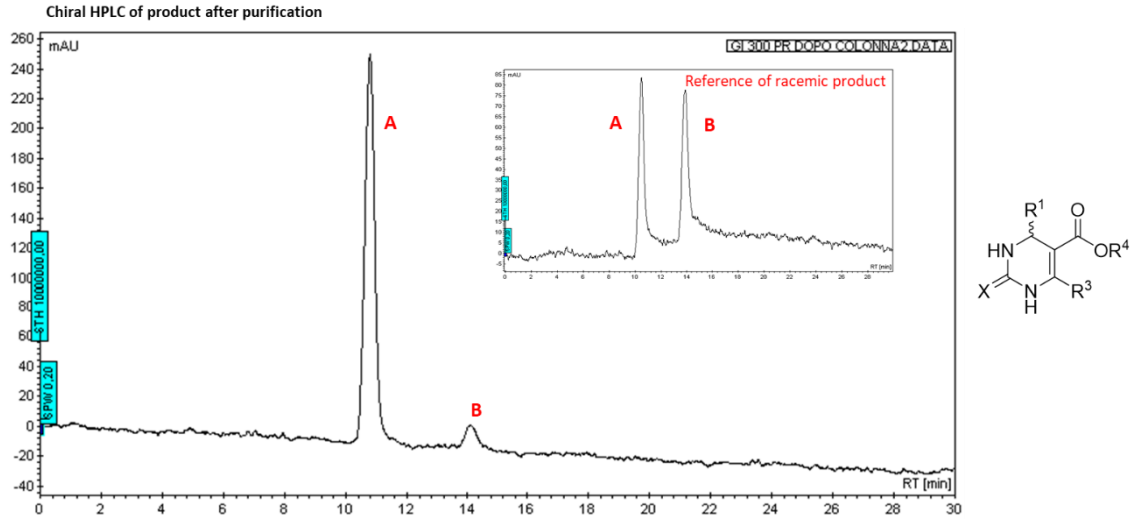

Figure 122- Chiral HPLC of product after purification. Enantiomer A (rt= 10.15): 95%; enantiomer B (rt= 14): 5%.

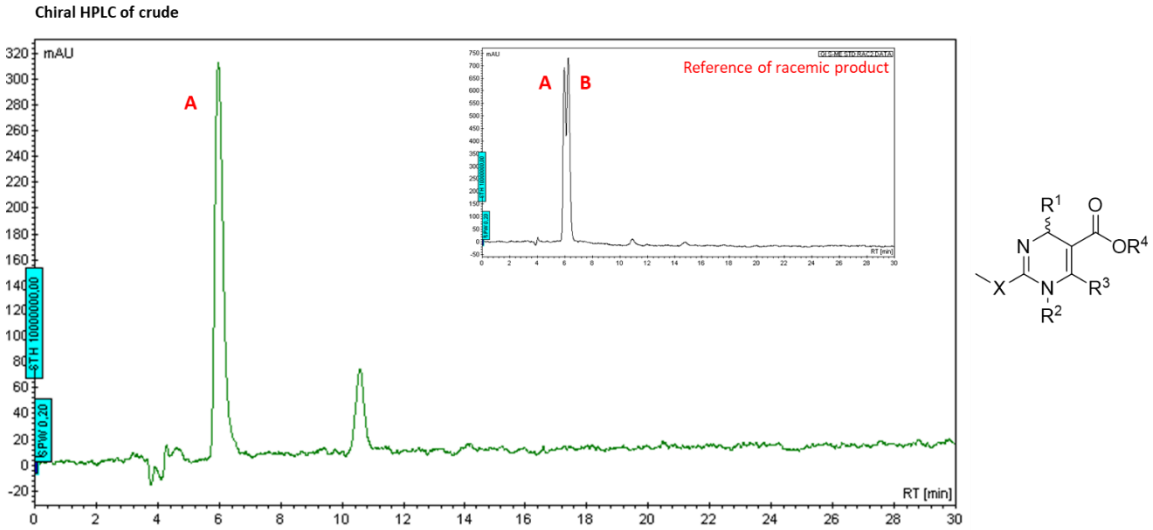

Figure 123- Chiral HPLC of crude. Enantiomer A (rt= 6): 99% (partial overlapping of peaks); starting material (rt= 10.15).

SECTION C

Bibliography

(1) Foreman, K. et al. *The Lancet* **2018**, *392*, 2052.

(2) https://www.who.int/en/news-room/fact-sheets/detail/cancer.

(3) DeVita Jr., V. T.; Chu, E. *Cancer Res.* **2008**, *68*, 8643.

(4) Loadman, P. *Br. J. Cancer* **2002**, *86*, 1665.

(5) Strebhardt, K.; Ullrich, A. *Nat. Rev. Cancer* **2008**, *8*, 473.

(6) Krall, N.; Scheuermann, J.; Neri, D. *Angew. Chem. Int. Ed.* **2013**, *52*, 1384.

(7) Berndt, N.; Karim, R. M.; Schönbrunn, E. *Curr Opin Chem Biol.* **2017**, *39*, 126.

(8) Roskoski, R. *Pharmacol. Res.* **2021**, *165*, 105463.

(9) Bhullar, K. S.; Lagarón, N. O.; McGowan, E. M.; Parmar, I.; Jha, A.; Hubbard, B. P.; Rupasinghe, H. P. V. *Mol. Cancer* **2018**, *17*, 48.

(10) Klaeger, S. et al. *Science* **2017**, *358*, eaan4368.

(11) Hafeez, U.; Gan, H. K.; Scott, A. M. *Curr Opin Pharmacol.* **2018**, *41*, 114.

(12) Kaplon, H.; Reichert, J. M. *mAbs* **2021**, *13*, 1860476.

(13) Baah, S.; Laws, M.; Rahman, K. M. *Molecules* **2021**, *26*.

(14) Chiu, M. L.; Goulet, D. R.; Teplyakov, A.; Gilliland, G. L. *Antibodies* **2019**, *8*.

(15) Hoffmann, R. M.; Coumbe, B. G. T.; Josephs, D. H.; Mele, S.; Ilieva, K. M.; Cheung, A.; Tutt, A. N.; Spicer, J. F.; Thurston, D. E.; Crescioli, S.; Karagiannis, S. N. *Oncoimmunology* **2018**, *7*, e1395127.

(16) Boekhout, A. H.; Beijnen, J. H.; Schellens, J. H. M. *Oncologist* **2011**, *16*, 800.

(17) Narayan, M.; Wilken, J. A.; Harris, L. N.; Baron, A. T.; Kimbler, K. D.; Maihle, N. J. *Cancer Res.* **2009**, *69*, 2191.

(18) Wolff, A. C. et al. *J. Clin. Oncol.* **2007**, *25*, 118.

(19) Srinivasarao, M.; Galliford, C. v; Low, P. S. *Nat. Rev. Drug Discov.* **2015**, *14*, 203.

(20) Patel, T. K.; Adhikari, N.; Amin, Sk. A.; Biswas, S.; Jha, T.; Ghosh, B. *New J. Chem.* **2021**, *45*, 5291.

(21) Leamon, C. P.; Reddy, J. A.; Dorton, R.; Bloomfield, A.; Emsweller, K.; Parker, N.; Westrick, E. *J. Pharmacol. Exp. Ther.* **2008**, *327*, 918.

(22) Leamon, C. P. *Curr Opin Investig. Drugs* **2008**, *9*, 1277.

(23) Das, S.; Al-Toubah, T.; El-Haddad, G.; Strosberg, J. *Expert Rev. Gastroenterol Hepatol.* **2019**, *13*, 1023.

(24) Barone, R.; Borson-Chazot, F.; Valkema, R.; Walrand, S.; Chauvin, F.; Gogou, L.; Kvols, L. K.; Krenning, E. P.; Jamar, F.; Pauwels, S. *J. Nucl. Med.* **2005**, *46*, 99S.

(25) Ambrosio, A. J.; Suzin, D.; Palmer, E. L.; Penson, R. T. *Expert Rev. Clin. Pharmacol.* **2014**, *7*, 443.

(26) Yarden, Y.; Sliwkowski, M. X. *Nat. Rev. Mol. Cell Biol.* **2001**, *2*, 127.

(27) Cini, E.; Faltoni, V.; Petricci, E.; Taddei, M.; Salvini, L.; Giannini, G.; Vesci, L.; Milazzo, F. M.; Anastasi, A. M.; Battistuzzi, G.; de Santis, R. *Chem. Sci.* **2018**, *9*, 6490.

(28) Nagayama, A.; Ellisen, L. W.; Chabner, B.; Bardia, A. *Target. Oncol.* **2017**, *12*, 719.

(29) Chau, C. H.; Steeg, P. S.; Figg, W. D. *The Lancet* **2019**, *394*, 793.

(30) Kalim, M.; Chen, J.; Wang, S.; Lin, C.; Ullah, S.; Liang, K.; Ding, Q.; Chen, S.; Zhan, *J. Drug Des. Devel. Ther.* **2017**, *11*, 2265.

(31) Ritchie, M.; Tchistiakova, L.; Scott, N. *mAbs* **2013**, *5*, 13.

(32) Mariathasan, S.; Tan, M.-W. *Trends Mol. Med.* **2017**, *23*, 135.

(33) E, K. S. H. *mBio* **2017**, *8*, e00117.

(34) Reichert, J. M.; Dewitz, M. C. *Nat. Rev. Drug Discov.* **2006**, *5*, 191.

(35) P, M. M.; C, F. B. *mSphere* **2017**, *2*, e00397.

(36) Gautam, S.; Kim, T.; Lester, E.; Deep, D.; Spiegel, D. A. *ACS Chem. Biol.* **2016**, *11*, 25.

(37) Kurokawa, K. et al. *J. Biol. Chem.* **2013**, *288*, 30956.

(38) Lehar, S. M. et al. *Nature* **2015**, *527*, 323.

(39) Junutula, J. R. et al. *Nat. Biotechnol.* **2008**, *26*, 925.

(40) Rima, M.; Rima, M.; Fajloun, Z.; Sabatier, J.-M.; Bechinger, B.; Naas, T. *Antibiotics* **2021**, *10*.

(41) Zhang, Q.-Y.; Yan, Z.-B.; Meng, Y.-M.; Hong, X.-Y.; Shao, G.; Ma, J.-J.; Cheng, X.-R.; Liu, J.; Kang, J.; Fu, C.-Y. *Mil. Med. Res.* **2021**, *8*, 48.

(42) Datta, S.; Roy, A. *Int. J. Pept. Res. Ther.* **2021**, *27*, 555.

(43) Huan, Y.; Kong, Q.; Mou, H.; Yi, H. *Front. Microbiol.* **2020**, *11*, 582779.

(44) Cavaco, M.; Andreu, D.; Castanho, M. A. R. B. *Angew. Chem. Int. Ed.* **2021**, *60*, 1686.

(45) Hutson, C.L. et al. *mSphere* **2021**, *6*, e00927.

(46) Effros, R. B. et al. *Clin. Infect. Dis.* **2008**, *47*, 542.

(47) Marano, G.; Vaglio, S.; Pupella, S.; Facco, G.; Catalano, L.; Liumbruno, G. M.; Grazzini, G. *Blood Transfus.* **2016**, *14*, 152.

(48) Simonovich, V. A. et al. *N. Engl. J. Med.* **2020**, *384*, 619.

(49) Umotoy, J. C.; de Taeye, S. W. *Front. Immunol.* **2021**, *12*, 708806.

(50) Dean, A. Q.; Luo, S.; Twomey, J. D.; Zhang, B. *mAbs* **2021**, *13*, 1951427.

(51) Bross, P. F.; Beitz, J.; Chen, G.; Chen, X. H.; Duffy, E.; Kieffer, L.; Roy, S.; Sridhara, R.; Rahman, A.; Williams, G.; Pazdur, R. *Clin. Cancer Res.* **2001**, *7*, 1490.

(52) Petersdorf, S. H.; Kopecky, K. J.; Slovak, M.; Willman, C.; Nevill, T.; Brandwein, J.; Larson, R. A.; Erba, H. P.; Stiff, P. J.; Stuart, R. K.; Walter, R. B.; Tallman, M. S.; Stenke, L.; Appelbaum, F. R. *Blood* **2013**, *121*, 4854.

(53) Tong, J. T. W.; Harris, P. W. R.; Brimble, M. A.; Kavianinia, I. *Molecules* **2021**, *26*, 5847.

(54) Katz, J.; Janik, J. E.; Younes, A. *Clin.l Cancer Res.* **2011**, *17*, 6428.

(55) Von Minckwitz, G. et al. *N. Engl. J. Med.* **2018**, *380*, 617.

(56) Lambert, J. M.; Chari, R. V. J. *J. Med. Chem.* **2014**, *57*, 6949.

(57) Lamb, Y. N. *Drugs* **2017**, *77*, 1603.

(58) DiJoseph, J. F.; Armellino, D. C.; Boghaert, E. R.; Khandke, K.; Dougher, M. M.; Sridharan, L.; Kunz, A.; Hamann, P. R.; Gorovits, B.; Udata, C.; Moran, J. K.; Popplewell, A. G.; Stephens, S.; Frost, P.; Damle, N. K. *Blood* **2004**, *103*, 1807.

(59) Dhillon, S. *Drugs* **2018**, *78*, 1763.

(60) Shitara, K.; Bang, Y.-J.; Iwasa, S.; Sugimoto, N.; Ryu, M.-H.; Sakai, D.; Chung, H.-C.; Kawakami, H.; Yabusaki, H.; Lee, J.; Saito, K.; Kawaguchi, Y.; Kamio, T.; Kojima, A.; Sugihara, M.; Yamaguchi, K. *N. Engl. J. Med.* **2020**, *382*, 2419.

(61) Modi, S. et al. *N. Engl. J. Med***. 2019**, *382*, 610.

(62) Brekke, O. H.; Sandlie, I. *Nat. Rev. Drug Discov.* **2003**, *2*, 52.

(63) Tsuchikama, K.; An, Z. *Protein Cell* **2018**, *9*, 33.

(64) Wang, W.; Wang, E. Q.; Balthasar, J. P. *Clin. Pharmacol. Ther.* **2008**, *84*, 548.

(65) Rudnick, S. I.; Lou, J.; Shaller, C. C.; Tang, Y.; Klein-Szanto, A. J. P.; Weiner, L. M.; Marks, J. D.; Adams, G. P. *Cancer Res.* **2011**, *71*, 2250.

(66) Polson, A. G.; Ho, W. Y.; Ramakrishnan, V. *Expert Opin. Investig. Drugs* **2011**, *20*, 75.

(67) Lyon, R. P.; Bovee, T. D.; Doronina, S. O.; Burke, P. J.; Hunter, J. H.; Neff-LaFord, H. D.; Jonas, M.; Anderson, M. E.; Setter, J. R.; Senter, P. D. *Nat. Biotechnol.* **2015**, *33*, 733.

(68) Burke, P. J. et al. *Mol. Cancer Ther.* **2017**, *16*, 116.

(69) Bargh, J. D.; Isidro-Llobet, A.; Parker, J. S.; Spring, D. R. *Chem. Soc. Rev.* **2019**, *48*, 4361.

(70) Lu, J.; Jiang, F.; Lu, A.; Zhang, G. *Int. J. Mol. Sci.* **2016**, *17*.

(71) Chalouni, C.; Doll, S. *J. Exp. Clin. Cancer Res.* **2018**, *37*, 20.

(72) McCombs, J. R.; Owen, S. C. *AAPS J.* **2015**, *17*, 339.

(73) Tumey, L. N.; Charati, M.; He, T.; Sousa, E.; Ma, D.; Han, X.; Clark, T.; Casavant, J.; Loganzo, F.; Barletta, F.; Lucas, J.; Graziani, E. I. *Bioconjug. Chem.* **2014**, *25*, 1871.

(74) Ravasco, J. M. J. M.; Faustino, H.; Trindade, A.; Gois, P. M. P. *Chem. Eur. J.* **2019**, *25*, 43.

(75) DiJoseph, J. F.; Khandke, K.; Dougher, M. M.; Evans, D. Y.; Armellino, D. C.; Hamann, P. R.; Damle, N. K. *Hematol. Meet. Rep.* **2009**, *2*.

(76) Kalia, J.; Raines, R. T. *Angew. Chem. Int. Ed.* **2008**, *47*, 7523.

(77) Zhang, X.; Lin, Y.; Gillies, R. J. *J. Nucl. Med.* **2010**, *51*, 1167.

(78) Zhang, A.; Yao, L.; An, M. *Chem. Comm.***2017**, *53*, 12826.

(79) Wang, Y.; Fan, S.; Xiao, D.; Xie, F.; Li, W.; Zhong, W.; Zhou, X. *Cancers* **2019**, *11*.

(80) Choy, C. J.; Geruntho, J. J.; Davis, A. L.; Berkman, C. E. *Bioconjug. Chem.* **2016**, *27*, 824.

(81) Kong, S. D.; Luong, A.; Manorek, G.; Howell, S. B.; Yang, J. *Bioconjug. Chem.* **2007**, *18*, 293.

(82) Jacques, S. A.; Leriche, G.; Mosser, M.; Nothisen, M.; Muller, C. D.; Remy, J.-S.; Wagner, A. *Org. Biomol. Chem.* **2016**, *14*, 4794.

(83) Leriche, G.; Nothisen, M.; Baumlin, N.; Muller, C. D.; Bagnard, D.; Remy, J.-S.; Jacques, S. A.; Wagner, A. *Bioconjug. Chem.* **2015**, *26*, 1461.

(84) Deslongchamps, P.; Dory, Y. L.; Li, S. *Tetrahedron* **2000**, *56*, 3533.

(85) Godwin, A. K.; Meister, A.; O'Dwyer, P. J.; Huang, C. S.; Hamilton, T. C.; Anderson, M. E. *Proc. Nat. Acad. Sci.* **1992**, *89*, 3070.

(86) Pillow, T. H.; Sadowsky, J. D.; Zhang, D.; Yu, S.-F.; del Rosario, G.; Xu, K.; He, J.; Bhakta, S.; Ohri, R.; Kozak, K. R.; Ha, E.; Junutula, J. R.; Flygare, J. A. *Chem. Sci.* **2017**, *8*, 366.

(87) Pillow, T. H. et al. *Mol. Cancer Ther.* **2017**, *16*, 871.

(88) Bernardes, G. J. L.; Casi, G.; Trüssel, S.; Hartmann, I.; Schwager, K.; Scheuermann, J.; Neri, D. *Angew. Chem. Int. Ed.* **2012**, *51*, 941.

(89) Dubowchik, G. M.; Firestone, R. A.; Padilla, L.; Willner, D.; Hofstead, S. J.; Mosure, K.; Knipe, J. O.; Lasch, S. J.; Trail, P. A. *Bioconjug. Chem.* **2002**, *13*, 855.

(90) Dorywalska, M. et al. *Bioconjug. Chem.* **2015**, *26*, 650.

(91) Dorywalska, M. et al. *Mol. Cancer Ther.* **2016**, *15*, 958.

(92) Anami, Y.; Yamazaki, C. M.; Xiong, W.; Gui, X.; Zhang, N.; An, Z.; Tsuchikama, K. *Nat. Commun.* **2018**, *9*, 2512.

(93) Caculitan, N. G. et al. *Cancer Res.* **2017**, *77*, 7027.

(94) Wang, Y.; Fan, S.; Zhong, W.; Zhou, X.; Li, S. *Int. J. Mol. Sci.* **2017**, *18*.

(95) Tiberghien, A. C.; Levy, J.-N.; Masterson, L. A.; Patel, N. v; Adams, L. R.; Corbett, S.; Williams, D. G.; Hartley, J. A.; Howard, P. W. *ACS Med. Chem. Lett.* **2016**, *7*, 983.

(96) Gébleux, R.; Stringhini, M.; Casanova, R.; Soltermann, A.; Neri, D. *Int. J. Cancer* **2017**, *140*, 1670.

(97) Dal Corso, A.; Cazzamalli, S.; Gébleux, R.; Mattarella, M.; Neri, D. *Bioconjug. Chem.* **2017**, *28*, 1826.

(98) Jeffrey, S. C.; Andreyka, J. B.; Bernhardt, S. X.; Kissler, K. M.; Kline, T.; Lenox, J. S.; Moser, R. F.; Nguyen, M. T.; Okeley, N. M.; Stone, I. J.; Zhang, X.; Senter, P. D. *Bioconjug. Chem.* **2006**, *17*, 831.

(99) Burke, P. J.; Senter, P. D.; Meyer, D. W.; Miyamoto, J. B.; Anderson, M.; Toki, B. E.; Manikumar, G.; Wani, M. C.; Kroll, D. J.; Jeffrey, S. C. *Bioconjug. Chem.* **2009**, *20*, 1242.

(100) Kolodych, S.; Michel, C.; Delacroix, S.; Koniev, O.; Ehkirch, A.; Eberova, J.; Cianférani, S.; Renoux, B.; Krezel, W.; Poinot, P.; Muller, C. D.; Papot, S.; Wagner, A. *Eur. J. Med. Chem.* **2017**, *142*, 376.

(101) Kern, J. C. et al. *J. Am. Chem. Soc*. **2016**, *138*, 1430.

(102) Bargh, J. D.; Walsh, S. J.; Isidro-Llobet, A.; Omarjee, S.; Carroll, J. S.; Spring, D. R. *Chem. Sci.* **2020**, *11*, 2375.

(103) Su, Z.; Xiao, D.; Xie, F.; Liu, L.; Wang, Y.; Fan, S.; Zhou, X.; Li, S. *Acta Pharm. Sin. B* **2021**, *11*, 3889.

(104) Ray, P. D.; Huang, B.-W.; Tsuji, Y. *Cell. Signal.* **2012**, *24*, 981.

(105) Song, C.-C.; Du, F.-S.; Li, Z.-C. *J. Mater. Chem. B* **2014**, *2*, 3413.

(106) Lallana, E.; Tirelli, N. *Macromol. Chem. Phys.* **2013**, *214*, 143.

(107) Yang, X.; Pan, Z.; Choudhury, M. R.; Yuan, Z.; Anifowose, A.; Yu, B.; Wang, W.; Wang, B. *Med. Res. Rev.* **2020**, *40*, 2682.

(108) Heggie, G. D.; Sommadossi, J.-P.; Cross, D. S.; Huster, W. J.; Diasio, R. B. *Cancer Res.* **1987**, *47*, 2203.

(109) Miura, K.; Kinouchi, M.; Ishida, K.; Fujibuchi, W.; Naitoh, T.; Ogawa, H.; Ando, T.; Yazaki, N.; Watanabe, K.; Haneda, S.; Shibata, C.; Sasaki, I. *Cancers* **2010**, *2*, 1717.

(110) Ai, Y.; Obianom, O. N.; Kuser, M.; Li, Y.; Shu, Y.; Xue, F. *ACS Med. Chem. Lett.* **2019**, *10*, 127.

(111) Kim, E.-J.; Bhuniya, S.; Lee, H.; Kim, H. M.; Cheong, C.; Maiti, S.; Hong, K. S.; Kim, J. S. *J. Am. Chem. Soc.* **2014**, *136*, 13888.

(112) Kuang, Y.; Balakrishnan, K.; Gandhi, V.; Peng, X. *J. Am. Chem. Soc.* **2011**, *133*, 19278.

(113) Peng, X.; Gandhi, V. *Ther. Deliv.* **2012**, *3*, 823.

(114) Pei, P.; Sun, C.; Tao, W.; Li, J.; Yang, X.; Wang, J. *Biomaterials* **2019**, *188*, 74.

(115) Taresco, V.; Alexander, C.; Singh, N.; Pearce, A. K. *Adv. Ther. (Weinh.)* **2018**, *1*, 1800030.

(116) Liu, B.; Wang, D.; Liu, Y.; Zhang, Q.; Meng, L.; Chi, H.; Shi, J.; Li, G.; Li, J.; Zhu, X. *Polym. Chem.* **2015**, *6*, 3460.

(117) Ji, X.; Pan, Z.; Yu, B.; de La Cruz, L. K.; Zheng, Y.; Ke, B.; Wang, B. *Chem. Soc. Rev.* **2019**, *48*, 1077.

(118) Matikonda, S. S.; Orsi, D. L.; Staudacher, V.; Jenkins, I. A.; Fiedler, F.; Chen, J.; Gamble, A. B. *Chem. Sci.* **2015**, *6*, 1212.

(119) Fan, X.; Ge, Y.; Lin, F.; Yang, Y.; Zhang, G.; Ngai, W. S. C.; Lin, Z.; Zheng, S.; Wang, J.; Zhao, J.; Li, J.; Chen, P. R. *Angew. Chem. Int. Ed.* **2016**, *55*, 14046.

(120) Rossin, R.; van Duijnhoven, S. M. J.; ten Hoeve, W.; Janssen, H. M.; Kleijn, L. H. J.; Hoeben, F. J. M.; Versteegen, R. M.; Robillard, M. S. *Bioconjug. Chem.* **2016**, *27*, 1697.

(121) Spangler, B.; Kline, T.; Hanson, J.; Li, X.; Zhou, S.; Wells, J. A.; Sato, A. K.; Renslo, A. R. *Mol. Pharm.* **2018**, *15*, 2054.

(122) Li, J.; Xiao, D.; Xie, F.; Li, W.; Zhao, L.; Sun, W.; Yang, X.; Zhou, X. *Bioorg. Chem.* **2021**, *111*, 104475.

(123) D'Orazio, J.; Jarrett, S.; Amaro-Ortiz, A.; Scott, T. *Int. J. Mol. Sci.* **2013**, *14*, 12222.

(124) Matsumura, Y.; Ananthaswamy, H. N. *Toxicol. Appl. Pharmacol.* **2004**, *195*, 298.

(125) Alouane, A.; Labruère, R.; Le Saux, T.; Schmidt, F.; Jullien, L. *Angew. Chem. Int. Ed.* **2015**, *54*, 7492.

(126) Walther, R.; Rautio, J.; Zelikin, A. N. *Adv. Drug Deliv. Rev.* **2017**, *118*, 65.

(127) Mosey, R. A.; Floreancig, P. E. *Org. Biomol. Chem.* **2012**, *10*, 7980.

(128) P. Hay, M.; M. Sykes, B.; A. Denny, W.; J. O'Connor, C. *J. Chem. Soc. Perkin Trans. 1* **1999**, 2759.

(129) Toki, B. E.; Cerveny, C. G.; Wahl, A. F.; Senter, P. D. *J. Org. Chem*. **2002**, *67*, 1866.

(130) Govindan, S. v; Cardillo, T. M.; Sharkey, R. M.; Tat, F.; Gold, D. v; Goldenberg, D. M. *Mol. Cancer Ther.* **2013**, *12*, 968.

(131) Staben, L. R. et al. *Nat. Chem.* **2016**, *8*, 1112.

(132) Jin, C.; Wen, S.; Zhang, Q.; Zhu, Q.; Yu, J.; Lu, W. *ACS Med. Chem. Lett.* **2017**, *8*, 762.

(133) Chen, E. K. Y.; McBride, R. A.; Gillies, E. R. *Macromolecules* **2012**, *45*, 7364.

(134) Shamis, M.; Lode, H. N.; Shabat, D. *J. Am. Chem. Soc.* **2004**, *126*, 1726.

(135) Zhao, R. Y.; Wilhelm, S. D.; Audette, C.; Jones, G.; Leece, B. A.; Lazar, A. C.; Goldmacher, V. S.; Singh, R.; Kovtun, Y.; Widdison, W. C.; Lambert, J. M.; Chari, R. V. J. *J. Med. Chem.* **2011**, *54*, 3606.

(136) Epenetos, A. A.; Snook, D.; Durbin, H.; Johnson, P. M.; Taylor-Papadimitriou, J. *Cancer Res***. 1986**, *46*, 3183.

(137) Beck, A.; Goetsch, L.; Dumontet, C.; Corvaïa, N. *Nat Rev. Drug Discov.* **2017**, *16*, 315.

(138) Akaiwa, M.; Dugal-Tessier, J.; Mendelsohn, B. A. *Chem. Pharm. Bull.* **2020**, *68*, 201.

(139) Park, M.-H.; Lee, B. ill; Byeon, J.-J.; Shin, S.-H.; Choi, J.; Park, Y.; Shin, Y. G. *Molecules* **2019**, *24*.

(140) Widdison, W. C. et al. *J. Med. Chem.* **2006**, *49*, 4392.

(141) Nittoli, T. et al. *Bioorg. Med. Chem.* **2018**, *26*, 2271.

(142) Tumey, L. N. *ACS Med. Chem. Lett.* **2016**, *7*, 977.

(143) Li, J. Y. et al. *Cancer Cell.* **2016**, *29*, 117.

(144) Liu, Y.; Zhang, X.; Han, C.; Wan, G.; Huang, X.; Ivan, C.; Jiang, D.; Rodriguez-Aguayo, C.; Lopez-Berestein, G.; Rao, P. H.; Maru, D. M.; Pahl, A.; He, X.; Sood, A. K.; Ellis, L. M.; Anderl, J.; Lu, X. *Nature* **2015**, *520*, 697.

(145) Shor, B.; Gerber, H.-P.; Sapra, P. *Mol. Immunol.* **2015**, *67*, 107.

(146) Shen, B.; Hindra; Yan, X.; Huang, T.; Ge, H.; Yang, D.; Teng, Q.; Rudolf, J. D.; Lohman, J. R. *Bioorg. Med. Chem. Lett.* **2015**, *25*, 9.

(147) Li, W. et al. *ACS Med. Chem. Lett.* **2019**, *10*, 1386.

(148) Leimgruber, W.; Stefanović, V.; Schenker, F.; Karr, A.; Berger, J. *J. Am. Chem. Soc.* **1965**, *87*, 5791.

(149) Kolakowski, R. v; Young, T. D.; Howard, P. W.; Jeffrey, S. C.; Senter, P. D. *Tetrahedron Lett.* **2015**, *56*, 4512.

(150) Miller, M. L. et al. *Mol. Cancer Ther.* **2016**, *15*, 1870.

(151) Mantaj, J.; Jackson, P. J. M.; Rahman, K. M.; Thurston, D. E. *Angew. Chem. Int. Ed.* **2017**, *56*, 462.

(152) Boger, D. L.; Johnson, D. S. *Angew. Chem. Int. Ed*. **1996**, *35*, 1438.

(153) Yao, H.-P.; Zhao, H.; Hudson, R.; Tong, X.-M.; Wang, M.-H. *Drug Discov. Today* **2021**, *26*, 1857.

(154) Boger, D. L.; Han, N. *Bioorg. Med. Chem.* **1997**, *5*, 233.

(155) Fujiwara, A.; Hoshino, T.; Westley, J. W. *Crit. Rev. Biotechnol.* **1985**, *3*, 133.

(156) Ma, Z.; He, H.; Sun, F.; Xu, Y.; Huang, X.; Ma, Y.; Zhao, H.; Wang, Y.; Wang, M.; Zhang, J. *J. Cancer Res. Clin. Oncol.* **2017**, *143*, 1929.

(157) Camacho, K. M.; Menegatti, S.; Vogus, D. R.; Pusuluri, A.; Fuchs, Z.; Jarvis, M.; Zakrewsky, M.; Evans, M. A.; Chen, R.; Mitragotri, S. *J. Control. Release* **2016**, *229*, 154.

(158) Lin, C. M.; Ho, H. H.; Pettit, G. R.; Hamel, E. *Biochemistry* **1989**, *28*, 6984.

(159) Singh, R.; Kaur, H. *Synthesis (Stuttg.)* **2009**, *2009*, 2471.

(160) Ho, T. C. S.; Chan, A. H. Y.; Ganesan, A. *J. Med. Chem.* **2020**, *63*, 12460.

(161) Hull, E. E.; Montgomery, M. R.; Leyva, K. J. *Biomed. Res. Int.* **2016**, *2016*, 8797206.

(162) Kim, H.-J.; Bae, S.-C. *Am. J. Transl. Res.* **2011**, *3*, 166.

(163) Yoon, S.; Eom, G. H. *Chonnam Med. J.* **2016**, *52*, 1.

(164) Giannini, G. et al. *J. Med. Chem.* **2014**, *57*, 8358.

(165) Cini, E.; Faltoni, V.; Petricci, E.; Taddei, M.; Salvini, L.; Giannini, G.; Vesci, L.; Milazzo, F. M.; Anastasi, A. M.; Battistuzzi, G.; de Santis, R. *Chem. Sci.* **2018**, *9*, 6490.

(166) Cianferotti, C.; Faltoni, V.; Cini, E.; Ermini, E.; Migliorini, F.; Petricci, E.; Taddei, M.; Salvini, L.; Battistuzzi, G.; Milazzo, F. M.; Anastasi, A. M.; Chiapparino, C.; de Santis, R.; Giannini, G. *Chem. Comm.* **2021**, *57*, 867.

(167) Lehmann, R.; Nüsslein-Volhard, C. *Nature* **1987**, *329*, 167.

(168) Chai, J. Y.; Sugumar, V.; Alshawsh, M. A.; Wong, W. F.; Arya, A.; Chong, P. P.; Looi, C. Y. *Biomedicines* **2021**, *9*.

(169) Jenkins, D. *Cell. Signal.* **2009**, *21*, 1023.

(170) Echelard, Y.; Epstein, D. J.; St-Jacques, B.; Shen, L.; Mohler, J.; McMahon, J. A.; McMahon, A. P. *Cell* **1993**, *75*, 1417.

(171) Ayers, K. L.; Thérond, P. P. *Trends Cell Biol.* **2010**, *20*, 287.

(172) Rohatgi, R.; Milenkovic, L.; Scott, M. P. *Science* **2007**, *317*, 372.

(173) Keeler, R. F.; Binns, W. *Can. J. Biochem.* **1966**, *44*, 829.

(174) Sanchez, P.; Ruiz i Altaba, A. *Mech. Dev.* **2005**, *122*, 223.

(175) Dahmane, N.; Sánchez, P.; Gitton, Y.; Palma, V.; Sun, T.; Beyna, M.; Weiner, H.; Ruiz i Altaba, A. *Development* **2001**, *128*, 5201.

(176) Berman, D. M.; Karhadkar, S. S.; Hallahan, A. R.; Pritchard, J. I.; Eberhart, C. G.; Watkins, D. N.; Chen, J. K.; Cooper, M. K.; Taipale, J.; Olson, J. M.; Beachy, P. A. *Science* **2002**, *297*, 1559.

(177) Winkler, J. D.; Isaacs, A.; Holderbaum, L.; Tatard, V.; Dahmane, N. *Org. Lett.* **2009**, *11*, 2824.

(178) Nguyen, N. M.; Cho, J. *Int. J. Mol. Sci.* **2022**, *23*, 1733.

(179) Theocharopoulos, C.; Lialios, P.-P.; Samarkos, M.; Gogas, H.; Ziogas, D. C. *Vaccines* **2021**, *9*, 1111.

(180) Cavaco, M.; Castanho, M. A. R. B.; Neves, V. *Pept. Sci.* **2018**, *110*, e23095.

(181) Cal, P. M. S. D.; Matos, M. J.; Bernardes, G. J. L. *Expert Opin. Ther. Pat.* **2017**, *27*, 179.

(182) Ventola, C. L. *P&T* **2015**, *40*, 277.

(183) Hashemian, S. M. R.; Farhadi, T.; Ganjparvar, M. *Drug Des. Devel. Ther.* **2018**, *12*, 1759.

(184) Hayakawa, M.; Toda, N.; Carrillo, N.; Thornburg, N. J.; Crowe Jr., J. E.; Barbas, C. F. *ChemBioChem* **2012**, *13*, 2191.

(185) Sajid Jamal, Q. M.; Alharbi, A. H.; Ahmad, V. *J. Biomol. Struct. Dyn.* **2022**, *40*, 7960.

(186) Backer, V.; Sjöbring, U.; Sonne, J.; Weiss, A.; Hostrup, M.; Johansen, H. K.; Becker, V.; Sonne, D. P.; Balchen, T.; Jellingsø, M.; Sommer, M. O. A. *Lancet Reg. Health Eur.* **2021**, *4*, 100084.

(187) Jain, N.; Smith, S. W.; Ghone, S.; Tomczuk, B. *Pharm. Res.* **2015**, *32*, 3526.

(188) Kline, T.; Steiner, A. R.; Penta, K.; Sato, A. K.; Hallam, T. J.; Yin, G. *Pharm. Res.* **2015**, *32*, 3480.

(189) Hu, X.; Bortell, E.; Kotch, F. W.; Xu, A.; Arve, B.; Freese, S. *Org. Process Res. Dev.* **2017**, *21*, 601.

(190) Anderson, G. W.; Zimmerman, J. E.; Callahan, F. M. *J. Am. Chem. Soc.* **1964**, *86*, 1839.

(191) Kalkhof, S.; Sinz, A. *Anal. Bioanal. Chem.* **2008**, *392*, 305.

(192) Kang, M. S.; Kong, T. W. S.; Khoo, J. Y. X.; Loh, T.-P. *Chem. Sci.* **2021**, *12*, 13613.

(193) Hettick, J. M.; Ruwona, T. B.; Siegel, P. D. *J. Am. Soc. Mass Spectrom.* **2009**, *20*, 1567.

(194) Wilbur, D. S.; Chyan, M.-K.; Nakamae, H.; Chen, Y.; Hamlin, D. K.; Santos, E. B.; Kornblit, B. T.; Sandmaier, B. M. *Bioconjug. Chem.* **2012**, *23*, 409.

(195) Dovgan, I.; Ursuegui, S.; Erb, S.; Michel, C.; Kolodych, S.; Cianférani, S.; Wagner, A. *Bioconjug. Chem*. **2017**, *28*, 1452.

(196) Asano, S.; Patterson, J. T.; Gaj, T.; Barbas III, C. F. *Angew. Chem. Int. Ed.* **2014**, *53*, 11783.

(197) Sun, M. M. C.; Beam, K. S.; Cerveny, C. G.; Hamblett, K. J.; Blackmore, R. S.; Torgov, M. Y.; Handley, F. G. M.; Ihle, N. C.; Senter, P. D.; Alley, S. C. *Bioconjug. Chem.* **2005**, *16*, 1282.

(198) Kuninori, T.; Nishiyama, J. *Agric. Biol. Chem.* **1985**, *49*, 2453.

(199) Alley, S. C.; Benjamin, D. R.; Jeffrey, S. C.; Okeley, N. M.; Meyer, D. L.; Sanderson, R. J.; Senter, P. D. *Bioconjug. Chem.* **2008**, *19*, 759.

(200) Lyon, R. P.; Setter, J. R.; Bovee, T. D.; Doronina, S. O.; Hunter, J. H.; Anderson, M. E.; Balasubramanian, C. L.; Duniho, S. M.; Leiske, C. I.; Li, F.; Senter, P. D. *Nat. Biotechnol.* **2014**, *32*, 1059.

(201) Walsh, S. J.; Bargh, J. D.; Dannheim, F. M.; Hanby, A. R.; Seki, H.; Counsell, A. J.; Ou, X.; Fowler, E.; Ashman, N.; Takada, Y.; Isidro-Llobet, A.; Parker, J. S.; Carroll, J. S.; Spring, D. R. *Chem. Soc. Rev.* **2021**, *50*, 1305.

(202) Junutula, J. R.; Bhakta, S.; Raab, H.; Ervin, K. E.; Eigenbrot, C.; Vandlen, R.; Scheller, R. H.; Lowman, H. B. J Immunol Methods **2008**, *332*, 41.

(203) Tumey, L. N.; Li, F.; Rago, B.; Han, X.; Loganzo, F.; Musto, S.; Graziani, E. I.; Puthenveetil, S.; Casavant, J.; Marquette, K.; Clark, T.; Bikker, J.; Bennett, E. M.; Barletta, F.; Piche-Nicholas, N.; Tam, A.; O'Donnell, C. J.; Gerber, H. P.; Tchistiakova, L. AAPS J **2017**, *19*, 1123.

(204) Shen, B.-Q. et al. *Nat. Biotechnol.* **2012**, *30*, 184—189.

(205) Yin, G. et al. *Sci. Rep.* **2017**, *7*, 3026.

(206) Roy, G.; Reier, J.; Garcia, A.; Martin, T.; Rice, M.; Wang, J.; Prophet, M.; Christie, R.; Dall'Acqua, W.; Ahuja, S.; Bowen, M. A.; Marelli, M. *mAbs* **2020**, *12*, 1684749.

(207) Hofer, T.; Skeffington, L. R.; Chapman, C. M.; Rader, C. *Biochemistry* **2009**, *48*, 12047.

(208) Griffin, M.; Casadio, R.; Bergamini, C. M. *Biochem. J.* **2002**, *368*, 377.

(209) Strop, P.; Tran, T.-T.; Dorywalska, M.; Delaria, K.; Dushin, R.; Wong, O. K.; Ho, W.-H.; Zhou, D.; Wu, A.; Kraynov, E.; Aschenbrenner, L.; Han, B.; O'Donnell, C. J.; Pons, J.; Rajpal, A.; Shelton, D. L.; Liu, S.-H. *Mol. Cancer Ther.* **2016**, *15*, 2698.

(210) Beerli, R. R.; Hell, T.; Merkel, A. S.; Grawunder, U. *PLoS One* **2015**, *10*, e0131177.

(211) Drake, P. M.; Albers, A. E.; Baker, J.; Banas, S.; Barfield, R. M.; Bhat, A. S.; de Hart, G. W.; Garofalo, A. W.; Holder, P.; Jones, L. C.; Kudirka, R.; McFarland, J.; Zmolek, W.; Rabuka, D. *Bioconjug. Chem.* **2014**, *25*, 1331.

(212) Qasba, P. K. *Bioconjug. Chem.* **2015**, *26*, 2170.

(213) O'Shannessy, D. J.; Dobersen, M. J.; Quarles, R. H. *Immunol. Lett.* **1984**, *8*, 273.

(214) Zuberbühler, K.; Casi, G.; Bernardes, G. J. L.; Neri, D. *Chem. Comm.* **2012**, *48*, 7100.

(215) Zhou, Q. et al. *Bioconjug. Chem.* **2014**, *25*, 510.

(216) Ramakrishnan, B.; Qasba, P. K. *J. Biol. Chem.* **2002**, *277*, 20833.

(217) Wei, Y.; Li, C.; Huang, W.; Li, B.; Strome, S.; Wang, L.-X. *Biochemistry* **2008**, *47*, 10294.

(218) Chen, Y. *Methods Mol. Biol.* **2013**, *1045*, 267.

(219) Petrović, M.; Hernando, M. D.; Díaz-Cruz, M. S.; Barceló, D. *J. Chromatogr. A* **2005**, *1067*, 1.

(220) Neupane, R.; Bergquist, J. *Eur. J. Mass Spectrom.* **2017**, *23*, 417.

(221) Birdsall, R. E.; Shion, H.; Kotch, F. W.; Xu, A.; Porter, T. J.; Chen, W. *mAbs* **2015**, *7*, 1036.

(222) Valliere-Douglass, J. F.; McFee, W. A.; Salas-Solano, O. *Anal. Chem.* **2012**, *84*, 2843.

(223) Lazar, A. C.; Wang, L.; Blättler, W. A.; Amphlett, G.; Lambert, J. M.; Zhang, W. *Rapid Comm.s in Mass Spectrom.* **2005**, *19*, 1806.

(224) Kommineni, N.; Pandi, P.; Chella, N.; Domb, A. J.; Khan, W. *Polym. Adv. Technol.* **2020**, *31*, 1177.

(225) Goyon, A.; Beck, A.; Veuthey, J.-L.; Guillarme, D.; Fekete, S. *J. Pharm. Biomed. Anal.* **2017**, *144*, 242.

(226) Sandra, K.; Vanhoenacker, G.; Vandenheede, I.; Steenbeke, M.; Joseph, M.; Sandra, P. *J. Chromatogr. B* **2016**, *1032*, 119.

(227) Beck, A.; Terral, G.; Debaene, F.; Wagner-Rousset, E.; Marcoux, J.; Janin-Bussat, M.-C.; Colas, O.; Dorsselaer, A. van; Cianférani, S. *Expert Rev. Proteomics* **2016**, *13*, 157.

(228) Pan, L. Y.; Salas-Solano, O.; Valliere-Douglass, J. F. *Anal. Chem.* **2014**, *86*, 2657.

(229) Debaene, F.; Bœuf, A.; Wagner-Rousset, E.; Colas, O.; Ayoub, D.; Corvaïa, N.; van Dorsselaer, A.; Beck, A.; Cianférani, S. *Anal. Chem.* **2014**, *86*, 10674.

(230) Chudasama, V.; Maruani, A.; Caddick, S. *Nat. Chem.* **2016**, *8*, 114.

(231) Yoder, N. C.; Bai, C.; Tavares, D.; Widdison, W. C.; Whiteman, K. R.; Wilhelm, A.; Wilhelm, S. D.; McShea, M. A.; Maloney, E. K.; Ab, O.; Wang, L.; Jin, S.; Erickson, H. K.; Keating, T. A.; Lambert, J. M. *Mol. Pharm.* **2019**, *16*, 3926.

(232) Shamsabadi, A.; Ren, J.; Chudasama, V. *RSC Adv,* **2017**, *7*, 27608.

(233) Salahi, F.; Purohit, V.; Ferraudi, G.; Stauffacher, C.; Wiest, O.; Helquist, P. *Org. Lett.* **2018**, *20*, 2547.

(234) Bourbon, P.; Peng, Q.; Ferraudi, G.; Stauffacher, C.; Wiest, O.; Helquist, P. *Bioorg. Med. Chem. Lett.* **2013**, *23*, 6321.

(235) Wood, M. J.; Irwin, W. J.; Scott, D. K. J Clin Pharm Ther **1990**, *15*, 291.

(236) Figueiras, T. S.; Neves-Petersen, M. T.; Petersen, S. B. *J. Fluoresc.* **2011**, *21*, 1897.

(237) Laubrock, N.; Hempel, G.; Schulze-Westhoff, P.; Würthwein, G.; Flege, S.; Boos, J. *Chromatographia* **2000**, *52*, 9.

(238) Davis, I. D. et al. *N. Engl. J. Med.* **2019**, *381*, 121.

(239) Nishimon, S.; Nishimon, M.; Nishino, S. *Expert Opin Pharmacother.* **2019**, *20*, 1065.

(240) Szijj, P. A.; Bahou, C.; Chudasama, V. *Drug Discov. Today Technol.* **2018**, *30*, 27.

(241) Li, W.; Veale, K. H.; Qiu, Q.; Sinkevicius, K. W.; Maloney, E. K.; Costoplus, J. A.; Lau, J.; Evans, H. L.; Setiady, Y.; Ab, O.; Abbott, S. M.; Lee, J.; Wisitpitthaya, S.; Skaletskaya, A.; Wang, L.; Keating, T. A.; Chari, R. V. J.; Widdison, W. C. *ACS Med. Chem. Lett.* **2019**, *10*, 1386.

(242) Nanda, J. S.; Lorsch, J. R. *Methods in Enzymol.* **2014**; Vol. 536, 87.

(243) Zeng, D.; Guo, Y.; White, A. G.; Cai, Z.; Modi, J.; Ferdani, R.; Anderson, C. J. *Mol. Pharm.* **2014**, *11*, 3980.

(244) Andreano, E. et al. *Cell* **2021**, *184*, 1821.

(245) Backer, V.; Sjöbring, U.; Sonne, J.; Weiss, A.; Hostrup, M.; Johansen, H. K.; Becker, V.; Sonne, D. P.; Balchen, T.; Jellingsø, M.; Sommer, M. O. A. *Lancet Reg. Health Eur.* **2021**, *4*, 100084.

(246) Takaoka, S.; Takaoka, N.; Minoshima, Y.; Huang, J.-M.; Kubo, M.; Harada, K.; Hioki, H.; Fukuyama, Y. *Tetrahedron* **2009**, *65*, 8354.

(247) Orlowska, E.; Roller, A.; Wiesinger, H.; Pignitter, M.; Jirsa, F.; Krachler, R.; Kandioller, W.; Keppler, B. K. *RSC Adv.* **2016**, *6*, 40238.

(248) Gryder, B. E.; Akbashev, M. J.; Rood, M. K.; Raftery, E. D.; Meyers, W. M.; Dillard, P.; Khan, S.; Oyelere, A. K. *ACS Chem. Biol.* **2013**, *8*, 2550.

(249) Bradford, M. M. *Anal. Biochem.* **1976**, *72*, 248.

(250) Barthel, B. L.; Rudnicki, D. L.; Kirby, T. P.; Colvin, S. M.; Burkhart, D. J.; Koch, T. H. *J. Med. Chem.* **2012**, *55*, 6595.

(251) Ruiz-Olalla, A.; Würdemann, M. A.; Wanner, M. J.; Ingemann, S.; van Maarseveen, J. H.; Hiemstra, H. *J. Org. Chem.* **2015**, *80*, 5125.

(252) Kemper, B.; von Gröning, M.; Lewe, V.; Spitzer, D.; Otremba, T.; Stergiou, N.; Schollmeyer, D.; Schmitt, E.; Ravoo, B. J.; Besenius, P. *Chem. Eur. J.* **2017**, *23*, 6048.

(253) undisclosed due to IP protection reasons.

(254) Rotstein, B. H.; Zaretsky, S.; Rai, V.; Yudin, A. K. *Chem. Rev.* **2014**, *114*, 8323.

(255) Biginelli, P. *Gazz. Chim. Ital.* **1893**, *23*, 360.

(256) Singh, K.; Kaur, T. *MedChemComm* **2016**, *7*, 749.

(257) Rashid, U.; Sultana, R.; Shaheen, N.; Hassan, S. F.; Yaqoob, F.; Ahmad, M. J.; Iftikhar, F.; Sultana, N.; Asghar, S.; Yasinzai, M.; Ansari, F. L.; Qureshi, N. A. *Eur. J. Med. Chem.* **2016**, *115*, 230.

(258) Chikhale, R.; Menghani, S.; Babu, R.; Bansode, R.; Bhargavi, G.; Karodia, N.; Rajasekharan, M. v; Paradkar, A.; Khedekar, P. *Eur. J. Med. Chem.* **2015**, *96*, 30.

(259) Treptow, T. G. M.; Figueiró, F.; Jandrey, E. H. F.; Battastini, A. M. O.; Salbego, C. G.; Hoppe, J. B.; Taborda, P. S.; Rosa, S. B.; Piovesan, L. A.; Montes D'Oca, C. D. R.; Russowsky, D.; Montes D'Oca, M. G. *Eur. J. Med. Chem.* **2015**, *95*, 552.

(260) Dhumaskar, K. L.; Meena, S. N.; Ghadi, S. C.; Tilve, S. G. *Bioorg. Med. Chem. Lett.* **2014**, *24*, 2897.

(261) Zhu, X.; Zhao, G.; Zhou, X.; Xu, X.; Xia, G.; Zheng, Z.; Wang, L.; Yang, X.; Li, S. *Bioorg. Med. Chem. Lett.* **2010**, *20*, 299.

(262) Lewis, R. W.; Mabry, J.; Polisar, J. G.; Eagen, K. P.; Ganem, B.; Hess, G. P. *Biochemistry* **2010**, *49*, 4841.

(263) Kappe, C. O. *Acc. Chem. Res.* **2000**, *33*, 879.

(264) Heravi, M. M.; Asadi, S.; Lashkariani, B. M. *Mol. Divers.* **2013**, *17*, 389.

(265) Folkers, K.; Johnson, T. B. *J. Am. Chem. Soc.* **1933**, *55*, 3784.

(266) Sweet, Frederick.; Fissekis, J. D. *J. Am. Chem. Soc.* **1973**, *95*, 8741.

(267) Kappe, C. O. *J. Org. Chem.* **1997**, *62*, 7201.

(268) De Souza, R. O. M. A.; da Penha, E. T.; Milagre, H. M. S.; Garden, S. J.; Esteves, P. M.; Eberlin, M. N.; Antunes, O. A. C. *Chem. Eur. J.* **2009**, *15*, 9799.

(269) Freitas, E. F.; Souza, R. Y.; Passos, S. T. A.; Dias, J. A.; Dias, S. C. L.; Neto, B. A. D. *RSC Adv***. 2019**, *9*, 27125.

(270) Puripat, M.; Ramozzi, R.; Hatanaka, M.; Parasuk, W.; Parasuk, V.; Morokuma, K. *J. Org. Chem.* **2015**, *80*, 6959.

(271) Khanina, E. L.; Silinietse, G. O.; Ozol, Ya. Ya.; Dubur, G. Ya.; Kimenis, A. A. *Pharm. Chem. J.* **1978**, *12*, 1321.

(272) Rovnyak, G. C.; Atwal, K. S.; Hedberg, A.; Kimball, S. D.; Moreland, S.; Gougoutas, J. Z.; O'Reilly, B. C.; Schwartz, J.; Malley, M. F. *J. Med. Chem.* **1992**, *35*, 3254.

(273) Fabian, W. M. F.; Semones, M. A.; Kappe, C. O. *J. Mol. Struct.* **1998**, *432*, 219.

(274) Atwal, K. S.; Rovnyak, G. C.; Kimball, S. D.; Floyd, D. M.; Moreland, S.; Swanson, B. N.; Gougoutas, J. Z.; Schwartz, J.; Smillie, K. M.; Malley, M. F. *J. Med. Chem.* **1990**, *33*, 2629.

(275) Atwal, K. S.; Rovnyak, G. C.; Schwartz, J.; Moreland, S.; Hedberg, A.; Gougoutas, J. Z.; Malley, M. F.; Floyd, D. M. *J. Med. Chem.* **1990**, *33*, 1510.

(276) Atwal, K. S.; Swanson, B. N.; Unger, S. E.; Floyd, D. M.; Moreland, S.; Hedberg, A.; O'Reilly, B. C. *J. Med. Chem.* **1991**, *34*, 806.

(277) Mayer, T. U.; Kapoor, T. M.; Haggarty, S. J.; King, R. W.; Schreiber, S. L.; Mitchison, T. J. *Science* **1999**, *286*, 971.

(278) Prokopcová, H.; Dallinger, D.; Uray, G.; Kaan, H. Y. K.; Ulaganathan, V.; Kozielski, F.; Laggner, C.; Kappe, C. O. *ChemMedChem* **2010**, *5*, 1760.

(279) Russowsky, D.; Canto, R. F. S.; Sanches, S. A. A.; D'Oca, M. G. M.; de Fátima, Â.; Pilli, R. A.; Kohn, L. K.; Antônio, M. A.; de Carvalho, J. E. *Bioorg. Chem.* **2006**, *34*, 173.

(280) Prashantha Kumar, B. R.; Sankar, G.; Nasir Baig, R. B.; Chandrashekaran, S. *Eur. J. Med. Chem.* **2009**, *44*, 4192.

(281) Da Silva, D. L.; Reis, F. S.; Muniz, D. R.; Ruiz, A. L. T. G.; de Carvalho, J. E.; Sabino, A. A.; Modolo, L. v; de Fátima, Â. *Bioorg. Med. Chem.* **2012**, *20*, 2645.

(282) Wright, C. M.; Chovatiya, R. J.; Jameson, N. E.; Turner, D. M.; Zhu, G.; Werner, S.; Huryn, D. M.; Pipas, J. M.; Day, B. W.; Wipf, P.; Brodsky, J. L. *Bioorg. Med. Chem.* **2008**, *16*, 3291.

(283) Sashidhara, K. v; Avula, S. R.; Sharma, K.; Palnati, G. R.; Bathula, S. R. *Eur. J. Med. Chem.* **2013**, *60*, 120.

(284) Dondoni, A.; Massi, A.; Sabbatini, S.; Bertolasi, V. *J. Org. Chem.* **2002**, *67*, 6979.

(285) Treptow, T. G. M.; Figueiró, F.; Jandrey, E. H. F.; Battastini, A. M. O.; Salbego, C. G.; Hoppe, J. B.; Taborda, P. S.; Rosa, S. B.; Piovesan, L. A.; Montes D'Oca, C. D. R.; Russowsky, D.; Montes D'Oca, M. G. Eur *J. Med. Chem.* **2015**, *95*, 552.

(286) Ristovski (Trifunović), J.; Minorics, R.; Bartha, S.; Janković, N.; Zupkó, I. *J. Mol. Struct.* **2022**, *1254*, 132373.

(287) Bérubé, G. *Expert Opin. Drug Discov.* **2016**, *11*, 281.

(288) Bansal, Y.; Silakari, O. Eur *J. Med. Chem.* **2014**, *76*, 31.

(289) Gireesh, T.; Kamble, R. R.; Kattimani, P. P.; Dorababu, A.; Manikantha, M.; Hoskeri, J. H. *Arch. Pharm*. **2013**, *346*, 645.

(290) Kwon, O. W.; Moon, E.; Chari, M. A.; Kim, T. W.; Kim, A.; Lee, P.; Ahn, K.-H.; Kim, S. Y. *Bioorg. Med. Chem. Lett.* **2012**, *22*, 5199.

(291) Gijsen, H. J. M.; Berthelot, D.; de Cleyn, M. A. J.; Geuens, I.; Brône, B.; Mercken, M. *Bioorg. Med. Chem. Lett.* **2012**, *22*, 797.

(292) Chikhale, R. v; Bhole, R. P.; Khedekar, P. B.; Bhusari, K. P. *Eur. J. Med. Chem.* **2009**, *44*, 3645.

(293) Tale, R. H.; Rodge, A. H.; Hatnapure, G. D.; Keche, A. P.; Patil, K. M.; Pawar, R. P. *Med. Chem. Res.* **2012**, *21*, 4252.

(294) Mokale, S. N.; Shinde, S. S.; Elgire, R. D.; Sangshetti, J. N.; Shinde, D. B. *Bioorg. Med. Chem. Lett.* **2010**, *20*, 4424.

(295) De Fátima, Â.; Braga, T. C.; Neto, L. da S.; Terra, B. S.; Oliveira, B. G. F.; da Silva, D. L.; Modolo, L. *J. Adv. Res.* **2015**, *6*, 363.

(296) Chitra, S.; Devanathan, D.; Pandiarajan, K. Eur *J. Med. Chem.* **2010**, *45*, 367.

(297) Trivedi, A. R.; Bhuva, V. R.; Dholariya, B. H.; Dodiya, D. K.; Kataria, V. B.; Shah, V. H. *Bioorg. Med. Chem. Lett.* **2010**, *20*, 6100.

(298) Yadlapalli, R. K.; Chourasia, O. P.; Vemuri, K.; Sritharan, M.; Perali, R. S. *Bioorg. Med. Chem. Lett.* **2012**, *22*, 2708.

(299) Sethiya, A.; Soni, J.; Manhas, A.; Jha, P. C.; Agarwal, S. *Res. Chem. Intermed.* **2021**, *47*, 4477.

(300) Marinescu, M. *Molecules* **2021**, *26*.

(301) Zabihollahi, R.; Fassihi, A.; Aghasadeghi, M. R.; Memarian, H. R.; Soleimani, M.; Majidzadeh-A, K. *Med. Chem. Res.* **2013**, *22*, 1270.

(302) Kim, J.; Ok, T.; Park, C.; So, W.; Jo, M.; Kim, Y.; Seo, M.; Lee, D.; Jo, S.; Ko, Y.; Choi, I.; Park, Y.; Yoon, J.; Ju, M. K.; Ahn, J.; Kim, J.; Han, S.-J.; Kim, T.-H.; Cechetto, J.; Nam, J.; Liuzzi, M.; Sommer, P.; No, Z. *Bioorg. Med. Chem. Lett.* **2012**, *22*, 2522.

(303) Kim, J.; Park, C.; Ok, T.; So, W.; Jo, M.; Seo, M.; Kim, Y.; Sohn, J.-H.; Park, Y.; Ju, M. K.; Kim, J.; Han, S.-J.; Kim, T.-H.; Cechetto, J.; Nam, J.; Sommer, P.; No, Z. *Bioorg. Med. Chem. Lett.* **2012**, *22*, 2119.

(304) Ramajayam, R.; Tan, K.-P.; Liu, H.-G.; Liang, P.-H. *Bioorg. Med. Chem. Lett.* **2010**, *20*, 3569.

(305) Stefani, H. A.; Oliveira, C. B.; Almeida, R. B.; Pereira, C. M. P.; Braga, R. C.; Cella, R.; Borges, V. C.; Savegnago, L.; Nogueira, C. W. *Eur. J. Med. Chem.* **2006**, *41*, 513.

(306) De Vasconcelos, A.; Oliveira, P. S.; Ritter, M.; Freitag, R. A.; Romano, R. L.; Quina, F. H.; Pizzuti, L.; Pereira, C. M. P.; Stefanello, F. M.; Barschak, A. G. *J. Biochem. Mol. Toxicol.* **2012**, *26*, 155.

(307) Mansouri, M.; Movahedian, A.; Rostami, M.; Fassihi, A. *Res. Pharm. Sci.* **2012**, *7*, 257.

(308) Dondoni, A.; Massi, A.; Sabbatini, S. *Tetrahedron Lett.* **2002**, *43*, 5913.

(309) Sidler, D. R.; Barta, N.; Li, W.; Hu, E.; Matty, L.; Ikemoto, N.; Campbell, J. S.; Chartrain, M.; Gbewonyo, K.; Boyd, R.; Corley, E. G.; Ball, R. G.; Larsen, R. D.; Reider, P. J. *Can. J. Chem.* **2002**, *80*, 646.

(310) Schnell, B.; Strauss, U. T.; Verdino, P.; Faber, K.; Kappe, C. O. *Tetrahedron Asymmetry* **2000**, *11*, 1449.

(311) Muñoz-Muñiz, O.; Juaristi, E. *Arkivoc* **2003**, *2003*, 16.

(312) Huang, Y.; Yang, F.; Zhu, C. *J. Am. Chem. Soc.* **2005**, *127*, 16386.

(313) Kamali, M. Int *J. ChemTech Res.* **2015**, *8*, 536.

(314) Fedorova, O. v; Titova, Y. A.; Vigorov, A. Yu.; Toporova, M. S.; Alisienok, O. A.; Murashkevich, A. N.; Krasnov, V. P.; Rusinov, G. L.; Charushin, V. N. *Catal. Lett.* **2016**, *146*, 493.

(315) Davydov, A. A.; Sheppard, N. T. *Molecular spectroscopy of oxide catalyst surfaces* Wiley Chichester, **2003**; Vol. 690.

(316) Gong, L.-Z.; Chen, X.-H.; Xu, X.-Y. *Chem. Eur. J.* **2007**, *13*, 8920.

(317) Kappe, C. O.; Uray, G.; Roschger, P.; Lindner, W.; Kratky, C.; Keller, W. *Tetrahedron* **1992**, *48*, 5473.

(318) Uraguchi, D.; Terada, M. *J. Am. Chem. Soc.* **2004**, *126*, 5356.

(319) Chen, X.-H.; Xu, X.-Y.; Liu, H.; Cun, L.-F.; Gong, L.-Z. *J. Am. Chem. Soc.* **2006**, *128*, 14802.

(320) Akiyama, T.; Morita, H.; Itoh, J.; Fuchibe, K. *Org. Lett.* **2005**, *7*, 2583.

(321) Rowland, G. B.; Zhang, H.; Rowland, E. B.; Chennamadhavuni, S.; Wang, Y.; Antilla, J. C. *J. Am. Chem. Soc.* **2005**, *127*, 15696.

(322) Li, N.; Chen, X.-H.; Song, J.; Luo, S.-W.; Fan, W.; Gong, L.-Z. *J. Am. Chem. Soc.* **2009**, *131*, 15301.

(323) Guo, Y.; Gao, Z.; Meng, X.; Huang, G.; Zhong, H.; Yu, H.; Ding, X.; Tang, H.; Zou, C. *Synlett* **2017**, *28*, 2041.

(324) An, D.; Fan, Y.-S.; Gao, Y.; Zhu, Z.-Q.; Zheng, L.-Y.; Zhang, S.-Q. *Eur. J. Org. Chem.* **2014**, *2014*, 301.

(325) Xin, J.; Chang, L.; Hou, Z.; Shang, D.; Liu, X.; Feng, X. *Chem. Eur. J.* **2008**, *14*, 3177.

(326) Xu, D.-Z.; Li, H.; Wang, Y. *Tetrahedron* **2012**, *68*, 7867.

(327) Ma, J.-A.; Cahard, D. *Angew. Chem. Int. Ed.* **2004**, *43*, 4566.

(328) Frings, M.; Thomé, I.; Bolm, C. *Beilstein J. Org. Chem.* **2012**, *8*, 1443.

(329) Jang, H. bin; Rho, H. S.; Oh, J. S.; Nam, E. H.; Park, S. E.; Bae, H. Y.; Song, C. E. *Org. Biomol. Chem.* **2010**, *8*, 3918.

(330) Barbero, M.; Cadamuro, S.; Dughera, S. *Green Chem.* **2017**, *19*, 1529.

(331) Hu, Q.-S.; He, Y.-Q.; Li, L.-C. *Asian J. Chem.* **2016**, *28*.

(332) Lillo, V. J.; Saá, J. M. *Chem. Eur. J.* **2016**, *22*, 17182.

(333) Hang, Z.; Zhu, J.; Lian, X.; Xu, P.; Yu, H.; Han, S. *Chem. Comm.* **2016**, *52*, 80.

(334) Yu, H.; Xu, P.; He, H.; Zhu, J.; Lin, H.; Han, S. *Tetrahedron Asymmetry* **2017**, *28*, 257.

(335) Wu, Y.-Y.; Chai, Z.; Liu, X.-Y.; Zhao, G.; Wang, S.-W. *Eur. J. Org. Chem.* **2009**, *2009*, 904.

(336) González-Olvera, R.; Demare, P.; Regla, I.; Juaristi, E. *Arkivoc* **2008**, *2008*, 61.

(337) Li, Z.; Xing, H.; Huang, G.; Sun, X.; Jiang, J.; Wang, L. *Sci. China Chem.* **2011**, *54*, 1726.

(338) Titova, Y.; Fedorova, O.; Rusinov, G.; Vigorov, A.; Krasnov, V.; Murashkevich, A.; Charushin, V. Catal Today **2015**, *241*, 270.

(339) Bariwal, J.; van der Eycken, E. *Chem. Soc. Rev.* **2013**, *42*, 9283.

(340) Ullmann, F.; Bielecki, J. *Ber. Dtsch. Chem. Ges.* **1901**, *34*, 2174.

(341) Ley, S. v; Thomas, A. W. *Angew. Chem. Int. Ed.* **2003**, *42*, 5400.

(342) Sambiagio, C.; Marsden, S. P.; Blacker, A. J.; McGowan, P. C. *Chem. Soc. Rev.* **2014**, *43*, 3525.

(343) Lo, Q. A.; Sale, D.; Braddock, D. C.; Davies, R. P. *ACS Catal.* **2018**, *8*, 101.

(344) Gurjar, K. K.; Sharma, R. K. *ChemCatChem* **2017**, *9*, 862.

(345) Daly, S.; Haddow, M. F.; Orpen, A. G.; Rolls, G. T. A.; Wass, D. F.; Wingad, R. L. *Organometallics* **2008**, *27*, 3196.

(346) Liu, Z.-J.; Vors, J.-P.; Gesing, E. R. F.; Bolm, C. *Adv. Synth. Catal.* **2010**, *352*, 3158.

(347) Zhang, Z.; Mao, J.; Zhu, D.; Wu, F.; Chen, H.; Wan, B. *Tetrahedron* **2006**, *62*, 4435.

(348) Wang, D.; Zheng, Y.; Yang, M.; Zhang, F.; Mao, F.; Yu, J.; Xia, X. *Org. Biomol. Chem.* **2017**, *15*, 8009.

(349) Zhou, W.; Fan, M.; Yin, J.; Jiang, Y.; Ma, D. *J. Am. Chem. Soc.* **2015**, *137*, 11942.

(350) Quivelli, A. F.; Vitale, P.; Perna, F. M.; Capriati, V. *Front. Chem.* **2019**, *7*.

(351) Yuan, C.; Zhang, L.; Zhao, Y. *Molecules* **2019**, *24*.

(352) Liu, W.; Xu, J.; Chen, X.; Zhang, F.; Xu, Z.; Wang, D.; He, Y.; Xia, X.; Zhang, X.; Liang, Y. *Org. Lett.* **2020**, *22*, 7486.

(353) Ruiz-Castillo, P.; Buchwald, S. L. *Chem. Rev.* **2016**, *116*, 12564.

(354) Maiti, D.; Fors, B. P.; Henderson, J. L.; Nakamura, Y.; Buchwald, S. L. *Chem. Sci.* **2011**, *2*, 57.

(355) Surry, D. S.; Buchwald, S. L. *Chem. Sci.* **2011**, *2*, 27.

(356) Ingoglia, B. T.; Wagen, C. C.; Buchwald, S. L. *Tetrahedron* **2019**, *75*, 4199.

(357) Dennis, J. M.; White, N. A.; Liu, R. Y.; Buchwald, S. L. *J. Am. Chem. Soc.* **2018**, *140*, 4721.

(358) Sánchez-Sancho, F.; Escolano, M.; Gaviña, D.; Csáky, A. G.; Sánchez-Roselló, M.; Díaz-Oltra, S.; del Pozo, C. *Pharmaceuticals* **2022**, *15*.

(359) Bellini, R.; Reek, J. N. H. *Chem. Eur. J.* **2012**, *18*, 7091.

(360) Li, L.; Liu, Y.; Peng, Y.; Yu, L.; Wu, X.; Yan, H. *Angew. Chem. Int. Ed.* **2016**, *55*, 331.

(361) Sai, M.; Yamamoto, H. *J. Am. Chem. Soc.* **2015**, *137*, 7091.

(362) Ryabukhin, S. v; Plaskon, A. S.; Ostapchuk, E. N.; Volochnyuk, D. M.; Tolmachev, A. A. *ChemInform* **2007**, *38*.

(363) García-García, P.; Lay, F.; García-García, P.; Rabalakos, C.; List, B. *Angew. Chem. Int. Ed.* **2009**, *48*, 4363.

(364) Cho, H.; Nishimura, Y.; Yasui, Y.; Kobayashi, S.; Yoshida, S.; Kwon, E.; Yamaguchi, M. *Tetrahedron* **2011**, *67*, 2661.

(365) Undisclosed experimental results.

(366) Bartoszek, M.; Beller, M.; Deutsch, J.; Klawonn, M.; Köckritz, A.; Nemati, N.; Pews-Davtyan, A. *Tetrahedron* **2008**, *64*, 1316.